COMPUTATIONAL AND EXPERIMENTAL INVESTIGATION OF CATALYTIC HYDROCARBON FUEL PROCESSING FOR AUTOTHERMAL HYDROGEN PRODUCTION

by

Ahmet Kerim Avcı

B. S. in Ch.E., Boğaziçi University, 1996

Submitted to the Institute for Graduate Studies in Science and Engineering in partial fulfillment of the requirements for the degree of Doctor of Philosophy

Graduate Program in Chemical Engineering

Boğaziçi University

2003

to my family

ACKNOWLEDGEMENT

Firstly, I would like to express my truthful gratitude to my thesis supervisor Prof. Zeynep İlsen Önsan – a world-class professor – for her guidance, encouragement and trust in me. My respect and admiration in her personality as well as her invaluable way of teaching inspired me all the time. It was a privilege for me to work with Prof. Önsan during my PhD thesis.

Very special thanks are due to Prof. David L. Trimm, Science Leader of Gas Processing Division in CSIRO, a 'champions league player' in the field of catalysis and visiting professor at Boğaziçi University between March 2000-June 2000 for generously offering so much of his knowledge, experience and patience as well as his lifestyle and scientific philosophy in such a short time and for keeping up his interest since then.

I would like to express my great appreciations for Assoc. Prof. Ahmet Erhan Aksoylu, Assoc. Prof. Ayşe Nilgün Akın, Assit. Prof. Ramazan Yıldırım and Dr. Ayşe İnci İşli who devoted their valuable time to guiding me, helping me all the time. It was a great opportunity for me to learn from their experiences and knowledge.

I would like to thank to Prof. Mehmet Çamurdan, Prof. Mahir Arıkol and Prof. Kutlu Ülgen for their valuable support and for sharing their scientific background with me.

Very special thanks to Mete Altıntaş, Orhan Oruç,Alper Tunga Akarsubaşı and Emre Sayılaner for their everlasting help and encouragement. Their friendships are the biggest assets that I have gained in my life.

I was very lucky to work with the CATREL team, apart from those cited above, Murat Dönmez, Tülay Bülbül, Mustafa Ataman, Kerem Uğuz, Şeyma Özkara, Mine Gülmen, Gökhan Seçkin and Burcu Selen for giving me their true friendship and making me feel happy all the time. I also would like to thank to all my friends in Chemical Engineering Department for their support.

I will always appreciate Bilgi Dedeoğlu and Nurettin Bektaş for their significant efforts during the experimental part of my thesis and for their cordial friendship. Heartfelt thanks are for Mine Çek and for Fatma Coşkun for their help in office work and also for Yakup Bal for his friendly attitude.

I would like to express my thanks to Zülal Mısırlı for her assistance in electron microscopy studies conducted at Boğaziçi University Advanced Technologies R&D Center.

Finally, I think that no words or phrases can be used to thank to my family - closest of the closest and best of the best. This work would have never been possible without their everlasting support. I dedicate this work to them, but I am aware that this is very far from being a sufficient thank when I consider their enormous efforts.

Financial support provided by the Boğaziçi University Research Fund through projects **DPT-97K120640** and **DPT-01K120300**. I also acknowledge Boğaziçi University Foundation for partially funding this study through the Fahir İlkel PhD scholarship program.

ABSTRACT

COMPUTATIONAL AND EXPERIMENTAL INVESTIGATION OF CATALYTIC HYDROCARBON FUEL PROCESSING FOR AUTOTHERMAL HYDROGEN PRODUCTION

Catalytic conversion of hydrocarbon fuels within the context of the operation of a fuel processor for supplying hydrogen to vehicular and stationary fuel cells is investigated using computer-based modeling/simulation studies and experimental techniques. The computational part of this work involves the quantitative description of the proposed fuel processor/fuel cell system, and the assessment of various combinations of hydrocarbon fuels and fuel processing routes on the basis of their hydrogen yields. Computer simulations indicate the possible advantages of the conversions of liquefied petroleum gas (propane + n-butane) by an indirect partial oxidation (combined total oxidation/steam reforming) mechanism for use in mobile fuel cell applications and of methane (natural gas) by a direct, one-step partial oxidation mechanism in small-scale stationary fuel cell applications. Experimental studies involve the investigation of total oxidation and steam reforming of propane and n-butane over a bimetallic Pt-Ni catalyst. The catalyst is thought to have the potential of driving indirect partial oxidation efficiently by facilitating heat transfer between the two reactions. For both hydrocarbons (a) the oxidation activities are found to follow the order of Pt>Pt-Ni>Ni, (b) Pt metal seems to drive oxidation qualitatively, (c) dispersion of Pt over Ni is likely to affect the oxidation activities. Steam reforming of n-butane over Ni and Pt-Ni catalysts have shown different characteristics, particularly at 648 K in terms of hydrogen selectivities. Assessment of reaction kinetics at 648 K gave reaction orders of 1.20 and –0.18, with respect to n-butane and steam, respectively and an activation energy of 80.7 kJ mol^{-1} in the 603 K–668 K range.

ÖZET

HİDROKARBON YAKITLARIN OTOTERMAL HİDROJEN ÜRETİMİ İÇİN KATALİTİK DÖNÜŞÜMLERİNİN BİLGİSAYAR DESTEKLİ VE DENEYSEL YÖNTEMLERLE İNCELENMESİ

Taşıtlarda ve yerel uygulamalarda kullanılabilecek yakıt pillerine hidrojen sağlamak amacıyla, hidrokarbon yakıtların yakıt prosesörü çalışma koşullarında dönüşümleri, bilgisayar destekli modelleme/benzetim yöntemleri ve deneysel çalışmalarla incelenmiştir. Bilgisayar destekli çalışmalar, önerilen yakıt pili/yakıt prosesörü sistemi için genel bir matematiksel modelin geliştirilmesini ve bu modelin değişik yakıt/yakıt dönüşümü kombinasyonlarının hidrojen verimliliklerinin incelenmesi amacıyla kullanımını içermektedir. Bu çalışmalar, propan ve n-bütan hidrokarbonlarının karışımı olan sıvılaştırılmış petrol gazının ve çoğunlukla metan içeren doğal gazın sırasıyla dolaylı kısmi oksidasyon (toplam oksidasyon + buhar reformlama) ve tek aşamalı kısmi oksidasyon mekanizmalarıyla dönüşümlerinin, taşıtlar için yakıt pili ve yerleşik yakıt pili uygulamalarında hidrojen sağlamak amacıyla kullanılmalarının verimli olduklarını göstermiştir. Deneysel çalışmalar, propan ve n-bütan hidrokarbonlarının destekli, çift metalli Pt-Ni katalizörü üzerinde toplam oksidasyon dönüşümlerini ve buhar ile reformlanmalarını içermektedir. Pt-Ni katalizörün, bu reaksiyonlar arasındaki ısı transferini geliştirme ve böylece dolaylı kısmi oksidasyon mekanizmasını hızlandırma potansiyeline sahip olduğu düşünülmektedir. Her iki hidrokarbon için (a) toplam oksidasyon aktiviteleri Pt>Pt-Ni>Ni sırasıyla azalmış, (b) Pt metalinin toplam oksidasyon sırasında daha etkili olduğu görülmüştür. Pt metalinin Ni üzerinde dağılımının oksidasyon aktivitelerini etkilediği düşünülmektedir. n-Bütan'ın Ni ve Pt-Ni üzerinde buhar ile reformlanması incelenmiş ve özellikle 648 K'de hidrojen seçimliliği yönünden farklılıklar gözlemlenmiştir. 648 K'de yapılan kinetik çalışma sonucu, n-bütan ve buhar için reaksiyon dereceleri sırasıyla 1.20 ve –0.18 olarak bulunmuştur. 603 K-668 K arasındaki deneyler, aktivasyon enerjisinin 80.7 kJ mol^{-1} olduğunu göstermiştir.

TABLE OF CONTENTS

LIST OF FIGURES

LIST OF TABLES

LIST OF SYMBOLS/ABBREVIATIONS

a_j	Activity of component j
a_m	Exterior surface area per unit mass of catalyst
$c_{p,j}$	Gas phase heat capacity of component j
c_{pL,H_2O}	Liquid phase heat capacity of water
C_j	Bulk fluid concentration of component j
C_{sj}	Surface concentration of component j
D_e	Effective diffusivity inside catalyst
D_{jm}	Diffusivity of component j into a mixture
D_p	Particle diameter
D_t	Reactor diameter
E_A	Activation energy
f	Fraction of the recovered sensible heat from the partial oxidation reactor (Reactor 1) exit stream
f_3	Fraction of the recovered sensible heat from the afterburner (Reactor 3) exit stream
$F_{H_2,FC}$	Molar flow rate of hydrogen rejected from the fuel cell
$F_{H_2O,inj}$	Molar flow rate of liquid water injected
F_j	Molar flow rate of component j
F_j^o	Initial molar flow rate of component j
$F_{j,i}$	Molar flow rate of component j consumed in reaction i
$F_{j,M}$	Molar flow rate of component j flowing in reactor M
$F_{j,M}^o$	Molar flow rate of component j at the M^{th} reactor inlet
$F_{j,Mex}$	Molar flow rate of component j at the M^{th} reactor exit
$F_{j,1}^{sr,o}$	Molar flow rate of component j before steam reforming within partial oxidation reactor (Reactor 1)

$F_{j,3mid}$	Molar flow rate of component j after hydrogen oxidation within afterburner (Reactor 3)
$F_{j,ox}$	Molar flow rate of component j after methane total oxidation within the partial oxidation reactor
F_T	Total molar flow rate
F_T^o	Total molar flow rate at reactor inlet
G_j^o	Standard Gibbs free energy of formation of component j
H_j^o	Standard heat of formation of component j
h_s	Particle-to-fluid heat transfer coefficient
k_i, k_o	Specific rate of reaction i
k_{sj}	Particle-to-fluid mass transfer coefficient
$\tilde{k}$	Stoichiometric coefficient of oxygen in Reactions (5.7) and (5.8)
K_i, K_P	Pressure equilibrium constant of reaction i
K'_j, K''_j	Adsorption/desorption equilibrium constant of component j
K'''	Number of parameters
n	Reaction order
N'''	Number of data points
P_j	Partial pressure of component j
P_T	Total pressure
P_T^o	Total pressure at reactor inlet
Pr	Prandtl number
q	Heat input-removal terms in the energy balance equations
$-r_i$	Rate of reaction i
$-r_{i,s}$	Rate of reaction i evaluated at surface conditions
R	Gas constant
Re	Reynolds number
Sc	Schmidt number
T	Temperature of the gas mixture

T^o	Temperature of the gas mixture at reactor inlet
$T_l^{sr,o}$	Temperature of the gas mixture before steam reforming within partial oxidation reactor (Reactor 1)
$T_{l,exhr}$	Temperature of the gas mixture at the partial oxidation reactor (Reactor 1) exit after heat recovery
T_{LO}	Light-off temperature
$T_{M,ex}$	Temperature of the gas mixture at the M^{th} reactor exit
T_M^o	Temperature of the gas mixture at the M^{th} reactor inlet
T_{max}	Maximum catalyst bed temperature within the partial oxidation reactor (Reactor 1)
T_R	Reference temperature
T_{RxN}	Direct partial oxidation temperature
W	Catalyst weight
W/F_{AO}	Residence time
x_{CH_4}	Methane conversion
y_j	Yield of component j
α	Order of n-butane steam reforming with respect to n-butane
β	Order of n-butane steam reforming with respect to steam
β_o	Parameter in the pressure drop equation
$\Delta G_{i,T}$	Gibbs free energy of reaction i at temperature T
$\Delta H_{H_2O}^{vap}$	Latent heat of evaporation of water
ΔH_{298}^o, ΔH_i^o	Molar heat of reaction i at standard conditions
$\Delta H_{i,T}$, $\Delta H_{RxN,T}$	Molar heat of reaction i at temperature T
ϕ	Void fraction of the catalyst bed
γ_j	Activity coefficient of component j
η_i	Effectiveness factor for reaction i
λ_f	Thermal conductivity of the bulk fluid

λ_j	Thermal conductivity of component j
μ_f	Viscosity of the bulk fluid
μ_j	Viscosity of component j
ν_{ij}	Stoichiometric coefficient of component j in reaction i
ρ_b	Catalyst bed density
ρ_c	Solid density of the catalyst
ρ_f	Density of the bulk fluid
σ^2	Sum of squares of residuals
θ	Empirical constant

AFC	Alkaline fuel cell
ATR	Autothermal reforming
BET	Brunauer-Emmett-Teller
CH1	Channel 1 setting
CH2	Channel 2 setting
CH3	Channel 3 setting
CH4	Channel 4 setting
CHP	Combined heat-and-power
DMFC	Direct methanol fuel cell
EDX	Energy Dispersive X-ray Analysis
GC	Gas chromatograph
GHSV	Gas hourly space velocity
HC	Hydrocarbon
ICE	Internal combustion engine
IR	Infrared
LHHW	Langmuir-Hinshelwood Hougen-Watson
LNG	Liquefied natural gas
LPG	Liquefied petroleum gas
MCFC	Molten carbonate fuel cell
MEA	Membrane electrode assembly
MS	Molecular sieve

NASA	National Aeronautics and Space Administration
NAVC	Northeast Advanced Vehicle Consortium
ODE	Ordinary differential equation
PAFC	Phosphoric acid fuel cell
PEM	Proton exchange membrane
PEMFC	Proton exchange membrane fuel cell
POX	Partial oxidation
SEM-BCI	Scanning Electron Microscopy – Backscattered Composition Imaging
SOFC	Solid oxide fuel cell
SR	Steam reforming
TCD	Thermal conductivity detector
TGA	Thermogravimetric analysis
TOX	Total oxidation
TPR	Temperature programmed reduction
WGS	Water-gas shift
XPS	X-ray Photoelectron Spectroscopy
XRD	X-ray Diffraction

1. INTRODUCTION

The development of engines that operate efficiently and produce lower quantities of pollutants has been a major objective, particularly for the automobile industry, for many years. The legislative regulations (Cooper, 1994) have played important roles in achieving steady improvements in fuel economy and in lowering hazardous emissions by facilitating developments in the internal combustion engine (ICE) technology and in the catalytic converters. However, continuous increase in the number of vehicles, which is expected to double from 400 million to 800 million in the next 20 years (Golunski, 1998), has led to the release of much stringent regulations imposed on the emission levels of hazardous gases: In California, it is required that 10 per cent of all new light-duty vehicles sold are expected to have zero on-road emissions by 2003 (Raman, 1997). It is obvious that such regulations will require different power generation approaches. Among a number of alternatives, the use of fuel cells in vehicles is the option that excites most interest (Trimm and Önsan, 2001).

Compared with the conventional technologies, fuel cells offer significant advantages in clean and efficient power generation. They can operate at zero emission level when pure hydrogen is used as the fuel. They also have long life, produce very low noise emissions, and require much less maintenance since no moving parts are involved. Fuel cells involve direct conversion of chemical energy into electrical power without a heat generation step, and hence operate much more efficiently than internal combustion engines. These attractive features make fuel cells a significant option that would replace the existing energy conversion systems, such as combustion engines in automobiles (Gray and Petch, 2000; Hoogers and Thompsett, 1999). Apart from their potential use in powering vehicles, fuel cells, available in various types, can be employed in a vast range of markets ranging from small-scale portable/leisure applications to large-scale stationary power generation (Ralph and Hards, 1998).

A variety of fuel cells operating with different fuels and electrolytes are under investigation, but the Proton Exchange/Polymer Electrolyte Membrane Fuel Cell (PEMFC) fuelled by hydrogen seems to be the most promising option for both vehicular and small-

scale combined heat-and-power (CHP) facilities due to its compactness, modularity, high power density and fast response (Ahmed and Krumpelt, 2001; Ralph, 1999). PEMFC operation requires the continuous availability of hydrogen whose storage, transportation and availability are the major problems that will be encountered when it is directly used as a fuel. Hence, attention has been focused on the conversion of more readily available hydrocarbon fuels to hydrogen through compact and efficient catalytic devices called fuel processors.

Hydrogen is not only a fuel for proton exchange membrane fuel cells, but also a widely used feedstock in the chemical, petroleum refining and petrochemical industries. Hydrotreating and hydrocracking processes, synthesis gas applications such as production of ammonia and methanol, Fisher-Tropsch synthesis and the manufacture of chemicals having specific end uses such as pharmaceuticals are areas in which hydrogen is employed (Furimsky, 1998; Pena *et al.*, 1996). These applications make hydrogen, which is mostly produced by catalytic operations, a commodity of increasing demand in the world: In Western Europe and United States, hydrogen demand is expected to increase at an annual compound growth rate of 21 per cent and 10 per cent, respectively (Pena *et al.*, 1996). These factors make efficient and economic hydrogen production one of the most competitive topics in the field of catalysis.

The major objective of this research is to investigate catalytic autothermal hydrogen production using advanced computer simulations and experimental techniques. The simulation part of the thesis involves the development of a generalized fuel processor/fuel cell system and of mathematical models to investigate and to compare the conversion of a number of hydrocarbon fuels to hydrogen via different fuel processing routes and catalysts for use in vehicular and in small-scale combined heat-and-power applications. Based on the outcomes of the computer simulations, catalytic ignition of propane and n-butane in total oxidation and catalytic steam reforming of n-butane are studied in the experimental part of this work. The steam reforming tests involves the investigation of the reaction kinetics as well. Throughout the experiments, the major emphasis is the use of a bimetallic, thermally stable Pt-Ni catalyst that is expected to catalyze the oxidation and steam reforming by a thermally efficient route.

An extensive literature survey related with the fuel cell technology and catalytic oxidation, steam reforming and partial oxidation of hydrocarbons is presented in Section 2. The techniques, procedures, equipments and systems used in the experiments are described in Section 3. The algorithms and mathematical models employed to simulate fuel processor/fuel cell system are given in Section 4. The results of this research are presented and discussed in Section 5. Section 6 involves the major conclusions that can be drawn from this study and the recommendations for future work.

2. LITERATURE SURVEY

2.1. Fuel Cell Technology

2.1.1. Fuel Cell Operation

A fuel cell is a device that converts the chemical energy stored within a fuel directly into electrical energy and is composed of an anode, a cathode and an electrolyte which is also called a membrane. These units are combined to form the membrane electrode assembly (MEA), as shown in Figure 2.1 (Ralph and Hards, 1998).

In a basic fuel cell operation, atmospheric oxygen enters through the catalytic cathode and the fuel (usually hydrogen) is introduced at the catalytic anode. The hydrogen molecules split into electrons and protons at the anode via electrochemical oxidation. At this stage certain amount of heat is generated, but it is considerably less than that generated in a combustion process. The protons migrate through the electronically insulated electrolyte, and the electrons travel through an external circuit, both of which reach the cathode where they electrochemically react with oxygen to produce water. This operating scheme, presented in Figure 2.1, results in an electrical current and, therefore, can be used as a power source (Cameron, 1999; Vielstich and Iwasita, 1997).

The power generating MEA unit is sandwiched by two bipolar flow field plates, typically made of graphite or metal, in order to provide gas distribution to the anode and cathode in the MEA and to collect electric current from the surface of the MEA. These plates and the MEA combine to form a single fuel cell unit, as shown in Figure 2.2. Each cell generates about 0.7 eV, requiring an assembly (composed of 10-100 fuel cells) to obtain the desired electrical power (Cameron, 1999).

The process runs at temperatures less than 373 K, since the membrane needs to be humidified in order to conduct protons, as the protons migrate as hydrated species. However, the temperature should be kept high enough, i.e. greater than 333 K, to sustain reaction kinetics.

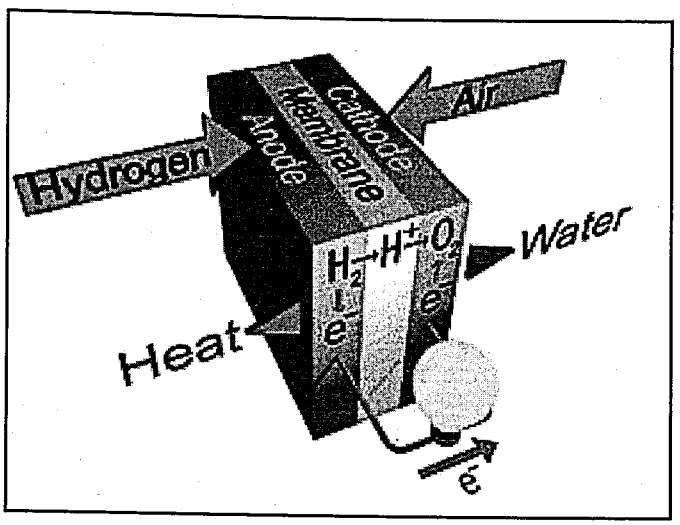

Figure 2.1. MEA and the basic fuel cell operation (Ralph and Hards, 1998)

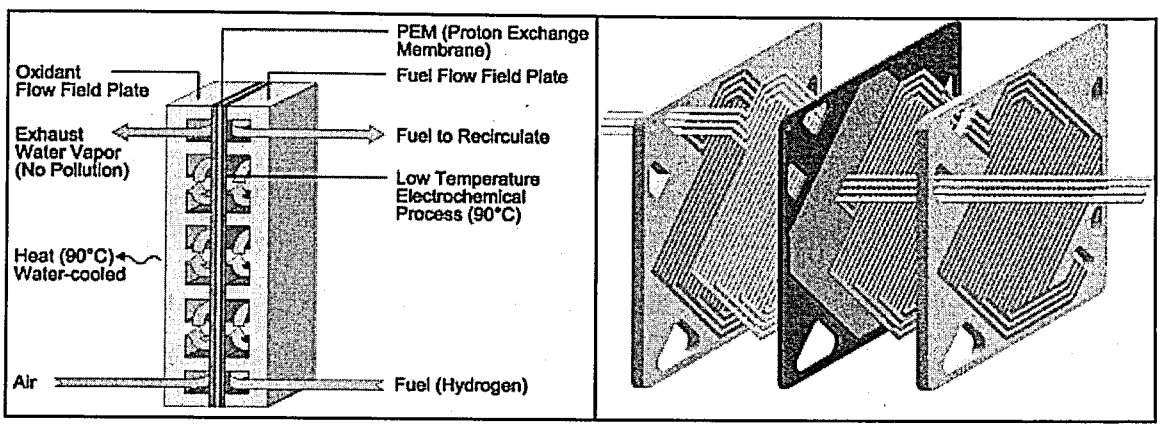

Figure 2.2. Flow field plates and MEA (Hoogers and Thompsett, 1999)

2.1.2. Types and Applications of Fuel Cells

Fuel cells are classified according to the electrolytes they employ, and are therefore distinguished into two major types as the ones operating at low temperature and at high temperature.

2.1.2.1. Low Temperature Fuel Cells. The three main types of low temperature fuel cells are Proton Exchange/Polymer Electrolyte Membrane (PEM) fuel cells, Phosphoric Acid Fuel Cells (PAFC) and Alkaline Fuel Cells (AFC).

PEM fuel cells use pure hydrogen as the fuel, a perfluorinated sulphonic acid membrane as the electrolyte and operate at temperatures between 333 K-363 K (Ralph and Hards, 1998). They offer high power densities and fast responses and have compact volumes, low weights and modular structures, which are highly desired in transportation facilities (Cameron, 1999; Ralph, 1999). This compatibility with mobile applications is confirmed by the utilization of hydrogen PEM fuel cell stacks in the majority of the fuel cell demonstration vehicles. Apart from mobile applications, their use in small-scale stationary combined heat and power (CHP) facilities and portable/leisure market are also considered (Ralph and Hards, 1998). The low tolerance against impurities such as sulphur and carbon monoxide (required to be less than 10 ppm) within the fuel is the major disadvantage of PEM fuel cells (Jost, 1997; Gray and Petch; 2000). Their modular structure allow PEMFCs to give diverse power outputs ranging from 25 W to 500 kW.

A special version of PEM fuel cells operating with methanol – Direct Methanol Fuel Cell (DMFC) – offers a less expensive fuel cell technology since it eliminates the requirement of hydrogen generation step. However, the slow electrochemical kinetics, formation of products that deactivate the catalyst and the existence of membrane problems associated with methanol cross-over from anode to cathode lead to much lower power densities and reduced efficiencies, making DMFCs unsuitable for use in mobile applications (Dicks, 1996; Hoogers and Thompsett, 1999). An extensive review of the DMFCs has been made by Urban and coworkers (2001).

PAFCs, the second type of low temperature fuel cells, operate at temperatures between 453 K-483 K and employ widely available phosphoric acid electrolytes. They operate on reformed natural gas, and have a slightly higher tolerance level (ca. one per cent) to carbon monoxide. PAFCs are the most commercially developed type of fuel cells and are being utilized in stationary combined heat and power applications, including hospitals, schools and utility power plants giving power outputs of ca. 200 kW (Cameron, 1999). However, their use in transportation is unlikely since they require a warm-up period before electrical energy is generated.

Alkaline fuel cells operate either at 333 K-393 K or at around 523 K depending on the concentration of the aqueous potassium hydroxide electrolyte, which can be either 35-

50 per cent or 85 per cent by weight, respectively. They can be built from relatively inexpensive components, but their low tolerance for carbon dioxide contamination requires both pure hydrogen and oxygen supplies, making them unsuitable to be employed in mobile applications. However, they are one of the most developed classes of fuel cells, since they are being utilized in space applications through the NASA space program (Ralph and Hards, 1998).

2.1.2.2. High Temperature Fuel Cells. The two major types of high temperature fuel cells are Molten Carbonate Fuel Cells (MCFC) and Solid Oxide Fuel Cells (SOFC). They have common features of operating at higher efficiencies than their low temperature counterparts in terms of electrical energy generation and of providing waste heat due to high temperatures involved, making them suitable to use in stationary cogeneration facilities rather than in vehicular applications.

MCFCs operate at high temperatures between 903 K-973 K, at which hydrocarbon fuels such as natural gas can be reformed internally. The corrosive nature and volatility of the lithium/potassium carbonate electrolyte, alkali poisoning during internal reforming and material problems encountered at high temperatures are the major disadvantages (Rostrup-Nielsen and Christiansen, 1995). However, MCFCs offer high efficiencies and are likely to be used in medium/large-scale stationary applications requiring electrical power in the range of 250 kW-2 MW (Cameron, 1999; Rastler, 2000).

Among other types of fuel cells, SOFCs involve the highest range of operating temperatures (ca. 1023 K-1273 K), which allows internal reforming of hydrocarbon fuels, particularly natural gas, into hydrogen-rich streams and therefore eliminates the requirement of an external fuel conversion unit (Cameron, 1999; Hart, 1998). The electrolyte is ceramic-based (zirconium and yttrium oxides), eliminating liquid electrolyte-based corrosion problems and has good tolerance against impurities within the fuel (Hart, 1998). It can be used for generating power ranging from 1 kW to several MW, but it is expected to be involved particularly in large-scale, MW-order power generation applications. Since they require warm-up and cool-down periods, they are unlikely to be used in transportation. However, their use as auxiliary power units in vehicles is being investigated (Hart, 1998).

Table 2.1 summarizes the types, features and applications of the fuel cells considered in this section.

Table 2.1. Features of different types of fuel cells

	PEMFC	AFC	PAFC	MCFC	SOFC
Operating temperature (K)	333-363	333-393 or ~523	453-483	903-973	1023-1273
Current density	High	High	Moderate	Moderate	High
Cathode /anode catalysts	Pt/Pt	Pt or Au/Pt	Pt/Pt	Ni/Ni	St-La manganite /Ni
Likely applications	Transportation, small-scale CHP, portable/leisure	Military and space	Small-scale CHP	Stationary power	Stationary power
Major advantages	Low temperature, quick start-up, solid electrolyte reduces corrosion	High performance	Can use impure hydrogen	Fuel flexibility	Fuel flexibility, solid electrolyte reduces corrosion
Major disadvantages	Low tolerance against impurities	Expensive removal of CO_2 from fuel and air	Low current & power, large size & weight	Corrosion & material problems at high T	Material problems at high T

2.1.3. Challenges in PEM Fuel Cell Operation

Although it has clear environmental and efficiency benefits, the fuel cell operation is challenging due to various cost-based and technology-based difficulties. Most of the fuel cells are currently manufactured using expensive techniques and materials. First of all, they include catalytic anode and cathode units, where platinum-based catalysts are found to satisfy the best combination of fast kinetics and required stability, particularly in the low-temperature ranges (Table 2.1). However, platinum is an expensive metal (US$ 565 per ounce of platinum vs. US$ 302 per ounce of gold) that significantly raises the cost of a fuel cell unit. In the present technology, 0.6-1.0 mg Pt per cm^2 is required to drive the anode/cathode reactions. The target is to reduce the quantity of platinum down to 0.1-0.2 mg Pt per cm^2 without any drop in operational performance, which is planned to be achieved by improving the dispersion of platinum over supports such as carbon (Ralph and Hards, 1998; Urban *et al.*, 2001). The machining and material costs associated with the flow field plates and the membrane costs are other factors that make it expensive to obtain electrical power from fuel cells. Therefore, in order to be competitive, a fuel cell in the automobile sector will have to cost between US$ 50-75 per kW versus the current cost of US$ 1000 to US$ 3000 per kW (Klaiber, 1996; Ralph, 1999). Efforts are being made to reduce these costs (Ledjeff-Hey *et al.*, 1998; Ralph and Hards, 1998), and the target figures appear to be possible to realize (Trimm and Önsan, 2001). Compared with the target cost set for the transportation facilities, the desired cost for stationary combined heat and power applications is around US$ 1500 per kW (Ralph and Hards, 1998), which seems to be within the bounds of current stack costs. This situation can be verified by the fact that stationary fuel cells have started to penetrate commercially to the market. On the other hand, although the fuel cell cars are at prototype level, they are expected to appear in the market within a period of 5-10 years (Thomas *et al.*, 2000).

In order to compete with the existing technologies, fuel cells must also meet the operational performance of the existing technologies. To illustrate, the fuel cell cars must provide the driving dynamics and robust operation at extreme conditions (eg. at temperatures between –30°C and 60°C). Therefore, besides cost issues, such performance-based problems should also be addressed (Klaiber, 1996).

Nevertheless, due to the fast improvements in related technologies, the challenges mentioned above are expected be overcome in a short term. Finding the optimal fuelling solution for driving fuel cells remains as the most important problem, since there are a vast number of possibilities. Therefore, this topic is considered separately in the next section.

2.2. Driving PEM Fuel Cells: Fuelling Issues

Due to a number of advantages mentioned previously, PEM fuel cells are considered for use in supplying both motive and stationary power. As in other types of fuel cells, PEM fuel cells use hydrogen as the fuel as well, but hydrogen purity requirement is much more strict. The use of hydrogen as a primary fuel has also introduced several technical problems associated with its storage, availability and distribution. This section reviews the different approaches and solutions that have been proposed to address hydrogen-based problems in the context of transportation applications unless otherwise specified. Off-board production + on-board storage of hydrogen and on-board conversion of readily available hydrocarbon fuels to hydrogen are the two major approaches proposed for fuelling PEM fuel cells.

2.2.1. On-board Storage of Hydrogen

It is obvious that, a true zero-emission car is only possible when fuelled with pure hydrogen (Thomas *et al.*, 2000). However, hydrogen is difficult to store on-board the vehicle since it is in the gas phase under ambient conditions. Several storage techniques such as using pressurized cylinders, metal hydrides, cryogenic methods and carbon nanotubes are proposed. These techniques are reviewed below.

2.2.1.1. Gaseous Hydrogen. This method is known to be the most traditional one and involves the storage of hydrogen gas in pressurized cylinders. Storage pressures between 175 atm and 345 atm have been reported (Browning *et al.*, 1997; Thomas *et al.*, 2000). Heavier vehicles such as buses are designed to employ hydrogen gas cylinders placed on their roofs, a solution which is reported to be promising (Hoogers and Thompsett, 1999; Ralph and Hards, 1998; Raman, 1997). Therefore, the use of zero-emission bus fleets is in the phase of commercialization. However, pressurized vessels are usually heavy and

occupy significant space, lead to pronounced weight and volume penalties and hence are unlikely to be used in passenger vehicles (Jamal and Wyszynski, 1994).

2.2.1.2. Liquid Hydrogen. This method involves storing hydrogen under cryogenic conditions, i.e. in the liquid phase, and offers advantages in terms of volume and weight. However, the low boiling point of hydrogen (20 K at 1 bar) requires storage in extremely well insulated containers to minimize loss due to vaporization (Browning *et al.*, 1997). In addition, liquefaction is an expensive and energy demanding process. Therefore, this route seems far from being practical for vehicular hydrogen storage, although it is under consideration by car manufacturers such as BMW (Raman, 1997).

2.2.1.3. Metal Hydrides. In this method, hydrogen is chemisorbed reversibly at a lower temperature on a metal or alloy as a metal hydride, and released by heating it to a higher temperature (Jamal and Wyszynski, 1994). Nickel-metal hydrides are considered in detail, and use of FeTi based and $LaNi_5$ based alloys are being investigated.

Although their use is considered in several prototype cars (Ralph and Hards, 1998), metal hydrides are expensive and possess very low energy density. In other words, they do not achieve better than two per cent hydrogen stored by weight at ambient conditions. However they are promising in terms of volume occupied. Finally, the necessity of using a heat exchange system to manage the hydrogen adsorption/desorption may cost extra weight and volume (Browning *et al.*, 1997).

Apart from metal hydrides above, different hydrides that involve non-reversible operation are available. These single-use hydrides, which can store higher amounts of hydrogen per unit weight, are desired in cases where smaller amounts of hydrogen are required. Examples are LiH, $LiAlH_4$, $NaBH_4$, which react with water to liberate hydrogen. Compared with their reversible counterparts, these hydrides give twice the amount of hydrogen stored, since half the hydrogen is derived from water. This option may be promising due the possibility of using waste water rejected by the fuel cell (Figure 2.1) in reacting with the hydride (Browning *et al.*, 1997).

2.2.1.4. Carbon Nanotubes. This recently emerging technology makes use of carbon nanotubes – microscopic carbon tubes synthesized in the laboratory – that absorb hydrogen. This route offers the most realistic volumetric and gravimetric figures for storing hydrogen on-board the vehicle, since it is possible to store large quantities of hydrogen between microscopic graphite fibers. Satisfactory storage is reported only at sub-ambient conditions, though research is focused on improving ambient storage performance.

Direct hydrogen storage technology together with hydrogen production from renewable sources is accepted to be the ultimate sustainable way of driving fuel cells in the long run (Dicks, 1996; Raman, 1997). However, the existing hydrogen storage technologies explained above are expensive and are far from satisfying the ideal vehicular performance, unless the last option, carbon nanotubes, is greatly improved (Ahmed and Krumpelt, 2001; Trimm and Önsan, 2001). Apart from storage-based problems, the availability and distribution of hydrogen remain as serious problems against the commercialization of fuel cell driven vehicles (Brown, 2001; Trimm and Önsan, 2001). This situation has led to the consideration of compact, efficient devices called fuel processors that can convert the readily available liquid hydrocarbon fuels into hydrogen on board the vehicle (Golunski, 1998; Hoogers and Thompsett, 1999; Jenkins and Shutt, 1989; Jiang *et al.*, 1995; Ralph and Hards, 1998; Vielstich and Iwasita, 1997). Fuels and processes that are proposed for use in fuel processor technology are reviewed in the following section.

2.2.2. On-board Fuel Conversion

2.2.2.1. Processes. The conversion of hydrocarbon fuels to hydrogen can carried out by several processes such as thermal cracking, steam reforming, carbon dioxide reforming, partial oxidation, autothermal reforming (Dicks, 1996):

$$CH_4 = C + 2H_2, \quad \Delta H^{\circ}_{298} = 74.8\,kJ\,mol^{-1} \tag{2.1}$$

$$CH_4 + H_2O = CO + 3H_2, \quad \Delta H^{\circ}_{298} = 206.2\,kJ\,mol^{-1} \tag{2.2}$$

$$CH_4 + CO_2 = 2CO + 2H_2, \quad \Delta H^{\circ}_{298} = 247.0\,kJ\,mol^{-1} \tag{2.3}$$

$$CH_4 + \tfrac{1}{2}O_2 = CO + 2H_2, \quad \Delta H^{\circ}_{298} = -35.7\,kJ\,mol^{-1} \tag{2.4}$$

It is possible to increase hydrogen production and lower carbon monoxide production in steam reforming (Reaction (2.2)), carbon dioxide reforming (Reaction (2.3)) and partial oxidation (Reaction (2.4)) via the water-gas shift reaction:

$$CO + H_2O = CO_2 + H_2, \quad \Delta H^{\circ}_{298} = -41.2\,kJ\,mol^{-1} \tag{2.5}$$

Direct decomposition of methane described in Reaction (2.1) has several penalties in terms of heat requirement and carbon formation. Although carbon monoxide is not produced, thermal cracking is not considered to be a promising way of conducting on-board fuel conversion. Several groups are interested in direct cracking of methane (Ferreira-Aparicio *et al.*, 1997; Zhang and Amiridis, 1998) and propane (Ledjeff-Hey *et al.*, 1998; Ledjeff-Hey *et al.*, 2000).

Steam reforming run on Ni-based catalysts is the cheapest and the most well-known route in large-scale hydrogen production (Aasberg-Petersen, *et al.*, 2001; Dicks, 1996; Rostrup-Nielsen, 1984; Rostrup-Nielsen and Alstrup, 1999). It is the process that gives the highest quantities of hydrogen (ca. 70-80 per cent of hydrogen in the product stream) (Brown, 2001). On the other hand, considerable heat input, higher catalyst loadings and larger reactors are required to drive the process, which make steam reforming unlikely to be used in mobile applications. However, the energy requirement can be met by oxidizing part of the fuel to supply heat into the system (Jenkins and Shutt, 1989; Jiang *et al.*, 1995; Golunski, 1998):

$$CH_4 + 2O_2 = CO_2 + 2H_2O, \quad \Delta H^{\circ}_{298} = -802.3\,kJ\,mol^{-1} \tag{2.6}$$

The combination of total oxidation (Reaction (2.6)), steam reforming and water-gas shift reaction is called indirect partial oxidation (Avcı *et al.*, 2001a; Avcı *et al.*, 2002; Avcı *et al.*, 2003; Trimm and Önsan, 2001). The strong exothermicity of total oxidation can

supply sufficient heat into the system. Since the water produced is insufficient to drive the steam reforming and water-gas shift, further water injection is necessary. Extra water is also required for suppressing coke formation which is likely to occur at steam reforming conditions (Pena *et al.*, 1996; Rostrup-Nielsen, 1984), and for temperature control (Avcı *et al.*, 2000; Avcı *et al.*, 2001a,b). It is worth noting that when water is fed together with the fuel and air, the process is also named as autothermal reforming (ATR) (Ahmed and Krumpelt, 2001; Dicks, 1996; Pena *et al.*, 1996).

Carbon dioxide produced by the water-gas shift may lead to carbon dioxide reforming of the fuel (Reaction (2.3)). However, this reaction is much slower than steam reforming in the presence of steam (Trimm and Önsan, 2001) and reported to be insignificant compared to Reaction (2.2).

Another possible route for hydrogen production is direct partial oxidation (dry oxidation), which is represented by Reaction (2.4). It is reported that this reaction runs at temperatures as high as 1373 K and at residence times as low as 10^{-4} - 10^{-2} s (Hickman and Schmidt, 1992), at which it is thermodynamically favored (Pena *et al.*, 1996). The flow rates and reactor/catalyst configurations affect product distribution, indicating the dominance of mass and heat transfer resistances over kinetics (Hickman and Schmidt, 1992; Hohn and Schmidt, 2001). The operating conditions mentioned above do not allow steam reforming, water-gas shift and carbon formation mechanisms, which require much higher residence times to run.

Mobile fuel cell applications require the fuel processors to be compact in size and to be able to respond fast in transient periods (Ahmed and Krumpelt, 2001). Thus, the partial oxidation/autothermal reforming routes explained above are accepted to be the most promising routes to address vehicular requirements (Ahmed and Krumpelt, 2001; Brown, 2001; Golunski, 1998; Moon *et al.*, 2001; Rampe, 2000), though direct hydrogen storage (Thomas *et al.*, 2000) and steam reforming (Emonts *et al.*, 1998; Emonts *et al.*, 2000; Ioannides, 2001) are also investigated. Apart from fuel cell applications, integration of the fuel processors and spark ignition engines are being considered (Jamal and Wyszynski, 1994; Isherwood *et al.*, 1998; Kirwan *et al.*, 1999). This combination is found to give much

lower vehicular emissions than those obtained in existing technologies, but still higher than the proposed fuel cell vehicle emissions.

2.2.2.2. Fuels. A number of fuels such as natural gas, LPG, gasoline, methanol and ethanol are considered for their conversion into hydrogen via processes explained above. Among these fuels, methanol and gasoline attract special interest, since they can be stored in liquid form which is highly desired in vehicles (Jost, 1997; Thomas *et al.*, 2000; Urban *et al.*, 2001). Another liquid fuel, diesel, deposits coke too easily and is not suitable for on-board conversion (Jamal and Wyszynski, 1994).

In addition to being a liquid fuel at ambient conditions, methanol is also considered for its easier reformation into a hydrogen rich stream, requiring temperatures less than 600 K (Emonts *et al.*, 1998; Emonts *et al.*, 2000; Geissler *et al.*, 2001; Jiang *et al.*, 1995; Ledjeff-Hey *et al.*, 1998; Urban *et al.*, 2001):

$$CH_3OH + H_2O = CO_2 + 3H_2, \quad \Delta H^{\circ}_{298} = 49.6\,kJ\,mol^{-1} \tag{2.7}$$

Methanol has advantages in terms of low impurities in the product stream after reforming. It is a synthetic fuel, and hence sulphur can be removed during methanol synthesis in the refinery (Brown, 2001). In contrast with the reformation of other fuels, carbon monoxide is not a major product, and its lower amounts may only come from the decomposition of methanol:

$$CH_3OH = CO + 2H_2, \quad \Delta H^{\circ}_{298} = 90.7\,kJ\,mol^{-1} \tag{2.8}$$

However, there are serious problems associated with the use of methanol. It is produced from synthesis gas – a mixture of carbon monoxide and hydrogen – which is obtained by steam reforming of natural gas. Current methanol production is estimated to meet the requirement of a maximum of one and a half million fuel cell cars, requiring extra synthesis plants in case of a greater demand (Thomas *et al.*, 2000). Apart from availability problems, methanol does not have a widespread distribution network (Brown, 2001), unless the existing gasoline infrastructure is technically upgraded to handle methanol,

which requires considerable investment. The most important problem is that methanol is a highly toxic commodity (Brown, 2001) which may result in death in case of inhalation of even a minute quantity.

Gasoline is considered to be the major opponent of methanol for use in mobile applications. It has clear advantages of being already available and of having a widespread refueling infrastructure. It is directly obtained by refining crude oil, without requiring an extra synthesis step as in the case of methanol. However gasoline is a complex fuel and includes a number of aromatics, which may lead to coke formation easily at the reforming conditions represented by temperatures as high as 1100 K (Rostrup-Nielsen, 1984). In addition, the higher amounts of sulphur within gasoline may interfere with the catalytic operations by deactivating the catalysts. It is proposed that the sulphur content should be decreased below 30 ppm to end up with fuel cell grade gasoline (Thomas *et al.*, 2000; Urban *et al.*, 2001). Nevertheless, the advantage of being the standard fuel outweighs the difficulties associated with its on-board conversion (Moon *et al.*, 2001).

Apart from methanol and gasoline, liquefied petroleum gas (LPG) is another fuel that can be stored in liquid form in pressurized vessels. LPG is obtained in crude oil processing as a byproduct and is a mixture of propane and n-butane, whose relative amounts depend on the region from which the oil is obtained. It is an available and cheap fuel with high energy density and relatively low sulphur content. The use of LPG in portable and in small-scale stationary fuel cell applications is of interest, but it can also be employed as a transportation fuel (Ahmed and Krumpelt, 2001; Ledjeff-Hey *et al.*, 1998; Ledjeff-Hey *et al.*, 2000).

Ethanol differs from the above fuels in the sense that it is classified as a renewable source, since it can be produced from any starch or sugar source such as corn and sugar cane via fermentation. It is currently used as an additive to gasoline in order to decrease emissions from internal combustion engines. Although not as much as methanol and gasoline, ethanol offers a potential, particularly in regions where it is produced, as an on-board fuel to be reformed. Ethanol steam reforming is investigated to a certain extent, but data about its partial oxidation are scarce (Ioannides, 2001).

Natural gas accounts for almost half the world's feedstock for hydrogen and has the lowest greenhouse emissions in terms of carbon dioxide (Armor, 1999). The major component of natural gas is methane, varying between 75 and 85 per cent, with the remainder being composed of higher alkanes (e.g. ethane and propane) and of traces of carbon dioxide (Chan and Wang, 2000; Dicks, 1996). Thus the number of hydrogen atoms per carbon atom is close to 4:1, which makes natural gas cleaner than other higher hydrocarbon fuels (Raman, 1997). Like LPG it is a very regionally dependent feedstock, since methane content can vary between 44.2 per cent and 92.6 per cent (Tindall and King, 1994).

Besides its environmental benefits, the availability of natural gas is considerable: it is available either through widespread pipeline networks in the form of gas or can be shipped in the form of liquefied natural gas (LNG) (Dicks, 1996). In addition, natural gas is more abundant than petroleum with proven and estimated reserves that are expected to supply feedstock for hydrogen production for several decades (Klaiber, 1996; Raman, 1997).

Nevertheless, the attractive features of natural gas are not sufficient to make it a candidate for being an on-board reformate. Firstly, it is in gaseous form at ambient conditions and requires heavy and bulky pressurized cylinders for on-board storage. In addition, methane is a very stable molecule and considerable energy input is required to trigger its conversion. Once it is started, it still requires high temperatures, because of the sluggish steam reforming kinetics (Rostrup-Nielsen, 1984). Therefore, natural gas is unlikely to be a suitable fuel for on-board conversion. However, off-board processing of natural gas at refueling stations to produce hydrogen on-site is thought to be a very promising solution for the distribution of hydrogen (Thomas *et al.*, 2000). In addition, this route allows the removal of carbon dioxide, which can then be compressed and sequestered into a depleted natural gas field. This method proposed for carbon dioxide removal is estimated to be only seven per cent more expensive than the case in which the gas is vented (Blok *et al.*, 1997). Therefore, off-board processing is likely to be significant if direct hydrogen storage techniques are within the commercial bounds. It is also worth noting that, natural gas is considered to be the ultimate fuel for processing in small to large-scale stationary applications (Dicks, 1996).

Apart from hydrogen generation, synthetic fuels (methanol, diesel, gasoline) can also be produced indirectly from natural gas. The process involves synthesis gas ($CO + H_2$) production from natural gas via well-established steam reforming technology and the conversion of the product gas to higher hydrocarbons, i.e. synthetic fuels via Fischer-Tropsch synthesis. This route is expected to have a pronounced importance in future when the petroleum reserves become scarce (Aasberg-Petersen *et al.*, 2001; Rostrup-Nielsen, 2000)

There are a number of fuels and fuel conversion routes available with several advantages and disadvantages. This situation increases the number of combinations that can be used for on-board fuel processing. Table 2.2 (Moon *et al.*, 2001) presents the existence of diverse fuel/fuel processing combinations, indicating the absence of a unique solution. One objective of this research is to compare various fuel/fuel processing combinations to extract some 'working' solutions for different cases.

Table 2.2. Commercial fuel/fuel processing combinations exercised

Corporation	Fuel selection		Fuel processing method	
	Methanol	Gasoline	Steam reforming	Partial oxidation
A. D. Little	Second	First		√
General Motors	First	Second	√	
Honda	Sole		√	
Hydrogen Burner Tech		Sole		√
International Fuel Cells	First	Second	√	√
Johnson-Matthey	First	Second	√	√
Mitsubishi	Sole		√	
Nissan	Sole		√	
Toyota	Sole		√	
Wellman	Second	First		√

2.2.2.3. CO Removal Techniques. The conversion of hydrocarbon fuels produces hydrogen-rich gas stream in which carbon monoxide exists as a byproduct. Usually the amount of carbon monoxide (ca. two-three mole per cent (Avcı *et al.*, 2001a)) is extremely higher than the limit (ca. 10 ppm (Urban *et al.*, 2001)), below which PEM fuel cells can safely operate. Therefore, several catalytic techniques should be employed for removing the carbon monoxide before the hydrogen-rich stream reaches the fuel cell.

As mentioned in the previous section, majority of the carbon monoxide can be removed by the water-gas shift reaction (Reaction (2.5)). This reaction is usually carried out in two modes – high temperature (623 K-673 K) water-gas shift over mixtures of Fe/Cr oxides and low temperature (453 K-523 K) water-gas shift over mixtures of Cu/Zn oxides (Amadeo and Laborde, 1995; Urban *et al.*, 2001). Therefore, separate high and/or low temperature shift converters are placed at the downstream of the fuel processor to remove carbon monoxide. It is worth noting that Reaction (2.5) running simultaneously with steam reforming is found to be effective in removing carbon monoxide during fuel conversion, particularly in cases where external water is injected (Avcı *et al.*, 2001a; Avcı *et al.*, 2002; Avcı *et al.*, 2003). However, sufficient carbon monoxide elimination cannot be achieved during shift conversion and other special techniques are necessary. These techniques should also operate effectively at low temperatures, since the PEM fuel cell operates at a temperature range of 333 K-363 K.

Several methods such as selective oxidation of CO to CO_2, methanation of CO and the use of hydrogen diffusion membranes are proposed to meet the above-mentioned criteria (Golunski, 1998; Trimm and Önsan, 2001). During methanation, significant amounts CO_2 may be converted along with CO, resulting in considerable H_2 loss. The method of using Pd-based diffusion membranes requires high-pressure differentials and high temperatures both of which can significantly reduce the overall efficiency. All these factors make the selective oxidation method the optimal choice for CO removal. Feeding oxygen into the shift reactor to combine water-gas shift and CO oxidation is also considered (Utaka *et al.*, 2000).

Trimm and Önsan (2001) have reviewed selective low temperature CO oxidation in hydrogen-rich streams. It is generally believed that a precious metal based catalyst such as Pt can exhibit optimal performance in terms of selectively removing carbon monoxide.

2.2.3. Efficiency of Fuel Cell Operation

As mentioned previously, fuel cells can convert chemical energy into electrical energy in a single step whereas in internal combustion engines, chemical energy is first converted into heat via combustion, followed by conversion into mechanical energy in pistons. Electricity is then produced using a generator (Gray and Petch, 2000). Therefore, as energy conversion devices, fuel cells are much more efficient than existing technologies which lose more than 80 per cent of the chemical energy mostly as waste heat. Theoretical efficiencies reported for internal combustion gasoline and diesel engines, and a hydrogen fuel cell are 40, 50 and 80 per cent, respectively.

Comparison of the efficiencies of the energy conversion units only will not be a realistic approach, and the processes that are used to deliver the fuel to the vehicle must also be taken into account. To illustrate, obtaining electrical power using pure hydrogen in a vehicle involves the production of the gas via steam reforming and related upstream/downstream processes, its distribution, its storage via techniques such as compression or liquefaction and its use in the fuel cell, all of which lead to losses in energy and efficiency. Therefore, the overall efficiencies or well-to-wheel efficiencies must be considered for a much realistic system analysis. Figure 2.3 presents a detailed energy loss analysis for a number of energy conversion systems.

Even though considerable energy is lost in the steps related with the handling and processing of the fuel (Figure 2.3), fuel cell efficiencies still remain to be higher than those obtained from existing internal combustion engines. Fuel cell based routes have efficiencies between 20 and 24 per cent, with the highest and lowest values estimated for on-board gasoline processing/fuel cell and on-board methanol processing/fuel cell combinations, respectively. Direct hydrogen storage is estimated to end up with an overall efficiency of 22 per cent. The conventional gasoline ICEs have efficiencies around 14 per cent while the diesel ICE can operate at values as high as 22-23 per cent.

Fuel processors and fuel cells can operate at high efficiencies if the variations in power load are minimum. In the cases of peak power requirements in vehicular operation, hybrid-electric drivetrains can be coupled with the fuel processor/fuel cell operation to handle transients and hence minimize efficiency losses. It is reported that the benefits of hybrid systems may increase the operating efficiencies of by ca. three per cent (Thomas *et al.*, 2000). This increase of efficiency is also valid in the case of hybrid electric-ICE combinations.

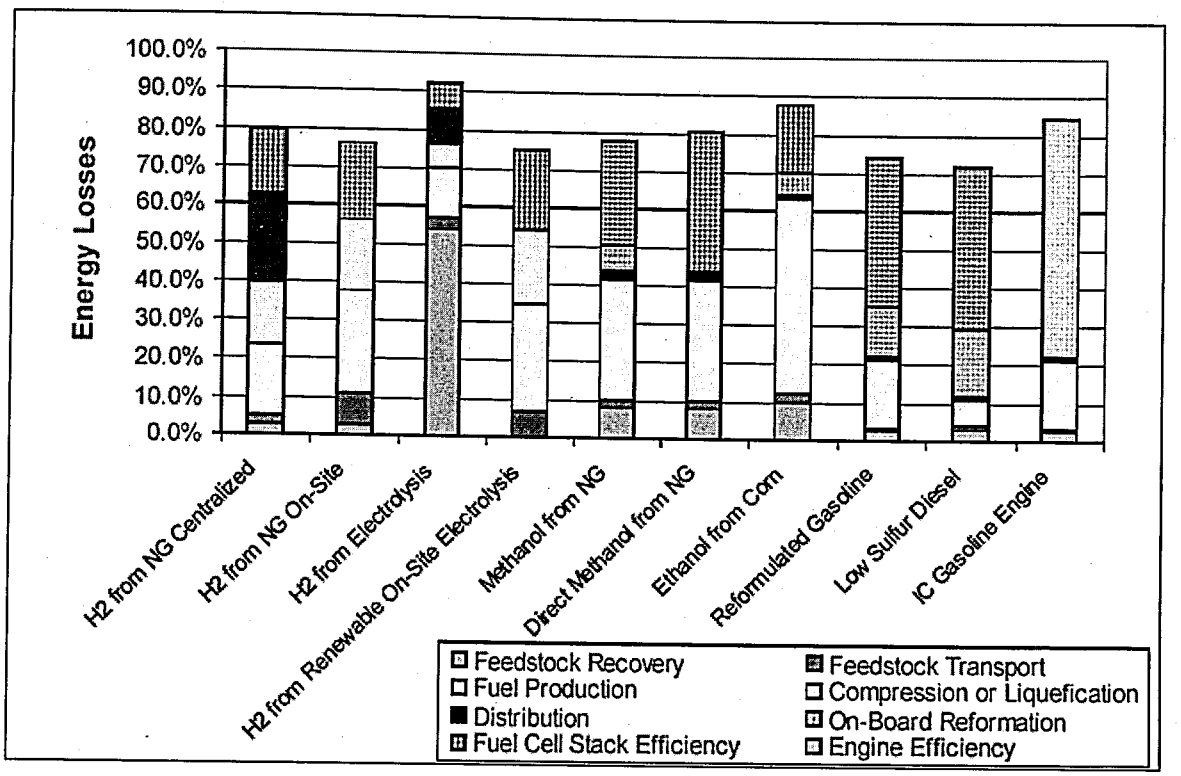

Figure 2.3. Well-to wheel energy losses for fuel cell vehicles using different fuelling routes and for an internal combustion engine (adapted from NAVC (2000))

It seems that the present vehicular fuel cell technology cannot offer significant efficiency increases over the ICE/hybrid electric ICE systems. However, the elimination of hazardous emissions such as nitrogen oxides, sulphur oxides, carbon monoxide and volatile organic compounds and reduction in greenhouse gas, i.e. carbon dioxide emissions make the use of fuel cells the only viable option for obtaining clean motive power.

2.3. Total Oxidation: The Heat Generation Step

Catalytic combustion/oxidation of hydrocarbons receives considerable attention in many basic and applied catalytic research facilities, since it has a vast range of applications. Removal of volatile organic compounds resulting from operations such as polymer processing, coating operations, domestic and other heating systems, industrial boilers, gas turbines, elimination of vehicular hydrocarbon, carbon monoxide and nitrogen oxide emissions and odor control are areas which involve catalytic combustion in lean-to-stoichiometric fuel regimes (Aryafar and Zaera, 1997; Lee *et al.*, 1999; Veser and Schmidt, 1996). In addition, catalytic partial oxidation under fuel-rich conditions is the basis for the production of many important chemicals (Trimm, 1983). In these applications, the use of catalysts serves basically for reducing the high reaction temperatures leading to the formation of nitrogen oxides, and for catalyzing the production of desired products within a complex reaction network (e.g. partial oxidation applications).

Hydrogen supply for fuel cells is usually achieved by steam reforming of a hydrocarbon fuel. This reaction needs high temperatures, hence some means of heat input to the reaction system. Electric heating using batteries is a possible method, but costs for a significant reduction in overall efficiency. Therefore, total oxidation of part of the fuel is a widely accepted route to generate the desired reaction heat (Trimm and Önsan, 2001):

$$CH_4 + 2O_2 = CO_2 + 2H_2O, \quad \Delta H^{o}_{298} = -802.3\,\mathrm{kJ\,mol^{-1}} \tag{2.6}$$

Once triggered, combination of total oxidation and steam reforming – indirect partial oxidation – is a thermally self-sustaining process. However, total oxidation of hydrocarbons does not occur at ambient conditions and requires higher temperatures. It is reported that hydrogen and methanol can be oxidized at room temperature over a precious metal catalyst like Pt and, therefore, can be used for triggering the partial oxidation (Jiang, 1992; Jiang *et al.*, 1995; Ma *et al.*, 1996).

Catalytic oxidation of methanol over supported Pt and Cu catalysts within the context of fuel processor/fuel cell operation was investigated (Jiang, 1992; Jiang *et al.*, 1995). It was found that the reduced forms of both catalysts oxidized methanol at room

temperature, whereas catalytic activity was observed at ca. 473 K when the catalysts were in their oxidic state. In contrast with Cu, Pt was observed to be hard to reoxidize, therefore could be used repeatedly without requiring further reduction. It was mentioned that, supported Pt catalysts were effective in facilitating methanol oxidation, and Pt loading did not affect catalytic activity. On the other hand, copper-based catalysts are usually employed in catalyzing steam reforming of methanol, which will be explained in the next section (Jiang *et al.*, 1995).

The catalytic oxidation of hydrogen over supported catalysts has also been investigated. It was found that hydrogen-rich mixtures (H_2:O_2 = 3.7:1) could be oxidized at room temperatures over a Pt/δ-Al_2O_3 catalyst with a metal content as low as 0.2 per cent by weight (Ma, 1995; Ma *et al.*, 1996). Ruth and coworkers (2000) have also reported a similar oxidation performance over a Au/TiO_2 catalyst. They also mentioned that hydrogen oxidation was mainly a surface catalyzed reaction and metal-support interactions were relatively insignificant.

Carbon monoxide oxidation in streams excluding/including hydrogen is considered for use in gas clean-up facilities such as gas filters and life rescue devices (Akın *et al.*, 2001) and in fuel cell applications (Korotkikh and Farrauto, 2000). The use of Pt and Au-based catalysts are usually proposed to achieve CO removal at temperatures as low as ambient (Ruth *et al.*, 2000). An excellent review covering low-temperature CO oxidation in detail is provided by Trimm and Önsan (2001).

2.3.1. Total Oxidation of Methane

In contrast with methanol and hydrogen, methane and other saturated hydrocarbons are oxidized at higher temperatures, preferably over precious metal catalysts. Methane is the most stable, and hence the least reactive hydrocarbon, and its catalytic oxidation has received considerable interest. It is generally accepted that Pd-based catalyst are the best to achieve methane oxidation in terms of obtaining lowest light-off temperatures (Aryafar and Zaera, 1997; Burch *et al.*, 1999; Ciuparu and Pfefferle, 2001; Lee *et al.*, 1999; Maillet *et al.*, 1997; Widjaja *et al.*, 1999), whereas Pt-based (Ma *et al.*, 1996; Trimm and Lam, 1980; Veser and Schmidt, 1996; Veser *et al.*, 1999) and Rh-based (Burch *et al.*, 1999) catalysts

are also considered for methane oxidation. Light-off temperature is defined as the value at which 10 per cent of the oxidation conversion of the hydrocarbon is obtained, and is used to indicate the oxidation activity of a specific catalyst. On the basis of their activities in methane oxidation, precious metals can be classified in the order of Pd>Pt>Rh (Aryafar and Zaera, 1997; Burch *et al.*, 1999).

The higher activity of Pd can be based on the high stability of its oxides: Burch and coworkers (1999) have proposed that the almost non-polar C-H bonds in methane could easily be activated by $Pd^{2+}O^{2-}$ ions at the surface of stable PdO by a heterolytic mechanism. In contrast with Pd, the oxides of Pt are unstable, and the proposed mechanism is unlikely to occur. They have also shown that the rate determining step for methane combustion on Pd catalysts could be the release of water from surface-OH groups rather than the initial C-H bond breaking step due to the relative stability of Pd(OH). The decomposition of the Pd oxides was found to trigger the deactivation of the Pd catalyst (Maillet *et al.*, 1997), which is another verification of the oxidic state of Pd.

2.3.2. Total Oxidation of Higher Hydrocarbons

Unlike methane oxidation, the use Pt-based catalysts gives lower light-off temperatures in the oxidation higher alkanes such as ethane, propane and butane. It is reported that, in ethane oxidation the light-off temperatures followed an order of Pt<Pd<Rh<Ir, with Pt and Pd being active at temperatures ca. 100-200°C less than Rh and Ir. Wider surface flammability limits were obtained with Pd foils allowing oxidation at very fuel-lean conditions, but coke deposition was reported at the fuel-rich conditions. No coke formation was detected within the flammability range of Pt (Veser and Schmidt, 1996; Veser *et al.*, 1999). Wu and coworkers (2001) have also reported light-off temperatures of 538 K and 623 K for propane oxidation over $Pt/\gamma\text{-}Al_2O_3$ and $Pd/\gamma\text{-}Al_2O_3$, respectively.

It is widely accepted that the site competition between the hydrocarbon and oxygen dictates the ignition characteristics of the fuel-oxygen-catalyst system, particularly those of higher alkanes (Burch *et al.*, 1999; Ma *et al.*, 1996; Veser *et al.*, 1999; Wu *et al.*, 2001). This situation can be explained by the fact that the light-off temperatures were found to

decrease with increased fuel-to-oxygen ratios: the more the oxygen was present in the feed, the more it occupied the catalyst surface, since the sticking probability of the oxygen was higher than those of alkanes. Veser and Schmidt (1996) have confirmed this situation using the metal-oxygen bond energies. The metals which had lower metal-oxygen bond energies facilitated the adsorption of hydrocarbons, hence surface ignition. In fact these bond energies followed an order of Pt<Pd<Rh<Ir, which was the same as the order of light-off temperatures. These results (a) explain that the oxide phase of the catalysts is not active for oxidation, and Pt, having the highest metallic stability, is the most active metal in the oxidation of higher alkanes and (b) indicate that surface competition is less significant in the case of methane oxidation.

Olefins have surface ignition characteristics that are different from those of paraffins. Olefin ignition temperatures increase at elevated fuel-to-oxygen ratios, since the sticking coefficients of alkenes are higher than that of oxygen and those of alkanes. Therefore, decreased amounts of alkenes in the feed facilitate oxygen adsorption for site competition, resulting in lower light-off temperatures (Burch *et al.*, 1999; Wu *et al.*, 2001). In addition, higher reactivity of olefins lead to the rapid C-C bond scission, which may result in the formation of carbonaceous deposits and, hence, poisoning of the catalyst surface (Veser and Schmidt, 1996).

Besides precious metals, Ni and Cu were also considered for hydrocarbon oxidation. Ma and coworkers (1996) have studied the oxidation of methane, ethane and propane over Pt/δ-Al_2O_3 and Ni/MgO-Al_2O_3 catalysts. They found that Pt was more active than Ni, resulting in lower light-off temperatures (Table 2.3). The results reported by Aryafar and Zaera (1997) also indicated that the catalytic activity for higher paraffins followed the order of Pt>Pd>Ni. However, they found Ni to be the best for methane oxidation, which is surprising. Neyestanaki and coworkers (1995) have compared Pt and Cu supported on ZSM-5 zeolites. Pt and Cu had resulted in light-off temperatures of 521 K and 611 K, respectively, though metal contents were 0.27 per cent and 3.60 per cent by weight. Methane oxidation on copper oxide-based catalyst has also been invetigated and light-off temperatures such as 803 K have been reported (Artizzu *et al.*, 1999).

The reactivity of paraffins increase with the chain length, and to a lesser extent with branching. This increase is much more significant within C_1-C_4 paraffins, however further improvement is negligible with alkanes higher than butane. In fact, the activation energies were found to decrease with chain length on Pt, Pd and Ni (Aryafar and Zaera, 1997). The effect of chain length can also be seen in Table 2.3.

Table 2.3. Light-off temperatures of the oxidation of C_1-C_3 alkanes over Pt and Ni-based catalysts (Ma *et al.*, 1996)

	Pt/δ-Al_2O_3		Ni/MgO-Al_2O_3	
Hydrocarbon (HC)	HC/O_2 (mol/mol)	Temperature (K)	HC/O_2 (mol/mol)	Temperature (K)
Methane	5.04	589	5.01	637
Ethane	0.89	515	0.85	588
Propane	0.48	485	0.48	583

2.3.3. The Effect of Catalyst Supports on Total Oxidation

The catalytic activity depends not only on the metal but also on the support. It has been found that Pt/SiO_2-Al_2O_3 catalyst was more active than Pt/ZrO_2 in catalyzing propane oxidation (Yazawa *et al.*, 2001). Similarly, propane oxidation over Pt/ZrO_2 and Pt/γ-Al_2O_3 catalysts gave light-off temperatures of 528 K and 538 K, respectively (Wu *et al.*, 2001). The difference in the catalytic activities can be attributed to the degree of acidity of the supports. Perhaps this phenomenon is best described by Wu and coworkers (2001), who have treated ZrO_2 and Al_2O_3 supports with NaOH and H_2SO_4. They found that base addition retards propane oxidation due to the increase in the electron density on the Pt surface, which prevents alkane adsorption and reduces site competition. However, acid addition leads to an opposite effect: reduction in the electron density facilitates propane adsorption and increases the rate of oxidation. This explanation confirms the differences between the catalytic activites reported (Yazawa *et al.*, 2001; Wu *et al.*, 2001), since the acidity decreases with the order of SiO_2-Al_2O_3>ZrO_2>γ-Al_2O_3.

The opposite behaviors of olefins and Pd catalyst in oxidation can also be explained by the support effect. It is reported that propylene oxidation over Pt/ZrO_2 and $Pt/\gamma\text{-}Al_2O_3$ catalysts gave light-off temperatures of 518 K and 493 K, respectively, and the acid/base addition gave the opposite effect. In addition, $Pd/\gamma\text{-}Al_2O_3$ (623 K) was found to be better than Pd/ZrO_2 (673 K) in catalyzing propane oxidation (Wu *et al.*, 2001). The latter result indicated that oxidation on Pd possibly involved a mechanism different from site competition between adsorbed hydrocarbon and adsorbed oxygen.

The importance of the support and metal-support interactions was also demonstrated by the treatment of Pt/Al_2O_3 and of Pt/SiO_2 catalysts using SO_2 (Burch *et al.*, 1999; Ruth *et al.*, 2000). SO_2 addition significantly improved the propane oxidation activity of Pt/Al_2O_3 (463 K/553 K with/without SO_2 treatment), whereas no effect was detected on Pt/SiO_2. It was proposed that SO_2 created an extra active site at the interface between the metal particle and the oxide support. The support effect has also been investigated in n-butane oxidation, and the positive effect of Mn stabilization of ZrO_2 against pure ZrO_2 has been reported (Keshavaraja and Ramaswamy, 1996).

2.3.4. Kinetics of Oxidation of Light Hydrocarbons

The kinetics of hydrocarbon oxidation is investigated in detail. In general, it is found that the reaction orders with respect to the hydrocarbon is positive, whereas negative orders are obtained for oxygen in oxidation over Pt-based catalysts (Table 2.4). However, this negative dependency with respect to oxygen is less pronounced when the hydrocarbon is present in over-stoichiometric quantites and even positive orders may be observed (Ma *et al.*, 1996). This can be explained by the poisoning of the Pt-surface by excessive amounts of hydrocarbon, though oxygen has a higher sticking probability (Veser *et al.*, 1999). However, hydrocarbon poisoning is much less significant than surface coverage of oxygen, and occurs only in the extreme portion of the fuel-rich side of the surface flammability region (Veser and Schmidt, 1996).

An interesting work related with methane oxidation over bimetallic $Pt\text{-}NiO/\delta\text{-}Al_2O_3$ was conducted by Opoku-Gyamfi and Adesina (1996). The positive and negative dependencies of methane and oxygen on the rate of methane oxidation were in agreement

with the results mentioned above, though oxygen presented a non-monotonic behaviour. The use of a bimetallic catalyst was found to introduce synergistic effects, which were proposed to come from the interaction of the two metal centers to form completely new sites. This has been verified by the fact that the activation energy calculated for the bimetallic catalyst (80.88 kJ mol^{-1}) was less than the composition weighted average of the individual activation energies of the monometallic Pt and NiO catalysts (103.56 kJ mol^{-1}).

Due to their different oxidation mechanisms (explained Section 2.3.2), the rate of oxidation of olefins over Pt increase and decrease at higher oxygen and hydrocarbon partial pressures, respectively. Reaction orders varying between one to two for oxygen and -0.6 to -1 for propylene have been reported (Wu *et al.*, 2001). For Pd-based catalysts, the dependence of the reaction rate on oxygen is much less significant. Aryafar and Zaerea (1997) have found that changes in the partial pressure of oxygen did not affect the rate of oxidation of C_1-C_4 alkanes and iso-butane over Pd foils. However, it has also been observed that propane oxidation over Pd/γ-Al_2O_3 increased as the partial pressure of oxygen is elevated (Marecot *et al.*, 1994).

The effects of oxidation products, i.e. water and carbon dioxide, on the rate have also been investigated. It is reported that steam has an inhibiting effect during oxidation over Pt-based catalyst, resulting in negative reaction orders (Marecot *et al.*, 1994). A similar trend has also been reported for ethene and propane oxidation over Pd/γ-Al_2O_3 catalyst, whereas carbon dioxide was found not to affect the reaction rate (van de Beld *et al.*, 1995). Inhibiting effect of water has also been found by Opoku-Gyamfi and Adesina (1996). Parameters of the power law rate expressions reported are presented in Table 2.4.

Mechanistic approaches for evaluating the kinetics of methane oxidation over Pt-based catalysts have also been reported. Ma and coworkers (1996) have derived a Langmuir-Hinshelwood type of rate law by considering the reaction of molecularly adsorbed hydrocarbon with the atomically adsorbed oxygen:

Trimm and Lam (1980) have also conducted a detailed study on the kinetics of methane oxidation over porous and non-porous Pt-alumina catalysts, based on the surface reaction of adsorbed methane and adsorbed oxygen or oxygen in the gas phase.

Table 2.4. Catalytic oxidation of light hydrocarbons over Pt-based catalysts

Catalyst/ support	HC	T (K)	Fuel regime	Reaction orders			E_A (kJ mol^{-1})	Reference
				HC	O_2	H_2O		
Pt/ δ-Al_2O_3	CH_4	633-733	HC rich	0.95	-0.17	-	88.5	Ma *et al.*, 1996
Pt-NiO/ δ-Al_2O_3	CH_4	773-893	HC rich	1.22	-0.38	-	80.8	Opoku-Gyamfi and Adesina, 1996
Pt/ γ-Al_2O_3	C_2H_4	453-493	O_2 rich	0.71	-	-0.12	43.2	van de Beld *et al.*, 1995
Pt/ δ-Al_2O_3	C_2H_6	473-543	HC rich	1.1	-0.6	-	80.4	Ma *et al.*, 1996
Pt/ δ-Al_2O_3	C_3H_8	423-463	HC rich	1.1	-0.6	-	104.7	Ma *et al.*, 1996
Pt/ γ-Al_2O_3	C_3H_8	553-603	O_2 rich	0.61	-	-0.46	119.3	van de Beld *et al.*, 1995
Pt/ ZrO_2	C_3H_8	473-593	HC rich	3.4	-2.9	-	215	Yazawa *et al.*, 2001
Pt/SiO_2-Al_2O_3	C_3H_8	473-523	HC rich	0.80	-0.52	-	100	Yazawa *et al.*, 2001
Pt/ ZrO_2	C_3H_8	473-593	O_2 rich	0.22	-1.0	-	215	Yazawa *et al.*, 2001
Pt/SiO_2-Al_2O_3	C_3H_8	473-523	O_2 rich	2.0	-1.5	-	100	Yazawa *et al.*, 2001

$$-r = \frac{k_o K''_A P_{CH_4} \sqrt{K''_B P_{O_2}}}{\left(1 + K''_A P_{CH_4} + \sqrt{K''_B P_{O_2}}\right)^2} \qquad (2.9)$$

2.4. Steam Reforming: The Hydrogen Generation Step

2.4.1. Description of the Process

Steam reforming is the process that produces the hydrogen required for fuel cells. It is a well-known and described technique (Rostrup-Nielsen, 1984) and is also known to be the largest and most economical way to produce hydrogen commercially (Armor, 1999). The process involves catalytic conversion of hydrocarbons, usually natural gas, i.e. methane, in the presence of steam to a mixture of hydrogen, carbon oxides and methane (Aasberg-Petersen *et al.*, 2001; Rostrup-Nielsen and Alstrup, 1999):

$$CH_4 + H_2O = CO + 3H_2, \quad \Delta H^{\circ}_{298} = 206.2\ kJ\ mol^{-1} \tag{2.2}$$

$$C_nH_m + nH_2O = nCO + (n + m/2)H_2, \quad \Delta H^{\circ}_{298} > 0 \tag{2.10}$$

An important side reaction, water-gas shift, favors the formation of carbon dioxide at lower temperatures. It is important particularly in fuel cell applications in terms of simultaneous elimination of carbon monoxide and production of hydrogen:

$$CO + H_2O = CO_2 + H_2, \quad \Delta H^{\circ}_{298} = -41.2\ kJ\ mol^{-1} \tag{2.5}$$

Methane formation can occur either due to the reverse of Reaction (2.2) or due to the following reactions, all of which are usually significant at lower temperatures:

$$CO_2 + 4H_2 = CH_4 + 2H_2O, \quad \Delta H^{\circ}_{298} = -165.0\ kJ\ mol^{-1} \tag{2.11}$$

$$C_nH_{2n+2} + \frac{n-1}{2}H_2O = \frac{3n+1}{4}CH_4 + \frac{n-1}{4}CO_2 \quad (n>1) \tag{2.12}$$

Steam reforming is thermodynamically favored at high temperatures, i.e. typically greater than ca. 1073 K, and at low pressures. However, in industrial practice, the product is usually desired to be at pressures greater than 20 atm (Armor, 1999). In the overall, the

process is highly endothermic and requires considerable external energy. The operation is fixed-bed in character; nickel-based catalyst is packed in a number of small diameter tubes, which are bundled together to form the reformer unit. The characteristics of the heat transfer across the tube walls usually affect the product distribution (Rase, 1990; Rostrup-Nielsen, 1984).

Use of membrane reactors in steam reforming was also demonstrated as a way to obtain conversions higher than the 'fixed-bed' values. These reactors include hydrogen selective membranes which remove hydrogen from the reaction medium. Therefore equilibrium can be shifted in the direction of increased reactant consumption resulting in higher conversions (Prabhu *et al.*, 1999; Tsotsis *et al.*, 1992). It was reported that Pd/Ag composite membranes gave satisfactory performance in methane steam reforming, though conversions greater than 80 per cent were only possible at temperatures and pressures greater than 873 K and 4 bar (Oklany *et al.*, 1998).

Methane may also be reformed with carbon dioxide to produce hydrogen:

$$CH_4 + CO_2 = 2CO + 2H_2, \quad \Delta H^{\circ}_{298} = 247.0\,kJ\,mol^{-1} \tag{2.3}$$

This reaction, which is also called dry reforming, is promising from the environmental point of view, since two greenhouse gases are reacted to produce a clean fuel. The reaction is also preferred when synthesis gas with low H_2-to-CO ratios are desired like in the case of methanol synthesis (Armor, 1999, 2000; Horiuchi *et al.*, 1996; Takano *et al.*, 1994). However, it is not feasible to operate in larger scales, since much severe operating conditions should be employed to overcome the inertness of carbon dioxide, and continuous availability of the gas may be problematic (Aasberg-Petersen *et al.*, 2001; Rostrup-Nielsen, 2000).

2.4.2. Catalysts

Ni-based catalysts are found to be optimal for facilitating both steam and carbon dioxide reforming in terms of sufficient activity and low cost/high availability. However, these catalysts have a high tendency of carbon formation under steam reforming conditions

represented by high temperatures. Carbon formation limits are closer to the actual operating conditions in carbon dioxide reforming (Armor, 1999; Rostrup-Nielsen and Bak Hansen, 1993). Presence of insufficient steam in the feed also leads to coke deposition over Ni. Usually, steam-to-carbon ratios should be kept above stoichiometric values to minimize coking; for methane the recommended ratios lie between 2.5 and 3, whereas other fuels may have different values (Rostrup-Nielsen, 1984). Further details of the tendency to form coke during methane steam reforming and of the thermodynamic carbon production limits in the presence of steam and carbon dioxide are presented in the summary of Rostrup-Nielsen (1984). Related reactions and mechanisms about carbon formation will be presented in Section 2.6.

In contrast with Ni-based ones, precious metal catalysts such as Rh and Ru are found to operate at high activities and selectivites without coke deposition. However, high cost and lower availability of Rh and Ru are major drawbacks. The activity of various catalysts for methane steam reforming is reported as follows (Rostrup-Nielsen and Bak Hansen, 1993):

$$\text{Ru, Rh} > \text{Ir} > \text{Pd, Ni, Pt} > \text{Re} > \text{Co}$$

Minimizing coke formation over nickel-based catalysts is also investigated. It was reported that addition of small amounts of molybdenum compounds (MoO_3) to nickel with quantities less than 0.1 per cent by weight significantly reduced coke deposition and increased the catalytic activity in n-butane steam reforming. Coking resistance was found to increase at elevated steam-to-carbon ratios, since water vapor was thought to stabilize surface molybdenum oxides that limited carbon formation (Borowiecki *et al.*, 1997). Addition of SnO_2 and WO_3 as well as oxides of K, Na, Mg, Ca and Ba was also found to suppress coking over nickel (Borowiecki *et al.*, 1997; Horiuchi *et al.*, 1996). The presence of these promoters basically prevented methane adsorption, and hence its decomposition on the nickel surface. In fact, after addition of alkaline earth oxides to nickel, Horiuchi and coworkers (1996) have found changes in the reaction orders of methane from positive to negative and of carbon dioxide from negative to positive in methane/carbon dioxide reforming. Apart from promoted ones, catalysts with low nickel contents such as $Ni_{0.03}Mg_{0.97}O$ were reported to give high activities in methane steam reforming and

demonstrated stabilities requiring steam-to-carbon ratios as low as unity (Yamazaki *et al.*, 1996).

Higher hydrocarbons, particularly olefins, which may appear as impurities in natural gas, can be decomposed to deposit carbon much easier than methane. In order to eliminate this, pre-reformer units are usually employed in industrial practice to reform higher hydrocarbons at lower temperatures before they enter the main reformer unit. Therefore coke formation due to the presence of higher hydrocarbons can be minimized (Aasberg-Petersen *et al.*, 2001).

2.4.3. Supports

The effects of catalyst supports on reforming activities have also been investigated. Bradford and Vannice (1996) have shown that TiO_2 supported nickel catalysts gave activities that were greater than other supports:

$$Ni/TiO_2 > Ni/C > Ni/SiO_2 > Ni/MgO$$

Similarly, it was demonstrated that Ni/Al_2O_3 was more active and more stable than Ni/SiO_2 (Takano *et al.*, 1994). Recently ceria supported catalyst are found to give higher activities and stabilities: Wang and Gorte (2001) have shown that one weight per cent Pd/ceria catalyst works under low steam-to-carbon ratios (between 1.0 and 2.0) and gives high activities without carbon formation during n-butane steam reforming. Pd/ceria was also found to be more active than one per cent Pd/alumina and 15 per cent Ni/silica. Use of ceria instead of silica enhanced steam reforming activities, but higher steam-to-carbon ratios were still required to eliminate coke formation over nickel in both cases (Wang and Gorte, 2001). It was also demonstrated that both Ni/MgO and Ni/La_2O_3 gave high activities close to the equilibrium conversion of methane during carbon dioxide reforming; however, the latter resulted in higher carbon formation (Prabhu *et al.*, 1999). Changes in activities due to the use of different supports were also reported for catalysts other than Ni. Nakamura and coworkers (1994) have shown that the activity sequence of the supports was $Al_2O_3 > TiO_2 > SiO_2$ for the carbon dioxide reforming of methane over Rh-based catalysts.

For the same reaction, Ir-based catalysts have exhibited an activity sequence of $TiO_2 \geqslant ZrO_2 \geqslant Y_2O_3 > La_2O_3 > MgO \geqslant Al_2O_3 > SiO_2$ (Nakagawa *et al.*, 1998b).

2.4.4. Kinetics of Steam Reforming of Light Hydrocarbons

Kinetics and mechanism of steam reforming of methane have been investigated and reviewed in detail (Rostrup-Nielsen, 1984). In general, the reaction rates were found to exhibit first order kinetics with respect to methane. However, the overall reaction orders were observed to have negative, zero and positive values, depending on the range of steam partial pressures employed (Elnashaie *et al.*, 1990). In fact, a comprehensive kinetic model proposed by Xu and Froment (1989a,b) (Table 2.5) exhibited results which were in contradiction with their previously reported counterparts. However these discrepancies were due to the non-monotonic dependency of the reaction rate on the partial pressure of steam (Elnashaie *et al.*, 1990).

The kinetics and mechanism of steam reforming of higher hydrocarbons are more complex than methane. Perhaps the most general kinetic model for describing the mechanism of steam reforming of higher hydrocarbons was proposed by Rostrup-Nielsen (1984). The model assumed that the hydrocarbon was chemisorbed on a dual site followed by successive α-scission of the carbon-carbon bonds. The resulting C_1-species was then considered to react with the adsorbed steam:

$$C_nH_m + 2* + \xrightarrow{k_A} C_nH_z{-}*_2 + \frac{m-z}{2}H_2 \qquad (2.13a)$$

$$C_nH_z{-}*_2 + n* + \xrightarrow{K_H^{\bullet}} C_{n-1}H_{z'}{-}*_2 + CH_x{-}*_n \qquad (2.13b)$$

$$CH_x{-}*_n + O{-}* \xrightarrow{k_r} CO + \frac{x}{2}H_2 + (n+1)* \qquad (2.13c)$$

$$H_2O + * \xleftrightarrow{K_W^{\bullet}} O{-}* + H_2 \qquad (2.13d)$$

$$H_2 + 2* \xleftrightarrow{K_H^{\bullet}} 2H{-}* \qquad (2.13e)$$

Table 2.5. Langmuir-Hinshelwood type rate expressions for methane steam reforming (adapted from Xu and Froment (1989a))

Reaction	Rate expression
$CH_4+H_2O=CO+3H_2$	$-r_1 = k_1\left(P_{CH_4}P_{H_2O} - \frac{P_{CO}\,P_{H_2}^3}{K_1}\right)P_{H_2}^{-5/2}(DEN)^{-2}$ $DEN=1+K''_{CO}P_{CO}+K''_{H_2}P_{H_2}+K''_{CH_4}P_{CH_4}+K''_{H_2O}\,P_{H_2O}/P_{H_2}$
$CH_4+2H_2O=CO_2+4H_2$	$-r_2 = k_2\left(P_{CH_4}P_{H_2O}^2 - \frac{P_{CO}\,P_{H_2}^4}{K_2}\right)P_{H_2}^{-7/2}(DEN)^{-2}$
$CO+H_2O=CO_2+H_2$	$-r_3 = k_3\left(P_{CO}P_{H_2O} - \frac{P_{CO_2}P_{H_2}}{K_3}\right)P_{H_2}(DEN)^{-2}$

The above mechanism resulted in a generalized rate expression assuming that the concentration of the species $C_nH_z{-}{*}_2$ was negligible:

$$r = \frac{k_A P_{C_nH_m}}{\left[1+\frac{nk_A}{k_r K''_w}\frac{P_{H_2}}{P_{H_2O}}P_{C_nH_m}+K''_W\left(\frac{P_{H_2O}}{P_{H_2}}\right)+\sqrt{K''_H P_{H_2}}\right]^{2n}} \qquad (2.14)$$

Reaction (2.13d) consisted of the following steps:

$$H_2O + \text{support} = H_2O\text{–support} \qquad (2.15a)$$

$$H_2O\text{–support} + * = O{-}* + H_2 \qquad (2.15b)$$

Reactions (2.15a) and (2.15b) represented the ability of the support and various promoters to enhance adsorption of steam, which was then transformed (spilled over) to the nickel surface. It was also indicated that strong support interaction might have caused the nickel surface to be covered by water.

Apart from mechanistic approaches, power law types of rate expressions have been proposed to describe steam reforming of various fuels. Related information about the power law kinetics is presented in Table 2.6.

2.4.4.1. Carbon Dioxide Reforming versus Steam Reforming. Investigation of the kinetics of methane carbon dioxide reforming has received some attention as well. Rostrup-Nielsen and Bak Hansen (1993) have observed no change in the methane reforming mechanism when steam was replaced with carbon dioxide. They have also shown that the kinetics of

Table 2.6. Steam reforming of light hydrocarbons over Ni-based catalysts (adapted from Trimm and Önsan (2001))

Hydrocarbon (HC)	Catalyst	T-range (K)	Pressure (MPa)	Orders			E_A (kJ mol^{-1})
				HC	H_2O	H_2	
CH_4	Ni/MgO	723-823	0.1	1.0	-	-	110
CH_4	Ni/MgO	623-673	0.1	0.96	-0.17	0.25	60
C_2H_6	Ni/MgO	723-823	0.1	0.60	-0.40	0.20	76
C_2H_6	Ni/MgO	583-623	0.1	0.95	-0.46	0.38	80.6
C_3H_8	Ni/MgO	583-623	0.1	0.93	-0.53	0.86	45
n-C_4H_{10}	Ni/γ-Al_2O_3	698-748	3.0	0	1.0	-	54
n-C_4H_{10}	Ni/SiO_2	673-723	0.1	0	1.0	-	

steam reforming was dominant to that of carbon dioxide reforming in the presence of steam. The latter result, however, was found to contradict with the results of Xu and Froment (1989a), i.e. when carbon dioxide was replaced with steam, the reforming rates were found to increase. Rostrup-Nielsen and Bak Hansen (1993) explained this behavior to be due to the negative heat of adsorption of steam estimated for the 'Xu and Froment' conditions, whereas positive values were told to be reported in various studies in the literature. This might be another explanation for the non-monotonic characteristic of the system.

Bradford and Vannice (1996) have also presented a detailed kinetic study about methane carbon dioxide reforming over TiO_2, SiO_2, MgO and carbon supported Ni

catalysts. They found positive reaction orders both for methane and carbon dioxide, with the values affected by the temperature and by the support. In some other studies involving Ni-based catalysts the reaction rates were found to be independent of the partial pressure of carbon dioxide (Takano *et al.*, 1994).

A recent study involving propane carbon dioxide reforming over Ru/Al_2O_3 catalyst has shown that (i) the reaction orders with respect to propane and carbon dioxide were zero and 0.3, respectively, (ii) carbon dioxide was involved in the rate determining step, and (iii) the mechanism of carbon dioxide reforming was different from that of steam reforming (Sutton *et al.*, 2001). The difference between these results and the ones mentioned previously might be due to the different catalysts employed.

In both steam and carbon dioxide reforming over nickel-based catalysts the water-gas-shift reaction is extremely rapid and goes to equilibrium (Rostrup-Nielsen, 1984):

$$CO + H_2O = CO_2 + H_2, \quad \Delta H^{o}_{298} = -41.2\ kJ\ mol^{-1} \tag{2.5}$$

In industrial practice, this reaction is employed in downstream processes called high-temperature shift and low-temperature shift either for adjusting the synthesis gas (H_2+CO) composition or for maximizing hydrogen production (Newsome, 1980). In general, chromia-stabilized magnetite iron oxide catalysts are employed in high-temperature water-gas shift operation (613 K – 633 K), whereas low temperature operation (ca. 473 K) involves the use of $CuO/ZnO/Al_2O_3$ catalyst (Armor, 1999; Pena *et al.*, 1996). Recently ceria supported catalysts are investigated and Pd and Ni are found to be more active than Co and Fe (Hilaire *et al.*, 2001). Kinetics of the water-gas shift reaction over both catalysts is studied in detail (Amadeo and Laborde, 1995; Gines *et al.*, 1997; Newsome, 1980).

2.4.5. Steam Reforming of Methanol

Steam reforming of methanol is also considered, since it is a much easier fuel to convert into hydrogen. The reaction is usually catalyzed by Cu-based catalysts at relatively lower temperatures around 600 K above which thermal sintering by a surface migration process is highly possible (Jiang, 1992; Twigg and Spencer, 2001). In contrast with the

other hydrocarbons, hydrogen generation from methanol does not involve carbon monoxide production, which is highly desired in fuel cell applications:

$$CH_3OH + H_2O = CO_2 + 3H_2, \quad \Delta H^{o}_{298} = 49.6\,kJ\,mol^{-1} \tag{2.7}$$

It was, however, reported that methanol decomposition may take place simultaneously with steam reforming to produce carbon monoxide, and water-gas shift can be important (Peppley *et al.*, 1999):

$$CH_3OH = CO + 2H_2, \quad \Delta H^{o}_{298} = 90.7\,kJ\,mol^{-1} \tag{2.8}$$

$$CO + H_2O = CO_2 + H_2, \quad \Delta H^{o}_{298} = -41.2\,kJ\,mol^{-1} \tag{2.5}$$

However, methanol decomposition may not be the only carbon monoxide production route. Some authors have also found that the formation of intermediate formaldehyde could take place, which would be followed by its decomposition to generate carbon monoxide (Velu *et al.*, 2001). It is worth noting that the importance of water-gas shift was emphasized in both routes.

Nevertheless, the above reactions are usually considered to describe the reaction network for methanol steam reforming. Mechanistic investigations and kinetic studies involving this network running over Cu/ZnO have been recently reported (Peppley *et al.*, 1999). An extensive review was also presented by Trimm and Önsan (2001).

2.5. The Partial Oxidation Process

Although steam reforming is the most desired route in terms of maximal hydrogen throughput, it is far from being suitable for use in fuel cell applications due to its high energy demand and reactor volumes and its sluggish kinetics. However, partial oxidation of hydrocarbons is much faster than steam reforming, requires smaller amounts of catalyst and is energetically self-sustaining once triggered, all of which are highly desired in supplying motive power for fuel cell vehicles.

The catalytic conversion of hydrocarbons to synthesis gas, i.e. a mixture of hydrogen and carbon monoxide, via partial oxidation is known to occur via two major routes:

- Indirect route in which total oxidation and steam reforming reactions are coupled.
- Direct route in which hydrocarbon is converted into synthesis gas in a single step.

These routes have some different characteristics which will be explained in the following sections. It is worth noting that the terms 'indirect' and 'direct' are not clearly specified in the literature, though the mechanisms proposed to characterize partial oxidation are grouped as shown above.

2.5.1. Indirect Partial Oxidation

Indirect partial oxidation is basically a combination of the total oxidation and steam reforming reactions. The most important feature of the process is its autothermicity, which is defined as supplying heat for endothermic steam reforming via exothermic oxidation. This feature is utilized in industrial practice in which non-catalytic combustion is used to supply heat for catalytic methane steam reforming (Pena *et al.*, 1996). Inclusion of steam can partially eliminate carbon formation during non-catalytic combustion around 2273 K, but material problems associated with excessive temperatures and coking are major disadvantages (Bharadwaj and Schmidt, 1995). Therefore, some other approaches must be employed for supplying hydrogen in fuel cell applications.

2.5.1.1. Partial Oxidation of Methane. Catalytic partial oxidation of methane to synthesis gas has received considerable interest, since it is possible to obtain synthesis gas at a ratio close to H_2:CO=2:1, which is the ideal feed for applications like methanol synthesis and Fisher-Tropsch process for producing synthetic fuels. The process can be carried out in a single reactor, whereas steam reforming route giving H_2:CO=3:1 requires water-gas shift reactors to adjust the desired ratio. Therefore, methane partial oxidation offers clear advantages particularly in synthesis gas production for large-scale applications.

It is generally accepted that at a feed composition of CH_4:O_2 ~ 2:1 and at temperatures and residence times around 1023 K and 0.1-1 sec., respectively, the reaction

follows a mechanism which can be explained by sequential occurrence of total oxidation and reforming reactions, and the product distribution can usually be predicted by the thermodynamic equilibrium. Dissanayake and coworkers (1991) studied methane oxidation over 25 weight per cent Ni/Al_2O_3 catalyst under oxygen deficient conditions at atmospheric pressure and at temperatures between 723 K and 1173 K. They obtained equilibrium yields of CO and H_2, with CO selectivities close to 95 per cent at a feed mixture of $CH_4:O_2 = 1.78:1$ and at contact times of ca. 0.1 s, and observed almost complete methane conversions at temperatures above 973 K. They also studied the oxidation state and phase composition of the catalyst by XPS and XRD techniques and showed that the previously calcined catalyst bed was composed of three distinct regions: The initial part of the bed was mainly Ni/Al_2O_4, which was moderately active for total oxidation of methane. The second region was found to be $NiO + Al_2O_3$, over which strong exotherms formed indicating high activity for complete oxidation. The third region mainly consisted of reduced Ni/Al_2O_3 phase, which catalyzed reforming of the remaining methane to CO and H_2 at thermodynamic compositions. Similarly, van Looij and Geus (1997) indicated the non-uniformity of the active phase of the nickel throughout the reactor depending on the partial pressure of oxygen and showed that methane combustion occurred over partially oxidized nickel whereas metallic nickel sites were active for reforming. The sequential mechanism was also confirmed by measurement of surface temperature by IR thermography techniques (Basile *et al.*, 2001). The surface temperature exceeded the gas phase temperature by ca. 200°C at the bed entrance, indicating strong exothermicity due to the occurrence of total oxidation. However, the dominance of endothermic reforming reactions in the second part of the catalyst bed was confirmed by the opposite trend observed between surface and gas phase temperatures.

It is worth noting that the nature of the operating conditions play important roles in the determination of the mechanism. It was reported that the sequential route was significant at lower flow rates, whereas the changes in mechanism towards direct formation of CO and H_2 were observed at higher flow rates in methane partial oxidation over Ru/TiO_2 catalyst (Boucouvalas *et al.*, 1996). The importance of the feed composition in the characterization of partial oxidation mechanism has also been reported (Boucouvalas *et al.*, 1996; Tsipouriari *et al.*, 1998). Apart from the operating conditions, the types of catalysts and supports affect the nature of the partial oxidation. It has been shown that the

temperature increased sharply and then dropped during methane partial oxidation over Ir/TiO_2 and Rh/SiO_2 catalysts, whereas an initial decrease in temperature was followed by a small temperature elevation in the case of Rh/TiO_2 and Rh/Al_2O_3 catalysts. It was concluded that total oxidation followed by steam reforming was dominant in the first case and the initial temperature drop in the latter case was due to the methane decomposition, which was the initial step of direct formation of synthesis gas (Nakagawa *et al.*, 1999b).

Ni-based catalysts are known to exhibit satisfactory activities during partial oxidation of methane to synthesis gas (Dissanayake *et al.*, 1991; Vermeiren *et al.*, 1992; Slagtern *et al.*, 1998). However, catalyst deactivation associated with coke formation over Ni is a significant problem which has been addressed by many researchers. Using promoters and various supports, and employing different catalyst preparation techniques suppress carbon formation and improve activity/selectivity features of the Ni-based catalysts. It was recently shown that preparation of Ni-based catalysts via the coprecipitation technique starting from Mg/Al hydrotalcite type precursors (Basile *et al.*, 2001) and via in-situ solid phase crystallization technique from layered double hydroxides (Morioka *et al.*, 2001) improve activity, selectivity and stability against coking basically due to the improved dispersion of nickel. Catalysts prepared by the impregnation technique gave comparable activities but poor stabilities due to coking (Morioka *et al.*, 2001).

Promoter and support effects in Ni-based catalysts are investigated in much more detail. Addition of alkali metal oxides (Li, Na, K) and rare-earth metal oxides (La, Ce, Y) to NiO/Al_2O_3 were found to improve activity and stability during methane partial oxidation. It was proposed that coke deposition is minimized due to higher metal dispersion resulting from the addition of promoters (Miao *et al.*, 1997). Lu and coworkers (1998) investigated the effect of $CaAl_2O_4$ spinel compound. They found that its existence between Ni and Al_2O_3 suppressed the formation of inactive $NiAl_2O_4$ phase and improved stability. Provendier and coworkers (1999) considered using perovskites and showed that $LaNi_xFe_{(1-x)}O_3$ type mixed perovskites were both active and stable during methane partial oxidation. They mentioned that La was basic in nature and prevented coking, Ni was active for partial oxidation and Fe limited the mobility of active Ni, thus increasing stability, and proposed that the use of these three key components led to higher activities and stabilities.

In fact, iron addition played an important role since $LaNiO_3$ gave poor thermal stability and coking resistance particularly in reductive atmospheres.

The catalyst supports were found to affect catalytic performance. Choudhary and coworkers (1998) studied different NiO-alkaline earth oxides catalysts and found that Ni-CaO, Ni-MgO-CaO and Ni-MgO gave much better performances than higher alkaline earth oxide (SrO, BaO) supported nickel catalysts. They verified their results by XPS studies, which have indicated a significant decrease in surface Ni/alkaline earth ratio in Ni-SiO and Ni-BaO catalysts. Tsipouriari and coworkers (1998) found that Ni/La_2O_3 catalyst presented exceptionally higher performance than any other Ni-supported catalyst due to the decoration of Ni particles by LaO_x species, which favored removal of excess carbon deposition. Diskin and coworkers (1998) found Ni-based catalysts to give carbon monoxide selectivities in the order of $Ni/SiO_2 > Ni/TiO_2 > Ni/CeO_2 > Ni/Al_2O_3$.

Catalysts other than Ni-based ones have been assessed on the basis of their activity, selectivity and stability features. Claridge and coworkers (1993) extensively studied carbon formation over various catalysts during methane partial oxidation and found the rate of coking to follow the order of Ni>Pd>Rh>Ir. Methane decomposition was the principal route for coking and electron micrographs showed that both whisker and encapsulated forms of carbon existed over the catalysts. The rate of coking was found to be 20 mg h^{-1} for Ni, 7.5 mg h^{-1} for Pd and less than 0.06 mg h^{-1} for other metals under the conditions employed ($CH_4:O_2$=2:1, 1050 K, GHSV = $4x10^4h^{-1}$). Ru-based catalysts were also studied in detail and found to exhibit satisfactory catalytic performance (Boucouvalas *et al.*, 1996). Ruckenstein and Wang (1999) studied the support effect over Rh-based catalysts by comparing reducible oxides (CeO_2, Nb_2O_5, Ta_2O_5, TiO_2, ZrO_2) and irreducible oxides (La_2O_3, SiO_2, Y_2O_3, γ-Al_2O_3, MgO) as the catalyst supports during methane partial oxidation at 1023 K, $CH_4:O_2$=2:1 and GHSV=720000 ml g^{-1} h^{-1}. They showed that, in general, irreducible oxides were much more active, selective and stable ($La_2O_3 < \gamma$-$Al_2O_3 \leqslant$ MgO) than reducible oxides due to the partial coverage of the active Rh sites in the latter case. Nakagawa and coworkers (1998a, 1998b, 1999a, 1999b) investigated Ir-based catalysts in detail. They found that 5 weight per cent Ir/TiO_2 catalyst gave partial oxidation activities (at 600°C and $CH_4:O_2$=5:1, 25 per cent conversion, CO and H_2 selectivities over 80 per cent) comparable with that of Rh/TiO_2. Much better activities were obtained in the

case of bimetallic 0.5 weight per cent Ir-Ni/La_2O_3 catalyst due to the synergistic effects: the monometallic catalysts were inactive at 873 K whereas 25.3 per cent methane conversion and 80 per cent selectivity to both CO and H_2 were observed over the bimetallic catalyst with minimal coke deposition. The support effect over Ir was also demonstrated. Supported 0.5 weight per cent Ir catalysts showed a decreasing activity trend of Ir/TiO_2 > Ir/La_2O_3 > Ir/Y_2O_3 > Ir/ZrO_2 > Ir/Al_2O_3 > Ir/MgO > Ir/SiO_2. They also showed that 5 per cent Ir/Al_2O_3 and Ir/SiO_2 catalyzed total combustion rather partial oxidation at 873 K.

Apart from changing the properties of catalysts, using different supports and modifying operating conditions, coke formation over nickel can be minimized by the addition of steam. Rostrup-Nielsen (1984) has shown that keeping the steam-to-carbon ratio at ca. 2.5 could minimize carbon formation over nickel-based catalysts. Presence of steam is usually required if the objective of the partial oxidation is not to meet the synthesis gas ratio (H_2:CO=2:1) but to maximize hydrogen production, which is highly desired in the fuel cell applications. Ma and Trimm (1996) have studied methane partial oxidation in the presence of steam over Pt and Ni based catalysts placed in various configurations. Pt-based and Ni-based catalysts are known to promote oxidation and steam reforming, as explained in Sections 2.3 and 2.4, respectively. They have investigated three configurations in which catalysts are placed as two different beds (Pt-upstream, Ni-downstream) and as physically mixed beds (Pt+Ni). The third configuration called uniform bed involved the existence of two metals on the same support. They found that, at the same feed properties, changes in the bed configurations came up with different conversion and selectivity figures, with the uniform bed composed of the bimetallic catalyst giving the best performance (ca. 92 per cent conversion and ca. 80 per cent product efficiencies at around 900 K and at carbon-to-oxygen and steam-to-carbon ratios of 1.55 and 2.34, respectively). The results indicated the significance of heat and mass transfer between exothermic oxidation and endothermic steam reforming.

2.5.1.2. Partial Oxidation of Higher Hydrocarbons. Although not as much as the conversion of methane, the partial oxidation of higher hydrocarbons have also been studied. Barbier and Duprez (1992) studied partial oxidation of propane over a bimetallic PtRh/CeO_2-Al_2O_3 catalyst (metal loadings in weight per cent: Pt: 1, Rh: 0.2). The

temperature-programmed oxidation between 473 K and 773 K under different values of oxygen deficient feed compositions has shown that total oxidation to CO_2 and H_2O dominated at temperatures below 623 K, but steam reforming and water-gas shift were significant at temperatures greater than 623 K at which oxygen was completely consumed and hydrogen started to appear. They have also studied the monometallic catalysts and found that Pt was more active than Rh in propane oxidation whereas the reverse order was valid for the steam reforming. The exit gas composition was close to the values predicted by the water-gas shift equilibrium which indicated that the reaction was rapid under the conditions employed, possibly due to the interaction between Pt and ceria.

Recently, Liu and coworkers (2001) have studied partial oxidation of propane to synthesis gas over Ni-based catalysts at a space velocity of $5.7x10^4$ h^{-1}, a feed composition of O_2:C_3H_8=1.65/1 and at temperatures between 773 K and 873 K. They studied the effect of catalyst support and found a decreasing activity trend of NiO/γ-Al_2O_3 > NiO/MgO > NiO/SiO_2. They also investigated the modification of NiO/γ-Al_2O_3 catalyst by addition of an alkali metal oxide (Li_2O) and a rare-earth metal oxide (La_2O_3), and observed increased resistance against coking due to the reduced Lewis acidity intensity of the catalyst. However, the coking was still significant (29.1 per cent by weight) even in the case of the modified nickel catalyst.

It was mentioned previously that the conversion of gasoline into hydrogen rich streams were of interest both for spark ignition engines (Jamal and Wyszynski, 1994; Kirwan *et al.*, 1999) and for fuel cell applications (Jost, 1997). The major problem associated with gasoline is the high possibility of coke formation due to the presence of aromatics. Coking is a much more significant problem when non-catalytic partial oxidation is of interest (Jamal and Wyszynski, 1994). It was mentioned that air-to-gasoline ratios greater than 5.2 were recommended to eliminate coking, whereas the ratios decreased to 3.5-4.0 in the presence of a catalyst (Trimm and Önsan, 2001). High quantities of sulphur in gasoline is another problem which leads to poisoning of the catalytic units (Heck and Farrauto, 1995).

A gasoline fuel processor developed by A. D. Little and Chrysler has been demonstrated (Jost, 1997). Spark ignition and electrical heating were used to trigger partial

oxidation and to provide initial energy to the system, respectively. Sulphur was removed in the form of H_2S and steam was added before passing the exit gases through a low-temperature shift catalyst. Finally CO removal was achieved by a Pt-based selective oxidation unit, which reduced CO levels below 10 ppm.

It is possible to control coke formation by adding steam to keep steam-to-carbon ratio around 2.5, at which coking does not take place (Rostrup-Nielsen, 1984). At a temperature and steam-to-carbon ratio of 973 K and 3, respectively, coke-free operation was reported for partial oxidation of iso-octane (hydrocarbon representing gasoline) over a commercial naphta reforming catalyst (Moon *et al.*, 2001). However addition of 100 ppm sulphur to the feed resulted with significant loss in catalytic activity (Moon *et al.*, 2001). As an alternative to steam addition, using a precious metal catalyst may minimize carbon formation (Rostrup-Nielsen and Bak Hansen, 1993).

Initiation of the fuel conversion system is also an important issue in fuel cell applications which has not been investigated in detail for gasoline. It was reported that the conversion of iso-octane was initiated at temperatures around 473 K over a Pt/chromia/silica catalyst, indirect partial oxidation was favored at temperatures less than 873 K and carbon formation related with carbon dioxide reforming was observed at higher temperatures (Trimm and Önsan, 2001). Further studies related with the conversion of C_{6+} hydrocarbons to hydrogen over $Pt/Cr_2O_3/SiO_2$ catalyst have been reported by Jenkins and Shutt (1989).

2.5.1.3. Partial Oxidation of Methanol. Among various fuel alternatives, perhaps methanol is the ideal one in terms of ease of conversion into a hydrogen-rich stream. An early work conducted by Jiang (1992) has demonstrated the partial oxidation (or autothermal reforming) of methanol by injecting methanol, air and water into a reactor in which Pt/Al_2O_3 and $Cu/ZnO/Al_2O_3$ catalysts were placed in a sequential order. It was found that air/methanol/water composition in the feed affected the temperature and product distribution in the catalyst beds. Considering that Cu-based catalysts tend to sinter at temperatures around 600 K (Twigg and Spencer, 2001), water injection plays a critical role in terms of controlling the maximum bed temperature in methanol-fed system, which has also been confirmed by Jiang (1992). More effective reactor configurations handling

methanol partial oxidation and steam reforming, i.e. HotSpot™ reactor technology, have been demonstrated by Golunski (1998). The process was based on the effective heat transfer between oxidation and steam reforming leading to improved hydrogen production efficiencies.

Recently, Velu and coworkers (2001) have investigated partial oxidation of methanol in the presence of water, i.e. oxidative steam reforming over CuZnAl(Zr) oxides. Presence of Zr was found to increase catalytic activity, requiring relatively lower temperatures around 500 K for selective hydrogen production. Optimum oxygen-to-methanol and water-to-methanol ratios were observed to exist between 0.2-0.3 and between 1.3-1.6, respectively. Methanol conversion was reported to exceed 60 per cent at 473 K. The importance of water addition can be explained by a previous work of the same group (Velu *et al.*, 1999). Methanol partial oxidation over CuZnAl-oxide type catalysts gave conversions between 40-60 per cent at 473 K in the absence of water, which is lower than the corresponding result reported recently (Velu *et al.*, 2001). Methanol conversion into hydrogen over Cu-based catalysts has also been addressed by several other groups (Emonts *et al.*, 1998; Geissler *et al.*, 2001; Ledjeff-Hey *et al.*, 1998)

The use of Pd/ZnO catalysts in the partial oxidation of methanol has also been considered. Cubeiro and Fierro (1998) have reported ca. 80 per cent conversion of methanol, which gave hydrogen selectivities around 80 per cent in the absence of water, and have proposed that higher values could be obtained in the presence of water as the reactant. Pd/ZnO catalyst offered improved thermal resistances above 600 K (at which Cu-based catalysts would start to sinter); however, alloy formation was observed at higher temperatures. Nevertheless, Pd-based catalysts can be an important alternative against Cu-based counterparts in terms of activity at low temperatures and stability at high temperatures.

2.5.2. Direct Partial Oxidation

In contrast with the indirect route explained above, the 'single-step' formation of synthesis gas is involved in direct partial oxidation:

$$CH_4 + \tfrac{1}{2}O_2 = CO + 2H_2, \quad \Delta H^{\circ}_{298} = -35.7\ kJ\ mol^{-1} \qquad (2.4)$$

The production of synthesis gas in its ideal composition, i.e. H_2:CO=2:1, without any steam requirements is the major advantage of the process. However, carbon monoxide, which is a serious poison for fuel cells, is a major product in direct oxidation, and post reactor applications involving water injection and water-gas shift are required to convert it into useful hydrogen in fuel cell applications.

Direct partial oxidation of methane to synthesis gas was studied initially by Ashcroft and coworkers (1990). They reported methane conversions above 90 per cent and hydrogen selectivities between 95-99 per cent over precious metal catalysts at temperatures and contact times around 1023 K and 0.1 s, respectively. However, Schmidt and his group have extensively studied the direct partial oxidation of methane (Bharadwaj and Schmidt, 1995; Hickman and Schmidt, 1993; Torniainen *et al.*, 1994) and higher hydrocarbons (Bodke *et al.*, 1998; Dietz III *et al.*, 1996; Huff and Schmidt, 1994; O'Connor *et al.*, 2000; Witt and Schmidt, 1996) to synthesis gas and olefins over Rh and Pt catalysts supported on various monoliths and gauzes. The major conclusions were that (i) Rh was selective to synthesis gas whereas Pt mainly catalyzed olefin formation (ii) synthesis gas selectivities close to the thermodynamic equilibrium were obtained at elevated temperatures usually exceeding 1273 K, at millisecond level contact times, at metal loadings greater than 10 per cent by weight and at near-stoichiometric feed mixtures (iii) mass transfer effects were significant in the determination of product distribution. Oxidation of methanol over Rh and Pt has also been studied (Zum Mallen and Schmidt, 1996). In contrast with high temperature requirements, the possibility of direct methane oxidation over Ru/TiO_2 at lower temperatures (between 873 K-1073 K) have also been reported (Boucouvalas *et al.*, 1996; Elmasides *et al.*, 2000).

Hickman and Schmidt (1992) have studied direct conversion of methane to synthesis gas over Pt and Pt-Rh coated monoliths at temperatures around 1373 K and at contact times between 10^{-4}-10^{-2} s. 80 per cent CH_4 conversion gave hydrogen and carbon monoxide selectivities around 50 per cent and 95 per cent, respectively, when the feed was composed of 15-20 per cent methane by volume. Replacement of oxygen with air and stoichiometric mixing of the reactants gave H_2 selectivities up to 70 per cent. Product

distribution changed at different flow rates, which was an indication of the importance of mass transfer effects. However, the higher H_2 selectivites reported for Rh (ca. 90 per cent) indicated the effect of kinetics of individual steps over product composition. Finally, the proposed mechanism for direct oxidation involved catalytic pyrolysis of CH_4 followed by H_2 desorption and oxidation of carbon to CO. They observed no coke deposition, which was thermodynamically favored at temperatures lower than 1273 K for CH_4:O_2=2:1, and no water formation under the conditions employed.

Different Al_2O_3-monolith supported catalysts were assessed on the basis of their activities and stabilities during methane partial oxidation (Torniainen *et al.*, 1994). It was shown that Rh gave the highest activity (conversion: 89 per cent, H_2 and CO selectivities: 90 and 95 per cent, respectively at 1273 K and ca. 10 ms residence time). Ni demonstrated similar activites but deactivated due to aluminate formation. Pt and Ir were found to be stable but gave activity/selectivity performances lower than Rh and Ni. In contrast with these catalysts, coke deposition was reported for Pd and Pd-La_2O_3. Cobalt deactivated due to aluminate formation and Re, Ru, Fe could not sustain autothermal operation. The authors have also investigated the significance of steam reforming (SR) and water-gas shift (WGS) by adding steam into the feed. They did not observe any SR and WGS effects under the conditions employed.

The importance of the heat transfer effects in direct oxidation has been demonstrated by Hohn and Schmidt (2001). They have compared Rh coated spheres and monoliths on the basis of their synthesis gas selectivities and have found that spheres gave more satisfactory results. The difference lied between heat transfer characteristics of the support geometries: spheres have facilitated conductive and radiative modes of heat transfer rather than convection which eventually allowed better distribution of 'high temperature' throughout the catalyst bed.

The effects of pore size in monoliths, washcoat addition and support material on the direct partial oxidation of methane, ethane and n-butane have been studied (Bodke *et al.*, 1998). Smaller pore size together with washcoat addition increased syngas selectivity by affecting mass transfer rates. Changing support material did not make any differences in

product distribution, although materials having higher thermal resistances like ZrO_2 would be preferred due to the high temperatures involved during the reaction.

Direct oxidation of C_3-C_4 alkanes (Huff and Schmidt, 1994) and C_5-C_6 alkanes (Dietz III *et al.*, 1996) over Pt-coated monoliths at contact times around 5 ms produced olefins rather than synthesis gas. This was observed for the entire range of fuel-to-oxygen ratios in the case of higher alkanes whereas stoichiometric feeds had a tendency to produce CO and H_2 in the case of propane and n-butane. The improved selectivity of Rh towards synthesis gas and rapid coking of Pd-based catalysts were confirmed in both studies.

The results above indicate that direct partial oxidation is favored at short contact times. However Witt and Schmidt (1996) have shown that much higher space velocities resulted in significant loss in activity. They observed that ethane conversion decreased from 90 per cent to 20 per cent when space velocity was increased from $5x10^4$ h^{-1} to $1x10^6$ h^{-1}. The possible reason was the cooling of the front region of the catalyst, which favored complete combustion and C_2 products via formation of CH_3 radicals. In fact, at elevated space velocities, a significant loss in ethylene selectivity was not observed.

The direct oxidation of cyclohexane, n-hexane, isooctane, toluene and commercial gasoline over Rh-coated monoliths has also been reported (O'Connor *et al.*, 2000). In general, the fuel conversions exceeded 95 per cent and synthesis gas yields were above 90 per cent at space velocities between $3x10^5$ h^{-1} and $3x10^6$ h^{-1}. Reduced pores sizes and washcoat addition were found to improve activity/selectivity performances. Direct conversion of commercial gasoline gave CO selectivites around 80 per cent, however the catalyst was poisoned primarily due to the sulphur in the gasoline. The authors have also mentioned the use of direct oxidation as an on-board fuel processing route and suggested water injection for maximizing hydrogen production.

Compared with indirect partial oxidation, the direct route has some serious operational challenges in supplying hydrogen for fuel cells in vehicles. The process requires high temperatures exceeding 1273 K, millisecond contact times and operates at nearly explosive feed conditions, all of which are significant drawbacks in applications involving frequent start-up/shut-down periods as in the case of vehicles. However,

computer simulations have shown that direct partial oxidation coupled with water injection and low-temperature water-gas shift conversion gives higher hydrogen yields than the indirect route (Avcı *et al.*, 2001a; Avcı *et al.*, 2002). In addition, the rapid response and requirements of smaller reactor volumes make direct partial oxidation a process to be further considered for use in fuel cell applications.

2.6. Inhibition of the Catalytic Processes

Deactivation of the catalysts is known to occur via three major routes defined as poisoning, fouling and thermal degradation (sintering). The following sections involve information about the fundamentals of these routes. At this point, it is worth noting that the first two type of deactivation can often be reversed, but sintering is usually irreversible.

2.6.1. Poisoning

The fundamental reason for catalyst poisoning is the interaction between a component existing within the feed or product and the active sites of the catalyst. The most common type of poisoning is known to be due to sulphur but also heavy metals or their ions can poison metallic catalysts, and organic bases may poison acidic catalysts. Three types of catalyst poisons have been identified, which are (i) Group 5A and 6A elements, including N, P, As and Sb (5A) and O, S, Se and Te (6A), (ii) toxic heavy metals such as Pb, Hg, Cd and Cu, and (iii) specific molecules that interact with catalyst surfaces (Bartholomew, 2001).

In the first type of poisons, the elements poison metal catalysts by interaction through their 's' and 'p' orbitals. Hence, the number of bonding electrons can be changed by oxidation or reduction, and the degree of poisoning can be modified. To illustrate, the poisoning effect of sulphur increases in the order of $SO_4^{2-} < SO_2 < H_2S$. It was reported that H_2S present at parts per billion levels is sufficient to result in significant surface coverage (Trimm, 2001).

Oxidation at high temperatures is proposed to regenerate catalysts poisoned by sulphur, since the sulphates, which can react with supports such as alumina, break up to

give SO_x that can be removed from the system in the gas phase. The sulphur compounds can also be removed before they reach the reactor. This process is known as hydrodesulphurization and involves the conversion of sulphur compounds to H_2S at temperatures between 623 K and 673 K over alumina supported cobalt and molybdenum oxides. The resulting H_2S can then be removed by adsorption on ZnO catalyst (Bartholomew, 2001; Dicks, 1996).

The removal of the second type of poisons is more complex, and involves processes known as abrasion or leaching, which were extensively reviewed by Trimm (2001).

Perhaps poisoning of the Pt-based catalysts within the PEM fuel cells by carbon monoxide is the best example for describing the third type of poisons. It is known that the existence of very small amounts of carbon monoxide as low as 10 ppm in hydrogen-rich streams is a serious threat for PEM fuel cell operation. Carbon monoxide adsorbs on the active Pt sites so strongly that almost no active sites are left for the dissociation of hydrogen into its protons and electrons.

Several techniques for improving the CO tolerance of the fuel cell catalysts have been reviewed (Ralph and Hards, 1998; Urban *et al.*, 2001). Use of bimetallic Pt/Ru alloy supported on carbon was found to be resistant against 50-100 ppm of CO in the feed, but stability (should be greater than 4000 h and 40000 h for mobile and stationary applications, respectively) of this formulation was questionable. Pt/Mo, Pt/W and Pt/Fe catalysts demonstrated better stabilities. Other solutions involve an air bleed, i.e. air or oxygen injection into the feed stream for oxidizing CO and addition of liquid H_2O_2 for driving CO oxidation. The CO resistances were reported to increase up to 150 ppm and 100 ppm, respectively, depending on the amounts of air and H_2O_2 injected.

2.6.2. Fouling

Fouling is defined as the physical blocking of the active sites due to the deposition of a substance on a catalyst surface. The most commonly known type of fouling is coke deposition which is usually observed in catalytic reactions involving hydrocarbons (Bartholomew, 2001).

The term "coke" is a collective description of various kinds of carbonaceous deposits, since the nature of the deposit can be different. Coking is usually favored under the conditions employed for catalytic steam reforming. It is more pronounced at higher temperatures and at lower quantities of steam and is known to occur via the following reactions (Trimm, 1999):

$$CH_4 = C + 2H_2, \quad \Delta H^{\circ}_{298} = 74.9\,kJ\,mol^{-1} \tag{2.16}$$

$$2CO = C + CO_2, \quad \Delta H^{\circ}_{298} = -172.4\,kJ\,mol^{-1} \tag{2.17}$$

$$CO + H_2 = C + H_2O, \quad \Delta H^{\circ}_{298} = -135.6\,kJ\,mol^{-1} \tag{2.18}$$

$$C_nH_{2n+2} = nC + (n+1)H_2, \quad \Delta H^{\circ}_{298} > 0 \tag{2.19}$$

The reactions are reversible and it is possible to minimize coke formation by adjusting operating conditions such as increasing the amounts of carbon dioxide and steam that will shift the directions of Reaction (2.17) (also known as Boudouard reaction) and Reaction (2.18) in the direction of coke minimization. The carbon limit diagrams that present the tendency of carbon formation over nickel catalyst as functions of O/C and H/C were presented by Rostrup-Nielsen (1984). Operating temperature defines the significance of the reactions above. Reactions (2.17) and (2.18) are exothermic, hence favored at lower temperatures. On the other hand cracking reactions (2.16) and (2.19) are likely to occur at higher temperatures due to their endothermic nature.

Three common types of carbon have been identified in nickel-catalyzed steam reforming. These are (i) pyrolytic carbon, (ii) whisker-like carbon, (iii) encapsulating carbon (Rostrup-Nielsen, 1984).

Pyrolytic carbon forms mainly due to the thermal cracking of hydrocarbons which are favored at temperatures higher than ca. 920 K (Rostrup-Nielsen, 1997). The process is further facilitated at lower steam-to-hydrocarbon ratios, at higher pressures and in the case of high surface acidity of the catalysts. This mode of carbon can also formed as a result of

higher residence times and of overheated gas films at the tube walls acting as a source of radicals and coke precursors. Therefore, the nature of catalyst packing, i.e. void fraction, affects the carbon formation by influencing residence time and the gas film volume. Pyrolytic carbon both deactivates the Ni-based catalyst by encapsulating it and blocks the reactor by accumulation within the voids between the particles (Rostrup-Nielsen, 1984). Suppressing the factors that facilitate it can minimize the formation of pyrolytic carbon.

The formation of whisker carbon and encapsulated carbon can be explained by the coking mechanism over nickel (Rostrup-Nielsen, 1997). The process is believed to start with the dissociation of hydrocarbons into highly reactive monatomic carbon (C_α), which can easily be gasified to form carbon monoxide. However, if C_α is formed in excessive quantities or gasification is slow, then polymerization to C_β is facilitated. It has been shown that C_β is much less reactive than C_α, and the gasification step is fairly slow (Trimm, 1999). As a result, C_β may either accumulate on the catalyst surface or dissolve in the nickel leading to encapsulated carbon and whisker carbon, respectively. Noble metal catalysts, on the other hand, do not dissolve carbon, i.e. do not favor whisker mechanism, and therefore are resistant against coking (Rostrup-Nielsen, 2000).

As the carbon has dissolved or formed a compound with nickel, diffusion through the metal particle to a grain boundary occurs. As a result, carbon precipitates out and lifts the nickel particle at the tip of a growing whisker. Nickel is still active in this mode of carbon formation, but accumulation of carbon whiskers leads to break-down of the catalyst and blocks the catalyst bed, which increases pressure drop dramatically. In general, the process is favored at temperatures greater than 720 K (Rostrup-Nielsen, 1984).

Some of the coke formed on the catalyst surface remains undissolved and eventually encapsulates nickel. At temperatures lower than ca. 770 K, encapsulation becomes more pronounced with time by the polymerization of C_nH_m radicals on the nickel surface, as explained above, and leads to progressive deactivation of the catalyst (Rostrup-Nielsen, 1984).

It was mentioned above that polymerization of C_α species to C_β was an intermediate step in the formation of dissolved or deposited carbon. It is obvious that polymerization is

possible by the presence of more than one C_α species, whose formation requires high number of surface sites. Therefore, it has been reported that it is possible to reduce C_α formation by controlling the number of sites in an ensemble, which will minimize coke formation but maintain steam reforming. The process is called ensemble size control (or sulphur passivation) and is achieved by addition of minimal quantities of sulphur (eg. $H_2S/H_2 < 7.5x10^{-7}$) in order to facilitate controlled sulphur adsorption on nickel. As a result, the rate of steam reforming is reduced but coke formation is almost eliminated (Rostrup-Nielsen, 1984; Trimm, 1999).

The addition of various promoters and use of different supports to suppress coke formation were already reviewed in Sections 2.4.2 and 2.4.3, respectively. Techniques developed for preventing carbide formation, which is an intermediate step in coke formation, have been presented by Trimm (1999).

2.6.3. Sintering

High surface area is a feature which is desired in catalysis, but it is not thermodynamically favored. Therefore, at high temperatures and in the presence or absence of a suitable chemical environment, the catalysts will transform into thermodynamically favored lower surface agglomerates. The process is known as sintering. This mechanism of deactivation is more pronounced in high temperature applications in which catalytic combustion is involved (Thevenin *et al.*, 2001).

In general, the thermal rearrangement of most of the solids occurs at around 0.3-0.5 times the melting point of the material (Trimm, 1980). The existence of particular atmospheres further accelerates sintering. To illustrate, hydrothermal conditions lead to catalyst deactivation due to sintering in steam reforming. In addition moist atmospheres are known to facilitate sintering of oxide supports (Trimm, 2001).

Unwanted chemical reactions can also occur at high temperatures. The formation of the inactive nickel aluminate phase as a result of the interaction between nickel and alumina demonstrates undesired component interactions at high temperatures. In addition, alloy formation or phase separation is likely to occur (Trimm, 2001).

γ-Al_2O_3 is a commonly used catalyst support, but starts to lose its high surface area (ca. 250 m^2 g^{-1}) at temperatures greater than 873 K. As the temperature is increased, γ phase transforms into δ and θ phases, respectively. The final transformation occurs at ca. 1373 K to a highly stable phase (α) which has a surface area as low as ca. 5 m^2 g^{-1}. The improvement of the thermal stability of alumina has been investigated by Arai and Machida (1996). They found that addition of oxides like BaO, La_2O_3, SiO_2, Li_2O and K_2O to alumina inhibited sintering, since these stabilizers filled vacancies in the lattice. Among these additives, SiO_2 introduced additional resistance against moist atmospheres. The change in the preparation method of alumina, which would have affected the rate of sintering due to the modified particle morphology and grain structure, was proposed as another method to improve thermal resistance.

3. EXPERIMENTAL

3.1. Materials

3.1.1. Chemicals

All the chemicals used for catalyst preparation are presented in Table 3.1.

Table 3.1. Chemicals used for catalyst preparation

Chemicals	Specification	Source	Molecular weight
Nickel nitrate	$Ni(NO_3)_2.6H_2O$ extra pure	Merck	290.81
Tetraammineplatinum(II) nitrate	$Pt(NH_3)_4(NO_3)_2$ 50.4 % Pt	Aldrich	387.22
Gamma alumina	γ-Al_2O_3	Alcoa	-

3.1.2. Gases and Liquids

All of the gases used in this research were supplied by Birleşik Oksijen Sanayi (BOS) and HABAŞ Companies, Istanbul, Turkey. Table 3.2 and Table 3.3 list the specifications and applications of the liquids and gases employed in this research.

Table 3.2. Specifications and applications of the liquids used

Liquid	Specification	Application
Nitrogen	HABAŞ	BET cold trap
Water	Distilled	Aqueous solutions, Reactant

Table 3.3. Specifications and applications of the gases used

Gas	Specification	Application
Hydrogen	99.99 % (BOS)	GC calibration, Reduction
Carbon Monoxide	99.999 % (BOS)	GC calibration
Helium	99.999 % (BOS)	GC carrier gas
Nitrogen	99.998 % (BOS)	Inert
Nitrogen	99.998 % (BOS)	BET
Dry Air	78.4 % N_2 + 21.5 % O_2 (BOS)	GC calibration, Reactant
Oxygen	99.999 % (BOS)	TGA purge gas
Methane	99.9 % (BOS)	GC calibration
Argon	99.999 % (BOS)	GC carrier gas, TGA protective gas
Propane	99.5 % (BOS)	GC calibration, Reactant
n-Butane	99.5 % (BOS)	GC calibration, Reactant

3.2. Experimental Systems

The experimental systems used in this research can be classified into four groups:

- Catalyst Preparation System: The set-up used for preparing catalysts by incipient-to-wetness impregnation technique represents this group of experimental systems.
- Catalyst Characterization Systems: This group of systems involves three different analytical techniques used to characterize the physical and structural properties of the catalyst samples prepared and to examine any carbonaceous deposits produced during the reactions.
- Catalytic Reaction System: This continuous flow microreactor system includes gas and liquid flow control, temperature controlled line heating, gas/liquid mixing, and reaction chamber, feed and product sampling sections. This system is used for assessing catalytic activity/selectivity and for measuring reaction kinetics.

- Product Analysis Systems: The quantitative determination of the composition of the species in the reactor exit stream is conducted by using two different gas chromatographs operating in parallel.

3.2.1. Catalyst Preparation System

The system used for preparing catalysts by incipient-to-wetness impregnation technique (Figure 3.1) includes a Retsch UR1 ultrasonic mixer, a vacuum pump, a buchner flask and a MasterFlex computerized-drive peristaltic pump.

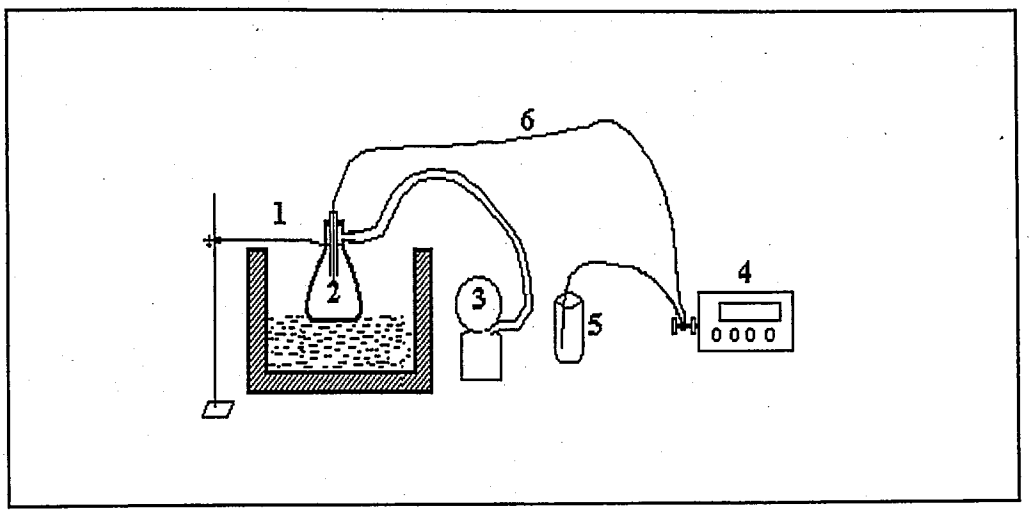

1. Ultrasonic mixer, 2. Buchner erlen, 3. Vacuum pump, 4. Peristaltic pump, 5. Reactant storage tank, 6. Silicone hoses

Figure 3.1. Schematic diagram of the impregnation system (Akın, 1996)

3.2.2. Catalyst Characterization Systems

The total surface area of the catalyst support materials was measured by using a Micromeritics Flowsorb II 2300 constant pressure dynamic apparatus (Figure 3.2). Coke formation over the spent catalysts was examined through Thermogravimetric Analysis (TGA) technique, using a Mettler-Toledo TGA/SDTA851^e system.

The structural analyses of the catalyst samples were carried out at Boğaziçi University Advanced Technologies R&D Center by Zülal Mısırlı through Scanning

Electron Microscopy-Backscattered Composition Imaging (SEM-BCI), Energy Dispersive X-ray Analysis (EDX) and particle size analysis techniques, using a Philips XL30 ESEM-FEG system which has a maximum resolution of 2 nm. In EDX analyses, the minimum detection limit was 50 ppm.

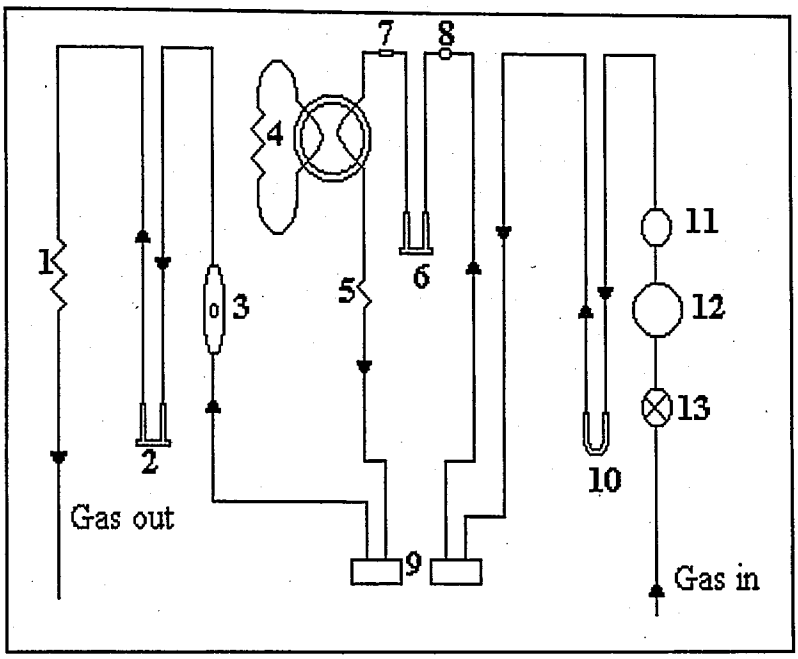

1. Back diffusion restrictor, 2. Degas, 3. Flowmeter, 4. Long path, 5. Short path, 6. Test sample, 7. Filter, 8. Septum, 9. Matched thermal conductivity cells, 10. Cold trap, 11. Flow adjustment valve, 12. Differential flow controller, 13. On-off valve

Figure 3.2. Schematic diagram of the BET equipment (Akın, 1996)

3.2.3. Catalytic Reaction System

The catalytic reaction system was designed and constructed in the Department and involves three characteristic sections:

- Feed section
- Reaction section
- Product analysis section

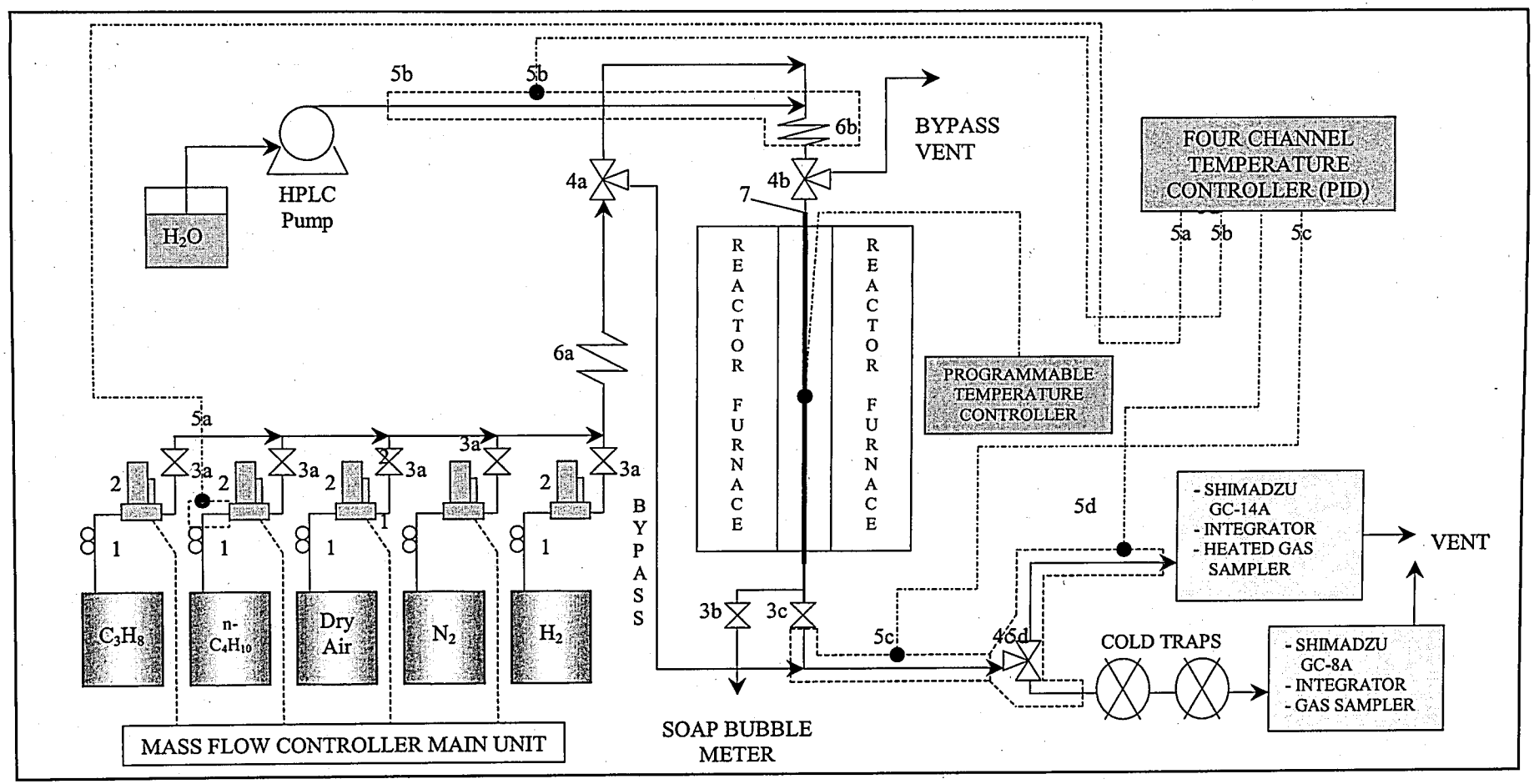

1. Gas regulator, 2. Mass flow controller, 3. On-off valve, 4. Three-way valve, 5. Heated zone, 6. Mixing zone, 7. Differential reactor

Figure 3.3. Schematic diagram of the flow microreactor system

The feed section was composed of mass flow control systems, 1/4", 1/8" and 1/16" stainless steel tubes and fittings for feeding liquid water and gaseous species, i.e. propane, n-butane, dry air, nitrogen and hydrogen (see Table 3.3 for specifications) at desired quantities accurately. The gases that were present in pressurized cylinders were passed through the gas flow regulators (items 1 in Figure 3.3) and the calibrated Omega Model 5878 mass flow controllers (items 2 in Figure 3.3), whose set values were adjusted by the main control unit. An Aalborg GFC171S series standalone controller was used to regulate hydrogen flow. The calibration curves of the mass flow controllers are presented in Appendix A. On-off valves (items 3a in Figure 3.3) were placed in front of the mass flow controllers to protect them from possible back-pressure fluctuations. In order to eliminate possible condensation of n-butane, the zone between the pressure regulator and the mass flow controller was kept at 333 K ± 3 K using a 0.6 m heating tape and the four channel temperature controller (Line 5a in Figure 3.3). Each gas was fed from its independent line, so that it was possible to meter the flow of individual species and adjust desired feed ratios. The gases were then passed through a primary mixing zone (zone 6a in Figure 3.3) to ensure the flow of a homogeneous reactant gas mixture into the reactor.

In the case of steam reforming experiments, the liquid reactant, water, was introduced into the reaction system at constant flow rates using a Jasco PU-1580 intelligent HPLC pump. The 1/16" tube, through which water was allowed to flow, was kept at 423 ± 3 K using a 1.4 m heating tape and the four channel temperature controller (Line 5b in Figure 3.3) to feed water in the form of steam. Steam and the homogeneous gas mixture were mixed in a secondary mixing zone (zone 6b in Figure 3.3) to introduce a homogeneous mixture of all the reactants into the reactor.

It was possible to divert the flow direction using three way valves 4a and 4b shown in Figure 3.3. The feed gases could be diverted in the direction of bypass line using valve 4a, so that feed composition could be assessed using gas chromatographs. Valve 4b played an important role, particularly in steam reforming experiments; the flow was diverted to the bypass vent line for establishing steady state flow and mixing of the steam and other gaseous reactants prior to the reaction.

The reactants, metered and mixed in the feed section, were allowed to flow through the reaction section. This section was composed of a 40 cm x 2.4 cm ID tube furnace controlled to ± 0.5 K by a Shimaden FP-21 programmable temperature controller (Figure 3.3) and a 1/4" (4 mm ID) stainless steel fixed-bed microreactor (item 7 in Figure 3.3). The reactor length was selected to be 50 cm so that it was longer than the furnace which was also constructed in the Department.

During the reaction tests, the catalyst bed was placed in the center of the reactor. The reaction temperature was controlled and measured by a 20-gauge wire K type sheathed thermocouple (insulation material: ceramic fiber braid) that was placed in the center of the furnace as shown in Figure 3.3. The position of the reactor and hence catalyst bed was adjusted to coincide with the constant-temperature zone of tube furnace.

Silane-treated glass wool (Alltech Associates Inc.) was used to hold the catalyst bed in a fixed position. Ceramic glass wool insulations were placed in top and bottom ends of the reactor furnace to prevent heat loss from the furnace and to provide a good temperature profile.

The product stream leaving the reactor involves steam. In order to prevent the condensation of steam, the line from the reactor to the three-way valve 4c and the line from valve 4c to both gas chromatographs were both kept heated at 398 ± 3 K using a 1.4 m and a 2.5 m heating tape and the four channel temperature controller (lines 5c and 5d respectively in Figure 3.3). The product stream (or the feed stream bypassed using valve 4a) was analyzed qualitatively and quantitatively using two separate gas chromatographs operating in a parallel scheme. Further details about product analysis involving the gas chromatographs are given in the following section.

The four channel temperature controller is a unit that can control the temperature of the four different zones independently. 16-gauge wire K type sheathed thermocouples (insulation material: fiberglass) were placed at the middle point of each heated zone to measure and control the temperatures. The degree of power input of the heating tapes was adjusted by the controller. The heating tapes were covered with ceramic wool insulation to prevent heat losses.

3.2.4. Product Analysis Systems

The product mixture contains groups of species with different characteristics, i.e. hydrocarbons involving methane, ethane, propane, n-butane, fixed gases involving hydrogen, oxygen, nitrogen, and others involving carbon monoxide, carbon dioxide and water. Considering that all these species excluding water needed to be analyzed quantitatively, use of two different gas chromatographs was essential: hydrocarbons were effectively analyzed using a Porapak Q column with He carrier gas whereas quantitative detection of hydrogen and other fixed gases were best achieved using a Molecular Sieve column with Ar carrier.

A Shimadzu GC-14A gas chromatograph equipped with a Thermal Conductivity Detector (TCD) and a Shimadzu CR-4A Chromatopac data processor was used interactively to analyze hydrocarbons and carbon dioxide. In order to analyze fixed gases, carbon monoxide and methane, a Shimadzu GC-8A gas chromatograph equipped with a Thermal Conductivity Detector (TCD) and a Shimadzu CR-1B Chromatopac data processor was employed. The latter involves a Molecular Sieve (MS) column which can easily be deactivated if it is contacted with a stream containing water vapor. Thus steam existing in the product stream was removed by placing two salt-ice cold traps held in Dewar flasks at 273 K before GC-8A inlet. The parallel operation of these gas chromatographs was achieved by diverting the product flow using the three-way valve 4c. The analysis conditions are presented in Table 3.4. For GC-14A, the previously optimized conditions by Aksoylu (1999) were used whereas analysis reports provided by the manufacturer were employed to finalize the operating conditions used in GC-8A.

Before proceeding with the experiments, the gas chromatographs were calibrated by injecting known volumes of the species to be analyzed from the injection ports to the column under the conditions given in Table 3.4 and by reading the area under the peak calculated by the integrator. Using this procedure, volume versus peak area curves were constructed for each gas – excluding carbon dioxide and methane in GC-14A, which were checked and found to be the same as the calibration curves obtained by Aksoylu (1999) – and the corresponding calibration factors were determined by linear regression. The calibration curves are presented in Appendix B.

Table 3.4. Product analysis conditions

GC Parameter	GC 1 – Shimadzu GC-14A	GC 1 – Shimadzu GC-8A
Detector type	TCD	TCD
Column temperature, K	363	333
Injector temperature, K	423	363
Detector temperature, K	423	363
TCD temperature, K	423	363
TCD current, μA	120	60
Carrier Gas (CG)	He	Ar
CG flow rate, ml min^{-1}	25	50
Column packing material	Porapak Q, 80-100 mesh	MS 5A, 60-80 mesh
Column tubing material	Stainless steel	Stainless steel
Column length & ID	3 m x 3mm	2 m x 3mm
Sample loop	1 ml kept at 398 K	1 ml kept at 298 K

3.3. Catalyst Preparation and Pretreatment

3.3.1. Support Preparation

The catalytic oxidation and steam reforming of hydrocarbons are known to be high-temperature reactions. Therefore, the catalyst supports should not only have high surface areas but also possess high thermal stabilities. γ-Al_2O_3 is a commonly used support material due to its high surface area. However it is reported to have low stabilities at temperatures greater than 873 K and tends to facilitate carbon formation in the presence of steam due to its high acidity (Ma, 1995). The most thermally stable version of alumina is obtained when γ-phase is transformed into α-phase at temperatures greater than 1400 K (Doesburg *et al.*, 1999). However, its low surface area, which is less than 5 m^2 g^{-1}, is likely to end up with poor catalytic activities due to the low dispersion of active metals. Hence using a support such as δ-alumina – an intermediate phase between γ and α -

having relatively high thermal stability and an acceptable surface area can be optimum in terms of obtaining an efficient catalytic performance (Ma, 1995).

In this study, three different support preparation procedures were investigated. These procedures, presented in Table 3.5, involved basically the calcination of γ-Al_2O_3 (BET surface area: 279 m^2 g^{-1}) at various temperatures. The comparison of the resulting materials was based on their BET surface areas.

Table 3.5. Support preparation procedures

Procedure	BET surface area (m^2 g^{-1})
Calcination at 1273 K for 4 h	46.8
Drying of γ-Al_2O_3 at 423 K for 2h followed by calcinations at 1173 K for 4h	81.6
Drying of γ-Al_2O_3 at 378 K overnight followed by calcination at 1148 K for 4h	73.2

It can be seen that the second procedure resulted with the highest BET surface area, possibly due to the low temperature removal of bonded water. It seems that the duration of drying is also important, since a longer period of drying at a lower temperature led to a lower BET surface area, though the calcination temperature was lower than 1173 K.

3.3.2. Preparation of Pt/δ-Al_2O_3 and Ni/δ-Al_2O_3

The monometallic Pt/δ-Al_2O_3 and Ni/δ-Al_2O_3 catalysts were prepared by the incipient-to-wetness impregnation technique using aqueous solutions of $Pt(NH_3)_4(NO_3)_2$ and $Ni(NO_3)_2.6H_2O$, respectively. The metal loadings were 0.2 weight per cent for platinum and 15 weight per cent for nickel. The aqueous solutions were prepared by dissolving the calculated amount of the precursor salts in definite amounts of distilled water (ca. 1 ml solution/g support). The support, δ-Al_2O_3, was put into the Buchner erlen and mixed ultrasonically for 25 min. under vacuum. The aqueous solution was then impregnated over the support via a peristaltic pump. The resulting slurries, which were

formed after ultrasonic mixing of the aqueous solutions and the support under vacuum for 1.5 h, were then dried overnight at 393 K and calcined either at 773 K ($PtO/\delta\text{-}Al_2O_3$) or at 873 K ($NiO/\delta\text{-}Al_2O_3$) for 4 h.

3.3.3. Preparation of $Pt\text{-}Ni/\delta\text{-}Al_2O_3$

The bimetallic $Pt\text{-}Ni/\delta\text{-}Al_2O_3$ catalyst (metal loadings were 0.2 weight per cent for Pt and 15 weight per cent for Ni) was prepared through a sequential route, in which Pt solution was impregnated over initially prepared and calcined Ni catalyst. The $NiO/\delta\text{-}Al_2O_3$ catalyst was prepared as explained above. The aqueous Pt solution was then impregnated over the $NiO/\delta\text{-}Al_2O_3$ and mixed ultrasonically under vacuum for 1.5 h. The resulting slurry involving two metals was dried overnight at 393 K and finally calcined at 773 K for 4 h.

3.3.4. Pretreatment

After calcination, the catalysts are in their oxide forms and usually inactive for the reactions. In order to obtain high catalytic activities, a pretreatment involving the reduction of the active metals from their oxide state to their metallic state is required prior to the reaction.

Elevated catalytic activities are possible if appropriate reduction procedures are developed for the reaction of interest. However, this requires temperature programmed reduction (TPR) studies to be conducted with several reducing agents. TPR studies have shown that reduction using pure hydrogen flow at 773 K for 4 h is a valid procedure for pretreating the catalysts above, although 873 K might also have been used for the monometallic Ni catalyst (Ma, 1995). Ma (1995) has also reported that during reduction, the water in the catalysts may cause their premature sintering, leading to a deactivation before the reaction. Considering these issues, the following stepwise reduction procedure was used for all the catalysts used in all of the experiments (Ma, 1995):

After placing the catalyst into the constant temperature zone of the microreactor, N_2 was allowed to flow at 50 ml min^{-1} for 10 min. to remove oxygen from the system. The

gas flow was switched from N_2 to H_2 and the latter was set to flow at 20 ml min^{-1}. Reduction was started by heating the catalyst from room temperature to 423 K at a rate of 10 K min^{-1}. The temperature was kept constant at 423 K for 30 min. for the removal of adsorbed water. Third step involved heating from 423 K to 573 K at a rate of 5 K min^{-1}, followed by a 30 min isothermal segment at 573 K for the removal of crystalline water. The temperature was then increased from 573 K to 773 K at a rate of 2 K min^{-1} and finally kept constant at 773 K for 4 h. After reduction, the system was allowed to cool down to ca. 423 K under H_2 flow. Below this temperature, the gas flow was switched from H_2 to N_2 and the latter was allowed to flow at a small flow rate, e.g. 3 ml min^{-1} overnight to sweep H_2 from the system.

3.4. Catalyst Characterization

Total surface area measurements were performed using the multi-point BET method. The equations used in the total surface area calculations are given as follows:

$$\frac{P}{V(P_o - P)} = \frac{1}{cV_m} + \left[\frac{(c-1)}{cV_m}\right]\frac{P}{P_o} \tag{3.1}$$

$$S = \frac{AV_mA_g}{M} \tag{3.2}$$

In Equations (3.1) and (3.2), A is the Avogadro's number (6.02×10^{23}), A_g is the area of an individually adsorbed molecule, which is 16.2×10^{-20} m^2 for nitrogen, M is the molar volume of the gas, and V_m is the monolayer volume. A straight line results for P/P_o values from about to 0.05 to 0.25 when experimental data are plotted as $P/V(P_o-P)$ on the ordinate against P/Po on the abcissa. Relative pressures within the prescribed range are typically obtained with gas compositions between about five per cent and 25 per cent nitrogen with the remainder being inert helium.

The sample was first dried and degassed under nitrogen flow for two and a half hours at 523 K and then cooled to room temperature. The Flowsorb 2300 unit was calibrated by injecting one milliliter of nitrogen at ambient conditions, calculating the

corresponding volume of gas at standard conditions and setting the instrument to indicate thereafter adsorbed and desorbed gas volumes at standard conditions. Then a flow of the measuring gas (five per cent to 25 per cent nitrogen-helium mixture) was allowed to pass over the sample at liquid nitrogen temperature of 77.4 K and equilibrate. After the adsorption equilibrium was established as indicated by the threshold indicator, the temperature of the sample was raised to ambient temperature and the amount of nitrogen desorbed was measured by the thermal conductivity detector. This nitrogen adsorption-desorption procedure was repeated at least four times with different nitrogen-helium gas mixtures. The total surface area was calculated from Equations (3.1) and (3.2) by using a software supplied by Micromeritics Inc. together with the Flowsorb 2300 unit.

In order to investigate the formation of the carbonaceous deposits over the catalysts used in the reaction tests, thermogravimetric analysis (TGA) technique was used. For this purpose a Mettler-Toledo TGA/SDTA851^e system was employed. The system was controlled by Star^e software which could also be used for conducting a number of post-experimental evaluations. In a typical experiment, catalyst sample of about 7 mg was put into a 1 ml aluminum oxide crucible which was placed on the sample holder of balance. The balance housing was thermostatted for ensuring good reproducibility of the weight signal. Oxygen and Argon were used as purge and protective gases, respectively. The protective gas was employed in order to prevent possible damages that might be caused by reactive gases which could be produced by the chemical reactions. The temperatures of the sample and the furnace were measured by platinum and platinum plus 13 per cent rhodium thermocouples (R-type).

3.5. Reaction Tests

3.5.1. Blank Tests

Blank tests were conducted to ensure that the material of construction, glass-wool and δ-alumina (used as inert material within the catalyst bed) did not interfere with the reaction test outputs. The results indicated that the items above were inactive under the conditions used in the reaction experiments.

3.5.2. Oxidation of Propane and n-Butane over Pt/δ-Al_2O_3, Ni/δ-Al_2O_3 and Pt-Ni/δ–Al_2O_3 Catalysts

Reaction tests were conducted using stainless steel tubular down-flow microreactors. In all experiments, 50 mg of fresh catalyst was diluted with 200 mg of inert δ-Al_2O_3. The temperature of the catalyst bed was controlled by a programmable temperature controller with ±0.1 K sensitivity. The catalysts were pretreated through reduction by 20 ml min^{-1} pure hydrogen flow at 773 K for 4 h as described in Section 3.3.4. The reaction temperature was increased at a rate of 1 K min^{-1}, starting from an initial temperature ranging between 378 K and 463 K to a final temperature ranging between 603 K and 678 K, depending on the fuel:oxygen ratio and the catalyst of interest. It is worth noting that 678 K is not exceeded in the temperature program due to the possibility of coke formation via thermal pyrolysis of the hydrocarbons.

The flow of the feed gases - C_3H_8, n-C_4H_{10}, dry air and N_2 at high purity (>99.5%) – were measured and controlled by Omega 5850 Series mass flow controllers. Hydrocarbon flow was kept at 1 ml min^{-1}, dry air (oxidant) and N_2 (balance gas) flow rates were adjusted according to the assigned fuel:oxygen ratio ($0.48<C_3H_8:O_2<2.00$; $0.37<n\text{-}C_4H_{10}:O_2<2.12$). The total inlet flow was kept constant at 140 ml min^{-1}. High flow rate together with catalyst dilution mentioned above were particularly preferred to eliminate any temperature rises and hot-spots that would occur due to the exothermicity of oxidation reactions.

Product samples were collected, and analyzed as much as possible during the reaction, to obtain conversion values at different temperatures. Parallel operation of the gas chromatographs was initiated by diverting the product stream initially to GC-8A using valve 4c. After injection of the sample collected in the sample loop of GC-8A, the product flow was then diverted to GC-14A followed by charging in the sample loop and sample injection into the Porapak Q column. This procedure was repeated in the successive product sampling and analysis periods. After the reaction, the reactor was bypassed by diverting the feed flow using valve 4a (Figure 3.3) and the feed analysis was conducted. Details of the analysis conditions are given in Table 3.4. The blank tests confirmed that the stainless steel reactor, alumina and glaswool were inert at the reaction conditions.

3.5.3. Steam Reforming of n-Butane over Ni/δ-Al_2O_3 and Pt-Ni/δ-Al_2O_3 Catalysts

In steam reforming experiments, 100 mg of fresh catalyst was placed into the constant temperature zone of the microreactor. The catalysts were pretreated through reduction by 20 ml min^{-1} pure hydrogen flow at 773 K for 4 h as described in Section 3.3.4. After reduction, the temperature of the zones 5a and 5b (Figure 3.3) were raised to 333 K and 423 K, respectively. Zones 5c and 5d were heated up to 398 K. The temperature of reactor was also raised to the reaction temperature (578 K, 598 K, 648 K or 678 K) together with inert nitrogen flow of 50 ml min^{-1}. After reaching the pertinent reaction temperature, flow was decreased and nitrogen was trapped within the reactor by diverting the flow to the bypass vent using valve 4b and by closing the valves 3b and 3c (Figure 3.3). The feed gases – n-butane, steam and nitrogen – were then allowed to flow through the bypass vent line for three hours for ensuring steady-state homogeneous flow. In all experiments, n-butane, steam and nitrogen flow rates were kept at 1 ml min^{-1}, 12 ml min^{-1} and 37 ml min^{-1}, corresponding to a total inlet flow of 50 ml min^{-1}. The n-butane and steam flow rates were selected such that the steam:carbon ratio was equal to three, since it is recommended to keep this ratio greater than 2.5 to minimize coke formation during steam reforming over Ni catalysts (Rostrup-Nielsen, 1984). The maximum reaction temperature, 678 K, is decided after preliminary propane steam reforming tests, which indicated heavy coke formation at 698 K.

The reaction was started after three hours by diverting the feed flow into the reactor. Product samples were collected and analyzed at 0.5 h, 2 h, 3 h and 4 h after the initiation of the reaction. The rest of the gas chromatograph operations were conducted with the strategy explained in the last paragraph of Section 3.5.2.

3.5.4. Experiments for Evaluation of the Kinetics of Steam Reforming of n-Butane over Pt-Ni/δ-Al_2O_3 Catalyst

The experimental strategy employed in these sets of experiments were basically the same as explained in Section 3.5.3. However, several factors should be taken into account in evaluating intrinsic reaction rates, i.e. the conversions should be kept at low values, e.g. less than 15 per cent, external and internal heat/mass transfer resistances should be

minimized by selecting high flow rates and small particle sizes, respectively, axial dispersion should be eliminated and isothermicity of the catalyst bed should be ensured. Therefore the operating conditions were selected by considering these factors. The summary of the conditions employed in all experiments is presented in Table 3.6.

In order to keep conversions at low values, small amounts of catalyst varying between 25 mg and 35 mg were put into the reactor. The total inlet flow was kept constant at 100 ml min^{-1} and a 45-60 mesh (250 – 425 μm) particle size was selected. These conditions were reported to be sufficient for the elimination of the external and internal transport resistances, respectively (Akın, 1996; Aksoylu, 1997). In order to minimize axial dispersion, the catalyst bed was diluted using inert δ-Al_2O_3 such that the total bed weight remained constant at 250 mg. The elimination of axial dispersion requires the following criteria to be satisfied (Kapteijn *et al.*, 1999):

$$D_t/D_p > 10 \tag{3.3}$$

$$L_b/D_p > 50 \tag{3.4}$$

The first criterion was satisfied, since the ratio of the reactor diameter ($D_t = 4x10^{-3}$ m) to the particle diameter ($D_p = 3.4x10^{-4}$ m – average value) was equal to12. The addition of inert δ-Al_2O_3 increased the bed length ($L_b = 2.3x10^{-2}$ m), which made the ratio of bed length to particle diameter equal to 68, and helped in satisfying the second criterion. Based on these values, it was concluded that axial dispersion was not significant under the conditions selected. For the different amounts of catalyst used, the dilution ratio defined as the ratio of the volume of inert material to the volume of the catalyst was always between 1 and 10. This criterion indicated that the amount of dilution was sufficient to ensure the isothermicity of the catalyst bed.

Based on the results of the steam reforming experiments described in Section 3.5.3, the temperature at which the reaction rates were measured at different initial concentrations was selected to be 648 K. In order to evaluate the activation energy of the reaction, experiments were also conducted at 603 K, 618 K, 633 K, 641 K, 658 K and 668 K at a single initial composition value. Evaluation of the reaction rate at a single initial

concentration required two experiments to be conducted at different residence times, i.e. W/F_{AO} values (A: n-butane), which were achieved by using different catalyst quantities.

Table 3.6. Summary of the experimental conditions employed

	Surface ignition experiments	Steam reforming experiments	Steam reforming kinetics experiments
Feed gases	C_3/n-C_4, dry air, N_2	n-C_4, H_2O, N_2	n-C_4, H_2O, N_2
Total flow, ml min^{-1}	140	50	100
Hydrocarbon flow, ml min^{-1}	1.0	1.0	1.0 - 2.5
Hydrocarbon:O_2	$0.48<C_3:O_2<2.00$ $0.37<$n-$C_4:O_2<2.12$	-	-
Steam:Carbon	-	3.0	1.2 – 3.0
Temperature, K	$378<T_i<463 \rightarrow$ $603<T_f<678$ (1 K min^{-1})	578, 598, 648, 678	603, 618, 633, 641, 648, 658, 668
Pressure, atm	~1.0	~1.0	~1.0
Bed weight, mg	50 (cat.) + 200 (al.)	100 (cat.)	25 (cat.) + 225 (al.) 35 (cat.) + 215 (al.)

4. MODELING STUDIES FOR SIMULATION OF HYDROCARBON FUEL CONVERSION TO HYDROGEN

This section describes the algorithms and mathematical models developed for simulating catalytic hydrogen production within the context of a generalized fuel processor/fuel cell operation. In addition, fixed-bed reactor operation is considered in detail together with the reactor models to describe the dual-catalyst autothermal hydrogen production quantitatively. The reactions and rate laws that appear in Section 2 are numbered here again to make them compatible with the indicial notation.

4.1. Introduction

The replacement of internal combustion engines with electric motors associated with fuel cells is an attractive alternative for eliminating pollutants and for meeting stringent clean air standards required by the recent legislative regulations (Cooper, 1994; Heck and Farrauto, 1995). Apart from the use of fuel cells in transportation, stationary power generation for applications such as hospitals and residential use is another emerging market for the use of fuel cells (Gray and Petch, 2000; Ralph and Hards, 1998).

The most promising fuel cells for vehicular and small-scale stationary applications would seem to be the ones equipped with proton exchange membranes (PEM) using hydrogen as the fuel (Ralph and Hards, 1998). Problems associated with the production, distribution and on-board storage of the hydrogen gas have led to the consideration of compact and efficient devices, i.e. fuel processors to convert available fuels to hydrogen (Golunski, 1998; Hoogers and Thompsett, 1999; Jiang *et al.*, 1995; Ralph and Hards, 1998; Trimm and Önsan, 2001). Among these fuels, methanol has been considered in some detail (Jiang *et al.*, 1995). However, the production capacities and the distribution network for methanol are not as extensive as for the other fuels, which makes the generation of hydrogen from natural gas, liquefied petroleum gases (LPG), gasoline or diesel attractive alternatives. Diesel has a high tendency of coke formation and is not suitable (Jamal and Wyszynski, 1994) but conversion of the other fuels is possible.

Hydrogen production that will ensure optimal fuel cell operation requires investigation of the conversion of different fuels via alternative routes. In the following sections, hydrogen generation from methane (model hydrocarbon for natural gas), propane (model hydrocarbon for LPG), isooctane (model hydrocarbon for gasoline) and methanol by two different fuel conversion mechanisms – the combined oxidation/steam reforming, i.e. indirect partial oxidation, and the one-step, direct partial oxidation are considered. For this purpose, algorithms, mathematical models and software are developed to simulate complete fuel processor/PEM fuel cell operations specialized for different conversion routes, hydrocarbons and catalysts in order to obtain hydrogen yields as functions of quantities of water and fuel fed into the systems. Methane is selected as the descriptive hydrocarbon to introduce the process and the model equations.

4.2. The Basis of the Fuel Processor/Fuel Cell Operation

4.2.1. Hydrogen Production in Fuel Processing Unit

4.2.1.1. Indirect Partial Oxidation. Methane, which is the model hydrocarbon for natural gas, can be converted to hydrogen on a bimetallic Pt-Ni catalyst (Ma and Trimm, 1996) by indirect partial oxidation, which is a combination of total oxidation (TOX), steam reforming (SR) and water-gas shift (WGS) reactions:

$$CH_4 + 2O_2 = CO_2 + 2H_2O, \quad \Delta H_1^o = -802.3\,kJ\,mol^{-1} \tag{4.1}$$

$$CH_4 + H_2O = CO + 3H_2, \quad \Delta H_2^o = 206.2\,kJ\,mol^{-1} \tag{4.2}$$

$$CO + H_2O = CO_2 + H_2, \quad \Delta H_3^o = -41.2\,kJ\,mol^{-1} \tag{4.3}$$

This operation, running in an adiabatically operating fixed-bed reactor, is autothermal in character, i.e. heat and part of the steam required by the endothermic steam reforming is supplied by the exothermic total oxidation. The catalyst, Pt-Ni/δ-Al_2O_3, can safely operate at temperatures up to 1100 K, above which thermal sintering is significant. Careful control of the bed temperature is therefore required to prevent catalyst deactivation

due to sintering. In addition, coke formation is likely to occur under steam reforming conditions by several mechanisms (Trimm, 1999), but it can be eliminated by keeping the steam/carbon ratio around 2.5 (Rostrup-Nielsen, 1984). This ratio is different from the water/methane ratio which is related with the water and methane at the system inlet. The effect of total oxidation is taken into account in the steam/carbon ratio:

$$\text{steam/carbon ratio} = \frac{\text{moles of water fed} + \text{moles of water produced by TOX}}{\text{moles of methane fed} - \text{moles of methane consumed in TOX}} \quad (4.4)$$

Steam produced by total oxidation is usually not sufficient to meet the above requirements, and additional water should be fed into the partial oxidation reactor (Figure 4.1) to control the catalyst bed temperature and to prevent carbon formation. This will also change the WGS equilibrium in the direction of increasing hydrogen yield and will remove an important portion of the CO which significantly deactivates the Pt-based anode of the PEMFC. However, this reduction in CO content is usually insufficient, and the use of a water-gas shift converter for further removal of CO is still required (Figure 4.1).

Sulphur is present in natural gas in the form of simple compounds such as H_2S, COS, $(C_2H_5)_2S$, which are usually added to act as odorants. However, their presence can affect steam reforming in indirect partial oxidation as well as the operation of other catalytic units by reducing the lifetime of the pertinent catalysts (Dicks, 1996; Rostrup-Nielsen, 1984). In order to eliminate catalyst deactivation, a sulphur trap, packed with a mixture of cobalt and molybdenum oxides supported on alumina and ZnO particles (Dicks, 1996), can be placed in front of the natural gas feed stream, as shown in Figure 4.1. The use of sulphur-free natural gas is another solution which eliminates the requirement of a sulphur trap.

The first step in indirect partial oxidation is the initiation of catalytic combustion called surface ignition, which is the direct indication of the energy needed to be supplied for triggering the fuel conversion. Surface ignition is also important for the heat management of the fuel processor/fuel cell system and is dictated quantitatively by the light-off temperatures. Light-off temperature is defined as the value at which 10 per cent of the oxidation conversion of a hydrocarbon is obtained (Ma *et al.*, 1996). Table 4.1 summarizes the light-off temperatures for the hydrocarbons of interest.

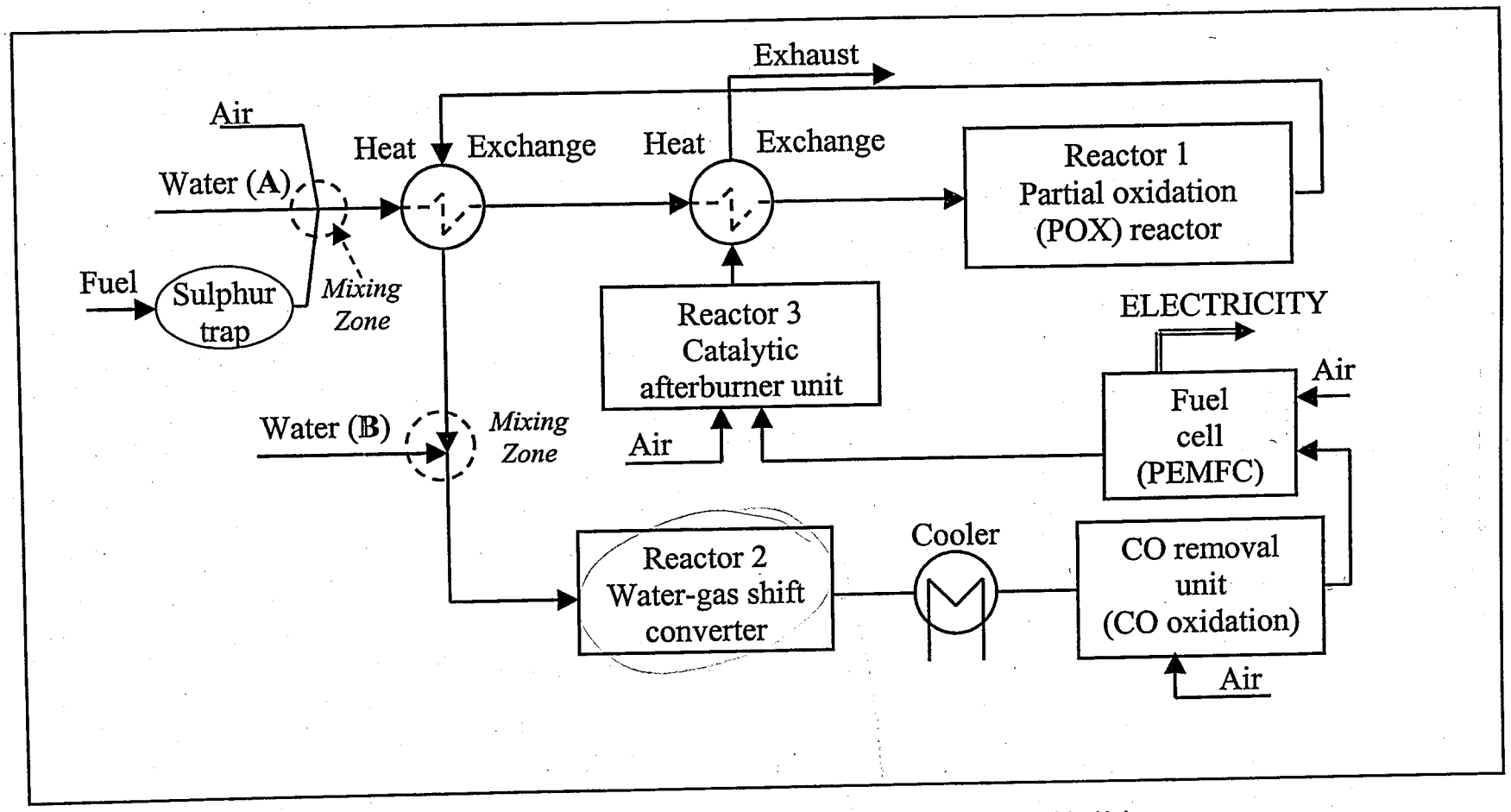

A: location of water injection in indirect partial oxidation; B: location of water injection in direct partial oxidation

Figure 4.1. Fuel processor/fuel cell operation

Table 4.1. Light-off temperatures

Hydrocarbon	Light-off Temperature (K)	Catalyst	Reference
Methane	673	Pt/Al_2O_3	Ma *et al.*, 1996
Methanol	298	Pt/Al_2O_3	Jiang *et al.*, 1995
Propane	442	Pt/Al_2O_3	Ma *et al.*, 1996
Octane	513	Pt/Al_2O_3	Trimm and Önsan, 2001

4.2.1.2. Direct Partial Oxidation. An alternative route for catalytic hydrogen production is direct partial oxidation (dry oxidation) and can be represented by the following reaction:

$$CH_4 + \tfrac{1}{2}O_2 = CO + 2H_2, \quad \Delta H_5^o = -35.7\ \text{kJ mol}^{-1} \tag{4.5}$$

Hickman and Schmidt (1992) reported 80 per cent methane conversion on Pt-monoliths at temperatures around 1373 K and at contact times between 10^{-4} and 10^{-2} s. Thus, in contrast to indirect oxidation, mass transfer limitations are much more significant than kinetics in the direct conversion of methane (Hickman and Schmidt, 1992). These operating conditions (Table 4.2) do not allow steam reforming, water-gas shift and carbon formation mechanisms, which require much higher residence times to run.

In order to make use of the water-gas shift reaction, a separate water-gas shift converter is placed after the partial oxidation reactor, as shown in Figure 4.1. In this operation, water is injected at the reactor exit, just after the sensible heat recovery of the hot exit gas stream and before the water-gas shift converter (Figure 4.1). Water addition adjusts the water-gas shift equilibrium to reduce the CO level to values suitable for the operation of the CO removal unit and to increase the H_2 yield. Moreover, water injection further cools down the gas stream after heat recovery and satisfies the low temperature requirements of the shift converter, CO removal unit and the PEM fuel cell.

Table 4.2. Operating conditions used in direct partial oxidation of various fuels

Fuel	Conversion (per cent)	Temperature (K)	Residence Time (ms)	Catalyst	Reference
Methane	80	1373	~1-5	Pt-monolith	Hickman and Schmidt, 1992
Methanol	30	1000	-	Rh-gauze	Zum Mallen and Schmidt, 1996
Propane	95	1273	~5	Pt-monolith	Huff and Schmidt, 1994
Octane[1]	93	1243	~5	Pt-monolith	Dietz III *et al.*, 1996

[1] The behavior of n-hexane in Dietz III *et al.*, 1996 is assumed to be the same as that of octane

4.2.2. Water-Gas Shift Converter

The water-gas shift converter is a separate fixed-bed reactor placed after the hydrogen generator in order to remove CO from the H_2-rich stream. It is packed with Cu/ZnO catalyst and operates at relatively low temperatures around 473 K. In indirect partial oxidation, water-gas shift runs simultaneously with methane steam reforming and removes most of the CO produced by the latter reaction. In dry oxidation, however, CO is a major product, but can be removed significantly in a single shift conversion when sufficient quantities of water are supplied. Moreover, energy integration allows temperature reduction down to low-temperature shift ranges (ca. 473 K). Therefore, another high temperature shift converter is not required in either operation.

The water-gas shift reaction is slightly exothermic and results in temperature elevations. Therefore, a cooler is employed in order to reduce the shift converter exit temperatures down to the operating ranges of the selective CO oxidation unit and the PEMFC.

4.2.3. CO Removal Unit

CO is a poison for the anode catalyst of the PEMFC, since it strongly chemisorbs onto Pt and deactivates the catalyst for the anode reaction (H_2 oxidation). The Pt-based anode catalyst can tolerate a maximum of 40 ppm CO (Golunski, 1998), which cannot be achieved by a single water-gas shift converter. Hence, the CO concentration within the hydrogen rich stream should further be reduced by a separate operation. Moreover, this removal operation should work efficiently at low temperatures, since the PEM fuel cell operates at a temperature range of 333 K-363 K.

Several methods such as selective oxidation of CO to CO_2, methanation of CO and the use of hydrogen diffusion membranes are proposed to meet the above-mentioned criteria (Ralph and Hards, 1998; Trimm and Önsan, 2001). During methanation, CO_2 may be converted along with CO, resulting in considerable H_2 loss. The use of Pd-based membranes requires high-pressure differentials and high temperatures both of which can significantly reduce the overall efficiency. All these factors make the selective oxidation method the optimal option for CO removal.

Trimm and Önsan (2001) have reported the details of selective CO oxidation at low temperatures, indicating a precious metal based catalyst such as Pt to exhibit optimal performance.

4.2.4. Fuel Cell and Catalytic Afterburner Unit

The proton exchange membrane fuel cell (PEMFC) is the unit producing the desired electrical power by converting the chemical energy stored within hydrogen into electricity. The PEMFC operation is represented by the following reactions occurring on the Pt-based cathode and anode at temperatures between 333 K and 363 K (Ralph and Hards, 1998):

Anode reaction: $$H_2 = 2H^+ + 2e^- \quad (4.6)$$

Cathode reaction: $$\tfrac{1}{2}O_2 + 2H^+ + 2e^- = H_2O \quad (4.7)$$

The PEMFC rejects about 25 per cent of the hydrogen that is fed into it (Golunski, 1998). There is also some unconverted methane within the gas mixture. These components – hydrogen and methane – are oxidized in a separate, adiabatic afterburner unit packed with a Pt-based catalyst to enable energy recovery within the entire system and to exhaust a clean gas free of hydrocarbons (Figure 4.1):

$$H_2 + \tfrac{1}{2}O_2 = H_2O, \quad \Delta H_8^o = -241.8\,kJ\,mol^{-1} \tag{4.8}$$

$$CH_4 + 2O_2 = CO_2 + 2H_2O, \quad \Delta H_1^o = -802.3\,kJ\,mol^{-1} \tag{4.1}$$

Part of the sensible heat of the hot afterburner effluent stream is then recovered for providing additional energy to the feed stream in order to trigger the partial oxidation conversion (Figure 4.1).

4.2.5. Energy Integration

In both indirect and direct partial oxidation mechanisms, heat is required to overcome the low reactivity of methane, to evaporate the extra liquid water fed into the system and to sustain the H_2-generating reactions (Reactions (4.2) and (4.5)). On the other hand, the PEMFC, and hence the CO removal unit and the water-gas shift converter, operate at relatively low temperatures. Therefore, energy integration becomes vital for optimizing these operations.

One energy source is the high sensible heat of the partial oxidation reactor exit stream, which can be recovered either by heat exchange with the cold inlet stream or by water injection, as proposed in the direct route (Figure 4.1). Such energy recovery also helps in reducing the temperature of the gas mixture to the fuel cell operating ranges. The hot exit stream from the catalytic afterburner is another energy source that contributes to the overall heat recovery of the operation (Figure 4.1).

4.3. Modeling and Simulation of Fuel Processor/Fuel Cell Operation

In order to evaluate the product yields as functions of water/methane and methane/oxygen ratios, computational algorithms specific for the two partial oxidation mechanisms are developed. In these algorithms, the aforementioned process considerations are taken into account in the light of the reaction kinetics. A methane feed of 1 kmol h^{-1} is taken as basis in both systems.

4.3.1. Indirect Partial Oxidation

As mentioned in Section 4.2.1.1, this route is based on steam reforming, the heat needed being supplied by total oxidation of part of the fuel. Since both steam and the fuel must be present in the POX reactor to facilitate hydrogen production, fuel, air and water are injected at point A (Figure 4.1) and no further injection is needed. In addition, most of the CO produced by steam reforming is removed by the water-gas shift reaction within the partial oxidation reactor such that the exit CO concentration is less than two mole percent – a level which is appropriate for the selective CO oxidation unit (Golunski, 1998). Therefore the use of a separate water-gas shift converter and a cooler is not required. The iterative algorithm developed for indirect partial oxidation assumes that the partial oxidation reactor operates adiabatically:

i. TOX (Reaction (4.1)) is very fast compared with steam reforming (Reaction (4.2)) and water-gas shift (Reaction (4.3)). Its effect is dictated by the degree of conversion achieved. Hence, a conversion value is assumed for the TOX. To illustrate, methane/oxygen ratios in the feed should be above the stoichiometric value (0.5) in order to leave some methane for steam reforming.
ii. A value is assumed for the amount of water fed into the reactor, thus specifying the molar water/fuel ratio at the inlet.
iii. For assumed values of oxidation conversion and water injected into the POX reactor, the molar flow rates of the components after total oxidation and the maximum bed temperature (ca. 1100 K for methane, propane and octane, ca. 600 K for methanol) are used as the initial conditions in order to integrate the differential mole and energy

balances, i.e. solve the one-dimensional pseudohogeneous reactor model (see Section 4.4 for details about reactor models) along a one kg bed of catalyst:

$$\frac{dF_{j,1}}{dW} = \sum_i (\nu_{ij})(-r_{ij}) \tag{4.9}$$

$$\frac{dT_1}{dW} = \frac{\sum_i (-\Delta H_{i,T_1})(-r_i)}{\sum_j F_{j,1} c_{p,j}} \tag{4.10}$$

$$\text{At } W = W_o, F_{j,1}^{sr,o} = F_{j,ox}; T_1^{sr,o} = T_{max} \tag{4.11}$$

In Equations (4.9)-(4.11), $c_{p,j}$ is the temperature dependent gas-phase heat capacity of component j in kJ kmol^{-1} K^{-1}, $F_{j,1}$ is the molar flow rate of component j in Reactor 1 in kmol h^{-1}, $F_{j,ox}$ is the molar flow rate of component j after total oxidation (Reaction (4.1)) in kmol h^{-1}, $\Delta H_{i,T_1}$ is the heat of Reaction i at temperature T_1 in kJ kmol^{-1}, $-r_i$ is the rate of Reaction i in kmol kgcat^{-1} h^{-1}, T_{max} is the maximum bed temperature in K, W_o is the initial value of the catalyst weight in kg and ν_{ij} is the stoichiometric coefficient of component j in reaction i. $F_{j,1}^{sr,o}$ and $T_1^{sr,o}$ are the initial molar flow rate of component j in kmol h^{-1} and temperature of the gas mixture just before steam reforming (after total oxidation) in K, respectively. The steam reforming rate laws used in Equations (4.10) and (4.11) are given in Table 4.3. It is worth noting that, 1100 K is the temperature above which thermal sintering deactivates the Ni catalyst driving methane, propane and octane steam reforming (Rostrup-Nielsen, 1984). Similarly, Cu/ZnO catalyst, which drives methanol steam reforming, is thermally sintered above 600 K (Wainwright and Trimm, 1995).

Water-gas shift is reported to be fast on Ni catalysts during steam reforming of methane, propane and octane (Rostrup-Nielsen, 1984). Therefore the water-gas shift reaction is considered to be at equilibrium along with the kinetics of the steam reforming reaction. This requires the simultaneous solution of the differential mole

and energy balance equations with the initial conditions given in Equations (4.9)-(4.11) and the algebraic, nonlinear water-gas shift equilibrium expression:

$$K_3 = \frac{P_{CO_2} P_{H_2}}{P_{CO} P_{H_2O}} \tag{4.12}$$

The value of the reaction equilibrium constant in Equation (4.12), K_3, at different temperatures is calculated using the integrated form of the van't Hoff equation (see Appendix D). In Equation (4.12), P_j is the partial pressure of component j in atm. In contrast with the steam reforming of other fuels, the kinetics of the water-gas shift reaction on Cu/ZnO catalyst, quantified by the second kinetic expression given in Table 4.4, is considered instead of its thermodynamic equilibrium during methanol steam reforming, whose rate law is given in Table 4.3.

iv. The temperature at the exit of the catalytic afterburner, $T_{3,ex}$, is calculated from the following energy balance:

$$q_{3,1} = F_{H_2,FC} \Delta H_{8,T_3^o} \tag{4.13}$$

$$q_{3,2} = \sum_j F_{j,3mid} \int_{T_3^o}^{T_{LO}} c_{p,j} dT \tag{4.14}$$

$$q_{3,3} = F_{CH_4,1ex} \Delta H_{1,T_{LO}} \tag{4.15}$$

$$q_{3,4} = \sum_j F_{j,3ex} \int_{298}^{T_{3,ex}} c_{p,j} dT \tag{4.16}$$

$$\sum_{m=1}^{4} q_{3,m} = 0 \tag{4.17}$$

Table 4.3. Kinetic expressions for the steam reforming reactions

Reaction	Rate expression (kmol kgcat^{-1} h^{-1})	Catalyst	Reference
$CH_4 + H_2O = CO + 3H_2$	$-r_2 = k_2 \dfrac{P_{C_1}^{0.96} P_W^{-0.17}}{1+\theta P_H^{0.25}}$	Ni/MgO-Al_2O_3	Ma, 1995
$CH_3OH + H_2O = CO_2 + 3H_2$	$-r_2 = k_2 \dfrac{K_1'\left(\dfrac{P_M}{P_H^{1/2}}\right)\left(1-\dfrac{P_H^3 P_C}{K_2 P_M P_W}\right) C_{S_1} C_{S_2}}{\left(1+K_1'\left(\dfrac{P_M}{P_H^{1/2}}\right)+K_2' P_C P_H^{1/2}+K_3'\left(\dfrac{P_W}{P_H^{1/2}}\right)\right)\left(1+K_4'^{1/2} P_H^{1/2}\right)}$	Cu/ZnO-Al_2O_3	Peppley *et al.*, 1999
$C_3H_8 + 3H_2O = 3CO + 7H_2$	$-r_2 = k_2 \dfrac{P_{C_3}^{0.93} P_W^{-0.53}}{1+\theta P_H^{0.86}}$	Ni/MgO-Al_2O_3	Ma, 1995
$C_8H_{18} + 8H_2O = 8CO + 17H_2$ [2]	$-r_2 = k_2 \dfrac{P_{C_7}}{\left(1+252 P_{C_7}\dfrac{P_H}{P_W}+0.08\dfrac{P_W}{P_H}\right)^2}$	Ni/MgO	Rostrup-Nielsen, 1984

[2] The behavior of heptane in Rostrup-Nielsen, 1984 is assumed to be the same as that of octane.

C: carbon dioxide
CO: carbon monoxide
C_1: methane
C_3: propane
C_7: heptane
C_{S_1}, C_{S_2} : site concentrations
H: hydrogen
k_3: rate constant of steam reforming
K_2: equilibrium constant of methanol steam reforming
K'_m : adsorption coefficient, atm^{-1}
M: methanol
P_j : partial pressure of component j, atm
$-r_i$: rate of Reaction i
W: water
θ : empirical constant

Table 4.4. Kinetic expressions for the water-gas shift reaction

Reaction	Rate expression (kmol $kgcat^{-1}$ h^{-1})	Catalyst	Reference
$CO + H_2O = CO_2 + H_2$	$-r_3 = k_3 \dfrac{P_{CO}P_W\left(1-\dfrac{P_H P_C}{K_3 P_{CO} P_W}\right)}{\left(1+K'_{CO}P_{CO}+K'_W P_W+K'_C P_C+K'_H P_H\right)^2}$ [3]	$Cu/ZnO-Al_2O_3$	Amadeo and Laborde, 1995
	$-r_3 = k_3 \dfrac{K'_3\left(\dfrac{P_{CO}P_W}{P_H^{1/2}}\right)\left(1-\dfrac{P_H P_C}{K_3 P_{CO} P_W}\right)C_{S_1}^2}{\left(1+K'_1\left(\dfrac{P_M}{P_H^{1/2}}\right)+K'_2 P_C P_H^{1/2}+K'_3\left(\dfrac{P_W}{P_H^{1/2}}\right)\right)^2}$ [4]	$Cu/ZnO-Al_2O_3$	Peppley *et al.*, 1999
	$-r_3 = 0$ (Ni catalyses Reaction (4.3) to equilibrium)	Ni	Rostrup-Nielsen, 1984

[3] This rate law is used in simulating Reactor 2 (water-gas shift converter) operation in direct partial oxidation.
[4] This rate law is used to describe the kinetics of the water-gas shift reaction during methanol steam reforming only.

C: carbon dioxide
CO: carbon monoxide
C_{S_1} : site concentration
H: hydrogen
k_2: rate constant of Reaction 2
K'_m, K'_j : adsorption coefficient, atm^{-1}
K_3: equilibrium constant of Reaction (4.3)
M: methanol
P_j : partial pressure of component j, atm
$-r_i$: rate of Reaction i
W: water

In Equations (4.13)-(4.17), $F_{H_2,FC}$ is the molar flow rate of hydrogen rejected by the fuel cell in kmol h^{-1}, $F_{j,3mid}$ is the molar flow rate of component j just after the hydrogen combustion and before octane oxidation in kmol h^{-1}, $F_{CH_4,1ex}$ is the molar flow rate of methane remaining unconverted and leaving Reactor 1 in kmol h^{-1}, $F_{j,3ex}$ is the exit molar flow rate of component j leaving Reactor 3 in kmol h^{-1}, T_3^o is the inlet temperature to Reactor 3, which is equal to taken to be equal to 353 K, T_{LO} is the light-off temperature for methane in K, $T_{3,ex}$ is the exit temperature from Reactor 3 in K, $\Delta H_{8,T_3^o}$ and $\Delta H_{1,T_{LO}}$ are the heat released by Reactions (4.8) and (4.1) at temperatures T_3^o and T_{LO}, respectively in kJ mol^{-1}, $q_{3,1}$ is the exothermal heat released by hydrogen combustion in kJ, $q_{3,2}$ is the energy required to raise the temperature of the gas mixture after hydrogen oxidation from T_3^o to T_{LO} in kJ, $q_{3,3}$ is the exothermal heat released by octane combustion in kJ and $q_{3,4}$ is the sensible heat of the Reactor 3 exit stream in J.

v. The amount of injected water assumed in Step (ii) is checked by solving the energy balance around the partial oxidation reactor given in Equation (4.25) for the maximum catalyst bed temperature, T_{max}:

$$q_{1,1} = F_{CH_4,2}\Delta H_{2,T_{max}} \tag{4.18}$$

$$q_{1,2} = F_{H_2O,inj}\left(c_{PL,H_2O}(373-298)+\Delta H_{H_2O}^{vap}\right) \tag{4.19}$$

$$q_{1,3} = \left[\sum_j \left(F_{j,ox}\right)\int_{T_{LO}}^{T_{max}} c_{p,j}\,dT\right] \tag{4.20}$$

$$q_{1,4} = F_{CH_4,1}\Delta H_{1,T_{LO}} \tag{4.21}$$

$$q_{1,5} = -0.7\left[\sum_{j}\left(F_{j,1ex}\right)\int_{298}^{T_{1,ex}} c_{p,j}dT\right] \tag{4.22}$$

$$q_{1,6} = -0.7\left[\sum_{j}\left(F_{j,3ex}\right)\int_{298}^{T_{3,ex}} c_{p,j}dT\right] \tag{4.23}$$

$$q_{1,7} = F_{CO,3}\Delta H_{3,T_{1,ex}} \tag{4.24}$$

$$\sum_{m=1}^{7} q_{1,m} = 0 \tag{4.25}$$

In Equations (4.18)-(4.25), c_{PL,H_2O} is the liquid phase heat capacity of water in kJ kmol^{-1} K^{-1}, $F_{CH_4,1}$ and $F_{CH_4,2}$ are the amounts of methane converted in Reactions (4.1) and (4.2), respectively in kmol h^{-1}, $F_{CO,3}$ is the amount of CO converted in Reaction (4.3) in kmol h^{-1}, $F_{j,1ex}$ is the exit molar flow rate of component j from Reactor 1 in kmol h^{-1}, $\Delta H_{3,T_{1,ex}}$ and $\Delta H_{2,T_{max}}$ are the heat of Reactions (4.3) and (4.2) at temperatures $T_{1,ex}$ and T_{max}, respectively in kJ mol^{-1}, $\Delta H^{vap}_{H_2O}$ is the latent heat of evaporation of water in kJ kmol^{-1}, $q_{1,1}$ is the energy required by the steam reforming of methane in kJ, $q_{1,2}$ is the energy required for heating and evaporating the liquid water injected to Reactor 1 in kJ, $q_{1,3}$ is the energy required for heating the reaction mixture after oxidation from the light-off temperature to maximum bed temperature in kJ, $q_{1,4}$ is the energy generated by total oxidation of methane in kJ, $q_{1,5}$ is the energy recovered from the exit stream of Reactor 1 in kJ, $q_{1,6}$ is the energy recovered from the exit stream of Reactor 3 in J and $q_{1,7}$ is the energy generated by the water-gas shift reaction in kJ. Seventy per cent heat recovery from the exit streams of Reactors 1 and 3 is assumed in evaluating $q_{1,5}$ and $q_{1,6}$.

vi. Steps (ii-v) are repeated until the amount of water fed into the reactor, i.e. water/methane ratio, satisfying the maximum bed temperature criterion (T_{max} = 1100 ± 10 K) is obtained.

vii. The algorithm above is repeated for different values of the total oxidation conversions to obtain product yields as functions of methane/oxygen and water/methane ratios. A compact version of this algorithm is presented as a flow diagram in Figure 4.2.

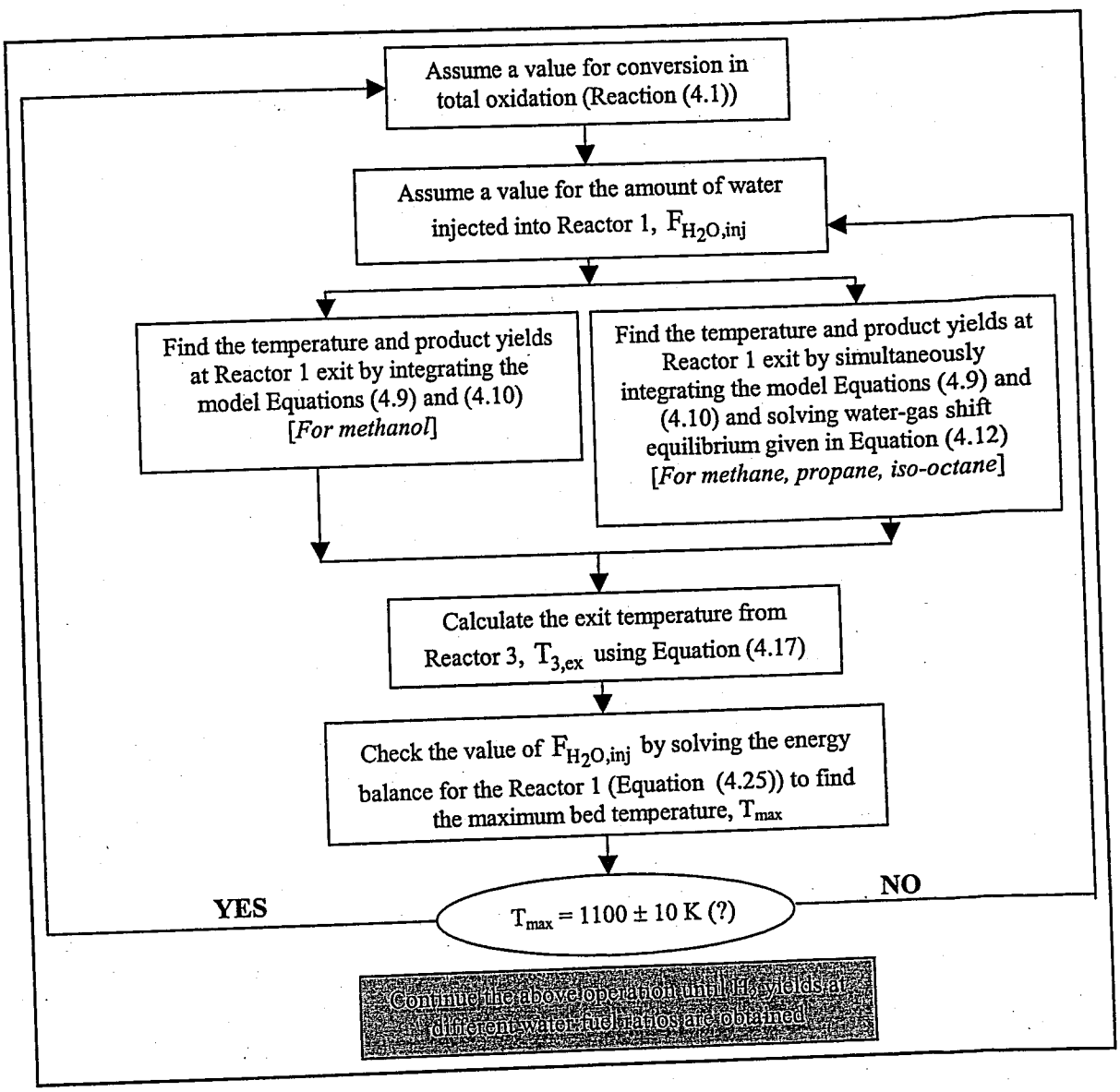

Figure 4.2. Flow diagram for the quantitative description of the indirect partial oxidation based fuel processing system

4.3.2. Direct Partial Oxidation

It has been shown that direct partial oxidation (Reaction (4.5)) is favored at high temperatures between 1000 K and 1373 K and at low residence times around 1-5 ms, using fuel:air ratios close to the stoichiometric values (Dietz III *et al.*, 1996; Hickman and Schmidt, 1992; Huff and Schmidt, 1994; Zum Mallen and Schmidt, 1996). The kinetics of the direct oxidation reaction over Pt monolith and Rh gauze catalysts are very fast and have not been investigated in detail for all fuels. Hence, results given in Table 4.2 have been used in the algorithm below to describe the conversions achieved in the direct oxidation reaction in Reactor 1 (Figure 4.1):

i. The composition of the gas mixture leaving Reactor 1 can simply be determined using the conversion values reported for different hydrocarbons given in Table 4.2. To illustrate, 0.20 moles of methane, 0.80 moles of carbon monoxide, 1.60 moles of hydrogen and 1.504 moles of nitrogen are obtained per mole of methane fed into the partial oxidation reactor in which 80 per cent octane conversion is achieved. Note that air is considered to be the limiting reactant and no oxygen leaves Reactor 1. In order to evaluate the temperature of this exit gas stream, $T_{1,ex}$, raised from 1373 K (temperature at which direct methane combustion becomes significant (Hickman and Schmidt, 1992)) by the exothermic heat released by Reaction (4.5), the following energy balance is used:

$$F_{CH_4,5}\Delta H_{5,1373} = \sum_j \left(F_{j,1ex}\right) \int_{1373}^{T_{1,ex}} c_{p,j}\,dT \qquad (4.26)$$

In the above equation, $F_{CH_4,5}$ is the amount of methane converted in Reaction (4.5) in mol/h, $\Delta H_{5,1373}$ is the heat of Reaction (4.5) at 1373 K and $T_{1,ex}$ is the temperature at the exit of the partial oxidation reactor in K.

ii. The exit gases, unconverted methane, hydrogen, carbon monoxide and nitrogen, are at high temperature and heat exchange with the inlet gases, methane and air, to Reactor 1 is essential. This will both help in increasing the temperature of the feed from 298 K to 1373 K and in reducing the temperature of the exit stream to water-

gas shift converter operating ranges. The following equation is used to represent this heat exchange as a reduction in the sensible heat of the hot exit stream:

$$(1-f)\sum_j \left(F_{j,1ex}\right) \int_{298}^{T_{1,ex}} c_{p,j}dT = \sum_j \left(F_{j,1ex}\right) \int_{298}^{T_{1,exhr}} c_{p,j}dT \qquad (4.27)$$

Solution of Equation (4.27) leads to the evaluation of the temperature of the gas stream after heat recovery, $T_{1,exhr}$, in K. In the above equation, f is the assumed fraction of sensible heat recovery.

iii. In the exit stream, there is a considerable quantity of carbon monoxide, whose level should be reduced since the gas is a poison for fuel cells as mentioned before. The selective oxidation unit that can reduce the carbon monoxide level below 40 ppm accepts a gas mixture with a carbon monoxide content of 2 mole per cent (Golunski, 1998; Trimm and Önsan, 2001). The latter criterion can be achieved using a low-temperature water-gas shift converter packed with $Cu/ZnO-Al_2O_3$ catalyst (Reactor 2 in Figure 4.1). Since these reactors can feasibly operate above 453 K (Amadeo and Laborde, 1995), 473 K is selected as the inlet temperature of Reactor 2. Therefore, in order to cool the gases further to 473 K, liquid water is injected at point B after heat exchange, as shown in Figure 4.1. This will also balance the water-gas shift equilibrium to favor hydrogen production and hence minimize carbon monoxide level. The amount of liquid water required for cooling the gas stream entering to Reactor 2 to 473 K, $F_{H_2O,inj}$, is evaluated by solving the energy balance given in Equation (4.28):

$$q_1 = F_{H_2O,inj}\left(c_{pL,H_2O}(373-298) + \Delta H^{vap}_{H_2O} + \int_{373}^{473} c_{p,H_2O}dT \right) \qquad (4.28)$$

$$q_2 = \sum_j \left(F_{j,1ex}\right) \int_{T_{1,exhr}}^{473} c_{p,j}dT \qquad (4.29)$$

$$\sum_{m=1}^{2} q_m = 0 \tag{4.30}$$

In Equations (4.28)-(4.30), q_1 is the energy required to evaporate and heat the injected water to 473 K in kJ and q_2 is the sensible heat needed to be given for reducing the gas mixture temperature from $T_{1,exhr}$ to 473 K in kJ.

iv. In order to find the flow rates of the components and the temperature of the gas mixture at Reactor 2 exit, the differential mole and energy balances given in Equations (4.31) and (4.32), respectively, together with the initial conditions given in Equation (4.33) are integrated along 0.25 kg of $Cu/ZnO-Al_2O_3$ catalyst:

$$\frac{dF_{j,2}}{dW} = (\nu_{2j})(-r_{2j}) \tag{4.31}$$

$$\frac{dT_2}{dW} = \frac{(-\Delta H_{2,T_2})(-r_2)}{\sum_j F_{j,2} c_{p,j}} \tag{4.32}$$

$$\text{At } W = 0, F_{j,2}^{o} = F_{j,1ex}\ (j \neq H_2O); F_{H_2O,2}^{o} = F_{H_2O,inj};\ T_2^{o} = 473\ K \tag{4.33}$$

In Equations (4.31)-(4.33), $F_{j,2}^{o}$ and $F_{j,2}$ are the molar flow rates of component j at the inlet and within Reactor 2, respectively, in kmol h^{-1}, $F_{H_2O,2}^{o}$ is the molar flow rate of steam at the inlet of Reactor 2 in kmol h^{-1}, $\Delta H_{3,T_2}$ is the heat of Reaction (4.3) at temperature T_2 in kJ mol^{-1}, $-r_3$ is the rate of Reaction (4.3) in kmol $kgcat^{-1}$ h^{-1} (the first rate law given in Table 4.4), T_2^{o} and T_2 are the gas mixture temperatures at the inlet and within Reactor 2, respectively, in K, W is the catalyst weight in kg and ν_{2j} is the stoichiometric coefficient of component j in Reaction (4.3).

v. The temperature at the afterburner exit is calculated as explained in Step (iv) of the indirect partial oxidation algorithm.

vi. In order to heat the feed gases injected at point A (Figure 4.1) from 298 K to the direct oxidation reaction temperature, 1373 K, the sensible heat generated in Reactor 3 can be used. The amount of this energy utilization can be determined in terms of the fraction of heat recovery from Reactor 3 effluent stream, f_3, using the relationship given below:

$$(1-f_3)\sum_j F_{j,3ex}\int_{298}^{T_{3,ex}} c_{p,j}dT = \sum_j F^o_{j,1}\int_{298}^{T_{RxN}} c_{p,j}dT \qquad (4.34)$$

In this equation, $F^o_{j,1}$ is the molar flow rate of component j in the feed stream, i.e. at injection point A (Figure 4.1) in kmol h^{-1} and T_{RxN} is the direct oxidation reaction temperature, which should be equal to 1373 K.

vii. Steps (ii-vi) are repeated for different values of the sensible heat recovery to obtain product yields as a function of water/fuel ratio. It is worth noting that the fuel/oxygen ratio at the inlet is fixed at the stoichiometric value for Reaction (4.5). A compact version of this algorithm is presented as a flow diagram in Figure 4.3.

4.3.3. Thermodynamic Predictions

In order to check whether the results based on kinetic data are within thermodynamic limits, the simulations are repeated using the same algorithms above with the following differences in respective steps:

- In indirect partial oxidation, a temperature rise occurs after light-off due to the high exothermicity of the total oxidation reaction. The maximum bed temperature is 1100 K, which is controlled by water injection into the reactor. Steam reforming, which runs after total oxidation, is endothermic, leading to a decrease in the bed temperature. The hydrogen rich effluent, whose composition is dictated by steam reforming and water-gas shift equilibria (Rostrup-Nielsen, 1984), leaves the reactor at a lower temperature. Therefore, solving steam reforming and water-gas shift equilibria simultaneously at the reactor exit conditions (eg. 850 K, 1.5 atm for methane) gives the product distribution at the reactor effluent stream:

$$K_2 = \frac{P_{CO} P_{H_2}^3}{P_{CH_4} P_{H_2O}} \tag{4.35}$$

$$K_3 = \frac{P_{CO_2} P_{H_2}}{P_{CO} P_{H_2O}} \tag{4.12}$$

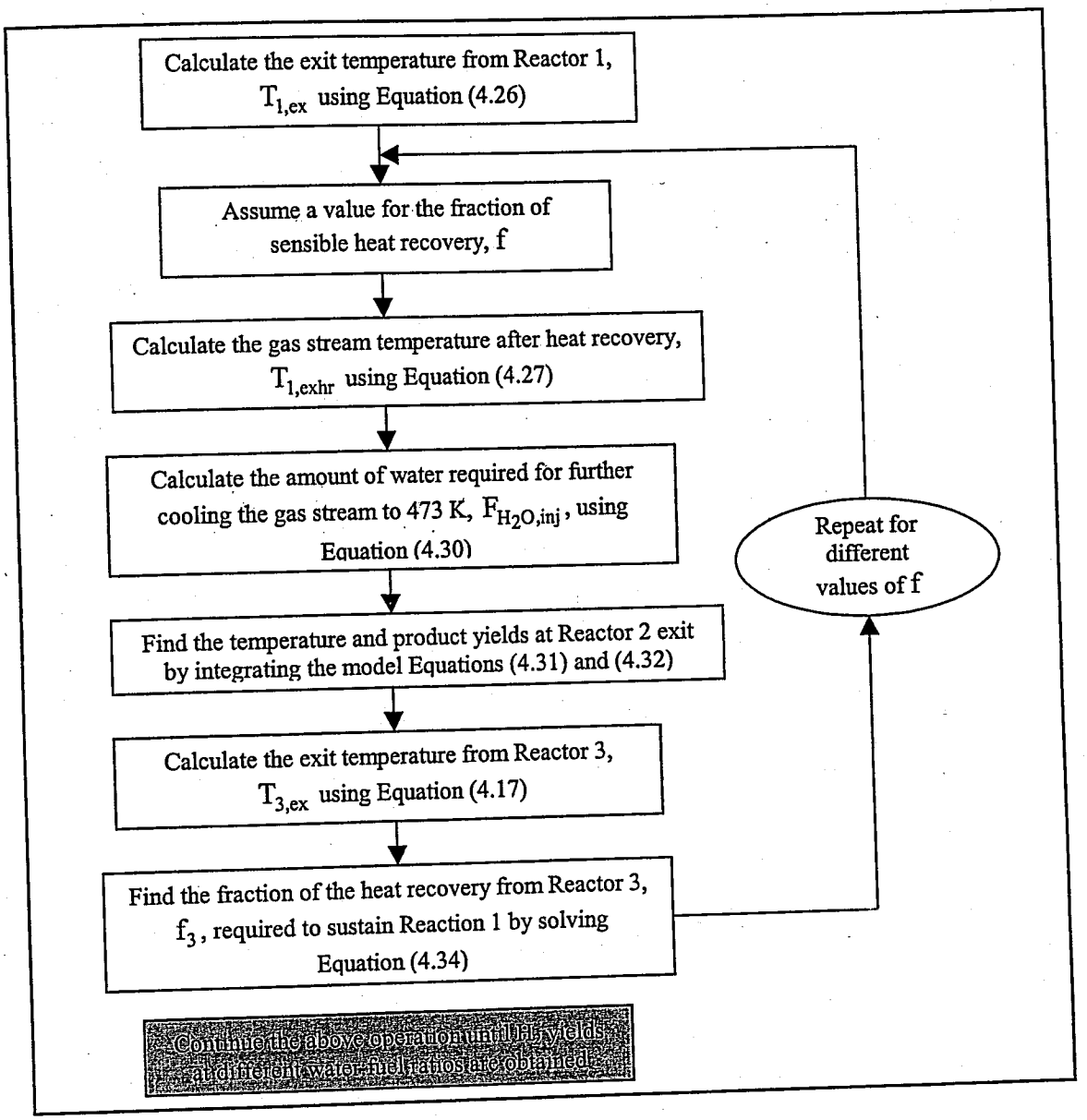

Figure 4.3. Flow diagram for the quantitative description of the direct partial oxidation based fuel processing system

Similarly, the product composition at the water-gas shift converter exit is determined by solving Equation (4.12) at 473 K.

- Due to the dominance of mass transfer effects over kinetics (Hickman and Schmidt, 1992) in direct partial oxidation, the reactor operation is considered to be the same as described in Section 4.3.2. The major difference is the use of Equation (4.12) instead of Equations (4.31)-(4.33) for calculating the product yields at the exit of the shift converter.

4.4. Fixed-Bed Operation and Reactor Models

The reactors employed in the fuel processor/fuel cell operation, (e.g. indirect partial oxidation reactor and water-gas shift converter) are fixed-bed in character. In this operation, the gas-phase reactants flow continuously into the reactor and pass over the solid catalysts on which reactions occur. The exit stream is composed of products, which are mostly formed on the catalyst surface and then desorbed into the gas phase, and unconverted reactants.

The reactor models used to describe the fixed-bed operation are the combination of equations and boundary conditions describing the conservation of mass, energy and momentum for the reaction system of interest. These models can be classified according to various criteria. Steady-state models do not consider time variations of operating parameters like temperature and species concentrations whereas unsteady-state models include time as a variable to be handled. One-dimensional models give the changes in the parameters as a function of a single spatial variable – the reactor length or the catalyst weight – whereas two-dimensional models consider radial variations in addition to axial changes. A third classification is related to the inclusion of external and/or internal transport resistances. Pseudohomogeneous reactor models describe the whole phenomenon in a single pseudo-entity, i.e. the bulk fluid gas phase and solid catalyst phase are assumed to possess the same temperature and species concentration throughout the operation. On the other hand, heterogeneous models include separate conservation equations for taking external and/or internal mass and/or heat transfer resistances into account (Froment and Bischoff, 1990; Rase, 1990).

Since the steady-state behavior of the systems is of interest, time is not considered as a variable in the models employed in this research. The reactors mentioned in the fuel processor/fuel cell unit in Section 4.2 are assumed to be in adiabatic. In addition, the autothermal hydrogen production (Section 4.5) is considered to take place in adiabatically operating fixed-bed tubular reactors. In adiabatic operation there is no heat transfer across the reactor walls, which greatly eliminates radial concentration and temperature gradients (Rase, 1990). Therefore, a two dimensional model, which includes partial differential conservation equations is not employed. Consequently, all the reactor simulations are conducted using one-dimensional steady-state fixed-bed reactor models.

Among one-dimensional models, the pseudohomogeneous one is the first choice, since it is possible to obtain the characteristic features of the reaction system at a relatively low cost of mathematical complexity. This model was used to simulate indirect partial oxidation and water-gas shift operation, as given in Equations (4.9)-(4.11) and (4.31)-(4.33), respectively. The pseudohomogeneous and the heterogeneous models are used to simulate the autothermal hydrogen production from natural gas, which is explained in much more detail in the rest of this chapter.

4.5. Autothermal Hydrogen Production

Steam reforming of light hydrocarbons run on nickel catalysts is the most widely employed route for hydrogen production due to its simple construction, operation and well-established technology. (Armor, 1999; Pena *et al.*, 1996; Rosen, 1991). On the other hand, the demand for considerable energy input resulting from the high endothermicity of the reforming reactions and the existence of catalyst deactivation turn out to be major drawbacks of catalytic steam reforming (Rostrup-Nielsen, 1984; Trimm, 1999).

In a recently proposed reaction system using integral microreactors, the endothermic heat and part of the steam required for methane steam reforming are balanced by exothermic methane oxidation in the presence of two different catalysts, Pt/δ-Al_2O_3 for total oxidation and Ni/MgO-Al_2O_3 for steam reforming (Ma and Trimm, 1996; Ma *et al.*, 1996). Increased hydrogen selectivities can thus be attained in autothermal operation. Moreover, the presence of two different catalysts introduces operational flexibility, i.e. the

reaction system can be adjusted in an object-oriented manner. For instance, the synthesis gas ratio may be adjusted for a specific end use such as Fischer-Tropsch synthesis.

4.5.1. Description of the Reaction System

The reaction system is an adiabatic fixed bed reactor in which Pt and Ni catalysts are packed in several configurations. During autothermal operation, oxidation, reforming and various side reactions exist within the reactor. Total oxidation of methane in the presence of air is catalyzed by the Pt/δ-Al_2O_3 catalyst and provides the exothermic heat to the system:

$$CH_4 + 2O_2 = CO_2 + 2H_2O, \quad \Delta H_1^o = -802.3\,kJ\,mol^{-1} \tag{4.1}$$

A large fraction of the endothermic heat is consumed by the steam reforming reactions:

$$CH_4 + H_2O = CO + 3H_2, \quad \Delta H_2^o = 206.2\,kJ\,mol^{-1} \tag{4.2}$$

$$CH_4 + 2H_2O = CO_2 + 4H_2, \quad \Delta H_2^o = 165.0\,kJ\,mol^{-1} \tag{4.36}$$

Water-gas shift and methane cracking are considered as side reactions running on the Ni/MgO-Al_2O_3 catalyst:

$$CO + H_2O = CO_2 + H_2, \quad \Delta H_3^o = -41.2\,kJ\,mol^{-1} \tag{4.3}$$

$$CH_4 = C + 2H_2, \quad \Delta H_{37}^o = 74.9\,kJ\,mol^{-1} \tag{4.37}$$

In order to implement these reactions into the model equations, their rate laws are required. Langmuir-Hinshelwood Hougen-Watson (LHHW) type rate laws for the above reactions obtained from the literature are presented in Table 4.5. Significant temperature changes are likely to occur due to the existence of reactions with high magnitudes of reaction enthalpies. Therefore temperature dependence of the rate law parameters in these

rate expressions, i.e. Arrhenius-type rate and adsorption/desorption equilibrium constants are taken into account for ensuring more realistic simulations and obtained from the corresponding references given in Table 4.5. Evaluation of the reaction equilibrium constants, K_i at any temperature is explained in detail in Appendix D.

4.5.2. Simulation of Autothermal Operation in Fixed-bed Reactors

Various configurations of the two catalysts, Pt/δ-Al_2O_3 and Ni/MgO-Al_2O_3, present within the reactor are possible. Experimental data reported show that a change in the catalyst bed arrangement results in different product distributions (Ma and Trimm, 1996). Two different bed arrangements are studied in this work. The configurations of interest are the consecutive dual-bed where Pt/δ-Al_2O_3 is placed in the upstream of the reactor followed by Ni/MgO-Al_2O_3, and the mixed-bed which involves a physical mixture of the two catalysts. In the simulation of autothermal operation in dual-bed scheme, steam reforming and other side reactions are assumed to be consecutive to methane oxidation, while the simultaneous occurrence of reactions given in Section 4.5.2 are considered in the mixed-bed scheme.

One-dimensional pseudohomogeneous and heterogeneous reactor models are used for the simulation of the adiabatic autothermal dual catalyst operation in fixed bed reactors. Model equations representing the pseudohomogeneous model are given in Equations (4.9)-(4.11). The working equations for the heterogeneous reactor model are as follows:

Model equations for the bulk fluid phase:

$$\frac{dF_j}{dW} = k_{sj} a_m \left(C_{sj} - C_j\right) \tag{4.38}$$

$$\frac{dT}{dW} = \frac{h_s a_m \left(T_s - T\right)}{\sum_j F_j c_{pj}} \tag{4.39}$$

Table 4.5. LHHW-type rate laws for the proposed reaction network

Reaction	Reaction Rate (kmol $kgcat^{-1}$ h^{-1})	Catalyst	Reference
(4.1)	$-r_1 = \frac{k_1 K_1'' P_{CH_4} \sqrt{K_2'' P_{O_2}}}{\left(1 + K_1'' P_{CH_4} + \sqrt{K_2'' P_{O_2}}\right)^2}$	$Pt/\delta\text{-}Al_2O_3$	Ma *et al.*, 1996
(4.2)	$-r_2 = \frac{k_2\left(P_{CH_4}P_{H_2O} - \frac{P_{CO}P_{H_2}^3}{K_2}\right)}{P_{H_2}^{5/2}(DEN)^2}$ $DEN = 1 + K_{CO}''P_{CO} + K_{H_2}''P_{H_2} + K_{CH_4}''P_{CH_4} + K_{H_2O}''\frac{P_{H_2O}}{P_{H_2}}$	$Ni/MgAl_2O_4$	Xu and Froment, 1989a
(4.36)	$-r_3 = \frac{k_3\left(P_{CH_4}P_{H_2O}^2 - \frac{P_{CO}P_{H_2}^4}{K_{36}}\right)}{P_{H_2}^{7/2}(DEN)^2}$		
(4.3)	$-r_4 = \frac{k_4\left(P_{CO}P_{H_2O} - \frac{P_{CO_2}P_{H_2}}{K_3}\right)}{P_{H_2}(DEN)^2}$		
(4.37)	$-r_5 = \frac{k_5\left(P_{CH_4} - \frac{P_{H_2}^2}{K_{37}}\right)}{\left(1 + K_H''P_{H_2}^{0.5}\right)^n}$	Ni	Kuvshinov *et al.*, 1998

$$\frac{dP}{dW} = -\frac{\beta_o}{A_c(1-\phi)\rho_c}\frac{P^o}{P}\frac{T}{T^o}\frac{F_T}{F_T^o} \tag{4.40}$$

Model equations for the solid phase:

$$k_{sj}a_m(C_{sj} - C_j) = \sum_i \eta_i(\nu_{ij})(-r_{ij,s}) \tag{4.41}$$

$$h_s a_m (T_s - T) = \sum_i \eta_i (-\Delta H_{i,T})(-r_{i,s}) \tag{4.42}$$

Boundary conditions:

$$\text{At } W = 0; \quad F_j = F_j^o, T = T^o, P = P^o \tag{4.43}$$

The particle-to-fluid mass and heat transfer coefficients in Equations (4.41) and (4.42), k_{sj} and h_s respectively, are evaluated by using the following correlations (Wakao and Kaguei, 1982):

$$\frac{h_s D_p}{\lambda_f} = 2 + 1.1 Pr^{1/3} Re^{0.6} \tag{4.44}$$

$$\frac{k_{sj} D_p}{D_{jm}} = 2 + 1.1 Sc^{1/3} Re^{0.6} \tag{4.45}$$

The temperature dependencies of physical properties such as viscosity, thermal conductivity, binary and effective diffusivities of the species present in the reaction mixture and their mixing rules have been reported (Rase, 1990; Wakao and Kaguei, 1982). The ideal gas approximation is employed in the evaluation of the density of the gas mixture.

In order to reduce the execution time in the reactor simulations, heterogeneous terms, i.e. interfacial heat and mass transfer resistances and the intraparticle diffusion limitations, are not incorporated into the reactor model if the criteria given in Table 4.6 indicating the degree of heterogeneity are satisfied (Fogler, 1999).

The criteria given in Table 4.6 are the versions modified for the multiple reaction cases and give approximate indications of the pertinent heterogeneous phenomenon (Rase, 1990). It is also worth noting that the intraparticle heat transfer resistance is not considered due to the relatively high thermal conductivity of the solid catalysts (Rase, 1990).

Table 4.6. Criteria for evaluating transport resistances in fixed-bed operation

Resistance	Criterion (Single reaction case)	Criterion (Multiple reaction case)
Interfacial mass transfer	$\frac{(-r_A)\rho_b D_p n}{2k_s C_{Ab}} < 0.15$	$\frac{\sum_i (\nu_{ij})(r_{ij})\rho_b D_p n}{2k_{sj} C_j} < 0.15$
Interfacial heat transfer	$\left\lvert\frac{(-\Delta H_{i,T})(-r_A)\rho_b D_p E_A}{2h_s T^2 R}\right\rvert < 0.15$	$\left\lvert\frac{\sum_i (-\Delta H_{i,T})(-r_i)\rho_b D_p E_A}{2h_s T^2 R}\right\rvert < 0.15$
Intraparticle mass transfer	$\frac{-r_{As}\rho_c D_p^2}{4D_e C_{As}} << 1$	$\frac{\sum_i (\nu_{ij})(r_{ij})_s \rho_c D_p^2}{4D_e C_{sj}} << 1$

In Equations (4.38)-(4.45) and in Table 4.6, a_m is the exterior surface area per unit mass of catalyst in m^2 $kgcat^{-1}$, C_{sj} is the surface concentration of component j in kmol m^{-3}, D_p is the particle diameter in m, D_e is the effective diffusivity inside catalyst in m^2 h^{-1}, D_{jm} is the diffusivity of component j into a mixture m in m^2 h^{-1}, E_A is the activation energy in kJ $kmol^{-1}$, F_T is the total molar flow rate in kmol h^{-1}, F_T^o is the total molar flow rate at reactor inlet in kmol h^{-1}, h_s is the particle-to-fluid heat transfer coefficient in kJ m^{-2} h^{-1} K^{-1}, k_{sj} is the particle-to-fluid mass transfer coefficient of component j in m h^{-1}, P_T is the total pressure in atm, P_T^o is the total pressure at reactor inlet in atm, Pr is the Prandtl number, Re is the Reynolds number, R is the gas constant in kJ $kmol^{-1}$ K^{-1}, Sc is the Schmidt number, T_s is the surface temperature in K, β_o is the parameter in the pressure drop equation, ϕ is the void fraction of the catalyst bed, η_i is the effectiveness factor for Reaction i, λ_f is the thermal conductivity of the bulk fluid in kJ m^{-1} h^{-1} K^{-1}, μ_f is the viscosity of the bulk fluid in kg m^{-1} h^{-1}, ρ_b is the catalyst bed density in kg m^{-3}, ρ_f is the density of the bulk fluid in kg m^{-3} and ρ_c is the solid density of the catalyst in kg m^{-3}.

4.6. Numerical Solution Techniques

The equilibrium expressions given in Equations (4.12) and (4.35), and the energy balances given in Equations (4.17), (4.25), (4.26), (4.27), (4.30) and (4.34) are nonlinear algebraic in character. A Gauss-Newton based optimization routine is employed for their mathematical solution. The differential mole and energy balances, Equations (4.31)-(4.32) are differential in character, and solved using a variable order, stiff ordinary differential equation (ODE) solver together with the initial conditions given in Equations (4.33). Equation sets (4.9)-(4.12) and (4.38)-(4.43) include both types of equations and are solved simultaneously using the algebraic and ODE solvers interactively. Different of ODE solvers, i.e. the variable order stiff solver mentioned above and a non-stiff solver, are used in combination in solving Equations (4.38)-(4.43) to obtain the best performance in terms of yielding the lowest CPU time. The computer codes are prepared using the MATLAB™ environment and executed using an IBM Netfinity M10 workstation.

4.6.1. Description of the Software Developed for Handling Reactor Models

The software developed for solving the reactor models is composed of a number of codes, i.e. subroutines with various functions. These codes can be classified into four different levels according to their specific features:

- Level 1 codes include basic information about the components existing in the reaction system. Enthalpy of formation data, Gibbs free energy of formation data, heat capacity data, thermal conductivity data and gas viscosity data are the set of information present in Level 1 codes (Geankoplis, 1993; Rase, 1990; Reid *et al.*, 1987).
- Level 2 codes are prepared for evaluating thermochemical data like enthalpy, Gibbs free energy and equilibrium constant of a chemical reaction at a specified temperature. The details of the calculation of thermochemical quantities are given in Appendix C.
- Level 3 codes include the temperature dependent forms of the Langmuir-Hinshelwood type rate expressions of the reactions that are considered in the reactor model. They are prepared in the form of a matrix, introducing an operational

flexibility to the reactor model. This feature enables this software to be employed in different fixed-bed reaction systems. In addition to the rate laws, criteria to determine the significance of interfacial/intraparticle transport resistances and some of the parameters of the model equations, such as physical properties of the mixture and heat and mass transfer coefficients, evaluated by using appropriate mixing rules and correlations, also exist at this level.

- Level 4 codes are based on the previous ones and include the reactor model equations to be solved and pertinent solvers to handle them. The codes in all levels are dependent on each other, so they should be considered simultaneously when solving the reactor model. Their dependence is presented in the flowchart given in Figure 4.4. Note that the solvers mentioned in this level are readily available as built-in subroutines in MATLAB™ (Hanselman and Littlefield, 1998).

The dashed-lined parts in Figure 4.4 represent the extra steps involved in the software in case of describing situations where heterogeneous phenomenon/phenomena is/are significant.

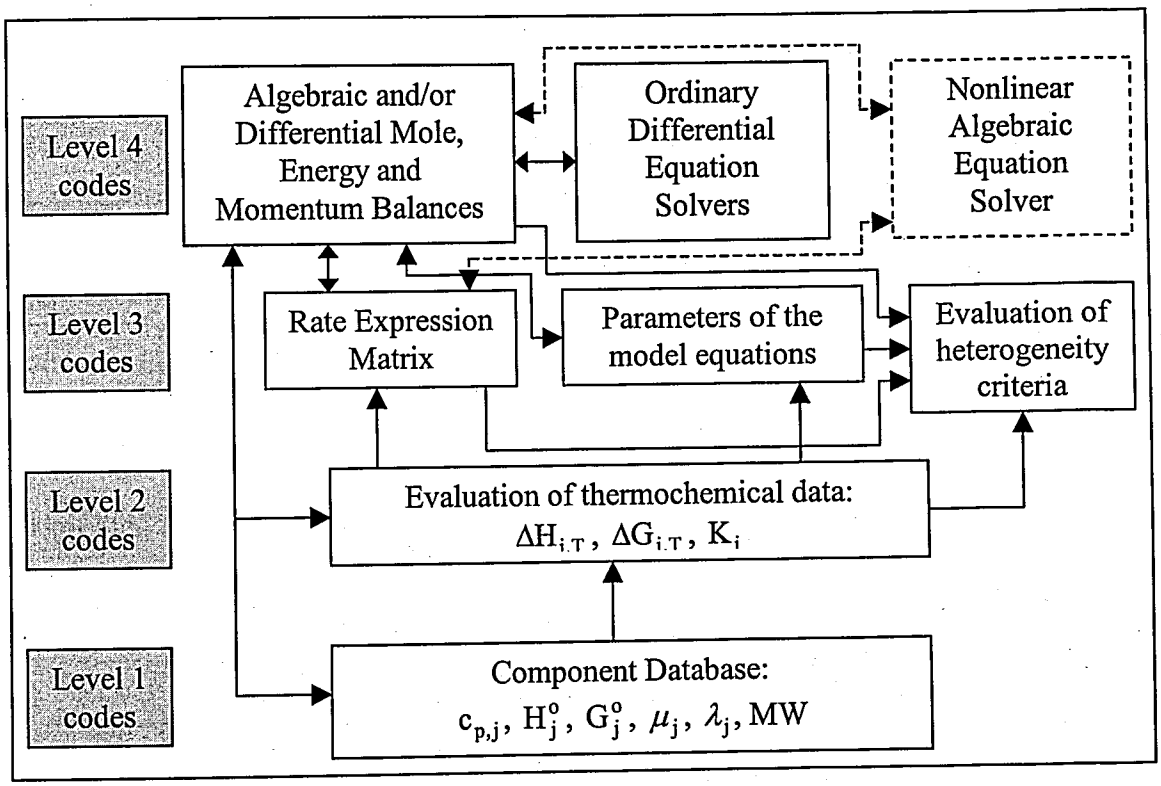

Figure 4.4. General structure of the software developed for handling the fixed-bed reactor model equations

5. RESULTS AND DISCUSSION

5.1. Simulation of Autothermal Hydrogen Production from Methane

An autothermal, dual catalyst, fixed bed reaction system proposed for hydrogen production from methane is mathematically investigated using different catalyst bed configurations and feed ratios. Consecutive placement or physical mixture of the oxidation and reforming catalysts, Pt/δ-Al_2O_3 and Ni/MgO-Al_2O_3 respectively, are the two configurations of interest. Reactor operation at different feed ratios is analyzed for both catalyst bed configurations on laboratory scale and industrial scale via a series of simulations by using the one-dimensional pseudohomogeneous and heterogeneous fixed bed reactor models. The type of heterogeneous components implemented into the model is decided by checking related criteria.

In order to test the reactor model, simulations are initially conducted at different feed ratios and catalyst bed configurations for bench scale integral reactors and compared with the experimental results reported by Ma and Trimm (1996). Autothermal operation is then analyzed under the same conditions in hypothetical industrial reactors whose dimensions are determined by scale-up and by using the industrial fixed bed reactor data available (Xu and Froment, 1989b). The ratio of the catalyst weight to the initial methane molar flow rate is used as the scale-up parameter. The operating conditions and reactor data used in the simulations are given in Table 5.1.

Further information related with the description of the reaction system and the reactor model is given in Sections 4.5.1 and 4.5.2, respectively.

5.1.1. Bench-Scale Simulations

Comparison of simulation outputs and their experimental counterparts for dual-bed and mixed-bed schemes are given in Tables 5.2 and 5.3, respectively.

Table 5.1. Operating conditions and reactor data

	Bench-scale reactor (Ma and Trimm, 1996)		Industrial-scale reactor (Xu and Froment, 1989b)	
	Dual-bed scheme	Mixed-bed scheme	Dual-bed scheme	Mixed-bed scheme
T^o (K)	640-665	800	815	800
P_T^o (atm)	2.5	2.9	28.6	28.6
$F_{CH_4}^o$ (kmol h^{-1})	$2.2x10^{-4}$	$1.7x10^{-4}$	62.2	44.4
W (kg)	$2x10^{-4}$ (Pt/δ-Al_2O_3) + $3x10^{-4}$ (Ni/MgO-Al_2O_3)	$5x10^{-4}$ (Pt/δ-Al_2O_3+ Ni/MgO-Al_2O_3)	53.2 (Pt/δ-Al_2O_3) + 79.8 ($Ni/MgAl_2O_4$)	133 (Pt/δ-Al_2O_3+ $Ni/MgAl_2O_4$)
D_t (m)	$1.3x10^{-3}$		$1.016x10^{-1}$	
D_p (m)	$3.4x10^{-4}$		$1.335x10^{-2}$	

Table 5.2. Experimental results and bench-scale simulation outputs in dual-bed scheme (heterogeneous model)

Feed conditions (Ma and Trimm, 1996)			Experimental results (Ma and Trimm, 1996)				Simulation outputs			
CH_4/O_2	H_2O/CH_4	GHSV (h^{-1})	x_{CH_4}	y_{H_2}[1]	y_{CO}[1]	T_{max} (K)	x_{CH_4}	y_{H_2}[1]	y_{CO}[1]	T_{max} (K)
3.53	0.88	37600	16.2	8.8	0	790	11.0	31.6	0.4	790
3.53	1.75	47700	15.0	10.1	0	781	13.1	39.8	0.4	782
2.98	1.75	50600	20.7	17.3	0	831	19.3	52.2	0.3	827
2.98	2.34	57500	19.9	17.3	0	823	20.9	58.0	0.5	822
2.51	1.75	59000	28.7	29.0	0	873	29.0	67.5	0.7	875

[1] Product yield: moles of product obtained/100 moles of methane fed

Table 5.3. Experimental results and bench-scale simulation outputs in mixed-bed scheme (heterogeneous model)

Feed conditions (Ma and Trimm, 1996)			Experimental results (Ma and Trimm, 1996)				Simulation outputs			
CH_4/O_2	H_2O/CH_4	GHSV (h^{-1})	x_{CH_4}	y_{H_2}[2]	y_{CO}[2]	T_{max} (K)	x_{CH_4}	y_{H_2}[2]	y_{CO}[2]	T_{max} (K)
2.24	1.17	37600	39.5	47.8	6.3	839	43.8	98.6	12.3	843
1.89	1.17	41100	53.3	74.9	11.7	888	53.9	125.7	24.1	902
1.89	1.56	44500	53.8	76.4	12.5	889	46.9	129.3	23.6	890
1.89	2.34	51300	54.9	82.9	9.9	851	31.0	129.7	20.0	869
1.55	1.56	49500	69.1	105.7	15.0	931	55.4	151.5	37.7	943
1.55	2.34	56000	70.1	107.1	19.6	908	40.5	153.6	31.9	913
1.35	2.34	60000	83.6	119.5	30.3	953	48.7	178.6	48.7	966
1.16	2.34	65000	91.7	120.6	35.9	1007	55.0	195.6	64.6	1009

[2] Product yield: moles of product obtained/100 moles of methane fed

When the product distributions obtained in the experiments and simulations are compared with each other, it is observed that the mixed-bed scheme gives higher hydrogen yields. Presence of the catalysts in the physically mixed state enhances heat and mass transfer characteristics, i.e. reduces the degree of heterogeneity of the reaction system, which is also confirmed by the relatively low values of the LHS of the criteria given by in Table 4.6 in Section 4.5.2.

The status of the criteria given in Table 4.6 is taken as a measure in the implementation of the heterogeneous components into the reactor model. In both catalyst bed configurations, it is observed that the interfacial heat transfer resistance is significant during the entire operation (LHS of interfacial heat transfer resistance criterion > 0.15). On the other hand, interfacial mass transfer resistance is observed to be important at temperatures higher than ca. 1100 K. Intraparticle diffusion limitations are neglected, i.e. effectiveness factor values are taken as unity due to the presence of small catalyst particles.

Each simulation of the dual-bed scheme is composed of two sub-simulations: one for the Pt bed where only methane oxidation is assumed to occur, the other for the Ni/MgO bed where steam reforming (Reactions (4.2) and (4.36)), water-gas shift (Reaction (4.3)) and methane decomposition (Reaction 4.37)) are considered to proceed. The bed temperature reaches to its maximum value at the bed interface where endothermic steam reforming reactions become significant. Experimentally determined maximum bed temperatures in dual-bed operation are less than 900 K (Table 5.2). Therefore, the interfacial mass transfer is neglected and only external heat transfer is considered as the heterogeneous component in both first and second sub-simulations. A single simulation is conducted for each run in the mixed-bed configuration where the reactions above including total oxidation (Reaction (4.1)) are assumed to proceed in a simultaneous fashion. The experimental values of maximum bed temperatures are less than 1010 K (Table 5.3). This leads to the implementation of interfacial heat transfer into the reactor model only. The heterogeneous characteristics of these reaction systems are also confirmed by checking the related criteria given in Table 4.6.

For both catalyst bed configurations, it is observed in the experiments and simulations that, at constant steam to methane ratio, a decrease in the methane to oxygen

ratio results in higher hydrogen yields and elevated maximum bed temperatures. Since the molar flow rate of methane is constant in all runs, any decrease in the methane to oxygen ratio, i.e. any increase in the molar flow rate of oxygen in the feed will lead to the combustion of more methane which will increase the amount of energy generated by total oxidation and hence the bed temperatures. Higher bed temperatures will facilitate endothermic steam reforming reactions and result in higher hydrogen yields. In addition, at constant methane to oxygen ratio, an increase in the initial molar flow rate of steam lowers the maximum bed temperature. It can be concluded that steam facilitates heat transfer between the two beds.

In both catalyst bed configurations, the maximum bed temperatures obtained from simulations are close to the experimental ones whereas predicted hydrogen and carbon monoxide yields seem to be positively deviating in all runs (Tables 5.2 and 5.3). One possible explanation is the absence of the following side reaction in the reactor model that removes hydrogen and carbon monoxide from the reaction medium:

$$CO + H_2 = C + H_2O, \quad \Delta H^{\circ}_{298} = -135.6\,\text{kJ mol}^{-1} \tag{2.18}$$

The change in the Gibbs free energy of the above reaction is negative at temperatures less than ca. 950 K, indicating its significance in existing reaction conditions. Hence, simulated H_2 and CO yields may approach experimental ones if this reaction were implemented into the model equations.

The methane conversion levels are predicted to be lower than the experimental values at low methane to oxygen and high steam to methane ratios in mixed-bed configuration (runs 4, 6, 7, 8 in Table 5.3). It seems that excess steam inhibits the steam reforming reaction in the simulations, which is not observed in the experiments. This difference may be due to the lower performance of the kinetic expressions in case of high amount of steam and oxygen, which appears to be a limitation for this model in larger scale simulations.

Pressure drop is observed to be negligible in both bed schemes. Maximum values are obtained to be 0.063 atm and 0.031 atm for the bench scale dual-bed and mixed-bed configurations, respectively.

Although the results of the one-dimensional heterogeneous model are presented in Tables 5.2 and 5.3, the use of pseudohomogeneous reactor model is also considered. In general, it is found that heterogeneous model gives outputs closer to the experimental results, whereas the deviation is higher in the case of pseudohomogeneous model. Such a trend is expected, since solid catalyst and bulk fluid phases are considered separately in the heterogeneous model. Some opposite trends are believed to be due to the nature of the ODE solvers. The comparative model outputs are presented in Figures 5.1-5.3.

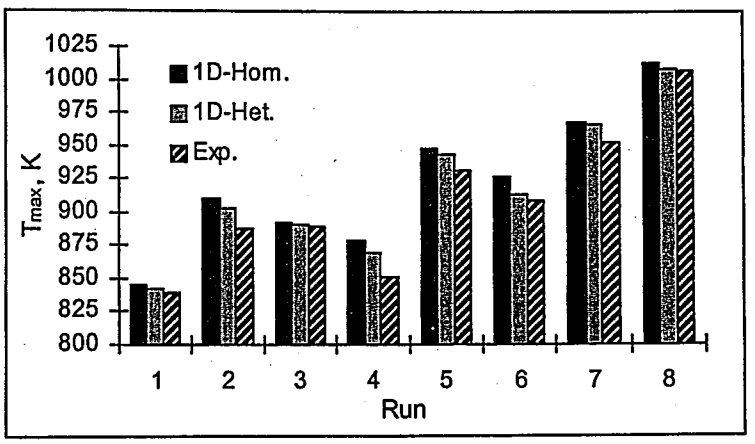

Figure 5.1. Comparison of the maximum bed temperatures in the mixed-bed case

5.1.2. Industrial-Scale Simulations

In order to predict characteristics of dual-catalyst autothermal operation on an industrial scale, a set of simulations are performed in hypothetical larger scale tubular reactors with the catalyst bed configurations of interest. Since steam is fed instead of liquid water into the reactors, the maximum bed temperatures obtained in industrial scale simulations are higher than ones given in Tables 5.2 and 5.3. As a result, in dual-bed operation, criteria related with interfacial mass and heat transfer resistances (Table 4.6) indicated their existence in Pt bed, both of which are considered in the first sub-simulation. However,

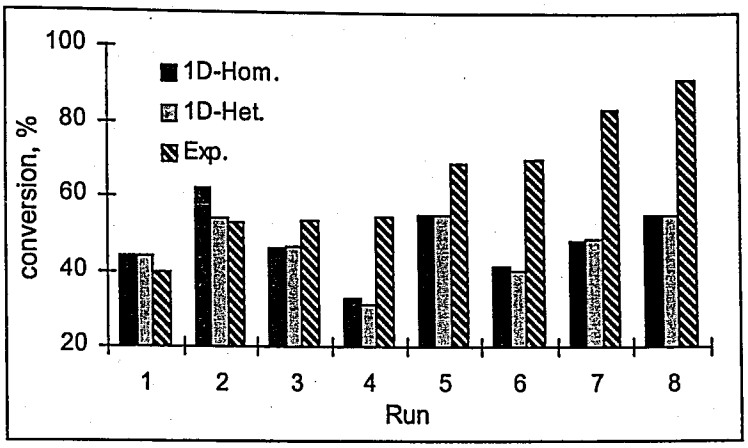

Figure 5.2. Comparison of methane conversions in the mixed-bed case

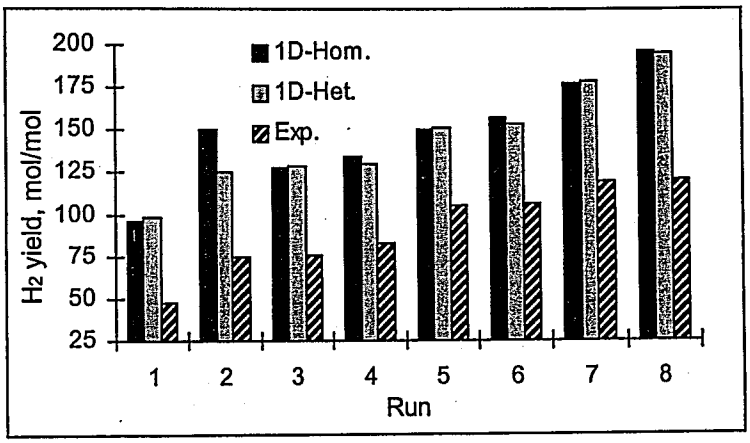

Figure 5.3. Comparison of hydrogen yields in the mixed-bed case

interfacial mass transfer resistance is found to be significant only at the bed interface, in an incremental layer of steam reforming catalyst. Therefore, interfacial heat transfer is the only external heterogeneous component considered in secondary sub-simulations. Similarly, only external heat transfer is considered in simulating the industrial scale reactor with mixed-bed configuration in which the local existence of external mass transfer is neglected.

Apart from the above external film resistances, intraparticle diffusion limitations are taken into account due to the presence of larger catalyst particles. For this purpose,

effectiveness factors for the model reactions given in Section 4.5.1 are taken from the literature (De Groote and Froment, 1996). Note that the similarity of the operating conditions given by De Groote and Froment (1996) and the ones exercised in this work allows the identification of the operating characteristics of the industrial scale reactor using the reported effectiveness factors.

Molar feed ratios given in Tables 5.2 and 5.3 are employed in the industrial scale simulations. Bed temperature and product yield trends obtained for different runs are similar to the bench scale simulations. Hydrogen yields are between 107 and 139 in the dual-bed and 122 and 218 in the mixed-bed configurations. The temperature and typical molar flow rate profiles for different bed configurations are given in Figures 5.4-5.7.

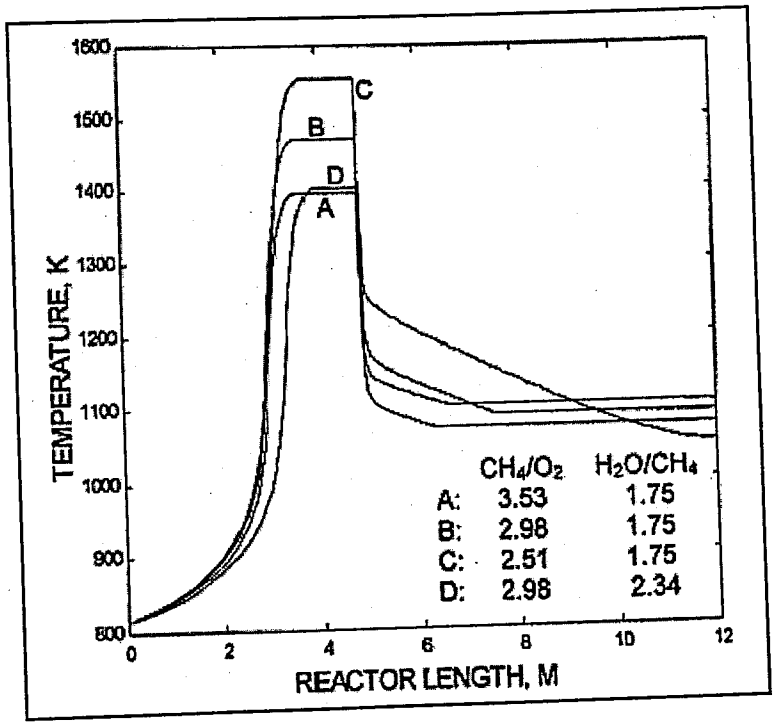

Figure 5.4. Temperature profiles obtained for industrial-scale reactor with dual-bed configuration

The bed temperatures obtained in dual-bed scheme are greater than those calculated for mixed-bed configuration. This is due to the complete consumption of oxygen in the feed, which allows total oxidation to proceed until completion and raise temperatures up to ca. 1600 K (Figure 5.4).

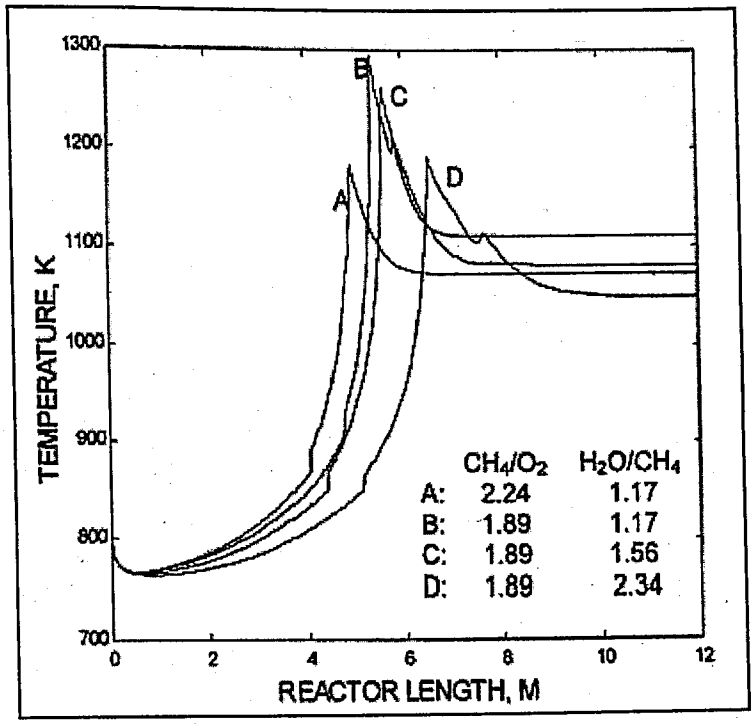

Figure 5.5. Temperature profiles obtained for industrial-scale reactor with mixed-bed configuration

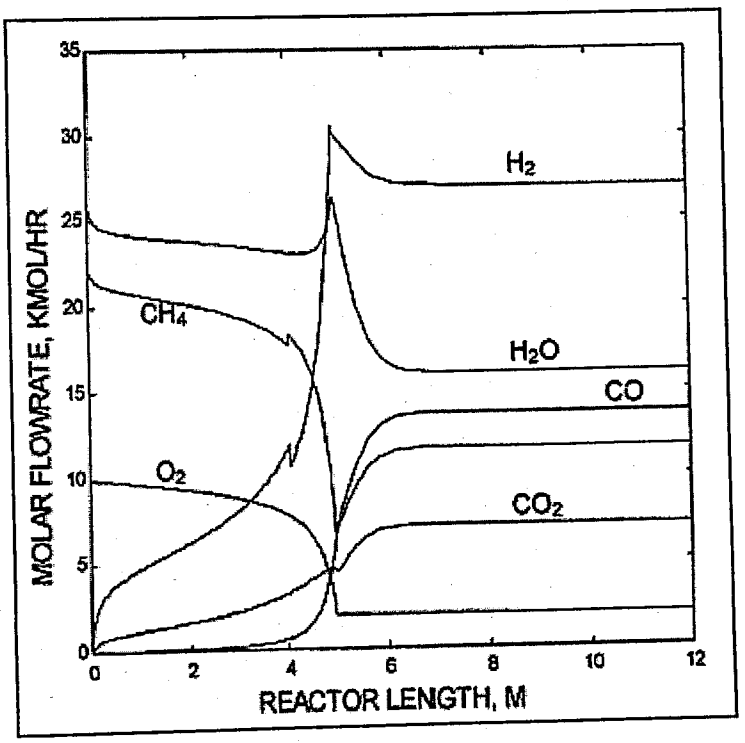

Figure 5.6. Product distribution obtained for industrial-scale reactor with mixed-bed configuration (CH_4/O_2=2.24, H_2O/CH_4=1.17)

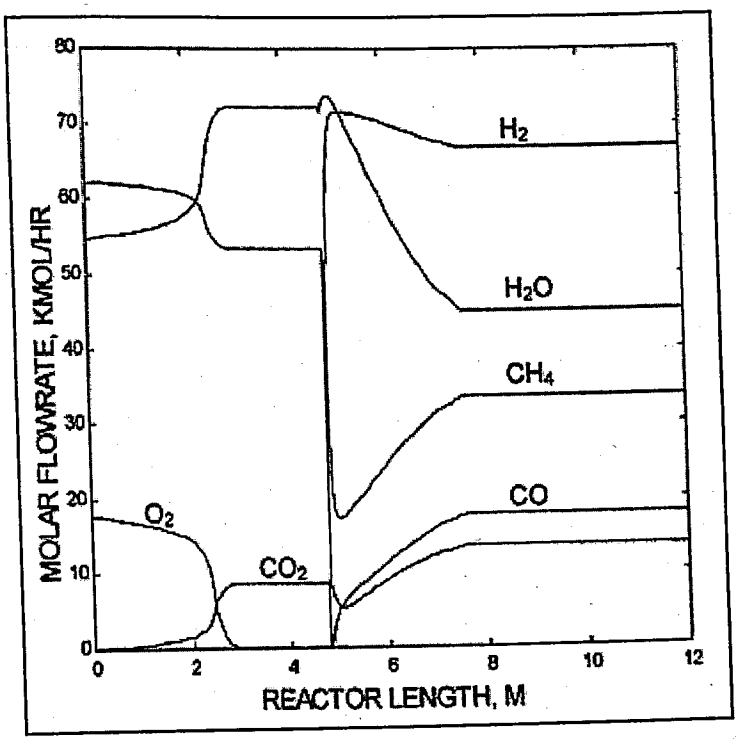

Figure 5.7. Product distribution obtained for industrial-scale reactor with dual-bed configuration (CH_4/O_2=3.53, H_2O/CH_4=0.88)

Dual-bed simulation results shown in Figure 5.4 indicate that the temperature in the bed rises first and then remains constant at a certain value, which is a typical temperature profile for methane oxidation whereas a peak is observed in temperature profiles obtained in mixed-bed simulations of Figure 5.5. The sharp temperature fall at the dual-bed interface is because of the high endothermicity of the reforming reactions running on Ni/MgO catalyst, whose existence is confirmed by a sharp increase in hydrogen flow rate in Figure 5.7. The increase in the methane flow rate and the decrease in the hydrogen flow rate after the maximum bed temperature location in Figures 5.6 and 5.7 indicate the occurrence of reverse Reactions (4.2), (4.3) and (4.36). Water-gas shift reaction seems to be important in the determination of CO and CO_2 distribution in both the dual-bed and the mixed-bed schemes.

The shift in the locations of the maximum bed temperatures in Figures 5.4 and 5.5 is due to the increase in the total molar flow rates at the reactor inlet where methane flow is kept constant. It is worth noting that the maximum pressure drop is estimated to be ca. 1 atm in larger scale reactor simulations.

5.1.3. Summary

Autothermal hydrogen production in the presence of two different catalysts is mathematically investigated by a series of simulations conducted for bench scale and hypothetical industrial scale reactors. Pt/δ-Al_2O_3 and Ni/MgO-Al_2O_3 catalyzing total methane oxidation and steam reforming, respectively, are either placed consecutively (dual-bed) or packed in the form of a physical mixture (mixed-bed). A one-dimensional heterogeneous reactor model is used for the simulations. Heterogeneous components describing heat and mass transfer resistances are incorporated into the simulations after checking the values of related criteria, and this greatly reduces the computation time. Mixed-bed configuration is observed to exhibit better performance when compared with dual-bed scheme in both reactor dimensions. Enhanced heat and mass transfer characteristics are believed to facilitate hydrogen production in mixed-bed scheme. Larger scale and bench scale operations possess the same external transport characteristics except that the interfacial mass transfer resistance is considered in addition to the external heat transfer resistance in simulating the Pt bed in industrial scale dual-bed operation. In both catalyst bed configurations, intraparticle diffusion limitations are significant in industrial scale operation.

5.2. Quantitative Investigation of Catalytic Natural Gas Conversion for Stationary Hydrogen Fuel Cell Applications

Hydrogen generation from natural gas for driving proton exchange membrane fuel cells in residential small-scale combined heat-and-power (CHP) applications is investigated by a series of computer simulations. Natural gas is converted into hydrogen either by the combined oxidation-steam reforming, i.e. indirect partial oxidation mechanism on Pt-Ni catalyst or by the direct, one-step partial oxidation mechanism on Pt monoliths. A water-gas shift converter and a catalytic selective carbon monoxide oxidation unit are used for reducing carbon monoxide levels to a value which the anode of PEMFC can tolerate. Unconverted hydrocarbons and hydrogen rejected from the fuel cell are considered to be oxidized in a Pt catalyst packed afterburner in order to supply energy to the system. Reactor simulations based on available kinetic data together with energy integration calculations indicate direct partial oxidation to give higher hydrogen yields corresponding to increased electrical power outputs and elevated efficiencies. Indirect partial oxidation has the advantage of operating simplicity, since the direct route runs only at millisecond level residence times and high temperatures. In both mechanisms, water injection and energy integration are critical issues in adjusting product yields and in temperature control. The simulation outputs are compared and validated by the results based on the thermodynamics of the pertinent mechanism.

The simulation results of the indirect and the direct partial oxidation of methane are given in Figures 5.8, 5.9 and in Figures 5.10, 5.11, respectively, and expressed in terms of product yields defined as the number of moles of product obtained per mole of methane fed into the system. The effects of water/methane and methane/oxygen ratios at the inlet and of sensible heat recovery levels on product yields are indicated on the pertinent plots.

5.2.1. Water Injection

It was previously mentioned that the steam/carbon ratio defined in Equation (4.4) should be kept above 2.5 to eliminate carbon formation in the oxidation/steam reforming case (Rostrup-Nielsen, 1984). Table 5.4 demonstrates the values of total oxidation conversions, corresponding methane/oxygen and steam/carbon ratios obtained without

water injection. The maximum value of the steam/carbon ratio is found to be 1.77, indicating the requirement for an external water supply into the system. It is worth noting that the steam produced by total oxidation would be sufficient if a precious metal catalyst such as Rh, which allows much less coke formation in reforming, was used instead of Ni (Rostrup-Nielsen and Bak Hansen, 1993; Trimm and Önsan, 2001).

The selective oxidation unit can successfully reduce the CO content down to 40 ppm, when a gas mixture with a CO composition below 2 mole per cent is fed into it (Golunski, 1998). In the direct oxidation route where methane conversion is taken to be 80 per cent (Hickman and Schmidt, 1992), the mole fraction of CO at the reactor exit is equal to ca. 0.2, which is ten times greater than the value that the CO cleanup unit can tolerate (0.02). Therefore, external water injection is required to eliminate coke formation and to drive the water-gas shift reaction for reducing CO levels in indirect and direct conversion routes, respectively.

5.2.2. Product Yields

Both thermodynamics and kinetics based H_2 yields obtained in indirect partial oxidation are found to have maximum values at certain water/methane and methane/oxygen ratios (Figure 5.8). Steam reforming is endothermic and gives higher hydrogen yields at high temperatures generated by the total oxidation. The more the methane is oxidized at lower methane/oxygen ratios, the higher the bed temperatures. However, this leads to lower amounts of methane reserved for steam reforming, meaning lower hydrogen yields. In the opposite case, where more methane is reserved for reforming, hydrogen production is expected to be lower, since oxidation is limited and bed temperature may not be adequate to drive steam reforming due to higher methane/oxygen ratios. This characteristic feature of the indirect partial oxidation leads to the existence of maxima in hydrogen yields.

In contrast with the indirect route, H_2 yields given in Figure 5.10 for direct oxidation seem to flatten at their maximum values. H_2 yields obtained in direct oxidation depend on the degree of sensible heat recovery, f, at the reactor exit, and hence, on the amount of water injected to cool the gas mixture for the shift conversion (Figure 4.1). The

higher the heat recovery, the lower the amount of water that needs to be injected. Therefore, at higher values of f, i.e. lower water/methane ratios, water will be the limiting reactant and H_2 yields will increase with increasing quantities of water (Figure 5.10). However, as the heat recovery decreases, CO becomes the limiting reactant after certain water/methane ratios (0.85 in thermodynamic case, 2.15 in kinetic case), and H_2 yields reach their maximum value and remain almost constant, since the amount of CO generated by the direct oxidation reaction is fixed (Figure 5.10). This reasoning is also valid for the trend of CO yields given in Figure 5.11.

In both indirect and direct partial oxidation, the amounts of CO decrease with increasing water/methane ratios (Figures 5.9 and 5.11). The water-gas shift reaction, driven by the externally injected water to a great extent, is considered as the major factor that reduces the CO yields.

Table 5.4. TOX conversion levels and related methane/air and steam/carbon ratios leading to converged solutions in thermodynamically and kinetically controlled cases in indirect partial oxidation

Kinetics			Thermodynamics		
TOX conversion	CH_4/air	steam/carbon	TOX conversion	CH_4/air	steam/carbon
0.25	0.53	0.67	0.10	1.33	0.22
0.27	0.49	0.74	0.13	1.02	0.30
0.31	0.43	0.90	0.16	0.83	0.38
0.33	0.40	0.99	0.20	0.66	0.50
0.36	0.37	1.13	0.25	0.53	0.67
0.47	0.28	1.77	0.30	0.44	0.86
-	-	-	0.35	0.38	1.08

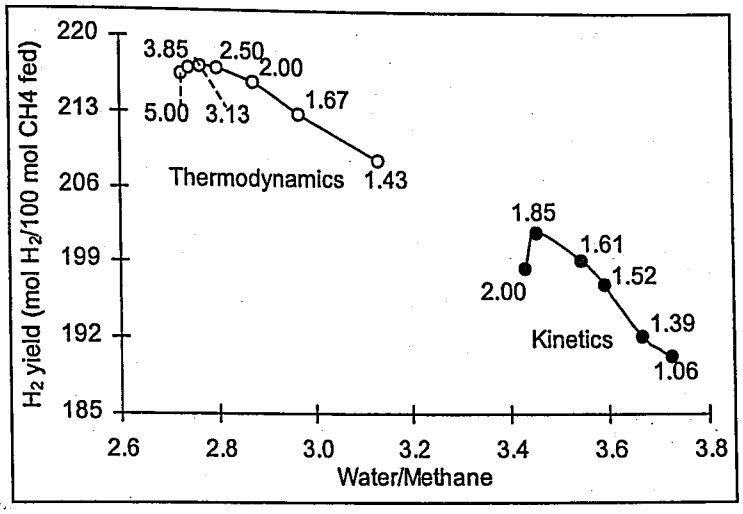

Figure 5.8. Effects of methane/oxygen (shown within the figure), and water/methane ratios at the system inlet on H_2 yield (moles of H_2 produced/mole of methane fed) in indirect partial oxidation of methane

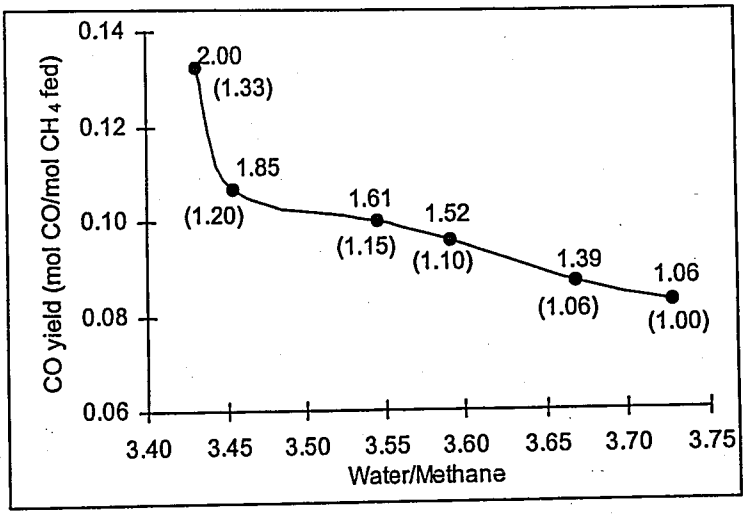

Figure 5.9. Effects of methane/oxygen (shown within the figure), and water/methane ratios at the system inlet on CO yield (moles of CO produced/mole of methane fed) in indirect partial oxidation of methane (molar percentage of CO within the gas mixture is shown within the figure in parenthesis)

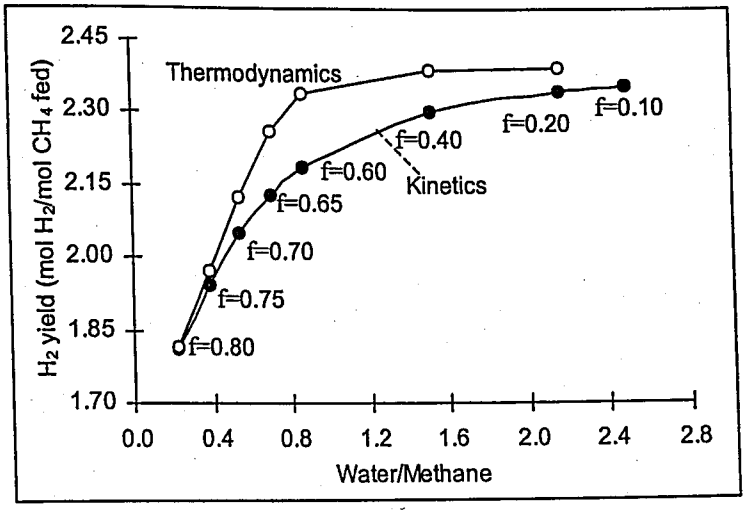

Figure 5.10. Effects of sensible heat recovery, f (shown within the figure), and water/methane ratio at the system inlet on H_2 yield (moles of H_2 produced/mole of methane fed) in direct partial oxidation of methane

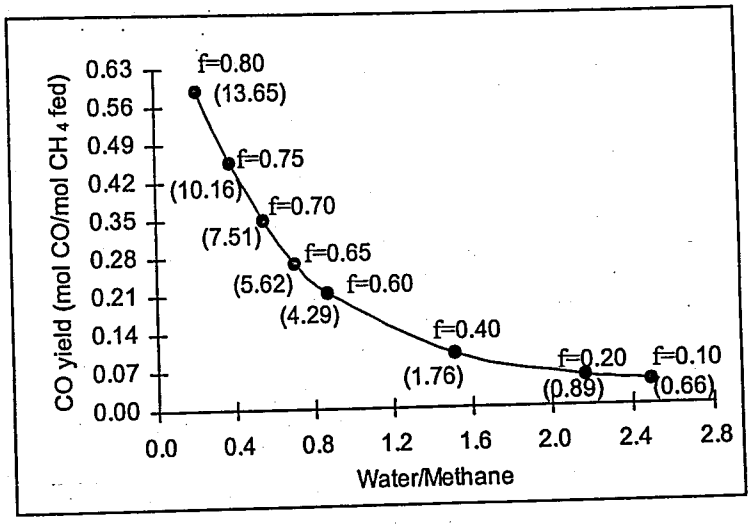

Figure 5.11. Effects of sensible heat recovery, f (shown within the figure), and water/methane ratio at the system inlet on CO yield (moles of CO produced/mole of methane fed) in direct partial oxidation of methane (molar percentage of CO within the gas mixture is shown within the figure in parenthesis)

5.2.3. Direct Partial Oxidation versus Indirect Partial Oxidation

The comparison of the two operations is based on product yields obtained in the kinetically controlled cases, as well as their electrical power production efficiencies, which is defined as follows:

$$\text{efficiency} = \frac{\text{actual PEMFC power obtained in kW}}{\text{theoretical PEMFC output in kW}} \times 100 \qquad (5.1)$$

The theoretical PEMFC power in the denominator is dictated by the maximum amount of hydrogen that could be expected from indirect and direct partial oxidation routes, which are 4 moles of hydrogen via Reactions (4.2) and (4.3), and 3 moles of hydrogen via Reactions (4.3) and (4.5), respectively. However, only 75 per cent of the hydrogen produced can be converted into electrical power, since the PEMFC rejects ca. 25 per cent of the hydrogen fed into it (Golunski, 1998). Therefore, the theoretical output would correspond to 87 kW and 65 kW power for oxidation/steam reforming and direct oxidation routes, respectively, assuming that 1000 l H_2 h^{-1} would correspond to 1 kW electrical power (Golunski, 1998), the PEMFC operates at 353 K and that 1 kmol h^{-1} of methane is fed into both systems.

An important point should be highlighted for the direct conversion route. It was mentioned that the selective CO oxidation unit, which reduces the CO levels to less than 40 ppm for the PEMFC operation, accepts a gas mixture with CO content below 2 mole per cent (Golunski, 1998). This condition, corresponding to a CO yield of ca. 0.1 mol CO/mol CH_4, is only valid above a water/methane ratio of 1.45 (Figure 5.11). In other words, the actual operating region for direct partial oxidation is determined by water/methane ratios greater than 1.45.

The actual maximum H_2 yield obtained in the direct conversion mechanism (2.36 mol H_2/mol CH_4) at a water/methane ratio of 2.49 is found to be higher than that estimated for the indirect partial oxidation (2.02 mol H_2/mol CH_4) at a water/methane ratio of 3.45 (Figures 5.8 and 5.10). These H_2 yields are equivalent to 51 kW and 44 kW power output, respectively, and corresponding to 78 per cent efficiency for direct

oxidation and 51 per cent efficiency for oxidation/steam reforming. Although the theoretical power output is higher in the indirect scheme, the direct route seems to be better in terms of higher H_2 yields and hence improved electrical power production efficiencies. The improved conversion of methane in direct oxidation (ca. 80 per cent at 1373 K (Hickman and Schmidt, 1992)) and the conversion of most of the CO formed in Reaction (4.5) to H_2 in the WGS converter via Reaction (4.3) lead to hydrogen quantities higher than those obtained in the indirect oxidation route in which approximately 28 per cent of the methane fed is lost during total oxidation and conversion of remaining methane during steam reforming is found to be reported at around 70 per cent (Trimm and Önsan, 2001). The WGS effect, i.e. conversion of the resulting CO into H_2, exercised both in the indirect partial oxidation reactor and in the shift converter is insufficient in reaching H_2 yields achieved in the direct route.

The CO yield and the corresponding molar CO composition are found to be 0.11 mol CO/mol CH_4 and 1.2 mole per cent of CO, respectively at a water/methane ratio of 3.45 in indirect partial oxidation (Figure 5.9). These figures are equivalent to 0.04 mol CO/mol CH_4 and 0.66 mole per cent of CO at a water/methane ratio of 2.49 in direct partial oxidation followed by water-gas shift conversion (Figure 5.11). These results indicate that the direct route gives lower amounts of CO, requiring reduced quantities of selective oxidation catalyst and hence a more compact CO cleanup unit.

Although the direct partial oxidation method seems to be promising in terms of the efficiency defined in Equation (5.1) and in terms of CO yields, it has serious operational challenges such as the requirement of high gas flow rates corresponding to millisecond-level contact times, high operating temperatures and the presence of near-explosive conditions (Hickman and Schmidt, 1992) that have to be overcome. These features are much more pronounced during transient periods such as start up and shut down operations which are exercised much less frequently in residential CHP facilities. The direct route may therefore be a promising fuel processing option for stationary applications. It is also worth noting that, a specific catalyst – Ru supported on TiO_2 – is reported to exhibit an exceptional behavior in terms of catalyzing direct partial oxidation at relatively lower temperatures (ca. 973 K – 1073 K) and at longer contact times (Elmasides *et al.*, 2000).

The latter mechanism is also preferable from an energetics point of view: it is found that a low sensible heat recovery of around 10 per cent from the mixture at reactor exit, together with 30 per cent heat recovery from the afterburner exit mixture, is sufficient to raise the temperature of the fuel and air feed stream (298 K) to 1373 K at which direct partial oxidation takes place. Therefore, higher levels of sensible heat and energy released from the afterburner can be used in applications such as central heating in addition to supplying electrical power.

5.2.4. Thermodynamics versus Kinetics

Thermodynamics-based H_2 yields are presented together with their kinetics-based counterparts in Figures 5.8 and 5.10 for indirect and direct partial oxidation mechanisms, respectively. In both operations, the results based on kinetics are within thermodynamic limit, as expected, verifying the kinetic data used in the simulations.

In order to drive the kinetics of the endothermic steam reforming, a higher amount of energy is required. This leads to elevated total oxidation conversions in the kinetically controlled case, as shown in Table 5.4, and to higher heat evolution within the catalyst bed. Increased amounts of water are, therefore, injected into the system for controlling the bed temperature at 1100 K, resulting in greater water/methane ratios in the kinetics-based simulation results (Figures 5.8 and 5.9).

5.2.5. Mobile Applications

The ease of operation and carried weight are issues that are much more critical in mobile fuel cell applications. Although direct oxidation is better in terms of power output efficiency, simpler indirect partial oxidation route seems to be the operation of choice for fuel conversion in hydrogen driven fuel cell vehicles, since the latter is much more suitable for handling transient periods usually exercised in mobile applications. However, if coupled with a natural gas engine to drive the vehicle, the high-efficiency direct oxidation based route can be integrated with a fuel cell based auxiliary power unit to feed the peripherals within a vehicle. Natural gas engines have good efficiency, can follow driving dynamics and therefore can handle the transient periods in vehicular operation. Electrical

power demand for the peripherals is much less variable and can easily be provided by a fuel cell based auxiliary power unit integrated with a direct partial oxidation based hydrogen generation unit.

Although natural gas has the advantages of high H:C ratio and lowest CO_2 emissions, if used in vehicles, it will require heavy gas storage cylinders, resulting in increased carried weight and higher fuel consumption, and hence is not recommended.

5.2.6. Summary

The use of natural gas (modeled as methane) as a fuel for catalytic conversion to hydrogen in fuel processor-fuel cell systems for small-scale stationary CHP applications is investigated by a series of computer simulations. Two systems specialized for different fuel conversion operations - combined total oxidation-steam reforming (indirect partial oxidation) and one step, dry oxidation (direct partial oxidation) – are of interest. In both systems, water injection is found to be necessary for product yield adjustment and temperature control. The indirect partial oxidation mechanism seems to be the operation of choice due to its practicality. The H_2 yields, calculated on the basis of kinetic data and verified by thermodynamics, are found to be higher in the direct oxidation route, leading to increased power outputs and efficiencies. The direct oxidation method, however, requires high temperatures, short contact times and near explosive conditions, but it may be exercised in stationary CHP applications in which start up and shut down are less frequent.

5.3. On-board Hydrogen Generation for Fuel Cell Powered Vehicles: The Use of Methanol and Propane

Although hydrogen has been found to be the most acceptable fuel for vehicle mounted fuel cells, the storage and transportation of the gas presents difficulties. As a result, attention has been focused on on-board conversion of more readily available fuels such as methanol. In this section comparisons are presented of hydrogen generation from methanol and propane. Simulations are based both on thermodynamic and kinetic data.

The molar hydrogen yields are defined as the number of moles of hydrogen produced per mole of fuel – methanol or propane – fed into the system multiplied by 100 ((mol H_2/mol fuel fed) x 100). Based on this definition, the maximum possible values of molar hydrogen yields are 300 per cent for methanol (Reaction (2.7)) and 1000 per cent for propane steam reforming and water-gas shift, i.e. Reactions (5.2) and (4.3), respectively:

$$CH_3OH + H_2O = CO_2 + 3H_2, \quad \Delta H^{\circ}_{298} = 49.6\,kJ\,mol^{-1} \tag{2.7}$$

$$C_3H_8 + 3H_2O = 3CO + 7H_2, \quad \Delta H^{\circ}_{298} = 497.7\,kJ\,mol^{-1} \tag{5.2}$$

$$CO + H_2O = CO_2 + H_2, \quad \Delta H^{\circ}_{298} = -41.2\,kJ\,mol^{-1} \tag{4.3}$$

Molar hydrogen yields calculated from thermodynamic data for indirect partial oxidation are shown in Figure 5.12. Maximum values are observed in both cases as the steam:carbon ratio increased, one at ca. 1.1, corresponding to 283 per cent H_2 yield from methanol, and one at ca. 2.0, corresponding to 770 per cent H_2 yield from propane (Figure 5.12), both of which are below the theoretical limits given above. The increase in H_2 yields at low steam:carbon ratios reflects the effect of adding more steam to the water-gas shift equilibrium. The decrease at higher ratios reflects the need to oxidize more fuel in order to gasify water, leaving less fuel to be steam reformed.

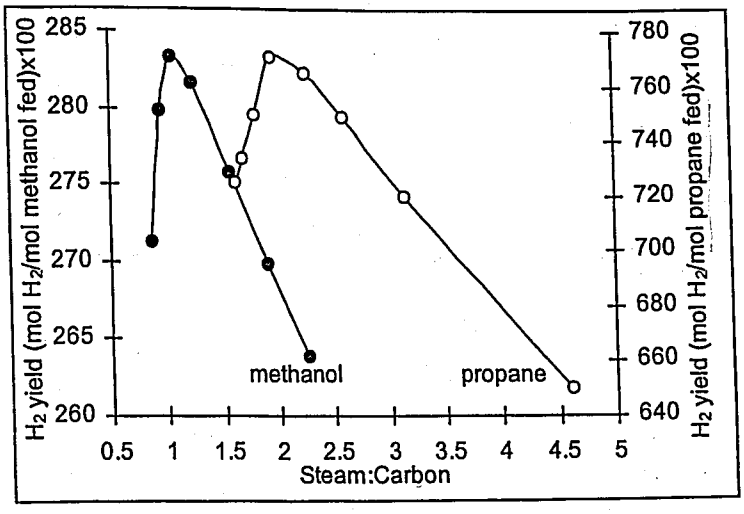

Figure 5.12. Thermodynamic investigation of the effect of steam:carbon ratio on H_2 yield (moles of H_2 produced/moles of fuel fed)x100 in indirect partial oxidation of methanol and propane

It is seen that the molar yield of hydrogen from methanol is lower than that of propane, which has an advantage of 2.7 x methanol. The maximum yield of hydrogen from propane is seen to occur at a steam:carbon ratio of ca. 2.0 (Figure 5.12) which may cause coking with a nickel based catalyst (Rostrup-Nielsen, 1984). The advantage of propane decreases to 2.6 if the system is operated at a steam:carbon ratio of 2.5. Alternatively, a noble metal catalyst may be preferred for operation at a ratio of 2.0 (Pena *et al.*, 1996). Methanol conversion over a Cu/ZnO catalyst is not subject to coking (Jiang *et al.*, 1995; Ma *et al.*, 1996; Peppley *et al.*, 1999) and can be operated at a ratio of 1.0.

Carried weight is an important issue, especially in passenger cars, and affects fuel consumption and overall performance. Therefore, the results were recalculated in terms of the volume of hydrogen produced per weight of fuel plus water added, and are presented in Figure 5.13. In contrast with the trends in Figure 5.12, the carried weight based hydrogen yields start directly from a maximum and decrease with increasing water:fuel ratios. When expressed in terms of carried weight, the molar yields observed at steam:carbon ratios lower than 1.1 for methanol and 2.0 for propane in Figure 5.12 increase, since lower quantities of water are required, and this leads to higher hydrogen yields per carried weight (Figure 5.13). The formation of trends shown in Figure 5.12 is

thus eliminated. Propane is again better than methanol when carried weight is considered, but its advantage is decreased to ca. 1.1 x methanol (Figure 5.13).

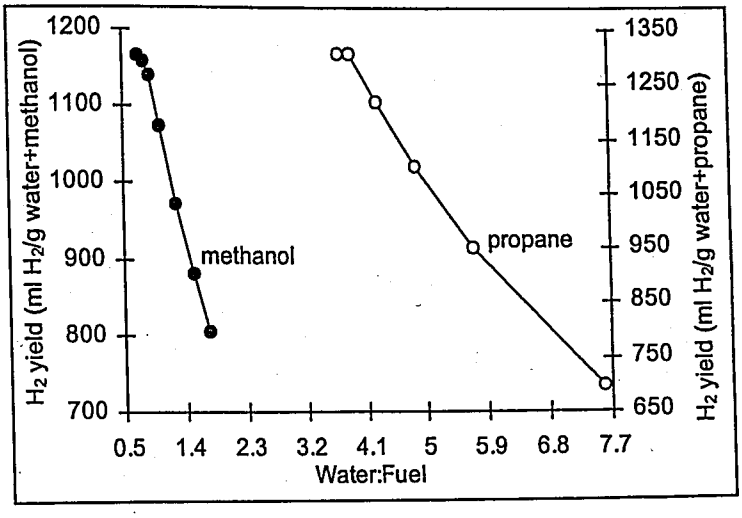

Figure 5.13. Thermodynamic investigation of the effect of injected water:injected fuel ratio on H_2 yield (volume of H_2 produced (ml)/mass of injected water and fuel (g)) in indirect partial oxidation of methanol and propane

Results of the simulations based on reaction kinetics are given in Figure 5.14. Steam:carbon ratios for both methanol and propane are higher than those calculated on the thermodynamics basis (Figures 5.12 and 5.14). In order to satisfy ca. 95 per cent overall fuel conversion, higher amounts of fuel must be oxidized, hence more water has to be fed to the reactor in order to control the bed temperature. As a result, the optimal values of the steam:carbon ratios increase to ca. 5.1 in the case of methanol and ca. 3.3 in the case of propane (Figures 5.12 and 5.14). The latter result indicates the use of Ni instead of a precious metal as catalyst in indirect partial oxidation of propane since the steam:carbon ratio is greater than 2.5. Finally, the yield of hydrogen is less than that predicted on thermodynamic grounds, as expected.

Results of the simulation of direct partial oxidation are reported in Figures 5.15 and 5.16. Maximal theoretical molar yields for methanol are 200 per cent (Reaction (5.3)) while those for propane are 700 per cent (Reactions (5.4) and (4.3)):

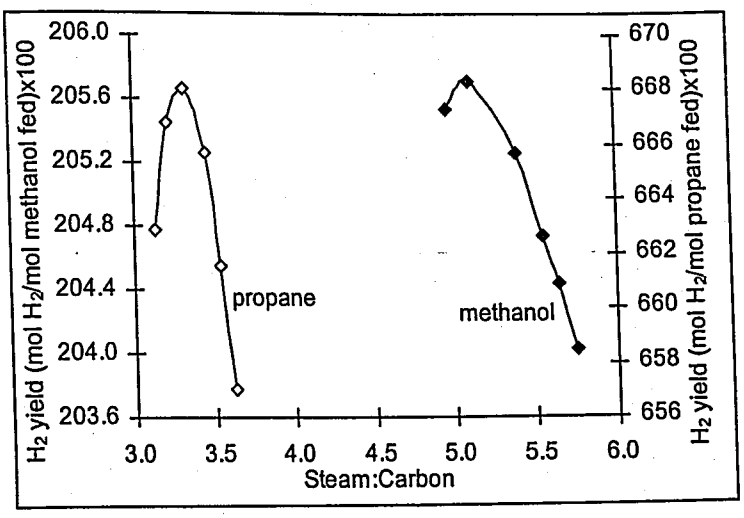

Figure 5.14. Kinetic investigation of the effect of steam:carbon ratio on H_2 yield (moles of H_2 produced/moles of fuel fed)x100 in indirect partial oxidation of methanol and propane

$$CH_3OH + 0.5O_2 = CO + H_2O + H_2, \quad \Delta H^{o}_{298} = -151.2\,kJ\,mol^{-1} \tag{5.3}$$

$$C_3H_8 + 1.5O_2 = 3CO + 4H_2, \quad \Delta H^{o}_{298} = -227.8\,kJ\,mol^{-1} \tag{5.4}$$

$$CO + H_2O = CO_2 + H_2, \quad \Delta H^{o}_{298} = -41.2\,kJ\,mol^{-1} \tag{4.3}$$

Since no water is injected into the reactor and only added to the product stream, no decrease in yield is expected at higher steam:carbon ratios. Again, the maximum yields calculated (ca. 60 per cent for methanol and 665 per cent for propane) are below theoretical limits, as expected (Figure 5.15).

More meaningful comparisons of the fuels can be made on carried weight based hydrogen yields that are given in Figure 5.16. Propane is seen to have an advantage of 4.6 x methanol (Figure 5.16) but to produce ca. 1.25 x more hydrogen than indirect partial oxidation (Figures 5.13 and 5.16). In the case of methanol, indirect partial oxidation gives ca. 3.5 x more hydrogen than direct partial oxidation (Figures 5.13 and 5.16).

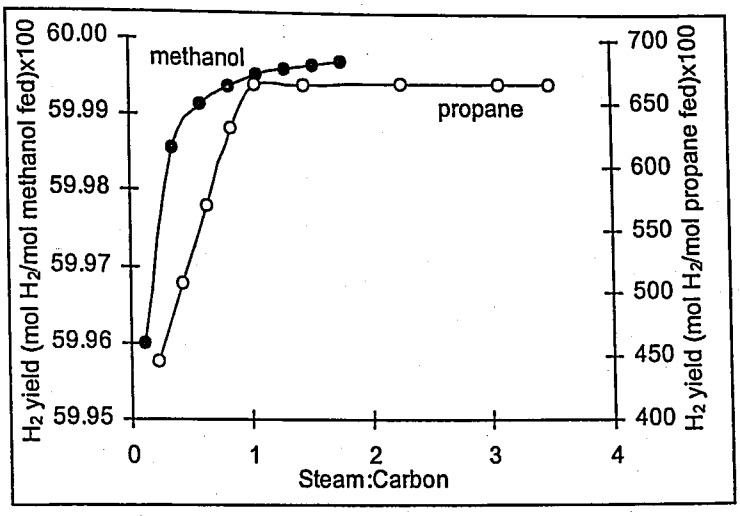

Figure 5.15. Thermodynamic investigation of the effect of steam:carbon ratio on H_2 yield (moles of H_2 produced/moles of fuel fed)x100 in direct partial oxidation of methanol and propane

Thus it is clear that propane will be a more efficient fuel for fuel cells than methanol, at least on thermodynamic grounds. Indirect partial oxidation yields more hydrogen in the case of methanol whereas the direct route seems to be better in the case of propane. However, thermodynamics-based calculations of the direct partial oxidation of propane show that the exit carbon monoxide levels are below 2 per cent only when the water:propane ratio is greater than or equal to ca. 2.8. At this ratio, the hydrogen yield obtained from the indirect route (ca. 1310 ml/g) seems to be slightly greater than that calculated for the direct route (ca. 1300 ml/g) (Figures 5.13 and 5.16). In addition, indirect partial oxidation of propane gives ca. 1.2 x more hydrogen than the direct partial oxidation when the molar hydrogen yields are considered (Figures 5.12 and 5.15). Consequently, indirect partial oxidation gives higher hydrogen yields but may demand that a vehicle be fuelled with both propane and water.

Although the simulations show that propane is the preferred source of hydrogen, which is also confirmed by kinetics-based calculations (Figure 5.17), the indirect system suffers from the disadvantage that propane oxidation does not start at room temperature as in the case of methanol and hydrogen (Jiang *et al.*, 1995; Ma *et al.*, 1996). Ma (1995) has shown that propane reactions will become significant above ca. 440 K, and combustion of

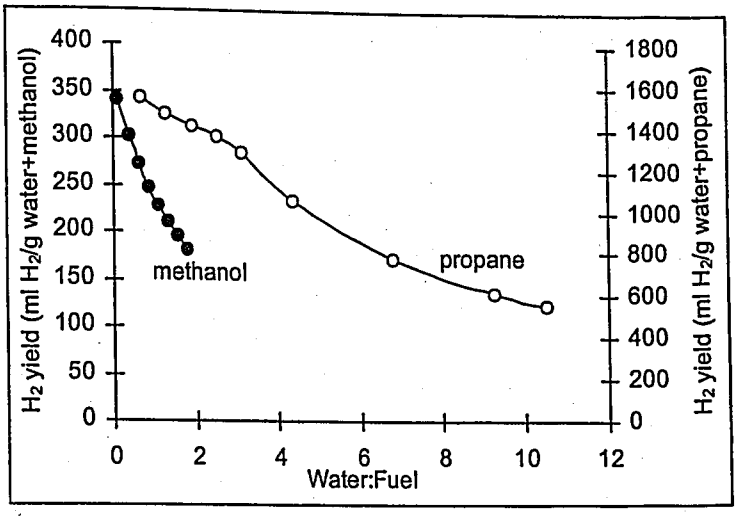

Figure 5.16. Thermodynamic investigation of the effect of injected water:injected fuel ratio on H_2 yield (volume of H_2 produced (ml)/mass of injected water and fuel (g)) in direct partial oxidation of methanol and propane

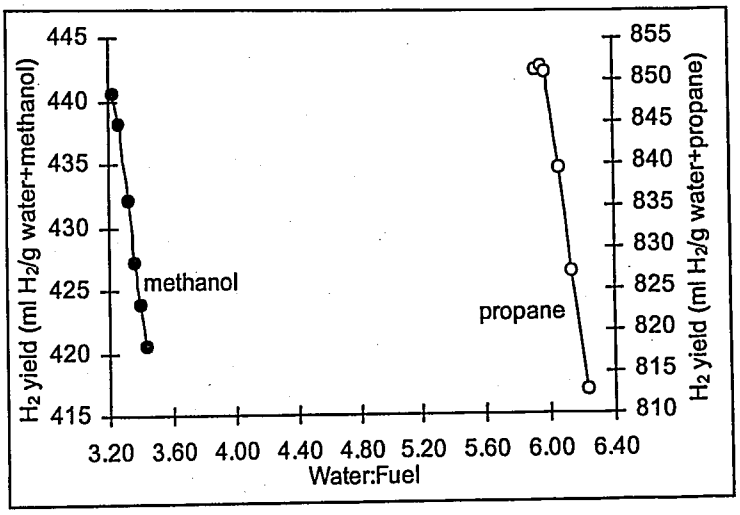

Figure 5.17. Kinetic investigation of the effect of injected water:injected fuel ratio on H_2 yield (volume of H_2 produced (ml)/mass of injected water and fuel (g)) in indirect partial oxidation of methanol and propane

methanol or hydrogen is needed to initiate the reaction at room temperature and to increase the bed temperature to this value. Storage of these amounts of hydrogen from a previous

run (ca. 15 l/kg-cat) (Ma, 1995) or battery heating of the catalyst bed is needed for operation with propane.

5.3.1. Summary

The use of methanol and propane in on-board hydrogen generation for mobile fuel cell applications is investigated by a series of computer simulations. A combination of total oxidation and steam reforming (indirect partial oxidation) on bimetallic catalysts (Pt-Ni for propane, Pt-Cu/ZnO for methanol) and one step, direct partial oxidation on Pt-coated monoliths for propane and Rh gauze for methanol are considered as the two alternative operations. The overall performance is evaluated by calculating the molar hydrogen yields and hydrogen yields based on carried weight. Simulations based on the thermodynamics of the two operations indicate indirect partial oxidation of propane as the best option in terms of hydrogen yield. The optimum hydrogen yield is calculated to occur at a steam:carbon ratio of ca. 2.0, which is below 2.5 and may lead to coking on Ni. Operating the system with ratios greater than 2.5 allows the use of Ni with lower hydrogen yield but which is still greater than that of methanol. Alternatively, using precious metal catalysts such as Rh, on which carbon formation is less likely to occur, provides the flexibility of operating at the desired steam:carbon ratio levels and results in higher hydrogen yields. Simulations based on the kinetics of the indirect partial oxidation reactions indicate that propane is the preferred fuel but that the system requires higher steam:carbon ratios thus favoring the use of Ni. Energy must be provided to start propane oxidation whereas methanol oxidation can be initiated at room temperature.

5.4. On-board Fuel Conversion for Hydrogen Fuel Cells: Comparison of Different Fuels by Computer Simulations

The present section compares on-board hydrogen generation from methane (model hydrocarbon for natural gas), propane (model hydrocarbon for LPG), isooctane (model hydrocarbon for gasoline) and methanol by two different conversion mechanisms – the combined oxidation/steam reforming, i.e. indirect partial oxidation and the one-step, direct partial oxidation. For this purpose, the complete fuel processor/fuel cell operations specialized for different conversion routes, hydrocarbons and catalysts are modeled and simulated to obtain hydrogen yields as functions of quantities of water and fuel fed into the systems.

5.4.1. Computer Simulations

Two major differences exist for methanol. In contrast to the direct partial oxidation of hydrocarbons for which fuel conversion is around 90 per cent, the maximum conversion reported for the direct reaction involving methanol is ca. 30 per cent (Zum Mallen and Schmidt, 1996). In the combined oxidation/steam reforming, i.e. indirect partial oxidation, the steam reforming of methanol is carried out over a Cu/ZnO catalyst where the maximum temperature is ca. 600 K (Wainwright and Trimm, 1995). Hydrocarbons are steam reformed over nickel-based catalysts, where the maximum temperature is of the order of 1100 K (Rostrup-Nielsen, 1984).

Results of the simulations are reported in Figures 5.18-5.25 and in Table 5.5. Figures 5.18-5.25 plot the yield of hydrogen expressed as a percentage of the theoretical amount that could be expected. Thus, for example, one mole of octane could be expected to yield up to 17 moles of hydrogen via Reactions 1 and 2 and 25 moles of hydrogen via reactions 2 and 3. An amount of 10 moles of hydrogen from one mole of octane thus corresponds to a yield of (10/17)x100 per cent via direct oxidation or (10/25)x100 per cent via oxidation/steam reforming:

$$C_8H_{18} + 4O_2 = 8CO + 9H_2, \quad \Delta H^{o}_{298} = -659.9\ \text{kJ mol}^{-1} \tag{5.5}$$

$$CO + H_2O = CO_2 + H_2, \quad \Delta H^{o}_{298} = -41.2\,kJ\,mol^{-1} \qquad (4.3)$$

$$C_8H_{18} + 8H_2O = 8CO + 17H_2, \quad \Delta H^{o}_{298} = 1274.8\,kJ\,mol^{-1} \qquad (5.6)$$

For direct partial oxidation, the maximum theoretical hydrogen yields are 3 moles from methane, 7 moles from propane, 17 moles from octane and 2 moles from methanol. For oxidation/steam reforming, the figures are 4 moles from methane, 10 moles from propane, 25 moles from octane and 3 moles from methanol.

The predicted yields are plotted as a function of water:fuel ratio injected into the system. This will not be the water:fuel ratio in the reactor since some water will be generated and some fuel removed by total oxidation. In that fuel economy is related to weight carried, more meaningful results are reported in Table 5.5, where the amount of hydrogen fed to the fuel cell is given as a percentage of the weight of fuel and water carried.

Table 5.5. Weight based hydrogen yields obtained from the simulations

Fuel	Indirect partial oxidation			Direct partial oxidation		
	T_{max} (K)	H_2 yield per weight at 353 K ((ml g^{-1})x100) [3]	Water: Fuel [4]	T_{max} (K)	H_2 yield per weight at 353 K ((ml g^{-1})x100) [3]	Water: Fuel [4]
Methane	1100	500	3.45	1490	1060	1.4
Methanol	600	440	3.26	1370	318	0.2
Propane	1100	850	5.98	1770	850	5.5
Octane	1100	1050	11.41	1840	770	14.4

[3] Weight based hydrogen yield = volumetric flow rate of hydrogen at 353 K (operating temperature of the fuel cell) (ml)/weight of the fuel+water injected into Reactor 1 (g))
[4] Water:Fuel = moles of water injected/moles of fuel injected

Considering first the results for direct partial oxidation (Figures 5.18-5.21), the amount of water added was calculated in terms of the amount needed to cool the gases

leaving Reactor 1 to 473 K (the inlet temperature for the water-gas shift reactor (Amadeo and Laborde, 1995)) and the amount needed to reduce the carbon monoxide level to 2 mole per cent - the maximum allowed level for the selective oxidation/fuel cell system (Golunski, 1998; Trimm and Önsan, 2001). This corresponded to water:fuel ratios shown as lines A, intersecting the carbon monoxide composition curves at 2 mole per cent as shown in Figures 5.18, 5.19 and 5.20 for methane, propane and octane, respectively. In contrast with the direct conversion of other fuels, carbon monoxide levels are calculated to be less than 1.2 mole per cent in methanol direct partial oxidation (Figure 5.21) due to the lower conversion levels in it (ca. 30 per cent).

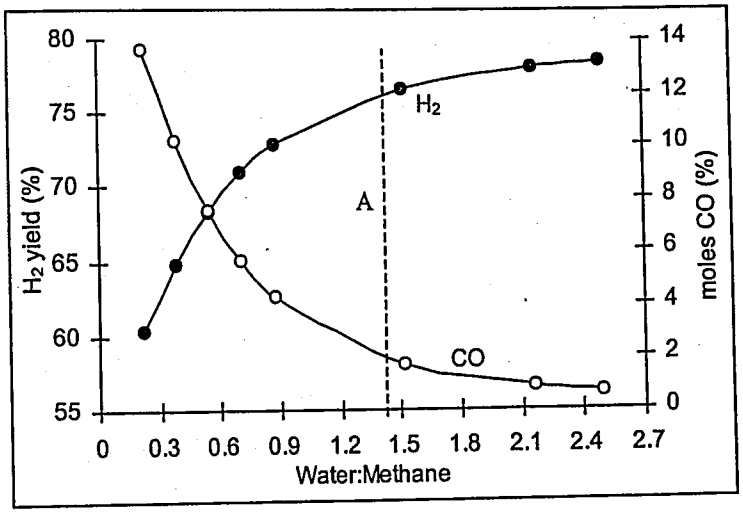

Figure 5.18. Effect of water:methane ratio injected into the system on H_2 yield [calculated amount of H_2 produced in moles/theoretical amount of H_2 produced in moles)x100] and on molar percentage of CO in direct partial oxidation of methane

The theoretical yield of hydrogen is seen to be much higher for hydrocarbons than for methanol, with propane and octane giving the highest yields (Figures 5.18-5.21). However, the maximum temperature, i.e. the exit temperature from Reactor 1 (Figure 4.1), calculated for octane is 1840 K (Table 5.5), which is approximately equal to the temperature at which the formation of nitrogen oxides becomes significant (ca. 1850 K). The maximum temperature for propane is 1770 K and for methane is 1490 K, inferring that the use of these two fuels may be preferred in order to avoid unwanted NO_x emissions.

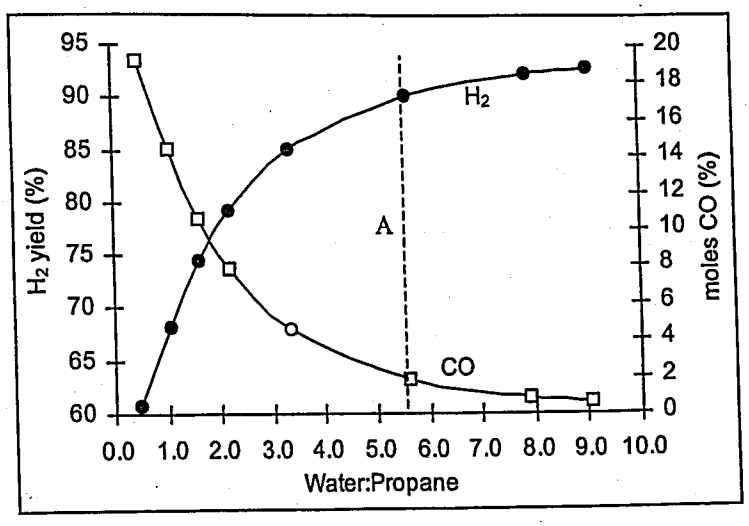

Figure 5.19. Effect of water:propane ratio injected into the system on H_2 yield [calculated amount of H_2 produced in moles/theoretical amount of H_2 produced in moles)x100] and on molar percentage of CO in direct partial oxidation of propane

In terms of hydrogen produced per weight carried, methane would seem to be preferred to propane, octane and methanol (Table 5.5), but these values do not include cylinder weight. Methane would require higher pressure storage than propane and would thus demand heavier cylinders. Octane and methanol could be stored in a normal gasoline tank, with minimal weight disadvantage.

Theoretical hydrogen yields from total oxidation/steam reforming are less than direct oxidation for hydrocarbons but greater for methanol (Figures 5.18-5.21 and 5.22-5.25). In the former conversion route, maximum bed temperatures, which are around 1100 K for hydrocarbons and 600 K for methanol, are much less than those needed to form nitrogen oxides. Effluent streams from Reactor 1 are found to contain carbon monoxide less than 2 mole per cent, and the inclusion of a water-gas shift reactor (Reactor 2 (Figure 4.1)) is not considered.

Water:fuel ratios calculated for methane, propane and methanol in the oxidation/steam reforming route are seen to be higher than those associated with direct oxidation (Table 5.5). Overall fuel conversion is taken to be 95±2 per cent in simulations

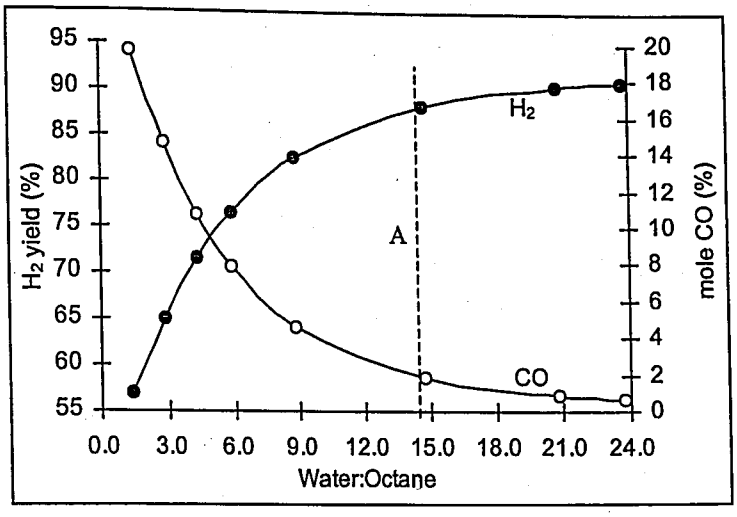

Figure 5.20. Effect of water:octane ratio injected into the system on H_2 yield [calculated amount of H_2 produced in moles/theoretical amount of H_2 produced in moles)x100] and on molar percentage of CO in direct partial oxidation of octane

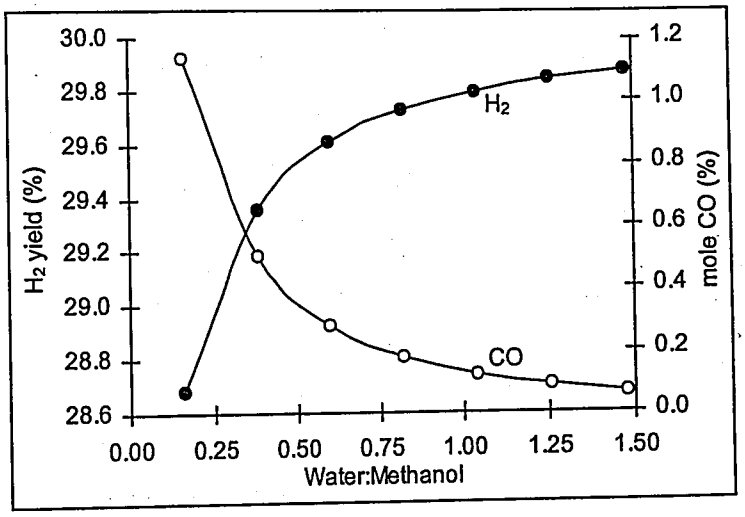

Figure 5.21. Effect of water:methanol ratio injected into the system on H_2 yield [calculated amount of H_2 produced in moles/theoretical amount of H_2 produced in moles)x100] and on molar percentage of CO in direct partial oxidation of methanol

of indirect partial oxidation of methanol, propane and octane (Jiang *et al.*, 1995; Ma, 1995). This leads the total oxidation conversions to be kept at their maximum possible values, which are calculated to be ca. 26 per cent for methanol and ca. 28 per cent for

propane and octane. Note that further oxidation leaves less fuel for steam reforming and lowers hydrogen production. Due to the excessive heat liberated by oxidation, higher amounts of water are injected into Reactor 1 in order to control the bed temperatures and hence prevent thermal sintering of the catalyst. Water is also used to facilitate steam reforming, which goes almost to completion (Jiang *et al.*, 1995; Ma, 1995). These factors lead to a difference between water:fuel ratios obtained in direct and indirect routes. This difference is particularly obvious with methanol, where extra water is needed to control the temperature of the Cu/ZnO catalyst (Table 5.5).

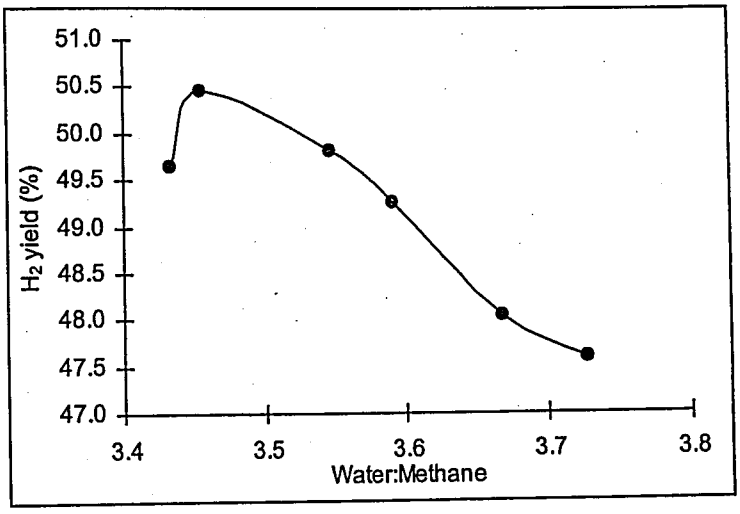

Figure 5.22. Effect of water:methane ratio injected into the system on H_2 yield [calculated amount of H_2 produced in moles/theoretical amount of H_2 produced in moles)x100] in indirect partial oxidation of methane

Octane has an opposite trend in terms of water:fuel ratios. The sensible heat of the Reactor 1 exit stream is considerably high due to the increased elevated exit temperature (1840 K) and higher molar flow rates of components leaving Reactor 1. Hence, a relatively higher amount of water injection at point B (Figure 4.1) is needed for cooling the gas stream to 473 K. Moreover, the amount of carbon monoxide generated in Reaction (5.5) is the highest in the case of octane, requiring much more water for its removal in the water-gas shift converter (Reactor 2 (Figure 4.1)). These extra water requirements in the direct oxidation are dominant to the ones needed to sustain the indirect conversion of octane, leading to higher water:fuel ratios in the former route (Table 5.5).

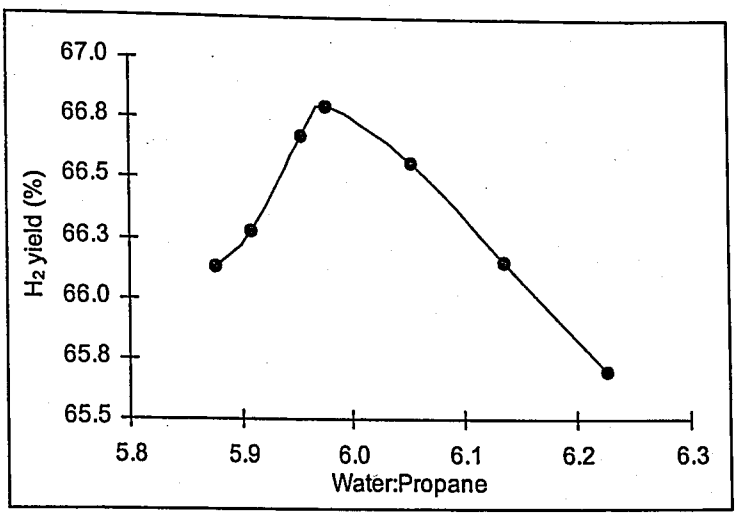

Figure 5.23. Effect of water:propane ratio injected into the system on H_2 yield [calculated amount of H_2 produced in moles/theoretical amount of H_2 produced in moles)x100] in indirect partial oxidation of propane

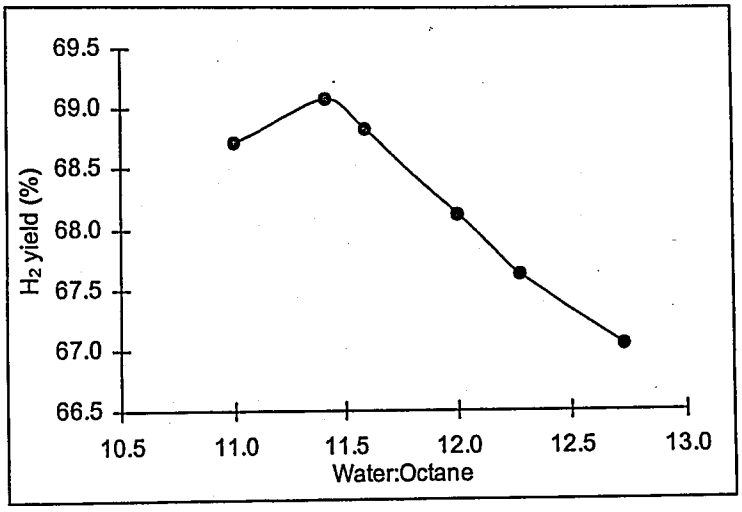

Figure 5.24. Effect of water:octane ratio injected into the system on H_2 yield [calculated amount of H_2 produced in moles/theoretical amount of H_2 produced in moles)x100] in indirect partial oxidation of octane

Although the total oxidation conversion levels for propane and octane are same (ca. 28 per cent), much more water is fed for the latter since the heat of combustion of octane (-5100.2 kJ mol^{-1}) is greater than that of propane (-2044.0 kJ mol^{-1}). Hence higher water:fuel ratios are required in the indirect partial oxidation of octane (Table 5.5).

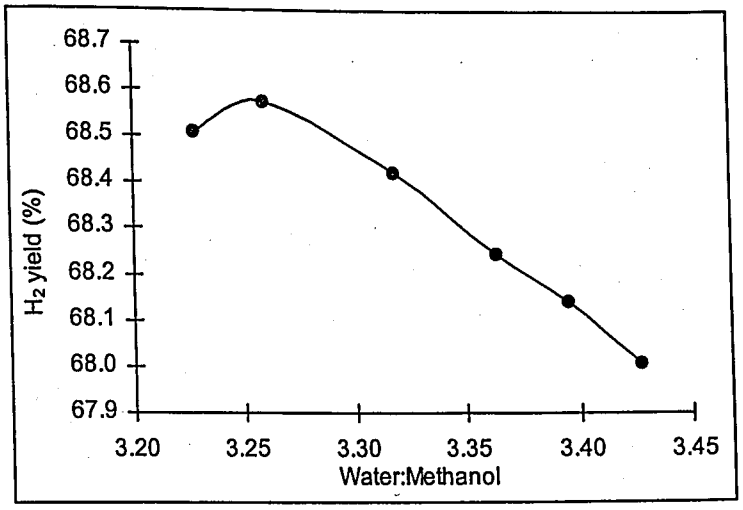

Figure 5.25. Effect of water:methanol ratio injected into the system on H_2 yield [calculated amount of H_2 produced in moles/theoretical amount of H_2 produced in moles)x100] in indirect partial oxidation of methanol

In contrast with other fuels, methane steam reforming conversion is limited (ca. 70 per cent) (Ma, 1995). Although the maximum oxidation conversion is calculated to be ca. 35 per cent for methane, the amount of water needed to be injected to control the bed temperature at ca. 1100 K will not be greater than required in the cases of propane and octane due to the relatively low heat of combustion of methane (-802.3 kJ mol^{-1}). Moreover, less water is used due to the lower extent of methane steam reforming, leading to water:fuel ratios lower than those calculated for propane and octane (Table 5.5).

5.4.2. Practical Applications

It is previously mentioned that methane would require high-weight, high-pressure cylinders and octane would lead to excessive temperatures. Methanol suffers from its significantly low weight based hydrogen yield (318 ml hydrogen/g carried). Therefore propane seems to be the optimal fuel for the direct conversion route. However, its hydrogen yield – 850 ml hydrogen/g carried - is lower than the one obtained for octane oxidized/steam reformed (1050 ml hydrogen/g carried). In addition, the cylinder weight will be greater in the propane. Thus it is possible that oxidation/steam reforming of gasoline/octane will offer the most efficient conversion, when weight-based hydrogen yields are considered.

The oxidation/steam reforming system seems to be advantageous to direct partial oxidation since the latter requires very short residence times (Dietz III *et al.*, 1996; Hickman and Schmidt, 1992; Huff and Schmidt, 1994; Zum Mallen and Schmidt, 1996) and operating conditions close to explosive limits, which may not be allowable in transportation facilities. In addition, the distribution network for gasoline is superior to that for LPG and methanol. Consequently, indirect partial oxidation of gasoline seems to be the ultimate choice again when the economics and simplicity of the operation is considered.

However, it is also possible that coke formation may be a problem particularly with gasoline. A steam:carbon ratio of ca. 2.5 is required for minimizing the coke formation on Ni catalysts (Rostrup-Nielsen, 1984). The steam:carbon ratios are found to be close to this limit (ca. 2.4-2.8) but the aromatics in gasoline may produce excess coke. Using a precious metal catalyst such as Rh instead of Ni may partially prevent coke formation (Rostrup-Nielsen and Bak Hansen, 1993). Apart from coking, high sulphur content of gasoline may also be a serious problem, since minute quantities of sulphur can easily poison the catalysts involved in the fuel processor/fuel cell system. A possible solution may be to use a 'fuel-cell grade' gasoline having reduced amount of sulphur. Alternatively propane, i.e. LPG may be used, since the fuel has much lower sulphur contents and has a lower possibility of coking when compared with gasoline.

It is seen from Figure 4.1 that heat exchange from the outlet gases to the inlet is required and that cooling of the gases may be required before entering the water-gas shift reactor or the fuel cell. In order to check that such cooling is realistic, the heat exchanger surface area is calculated for the various systems. The heat exchange efficiency in the indirect route is assumed to be 70 per cent (Equations (4.22) and (4.23)), whereas its value is between 20 per cent and 80 per cent in direct oxidation. The cooler needed to reduce the Reactor 2 exit temperatures from ca. 600 K (raised from 473 K by the exothermal heat released by the water-gas shift reaction) to 353 K is considered in calculating the total heat exchanger area in the latter operation. The results, summarized in Table 5.6, show that the predicted surface areas are within acceptable limits, although the area required in the case of octane is somewhat high due to the presence of the higher amount of water (Figures 5.20 and 5.24). It is worth noting that a low level of sensible heat recovery about 30 per cent (f_3=0.3) from Reactor 3 together with a heat exchange at Reactor 1 exit with 10 per

cent efficiency (f=0.1) is sufficient to increase the feed temperature from 298 K to 1243 K in the direct oxidation case, indicating the sufficiency of smaller heat exchange areas, which can also be seen in Table 5.6.

It is necessary to note that the oxidation of methane, propane and octane cannot be initiated at room temperature. Catalysts must be heated to light-off temperatures, either electrically or by combusting hydrogen from a previous run. Ma (1995) measured the amount of hydrogen to reach light-off for propane as 15 ml hydrogen/g catalyst. Methanol will light-off at room temperature (Jiang *et al.*, 1995) but gives a much worse performance.

It should also be noted that the introduction of the fuel conversion system will require vehicle fuelling with both water and fuel. In the case of methanol, a mixture is possible whereas with hydrocarbons, two tanks will be required.

Table 5.6. Heat exchange area required for cooling the exit gases from Reactor 1[5]

	Indirect partial oxidation[6]	Direct partial oxidation[7]
Methane	3.9 – 4.2	1.0 – 1.5
Methanol	0.4 – 0.5	0.6 – 1.0
Propane	3.4 – 3.7	2.7 – 3.3
Octane	11.1 – 12.2	6.5 – 8.4

[5] Overall heat transfer coefficient is taken to be 830 J m^{-2} K^{-1} s^{-1} (Perry *et al.*, 1984)
[6] 70 per cent of heat transfer efficiency is assumed
[7] The area of the cooler after Reactor 2 is included

5.4.3. Summary

On-board hydrogen generation for fuel cells from natural gas (modeled as methane), LPG (modeled as propane), gasoline (modeled as octane) and methanol by direct and indirect partial oxidation routes is investigated by a series of computer simulations. Direct partial oxidation of propane and indirect partial oxidation of octane are found to be the efficient options when hydrogen yields based on the weight of carried fuel and water are considered. Nevertheless, the former suffers from the requirement of very short residence

times, nearly explosive operating conditions and the presence of a fuel storage cylinder. On the other hand, coke formation is a potential problem in the latter option, which may be eliminated by using a precious metal catalyst such as Rh instead of Ni. High sulphur content in gasoline may be detrimental to the operation of the catalytic units. Therefore, propane (LPG) may be used in indirect partial oxidation due to the significant coking and sulphur content problems associated with gasoline. Relatively low reactivity and the requirement of a much heavier storage cylinder are the major drawbacks of methane. Methanol, which is often suggested as a fuel, reacts at room temperature but gives lower hydrogen yields.

5.5. Investigation of Ignition Characteristics of Propane and n-Butane over Supported Pt, Ni, and Pt-Ni Catalysts

The efficient operation of a fuel processor is mostly based on the successful selection of fuel, fuel conversion mechanism and catalyst combinations. Computer simulations of a number of such combinations have shown that the conversion of LPG – a mixture of propane and n-butane – to hydrogen via indirect partial oxidation, i.e. combined total oxidation and steam reforming route, over a supported bimetallic Pt-Ni catalyst is a promising option in terms of optimal hydrogen production. In this section, ignition characteristics of propane and n-butane over the bimetallic Pt-Ni catalyst are studied under conditions pertinent to fuel processor operation in the fuel rich regime. A number of fuel:oxygen ratios and the individual roles of the active metals, Pt and Ni, are studied through a series of reaction tests for the assessment of catalytic activity and via electron microscopy studies for detailed surface characterization of the catalysts.

The oxidation of propane and n-butane can be described by the following reactions:

$$C_3H_8 + 5O_2 = 3CO_2 + 4H_2O, \quad \Delta H^{\circ}_{298} = -2044.0\ \text{kJ mol}^{-1} \tag{5.7}$$

$$n\text{-}C_4H_{10} + 6.5O_2 = 4CO_2 + 5H_2O, \quad \Delta H^{\circ}_{298} = -2658.5\ \text{kJ mol}^{-1} \tag{5.8}$$

The fuel rich conditions used in this study involve fuel:oxygen ratios ($HC:O_2$) greater than the corresponding stoichiometric values, which are 0.200 for propane and 0.154 for n-butane. Oxygen is the limiting reactant, and hence hydrocarbon conversions are dictated by the amount of oxygen existing in the feed stream. Maximum conversions that can be achieved in Reactions (5.7) and (5.8) are equal to $\{1/[5(HC:O_2)]\}x100$ and $\{1/[(13/2)(HC:O_2)]\}x100$, respectively; 40 per cent is the highest propane conversion and 30.8 per cent is the highest n-butane conversion when a $HC:O_2$ ratio of 0.5 is used. Therefore, the actual conversions obtained in the experiments are normalized using these maximum values to define the 'conversion' employed in this study:

$$\text{conversion} = \frac{\text{actual hydrocarbon conversion}}{\text{maximum hydrocarbon conversion}} \text{x100} \qquad (5.9)$$

Thus, for example, 10 per cent of conversion observed in propane and n-butane oxidation at HC:O_2 ratio of 0.5 corresponds to conversions of 25 per cent and 32.5 per cent respectively after normalization.

The estimation of the actual conversion in the numerator of Equation (5.9) is based on the disappearance of the oxygen peaks, and is expressed by Equation (5.10):

$$\text{actual hydrocarbon conversion} = \frac{F^{o}_{O_2} - F_{O_2}}{\tilde{k}.F^{o}_{HC}} \text{x100} \qquad (5.10)$$

In Equation (5.10), F^{o}_{HC} and $F^{o}_{O_2}$ are the molar flow rates of hydrocarbon and of oxygen in the feed stream, F_{O_2} is the molar flow rate of oxygen remaining after reaction and $\tilde{k}$ is the stoichiometric coefficient of oxygen in Reactions (5.7) and (5.8). Note that at constant temperature and pressure the molar flow rates are proportional to volumetric flow rates. The latter can be calculated using the peak area/volume relationships obtained from calibrations. The actual conversion can also be estimated either from the disappearance of the hydrocarbon peaks or from the formation of the carbon dioxide peaks. When evaluated starting from different chromatographic data obtained from different gas chromatographs, the light-off temperatures, which are defined as the values at which 10 per cent of the conversion is obtained, are found to differ by a maximum of 15 K.

The light-off curves of propane and n-butane oxidation over Pt/δ-Al_2O_3, Ni/δ-Al_2O_3 and Pt-Ni/δ-Al_2O_3, and the corresponding SEM micrographs of the catalysts are presented in Figures 5.26, 5.27, in Figures 5.28, 5.29 and in Figures 5.30, 5.31, respectively. The fuel:oxygen ratio is kept at 0.48 for propane and 0.37 for n-butane, so that the maximum theoretical conversion that can be achieved is 42 per cent. Thus, the comparison is made for equal maximum conversion levels.

The conversion-temperature plots obtained for propane and n-butane oxidation over Pt/δ-Al_2O_3, Ni/δ-Al_2O_3 and Pt-Ni/δ-Al_2O_3 are given in Figures 5.26, 5.28 and 5.30, respectively. For all catalysts, it can be seen that n-butane is oxidized earlier than propane, and the light-off temperatures obtained for n-butane are therefore lower (Table 5.7). Since it is generally accepted that the reactivity of alkanes increases with increasing chain length (Aryafar and Zaera, 1997; Veser *et al.*, 1999; Veser and Schmidt, 1996), such a trend is expected. The difference between the light-off temperatures of propane and n-butane is not too significant; this difference decreases as the carbon number increases (Trimm and Önsan, 2001).

It is possible to obtain complete 'S' curves during temperature-programmed oxidation over the Pt-catalyst (Figure 5.26). In the case of Ni, however, the conversion levels achieved are less than 30 per cent within the 390-678 K temperature range (Figure 5.28). This pronounced gap between the oxidation activities of the two catalysts can also be seen quantitatively from the difference of ca. 140 K between the light-off temperatures (Table 5.7) which shows the superior performance of platinum in catalytic combustion (Ma *et al.*, 1996; Tomishige *et al.*, 2002; Veser and Schmidt, 1996). Although gas phase oxygen exists in the reaction medium, the Pt-sites tend to be in their active metallic state (Pt^0), since the oxides of Pt are known to be unstable. This resistance against transformation into the less active oxide forms makes Pt-based catalysts active in catalytic combustion. High activities of Pt-based catalysts are confirmed also in fuel-lean conditions involving excess oxygen (Aryafar and Zaera, 1997; Veser *et al.*, 1999). Nickel-based catalysts, on the other hand, are found to exhibit alkane oxidation activities lower than those of platinum (Table 5.7). Although poor oxidation performances have been reported for supported nickel (Ma *et al.*, 1996; Tomishige *et al.*, 2002), Aryafar and Zaera (1997) have found nickel more active than both platinum and palladium in methane oxidation.

In spite of their poor oxidation features, supported nickel catalysts are known to be effective in driving hydrogen producing reforming reactions. Therefore, if platinum and nickel metals coexist over the same catalyst exothermic oxidation and endothermic reforming reactions can run together due to improved heat transfer on the catalyst surface

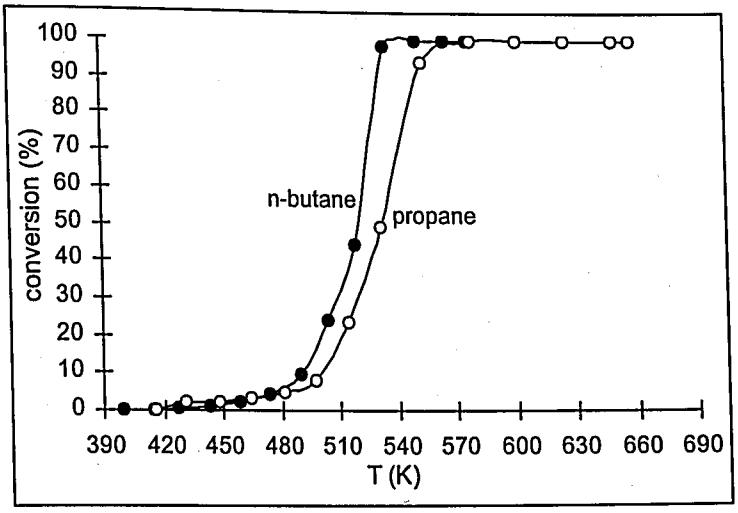

Figure 5.26. Conversion-temperature plots for oxidation of propane and n-butane over 0.2%Pt/δ-Al_2O_3 (C_3:O_2=0.48, n-C_4:O_2=0.37)

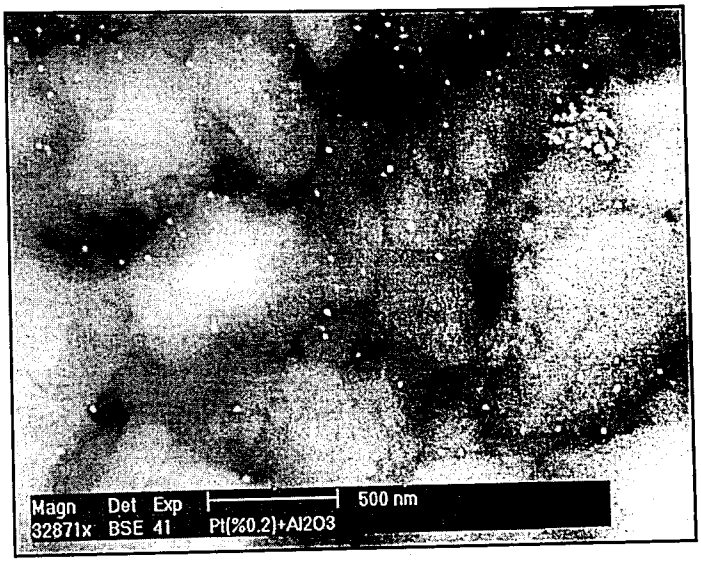

Figure 5.27. SEM micrograph of the 0.2%Pt/δ-Al_2O_3 catalyst (reduced, fresh sample)

which can lead to efficient hydrogen production for fuel cell applications. In the present work, the bimetallic Pt-Ni catalyst was tested for its oxidation characteristics. The oxidation of propane and n-butane over the Pt-Ni catalyst is shown in Figure 5.30. When compared with the monometallic nickel-catalyzed combustion (Figure 5.28), the light-off temperatures are found to be ca. 50 K lower in the case of Pt-Ni catalyst (Figure 5.30, Table 5.7) even though the amount of platinum is kept as low as 0.2 per cent by weight.

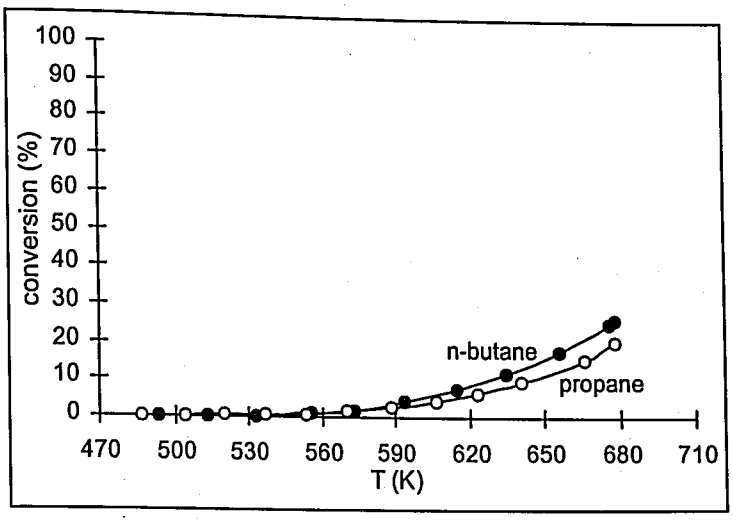

Figure 5.28. Conversion-temperature plots for oxidation of propane and n-butane over 15%Ni/δ-Al_2O_3 (C_3:O_2=0.48, n-C_4:O_2=0.37)

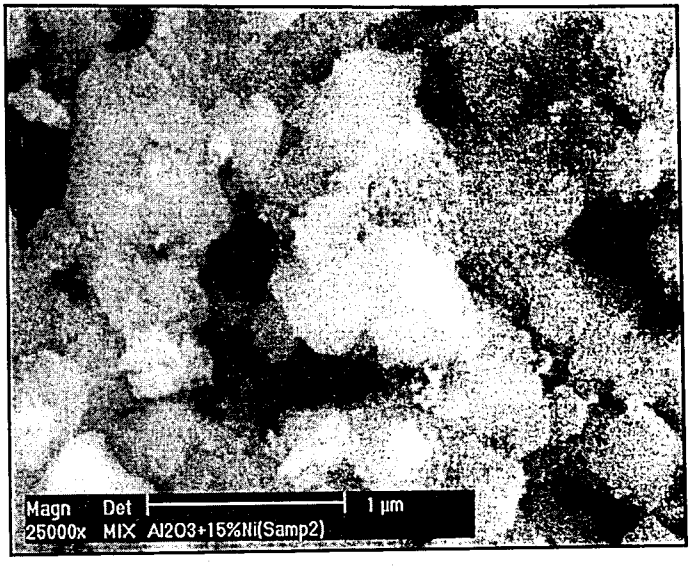

Figure 5.29. SEM micrograph of the 15%Ni/δ-Al_2O_3 catalyst (reduced, fresh sample)

However, the monometallic Pt catalyst seems to be much more active than the bimetallic Pt-Ni in terms of lower light-off temperatures (Table 5.7). The differences between these catalytic activities will be pointed out when the effect of the fuel:oxygen ratio on the ignition behavior of the catalysts is discussed.

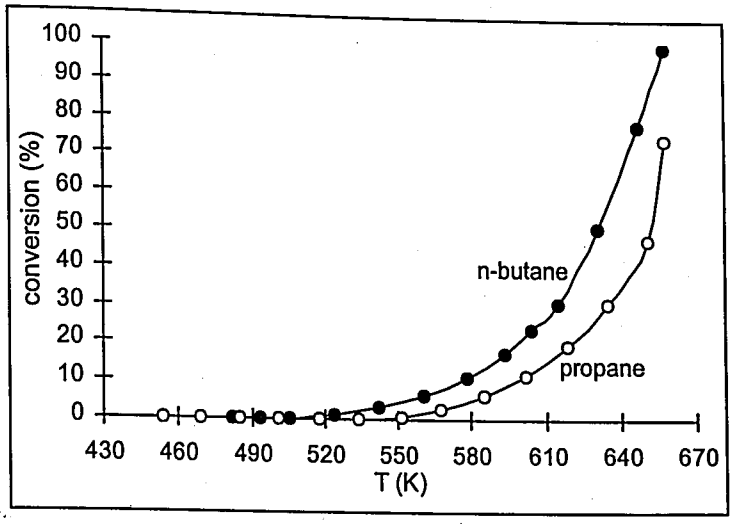

Figure 5.30. Conversion-temperature plots for oxidation of propane and n-butane over 0.2%Pt-15%Ni/δ-Al_2O_3 (C_3:O_2=0.48, n-C_4:O_2=0.37)

Figure 5.31. SEM micrograph of the 0.2%Pt-15%Ni/δ-Al_2O_3 catalyst (reduced, fresh sample)

The Pt-containing bifunctional catalyst seems to offer some additional features, apart from their better oxidation activities than the monometallic nickel catalyst. In the kinetically controlled regimes of Figures 5.26, 5.28 and 5.30, where conversion is below 10 per cent (Ma *et al.*, 1996), the rate of onset of oxidation (defined as the change in conversion with temperature) over Pt-Ni seems to be greater than those achieved over

Table 5.7. Light-off temperatures of propane and n-butane

Catalyst	Light-off temperature (K)	
	Propane (C_3:O_2=0.48)	n-Butane (n-C_4:O_2=0.37)
0.2%Pt/δ-Al_2O_3	501	489
15%Ni/δ-Al_2O_3	643	628
0.2%Pt-15%Ni/δ-Al_2O_3	597	573

either monometallic catalysts. The SEM micrograph of the Pt-Ni catalyst shown in Figure 5.31 indicates that platinum agglomerates, represented by the bright regions, are settled over a nickel environment (gray region in the background) which covers the alumina surface almost completely. However alloy formation or formation of some other type of new active sites was not detected; SEM-BCI did not indicate any relevant contrast difference. This finding is supported by the EDX results. It can be speculated that the source of this beneficial effect may be the synergistic interactions between Pt and Ni sites. Similar results have also been reported by Opoku-Gyamfi and Adesina (1999) who have studied kinetics of methane oxidation over Pt, NiO and Pt-NiO catalysts. Based on XRD and XPS analyses, they reported that a synergistic interaction existed between Pt and NiO centers rather than the formation of new Pt-Ni active phases. Finally, although SEM studies and literature information provide some ideas about the type of synergy, further detailed studies are required for unveiling the interactive characteristics of the bifunctional catalyst.

Fuel:oxygen ratio defines the balance between the amounts of the fuel oxidized/fuel reformed in indirect partial oxidation and has an optimum value that corresponds to maximum hydrogen production. The effect of the fuel:oxygen ratio on the light-off temperatures was therefore investigated and is presented in Figure 5.32. The quantitative differences between the light-off temperatures of different hydrocarbon-catalyst combinations presented in Table 5.7 can clearly be observed for different fuel:oxygen ratios in Figure 5.32. Moreover, these trends indicate several other features of the catalysts. Viewing the abscissa from right to left, it can be seen that, as the amount of

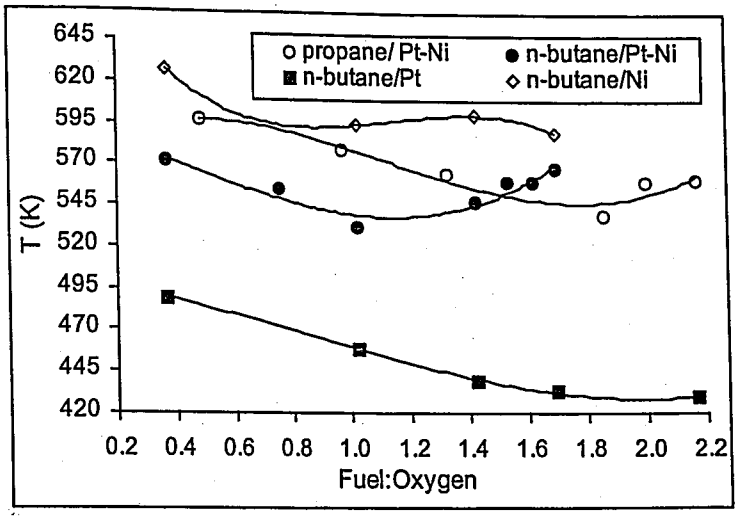

Figure 5.32. The effect of fuel:oxygen ratio on the light-off temperatures

oxygen in the feed increases, the light-off temperatures obtained for both propane and n-butane decrease down to a certain value and then start to increase again in the case of the Pt-Ni catalyst. The formation of minimum light-off temperatures at fuel:oxygen ratios of 1.1 for n-butane and 1.8 for propane over Pt-Ni catalyst can be explained by the possible interaction between two sites. It is very likely that the periphery of Pt agglomerates interacts with the dispersed Ni environment which modifies the properties of Pt and Ni sites in Pt-Ni/Al_2O_3 catalyst (Figure 5.31) and leads to increased oxidation activities represented by reduced light-off temperatures at certain fuel:oxygen ratios (Figure 5.32). It can also be speculated that Pt dominates in this interaction which can be supported by the fact that the sticking probability of the C_1-C_4 alkanes on the platinum surface, i.e. degree of competition with oxygen, increases with hydrocarbon chain length (Veser and Schmidt, 1996). The inhibiting effect of the hydrocarbon increases and, therefore, that of oxygen decreases in the case of higher alkanes. This phenomenon reported for Pt can also be observed in the case of Pt-Ni, since the minimum fuel:oxygen ratio of n-butane is smaller than that of propane, indicating that in the presence of higher quantities of oxygen in the feed, the surface ignition of the C_4-alkane is retarded earlier.

In order to understand the roles of each component further, n-butane oxidation is studied over monometallic Pt and Ni catalysts under conditions identical with those employed for Pt-Ni (Figure 5.32). At n-butane:oxygen ratios less than 1.8, the temperatures obtained over the Pt catalyst decrease steadily as the amount of oxygen fed

is decreased, and the rate of temperature decrease on Pt is almost the same as that of Pt-Ni until the minimum point (n-butane:oxygen = ca. 1.1) is reached for the latter. On the Pt catalyst, the temperatures remain almost constant beyond a ratio of 1.8, and the increase in the light-off temperatures, which is observed in the Pt-Ni catalyst, is not detected. This difference in behavior can be explained by comparing the SEM micrographs. The SEM micrograph of the monometallic Pt catalyst clearly indicates that platinum particles, represented by the bright specks, are well dispersed over the alumina support which is shown as a white cloud-like structure in the background (Figure 5.27). On the Pt-Ni catalyst, however, the Pt metal is not well dispersed but clustered in certain regions that correspond to bright locations in Figure 5.31. These clusters are composed of only Pt, since the EDX studies have shown that the bright regions in Figure 5.31 do not include any nickel agglomerates. The difference in platinum dispersion is also confirmed by the particle size analysis; the platinum particles are found to have diameters ranging between 10-60 nm and 70-330 nm over Pt/δ-Al_2O_3 and Pt-Ni/δ-Al_2O_3 catalysts, respectively. Therefore, due to the abundance of the active Pt sites over the well-dispersed Pt/δ-Al_2O_3 surface, it can be speculated that oxygen, which has a much higher sticking probability on the Pt surface than that of n-butane (Veser and Schmidt, 1996), is the dominant reactant in terms of surface coverage. Hence, the light-off temperatures follow a decreasing pattern even at low quantities of oxygen and the inhibiting effect of n-butane cannot be observed as clearly as in the case of the Pt-Ni catalyst. The relatively low number of active Pt sites over the Pt-Ni surface is likely to diminish the surface coverage of oxygen and thus facilitate competition with n-butane indicated by the increasing light-off temperatures at ratios greater than 1.1. This argument related with dispersion can probably explain the gaps between the light-off temperatures obtained for n-butane oxidation over Pt and Pt-Ni catalysts.

The increase in the light-off temperatures obtained for both hydrocarbons over the Pt-Ni catalyst at high fuel:oxygen ratios might also be due to possible carbon formation over Ni which would mask the "operation" of Pt and, therefore, result in lower oxidation activities. In order to investigate the possibility of this scenario, n-butane conversion over Pt-Ni/δ-Al_2O_3 was studied in the absence of dry air feed. The reaction temperature was increased from 453 K to 623 K at a rate of 1 K min^{-1}, with other conditions being kept identical to those explained in Section 3.5.2. The catalyst sample used in the reaction was

then analyzed on TGA by heating from 298 K to 873 K at a rate of 2 K min^{-1} under 25 ml min^{-1} flow of pure oxygen. A fresh, reduced catalyst sample was also analyzed on TGA under identical conditions. In both samples, a weight increase of ca. 2 per cent between 423-643 K was followed by a minute weight loss of around 0.7 per cent between 673-873 K. The identical TGA responses of spent and fresh catalyst samples show that no coke was deposited over the spent catalyst even in the absence of oxygen. Therefore a coking-driven inhibition is unlikely to occur during oxidation at low quantities of oxygen.

The oxidation activity of the Ni/δ-Al_2O_3 catalyst is relatively poor. Although the metal content of the catalyst is as high as 15 per cent by weight, the poor dispersion, i.e. agglomeration of the nickel particles shown in the SEM micrograph as bright regions (Figure 5.29), is likely to contribute to the highest light-off temperatures obtained among other catalysts (Table 5.7). In contrast with the trends obtained for the Pt and Pt-Ni catalysts, the light-off temperatures of n-butane oxidation over Ni seem to be less sensitive to the amount of oxygen in the feed (Figure 5.32). Although studies related with Ni-catalyzed oxidation under fuel-rich conditions are scarce, the active phase of the nickel catalyst during oxidation has been reported to be the relatively stable NiO phase, but not the metallic Ni^0 form (Dissanayake *et al.*, 1991; Ma, 1995). This may not be adequate to explain the oxygen dependency in alkane oxidation over Ni, but the differences in the trends between Ni and the Pt-containing catalysts are likely to support the importance of platinum during oxidation over the Pt-Ni catalyst.

5.5.1. Summary

The ignition characteristics of propane and n-butane over the monometallic 0.2%Pt/δ-Al_2O_3 and 15%Ni/δ-Al_2O_3 catalysts, and over the bimetallic 0.2%Pt-15%Ni/δ-Al_2O_3 catalyst which offers efficient hydrogen production through facilitating heat transfer between oxidation and reforming reactions, are investigated under fuel-rich conditions. Propane is found to have higher light-off temperatures than n-butane over all three catalysts, indicating the elevated paraffin reactivity with increasing chain length. The oxidation activities of the catalysts follow the order of Ni<Pt-Ni<Pt. Synergistic effects due to possible interactions between the periphery of Pt clusters and the Ni environment are likely to facilitate the rate of onset of oxidation and the achievement of

minimum light-off temperatures at optimum fuel:oxygen ratios ($n\text{-}C_4:O_2=1.1$, $C_3:O_2=1.8$) over Pt-Ni catalysts. Pt metal is likely to dominate in these interactions, since the order of optimum fuel:oxygen ratios are correlated with the order of sticking probabilities of paraffins to the Pt surface. The dispersion of Pt is thought to be responsible for the difference in the responses of Pt and Pt-Ni at high fuel:oxygen ratios and for the deviations between the light-off temperatures on the two catalysts. The Ni catalyst shows a non-monotonic response against changes in the amount of oxygen in the feed. Coke formation over Pt-Ni catalyst, which could drive the mechanism leading to elevations in the light-off temperatures at high fuel:oxygen ratios, is not observed. Lower light-off temperatures obtained by the addition of minute quantities of platinum to the steam reforming catalyst (Ni) indicate the possibility of initiating the hydrogen generating indirect partial oxidation route (total oxidation + steam reforming) with lower energy requirements.

5.6. Steam Reforming of n-Butane over the Supported Bimetallic Pt-Ni Catalyst

The second key reaction of indirect partial oxidation is steam reforming of the unoxidized hydrocarbon. The reaction is important, since it supplies the hydrogen that would be utilized by the fuel cell. This section involves an investigation of the steam reforming of n-butane over the bimetallic Pt-Ni catalyst whose ignition characteristics were reported in Section 5.5. Although LPG includes both propane and n-butane, the latter is selected as the model hydrocarbon to be considered in this study, since reported data related to propane steam reforming are more abundant. The first part of this study is related with the identification of the Pt-Ni catalyst by comparing its steam reforming features with those of the monometallic Ni catalyst under identical conditions. Based on an evaluation of the conditions in the first part, the kinetics of the reaction is studied in the second part, in which both power-law type and LHHW type rate laws describing the reaction rate within the selected range of operating conditions are proposed.

5.6.1. Identification of the Steam Reforming Characteristics of the Bimetallic Pt-Ni Catalyst

As mentioned in Section 5.5, Ni-based catalysts are efficient in driving the steam reforming of hydrocarbons, and platinum is found to be effective in the oxidation of hydrocarbons. Over the bimetallic Pt-Ni catalyst, nickel is expected to be the effective component in n-butane steam reforming, though further investigation would be necessary. The steam reforming characteristics of both Pt-Ni and Ni catalysts are therefore compared under identical conditions. 15%Ni/δ-Al_2O_3 and 0.2%Pt-15%Ni/δ-Al_2O_3 are used throughout the study.

The operating conditions for the experiments are given in Section 3.5.3 and in Table 3.6, but it is worth noting the bases for their selection. The preliminary propane steam reforming tests have indicated heavy coke formation at 698 K. Therefore, the maximum reaction temperature to be employed was selected as 678 K, considering the possible higher reactivity of n-butane. It was recommended that steam:carbon ratio should be kept above ca. 2.5 for suppressing any coke formation (Rostrup-Nielsen, 1984). Although this value was reported for methane, Ma (1995) did not detect any coke deposition in propane

steam reforming at a steam:carbon ratio of 3.0. Therefore, the feed composition in this study was also arranged so that the steam:carbon ratio was kept at 3.0 in all reaction tests. Steady state was reached within the first ca. 1.5 h of reaction; therefore, all data reported in this section are based on 2 h on stream.

Steam reforming of n-butane can be described by the following reactions:

$$n\text{-}C_4H_{10} + 8H_2O = 4CO_2 + 13H_2, \quad \Delta H^{o}_{298} = 485.3\ kJ\ mol^{-1} \tag{5.11}$$

$$n\text{-}C_4H_{10} + 4H_2O = 4CO + 9H_2, \quad \Delta H^{o}_{298} = 649.9\ kJ\ mol^{-1} \tag{5.12}$$

The water-gas shift reaction is fast over Ni-based catalysts and usually in equilibrium under steam reforming conditions (Rostrup-Nielsen, 1984):

$$CO + H_2O = CO_2 + H_2, \quad \Delta H^{o}_{298} = -41.2\ kJ\ mol^{-1} \tag{4.3}$$

The water-free composition of the gas phase obtained at different temperatures during n-butane steam reforming over 15%Ni/δ-Al_2O_3 and 0.2%Pt-15%Ni/δ-Al_2O_3 catalysts are presented in Figures 5.33 and 5.34, respectively. For both catalysts, it can be observed that methane is an important side product, and is possibly formed due to one of the following reactions:

$$4H_2 + CO_2 = CH_4 + 2H_2O, \quad \Delta H^{o}_{298} = -165.0\ kJ\ mol^{-1} \tag{5.13}$$

$$n\text{-}C_4H_{10} + 3H_2 = 4CH_4, \quad \Delta H^{o}_{298} = -174.7\ kJ\ mol^{-1} \tag{5.14}$$

Reaction (5.14), which is also called hydrogenolysis, is likely to be more significant in methane production, since the changes in molar compositions, particularly at temperatures higher than 650 K, are compatible with the stoichiometry of the reaction. On the other hand, the opposite trends of the CO_2 and H_2 distribution, which can be observed

both in Figures 5.33 and 5.34, do not confirm the occurrence of the CO_2 hydrogenation reaction, Reaction (5.13).

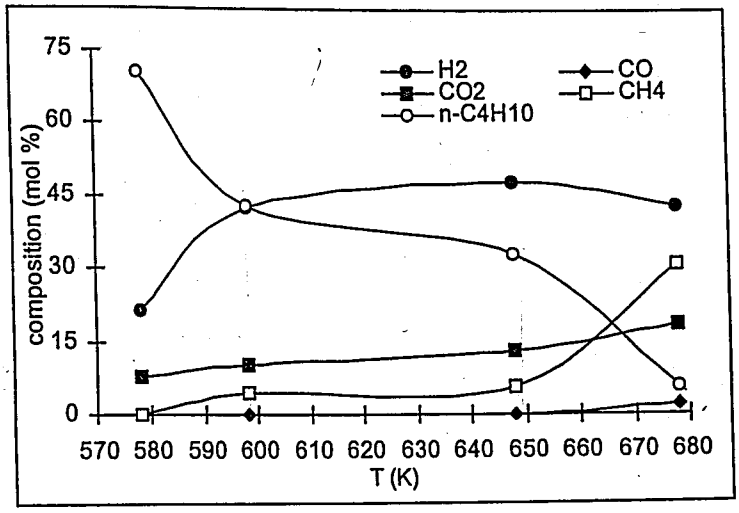

Figure 5.33. Molar gas phase compositions at different temperatures during n-butane steam reforming over 15%Ni/δ-Al_2O_3 catalyst (dry basis)

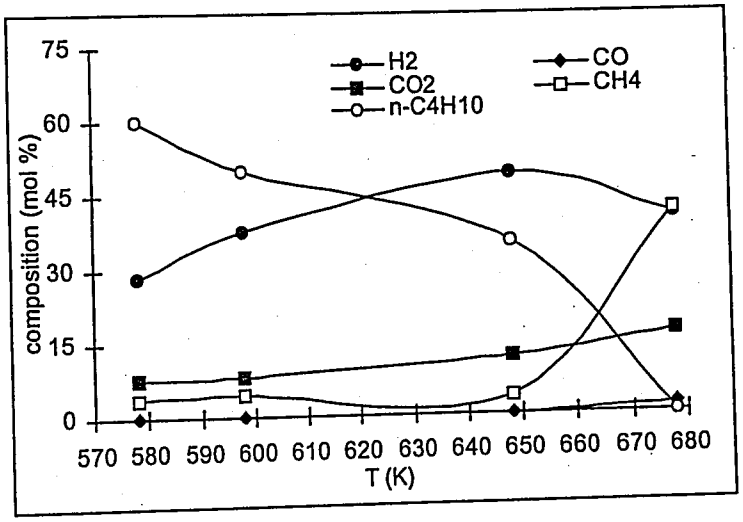

Figure 5.34. Molar gas phase compositions at different temperatures during n-butane steam reforming over 0.2%Pt-15%Ni/δ-Al_2O_3 catalyst (dry basis)

Apart from methane production, it can also be observed that CO is produced only in very small quantities at temperatures higher than 655 K. However, CO_2 can clearly be identified as a product at all temperatures. Thus, it can be concluded that n-butane steam

reforming can be represented by Reaction (5.11) rather than Reaction (5.12) under the operating conditions employed. At this point, it must be kept in mind that CO formation might have been suppressed by the water-gas shift reaction, but the apparent reaction data indicate the dominance of Reaction (5.11).

The behavior of both Ni and Pt-Ni catalysts during steam reforming are similar to each other, but there are some differences in the molar distribution of hydrogen with respect to temperature. It can be seen that hydrogen production reaches its maximum value at 648 K in the case of the Pt-Ni catalyst (Figure 5.34), whereas the hydrogen produced at 598 K over the Ni catalyst is much higher than Pt-Ni with no observable maximum at 648 K (Figure 5.33). In addition, at 648 K the amount of methane produced is around 6 mole per cent in the case of Ni, whereas it is below 4 per cent when Pt-Ni is used (Figures 5.33 and 5.34). These results indicate that the catalysts exhibit somewhat diverse characteristics at temperatures around 648 K. In fact, the comparative plot (Figure 5.35) giving the change in the selectivity (defined as the ratio of the hydrogen production rate to the methane production rate) versus reaction temperature clearly shows that Pt-Ni exhibits superior performance in terms of selective hydrogen production. Note that this feature is highly desired in fuel processing applications, since methane is a greenhouse

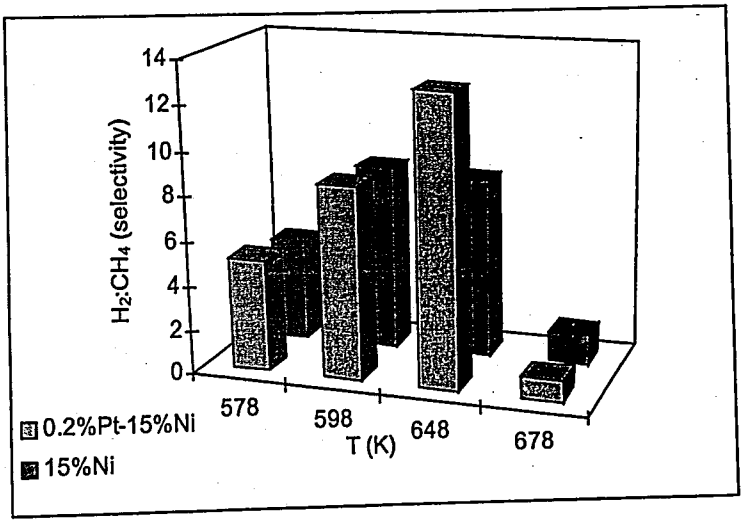

Figure 5.35. Selectivity versus temperature plot

gas that should be exhausted in minimal quantities. In addition, the formation of the gas consumes useful hydrogen by Reactions (5.13) and (5.14) which would reduce the overall efficiency of the fuel cell operation.

The hydrogen production rates of the catalysts given in Figure 5.36 indicate that the rates of hydrogen production over both catalysts are almost the same. This result confirms the outcome that the higher hydrogen selectivity of the bimetallic catalyst at 648 K is due to the suppressed methane production at this temperature.

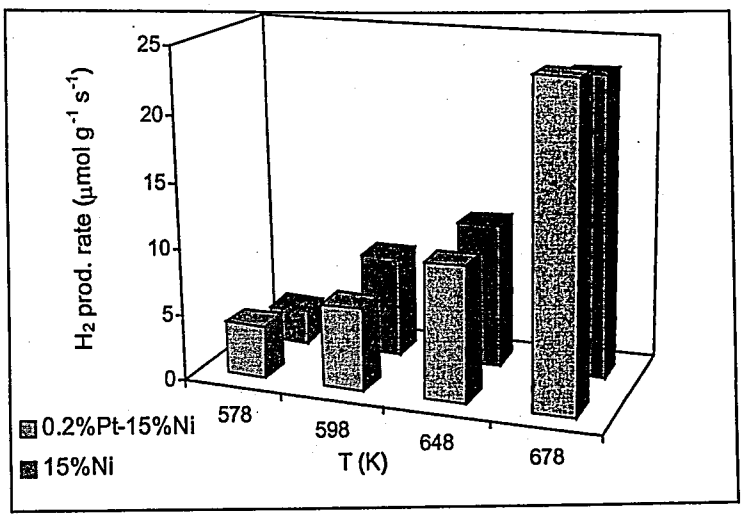

Figure 5.36. Hydrogen production rates obtained at different temperatures during steam reforming over both catalysts

Based on comparative steam reforming tests, it can be concluded that 648 K is the temperature at which the catalysts exhibit the most significant differences. It is believed that the effect of platinum on the catalytic activity is most pronounced at 648 K, and, therefore, this temperature is selected as the value at which the kinetic study of the n-butane steam reforming is conducted.

5.6.2. Kinetics of n-Butane Steam Reforming over the Pt-Ni/δ-Al_2O_3 Catalyst

The criteria for the selection of the operating conditions for evaluating the kinetics of n-butane steam reforming over Pt-Ni/δ-Al_2O_3 catalyst were given in Section 3.5.4. The

feed compositions, temperatures and residence times (W/F_{AO}, A: n-butane) employed, and conversions calculated in order to assess kinetics of steam reforming are given in Table 5.8.

Table 5.8. Conditions used for evaluating steam reforming kinetics

Experiment No.	H_2O (mole per cent)	n-C_4H_{10} (mole per cent)	T (K)	W/F_{AO} (mg.s μmol^{-1})	x_A (fractional)
1	16	1.0	648	36.66	0.0614
2	16	1.0	648	51.32	0.0760
3	12	2.5	648	14.66	0.0807
4	12	2.5	648	20.53	0.1033
5	12	1.5	648	24.44	0.0740
6	12	1.5	648	34.21	0.0982
7	16	2.0	648	18.33	0.0682
8	16	2.0	648	25.66	0.0991
9	16	1.0	603	36.66	0.0346
10	16	1.0	618	36.66	0.0647
11	16	1.0	633	36.66	0.0891
12	16	1.0	641	36.66	0.0855
13	16	1.0	658	36.66	0.1549
14	16	1.0	668	36.66	0.1751

Experiments 1-8 are conducted at four different feed compositions each at two different residence times to ensure the linear change of the n-butane conversion (x_A) with residence time (W/F_{AO}) in the initial rates region. These set of experiments are used for evaluating the order of the reaction with respect to n-butane and steam at 648 K. Experiments 9-14, in which the same feed composition/residence time combination is employed, are conducted at different temperatures to evaluate the activation energy of Reaction (5.11).

The power-law type rate expression describing the rate of consumption of n-butane can be expressed by the following general form:

$$-r_{n\text{-}C_4H_{10}} = \left\{k_o \exp\left(-\frac{E_A}{RT}\right)\right\}\left(P_{n\text{-}C_4H_{10}}\right)^{\alpha}\left(P_{H_2O}\right)^{\beta} \qquad (5.15)$$

Evaluation of the rate parameters, i.e. orders of reaction with respect to n-butane and steam – α and β, respectively – and the activation energy, E_A, requires initially the calculation of the reaction rates at the left hand side of Equation (5.15) which were evaluated from the slopes of the conversion versus residence time plots given in Figure 5.37.

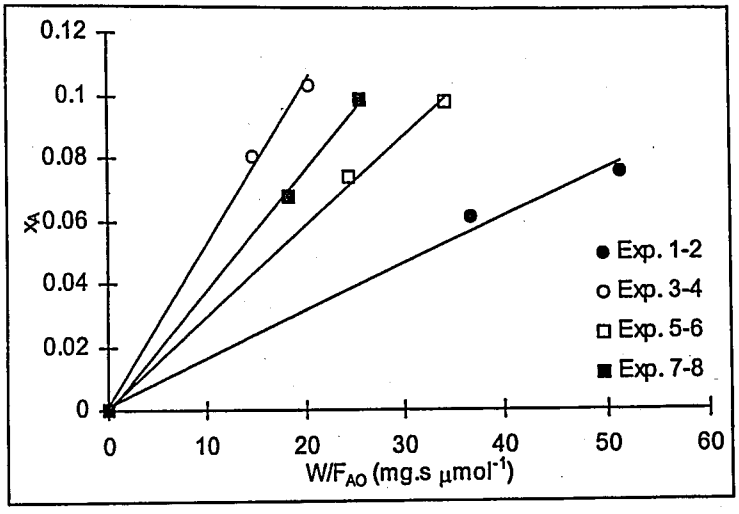

Figure 5.37. Conversion versus residence time plots

In all of the sets of experiments conducted at different feed concentrations, it can be observed that (i) the conversion of n-butane is less than 10 per cent, and (ii) the change in the conversion with residence time is linear (Figure 5.37). These outcomes ensure that the experiments are conducted in the region in which the reaction is kinetically controlled. The effect of the product hydrogen on the reaction rate is not considered due to the lower n-butane conversions obtained (initial rate region).

The initial rates of the reaction at each concentration set are calculated from the slopes of the lines shown in Figure 5.37 and are given in Table 5.9. The concentrations given in mole per cent can be converted into partial pressures, since the total pressure was equal to ca. 1 atm. Therefore, the resulting rate versus partial pressure data obtained at 648 K are used to estimate the reaction orders shown in Equation (5.15) using both linear and non-linear regression analysis, and the results are given in Table 5.10. Equation (5.15) was linearized by taking the natural logarithm of both sides.

Table 5.9. Initial rates calculated from conversion-residence time data

Experiment No.	Reaction rate (μmol $mg^{-1}s^{-1}$)
1-2	0.0015
3-4	0.0051
5-6	0.0029
7-8	0.0038

Table 5.10. Estimated reaction orders

	Reaction orders		$\sigma^2 = \frac{\sum_{i=1}^{N}(\text{rate}_{\text{calc.}} - \text{rate}_{\text{measured}})^2}{N''' - K'''}$
	α	β	
Linear reg.	1.26	-0.28	$4.7\text{x}10^{-3}$
Non-linear reg.	1.20	-0.18	$3.5\text{x}10^{-8}$

In Table 5.10, σ^2 is the sum of squares of residuals, N''' is the number of data points and K''' is the number of parameters. The expected smaller σ^2 value in the case of non-linear regression indicates a much better fit to the experimental data points, and, hence, the corresponding estimated parameters are utilized. The reaction orders ($\alpha = 1.20$ and $\beta = -0.18$) indicate that the reaction rate is directly proportional to the partial pressure of n-butane, whereas a minor inhibition is expected when the partial pressure of steam is

increased. The results are in agreement with those reported for the steam reforming of higher alkanes over Ni-based catalysts (Ma, 1995; Rostrup-Nielsen, 1984).

The activation energy (E_A) of Reaction (5.11) over the Pt-Ni catalyst can also be evaluated. For this purpose, the linearized form Equation (5.15) given below is employed:

$$\ln\left(-r_{n\text{-}C_4H_{10}}\right) = \ln(k_o) + \alpha\ln\left(P_{n\text{-}C_4H_{10}}\right) + \beta\ln\left(P_{H_2O}\right) - \frac{E_A}{RT} \qquad (5.16)$$

The linear Arrhenius plot between the natural logarithm of the reaction rate and the reciprocal of the temperature (1/T) is shown in Figure 5.38, and its slope gives the value of the quotient $-E_A/R$ from which the activation energy can be estimated.

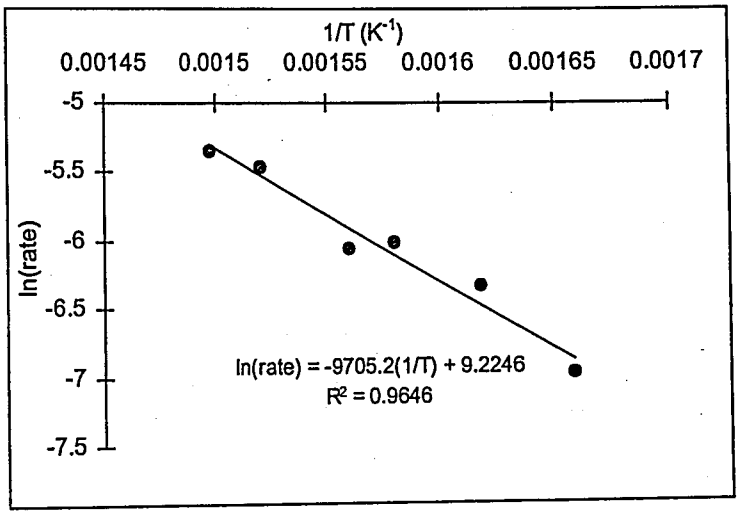

Figure 5.38. Arrhenius plot for steam reforming of n-butane over Pt-Ni catalyst

From the slope of the straight line in Figure 5.38, E_A is found either as 80.7 kJ mol^{-1} or as 19.3 kcal mol^{-1}, depending on the unit of the gas constant, R. This value is comparable with activation energies reported for the steam reforming of other hydrocarbons over supported nickel catalysts ranging from 54 kJ mol^{-1} to 96 kJ mol^{-1} (Ma, 1995; Rostrup-Nielsen, 1984).

In contrast with methane steam reforming, which has been studied to a large extent, mechanistic investigations related with the conversion of C_{2+} alkanes are scarce. A generalized mechanism for higher alkanes has been proposed by Rostrup-Nielsen (1984) (see Section 2.4.4), and the resulting LHHW rate law, whose general form is given below, was found to be successful in describing the steam reforming of ethane and n-heptane over a Ni/MgO catalyst:

$$-r_{C_{2+}} = \frac{k_1 P_{C_{2+}}}{\left(1 + K_1' P_{C_{2+}} \frac{P_{H_2}}{P_{H_2O}} + K_2' \frac{P_{H_2O}}{P_{H_2}}\right)^2} \qquad (5.17)$$

Equation (5.17) can possibly be used to quantify n-butane steam reforming, since it can be reduced to a power-law expression similar to Equation (5.15). However, a series of mixed-feed experiments, in which hydrogen is fed together with n-butane and steam, should be conducted to evaluate the rate parameters – k_1, K_1', K_2' – and to check the validity of the kinetic model proposed.

5.6.3. Summary

Comparative steam reforming experiments over Pt-Ni/δ-Al_2O_3 and Ni/δ-Al_2O_3 were conducted, and the characteristics features of the bimetallic catalyst were identified in order to set the conditions for the assessment of the reaction kinetics. The major difference between the responses of the catalysts was found to be at 648 K, at which the bimetallic catalyst has shown superior performance in terms of selective hydrogen production. Experimental studies for evaluating the kinetics of n-butane steam reforming over Pt-Ni/δ-Al_2O_3 catalyst conducted under differential conditions at 648 K gave the reaction orders of 1.20 and of –0.18 with respect to n-butane and steam, respectively. The activation energy of the reaction is found to be equal to 80.7 kJ mol^{-1}. Mixed feed experiments involving hydrogen are required to identify the mechanistic features of the reaction.

6. CONCLUSIONS AND RECOMMENDATIONS

6.1. Conclusions

The major objectives of this research were (i) to develop a complete mathematical model for simulating hydrogen production from different hydrocarbon fuel/fuel conversion mechanism/catalyst combinations within the context of the operation of a fuel processor that would supply hydrogen for driving fuel cells to be used in both vehicles and residential applications, (ii) to identify the optimum hydrocarbon fuel/fuel conversion mechanism/catalyst combination, and (iii) to highlight the characteristic features of this optimum combination using experimental techniques. The major conclusions that can be drawn from this study indicate that the planned objectives are satisfied. These conclusions are given as follows:

- Mathematical models were formulated for describing autothermal conversion of methane to hydrogen over various fixed-bed reactor configurations of Pt/δ-Al_2O_3 and Ni/MgO-Al_2O_3 catalysts. Heterogeneous reactor models gave results closer to experimental data reported for a bench-scale reactor.
- Feed compositions and catalyst-bed configurations modified heat transfer between exothermic oxidation and endothermic steam reforming, and, therefore affected temperature and product distribution.
- Indirect partial oxidation, i.e. combined total oxidation and steam reforming, of gasoline and LPG (propane+n-butane) over a bimetallic Pt-Ni catalyst were calculated to be efficient options for use in fuel processing for vehicular fuel cell applications. LPG seems to be better than gasoline due to its much lower possibility of coking and lower sulphur contents.
- Methanol, which is often suggested as an on-board fuel, demonstrated the worst performance for on-board vehicular hydrogen production.
- Methane, i.e. natural gas, was found to give the highest hydrogen yields when converted in the direct partial oxidation route. This combination seems to be most promising for use in residential, small-scale, combined heat-and-power applications.

- The results of the kinetics-based simulations were within thermodynamic limits which confirmed the correctness of the kinetic data collected from the literature.
- The balance between the extents of total oxidation and steam reforming in indirect partial oxidation gave maximum hydrogen yields at optimum water/fuel ratios.
- The requirement of water injection in suppressing carbon formation, in controlling the maximum bed temperature, in removing carbon monoxide and in increasing hydrogen yield was demonstrated.
- The activities of the catalysts in total oxidation of propane and n-butane under fuel-rich conditions were found to follow the order of 15%Ni/δ-Al_2O_3<0.2%Pt-15%Ni/δ-Al_2O_3<0.2%Pt/δ-Al_2O_3. n-Butane is found to be more reactive than propane.
- The possible dominance of the platinum metal during oxidation over the Pt-Ni catalyst was demonstrated. The dispersion of platinum seems to be a critical parameter in achieving oxidation at lower temperatures, which corresponds to lower energy requirements for triggering the indirect partial oxidation in fuel processing applications. It can be speculated that the possible synergistic interactions between Pt and Ni facilitate the rate of initiation of oxidation.
- The hydrogen selectivity of the bimetallic Pt-Ni catalyst was found to be higher than that of the Ni catalyst during steam reforming of n-butane at 648 K.
- The kinetics of n-butane steam reforming over Pt-Ni catalyst were studied at 648 K. The reaction orders with respect to n-butane and steam are found as 1.20 and –0.18, respectively. The activation energy of the reaction is found as 80.7 kJ mol^{-1}.

6.2. Recommendations

The following studies are recommended for obtaining further useful results:

- The dispersion of platinum can be increased by reducing the metal content of nickel. Therefore, it is worth preparing new bimetallic catalysts having nickel contents such as 10 or 5 per cent by weight and to test these catalysts in oxidation experiments.

- A series of mixed feed experiments involving hydrogen together with n-butane and steam should be conducted to estimate the effect of hydrogen on the rate of n-butane steam reforming and to obtain the parameters of the proposed LHHW type rate equation. The experiments may also be conducted at different temperatures to obtain the temperature dependency of the adsorption/desorption equilibrium constants.
- The Pt-catalyst has to be tested in n-butane steam reforming experiments in order to further understand the steam reforming characteristics of the Pt-Ni catalyst.
- The Pt-Ni catalyst should be tested in indirect partial oxidation experiments in which total oxidation and steam reforming occur simultaneously. It is recommended that the same experiments be conducted over the monometallic Pt and Ni catalysts in order to demonstrate the expected higher activity/selectivity features of the bimetallic catalyst. Stability tests should also be conducted.

APPENDIX A: CALIBRATION CURVES OF THE MASS FLOW CONTROLLERS

Calibration curves of the mass flow controllers used in the experiments are given below.

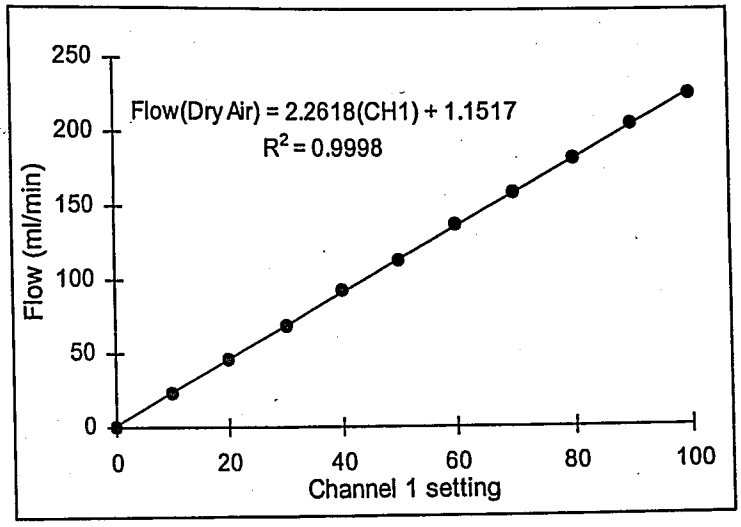

Figure A.1. Calibration curve of the dry air mass flow controller

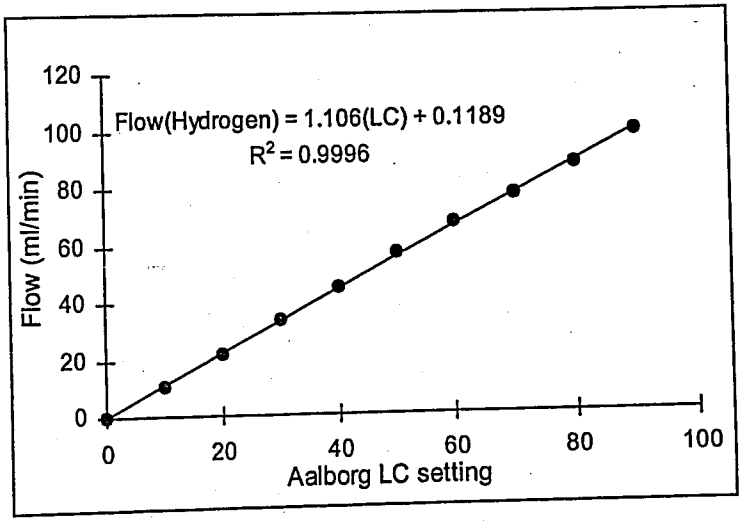

Figure A.2. Calibration curve of the hydrogen mass flow controller

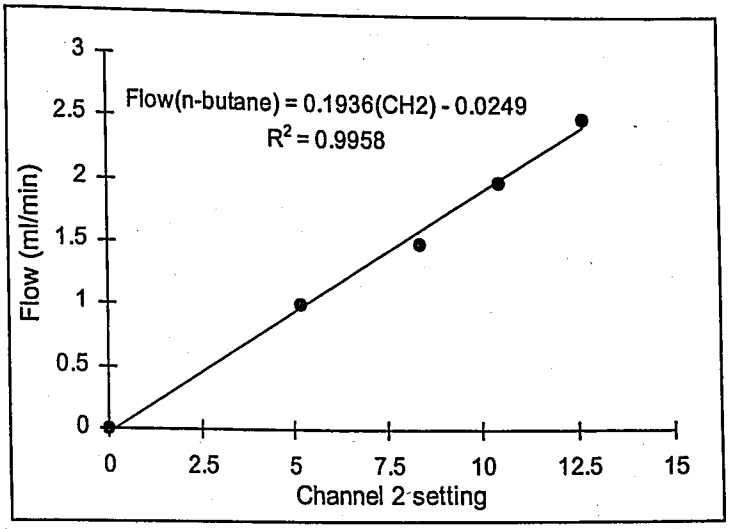

Figure A.3. Calibration curve of the n-butane mass flow controller

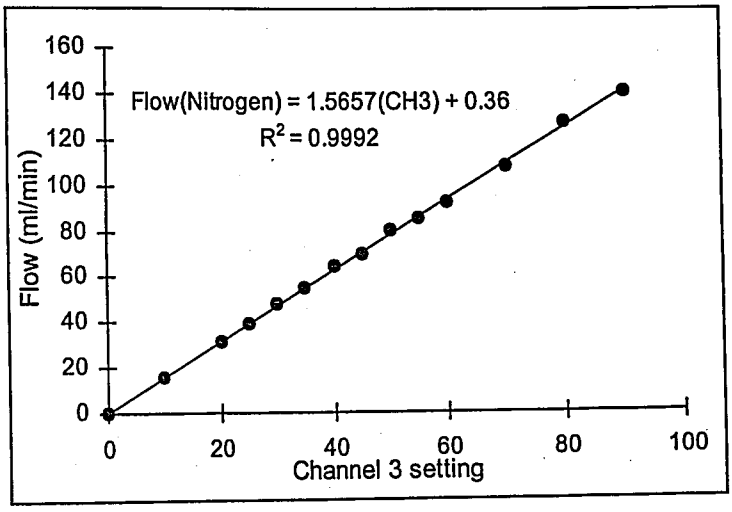

Figure A.4. Calibration curve of the nitrogen mass flow controller

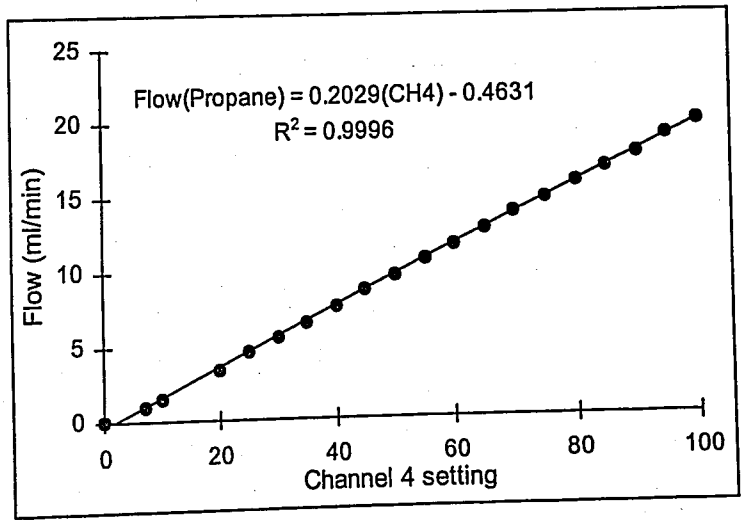

Figure A.5. Calibration curve of the propane mass flow controller

APPENDIX B: CALIBRATION CURVES OF THE GAS CHROMATOGRAPHS

Calibration curves of the gas chromatographs used in the experiments are given below.

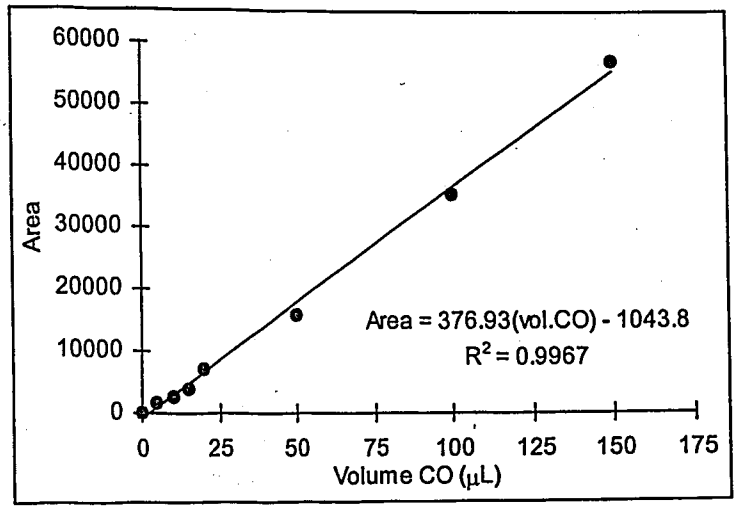

Figure B.1. Calibration curve of carbon monoxide (GC-8A)

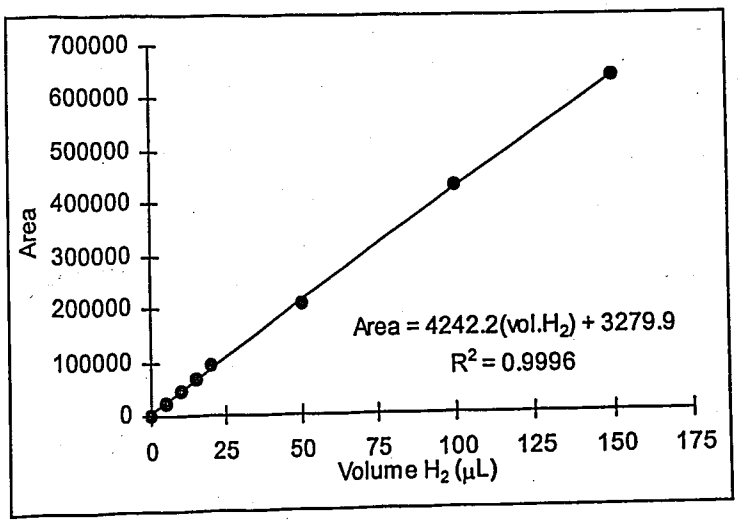

Figure B.2. Calibration curve of hydrogen (GC-8A)

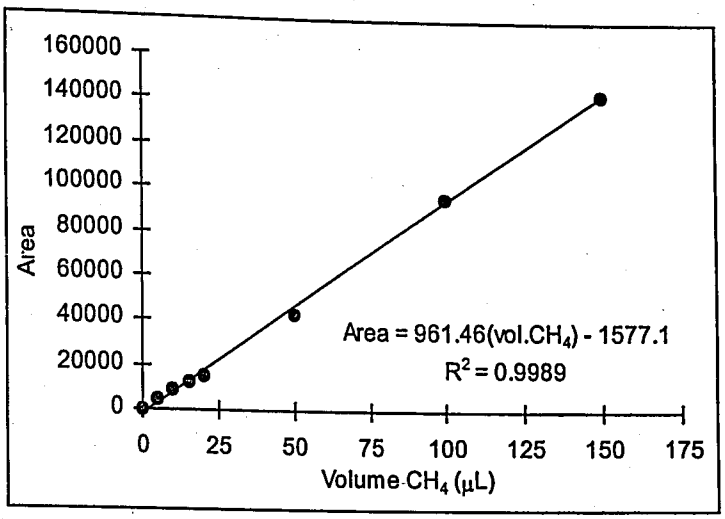

Figure B.3. Calibration curve of methane (GC-8A)

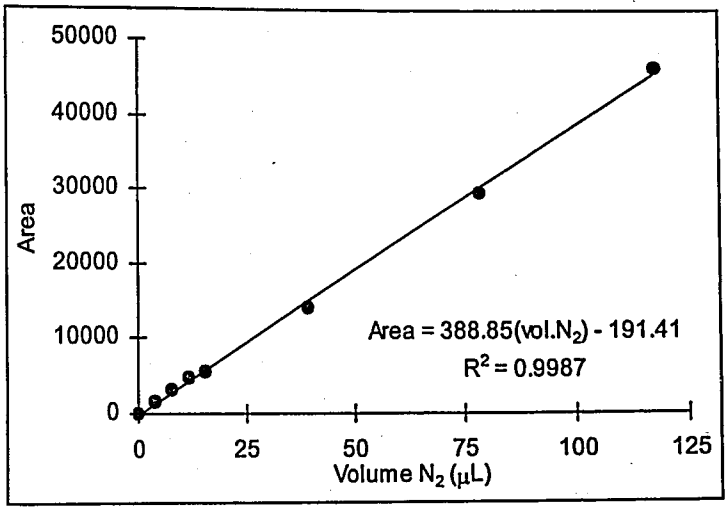

Figure B.4. Calibration curve of nitrogen (GC-8A)

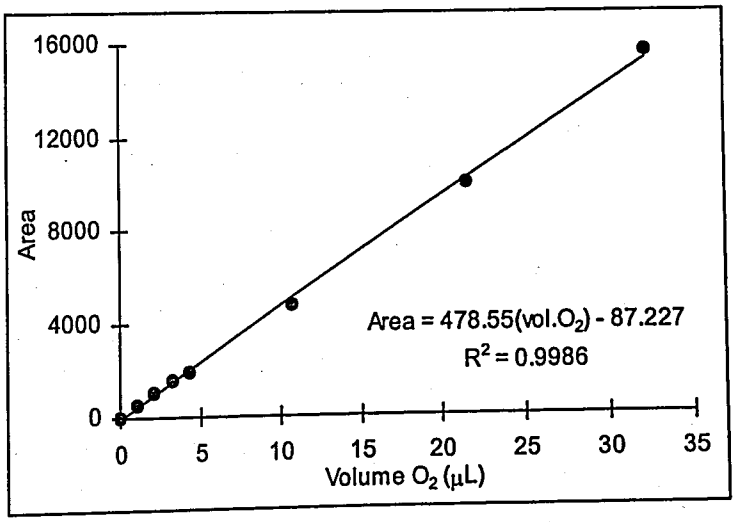

Figure B.5. Calibration curve of oxygen (GC-8A)

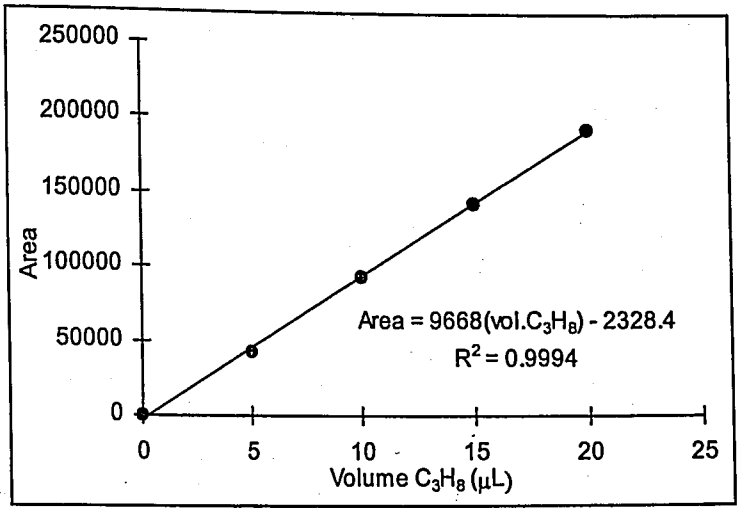

Figure B.6. Calibration curve of propane (GC-14A)

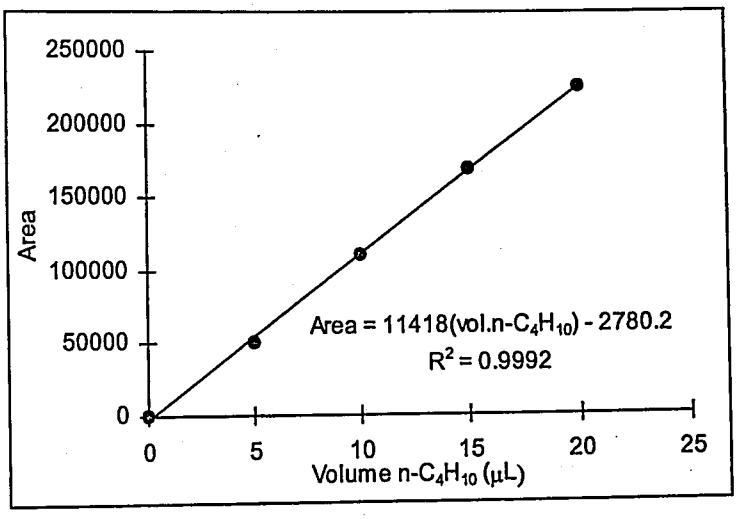

Figure B.7. Calibration curve of n-butane (GC-14A)

APPENDIX C: PHYSICAL PROPERTIES OF THE RELATED INORGANIC AND ORGANIC COMPOUNDS

Table C.1. Constants of the heat capacity equation and standard molar enthalpy and Gibbs free energy of formation of related inorganic and organic compounds (Reid *et al.*, 1987)

Compound	a_i	b_i ($\times 10^3$)	c_i ($\times 10^5$)	d_i ($\times 10^9$)	H^o_{fi} (kJ mol^{-1})	G^o_{fi} (kJ mol^{-1})
CO_2	19.795	73.436	-5.602	17.153	-393.5	-394.65
CO	30.869	-12.85	2.789	-12.72	-110.52	-137.37
H_2	27.143	9.274	-1.381	7.645	0	0
i-C_8H_{18}	-7.461	777.91	-42.87	91.733	-224.29	13.69
CH_4	19.251	52.126	1.197	-11.32	-74.85	-50.87
CH_3OH	21.152	709.24	2.587	-28.52	-201.2	-162.62
N_2	31.150	-13.57	2.680	-11.68	0	0
O_2	28.106	-0.00368	1.746	-10.65	0	0
C_3H_8	-4.224	306.26	-15.86	32.146	-103.8	-23.49
H_2O	32.243	7.779	-42.87	91.733	-241.83	-228.77

Table C.2. Molecular weight, thermal conductivity and viscosity of related inorganic and organic compounds (Geankoplis, 1993; Perry *et al.*, 1984)

Compound	Molecular weight (kg kgmol^{-1})	Thermal conductivity (W m^{-1} K^{-1})	Viscosity (kg m^{-1} s^{-1})
CO_2	44.01	$4.046\times10^{-3} + 6.369\times10^{-5}T$	$1.215\times10^{-6} + 4.5\times10^{-8}T$
CO	28.01	$6.555\times10^{-3} + 6.377\times10^{-5}T$	$1.281\times10^{-5} + 3.0\times10^{-8}T$
H_2	2.02	$8.070\times10^{-2} + 3.705\times10^{-4}T$	$7.014\times10^{-6} + 1.2\times10^{-8}T$
CH_4	16.04	$-2.503\times10^{-2} + 1.845\times10^{-4}T$	$4.402\times10^{-6} + 2.6\times10^{-8}T$
N_2	28.01	$1.295\times10^{-2} + 5.223\times10^{-5}T$	$1.156\times10^{-5} + 3.2\times10^{-8}T$
O_2	32.00	$1.210\times10^{-2} + 5.850\times10^{-5}T$	$1.228\times10^{-5} + 4.0\times10^{-8}T$
H_2O	18.02	$-3.484\times10^{-2} + 1.324\times10^{-4}T$	$-7.512\times10^{-6} + 4.4\times10^{-8}T$

Table C.3. Diffusion volumes of related inorganic and organic compounds (Rase, 1990)

Compound	Diffusion volumes, Σv_i's
CO_2	28.12
CO	22.01
H_2	4.62
CH_4	25.14
N_2	9.08
O_2	12.22
H_2O	10.73

APPENDIX D: EVALUATION OF THE THERMOCHEMICAL PARAMETERS

D.1. Heat Capacities of the Components

The temperature variations within the reaction system are significant due to the existence of exothermic oxidation, endothermic steam reforming and other side reactions having heat of reactions with relatively high magnitudes. Therefore temperature dependence of thermochemical properties of the gas phase species is taken into account for ensuring more realistic simulations of catalytic hydrogen production.

The heat capacity equation describing the temperature dependence of the heat capacity of component j is given as follows:

$$c_{pj} = a_j + b_j T + c_j T^2 + d_j T^3 \qquad \text{(D.1)}$$

The constants of Equation (D.1) for each component appearing in the reaction system are given in Table C.1 in Appendix C.

D.2. Enthalpy and Gibbs Free Energy of the Reactions

The most general form of a chemical reaction with two reactants, A and B, and two products, C and D, can be given as follows:

$$aA + bB = cC + dD \qquad \text{(D.2)}$$

In Reaction (D.2), a, b, c and d are the stoichiometric coefficients of the species A, B, C and D, respectively. Since the enthalpy and Gibbs free energy of a reaction are given for a basis of one mole of reactant, coefficients of Reaction (D.2) are rearranged as follows:

$$A+\frac{b}{a}B=\frac{c}{a}C+\frac{d}{a}D \tag{D.3}$$

Based on this definition, the enthalpy, and Gibbs free energy for Reaction (D.3) at normal operating conditions (298 K, 1 atm) can be expressed as follows:

$$\Delta H^{o}_{RxN}=\left(\frac{d}{a}H^{o}_{D}+\frac{c}{a}H^{o}_{C}\right)-\left(\frac{b}{a}H^{o}_{B}+H^{o}_{A}\right) \tag{D.4}$$

$$\Delta G^{o}_{RxN}=\left(\frac{d}{a}G^{o}_{D}+\frac{c}{a}G^{o}_{C}\right)-\left(\frac{b}{a}G^{o}_{B}+G^{o}_{A}\right) \tag{D.5}$$

In Equations (D.4) and (D.5), ΔH^{o}_{RxN} and ΔG^{o}_{RxN} correspond to the standard molar enthalpy and Gibbs free energy of Reaction (D.3), respectively. The latter will be used in the evaluation of equilibrium constants, which will be given in Section D.3. H^{o}_{j} and G^{o}_{j}, the molar enthalpy and Gibbs free energy of formations of component j, respectively, are also given in Table C.1 in Appendix C.

The molar enthalpy of Reaction (D.3) at any temperature, ΔH_{RxN}, which is a critical parameter appearing in model equations, is evaluated using the following equation:

$$\Delta H_{RxN,T}=\Delta H^{o}_{RxN}+\int_{298}^{T}(\Delta c_p)dT \tag{D.6}$$

where, Δc_p term is given as follows:

$$\Delta c_p=\left(\frac{d}{a}c_{pD}+\frac{c}{a}c_{pC}\right)-\left(\frac{b}{a}c_{pB}+c_{pA}\right) \tag{D.7}$$

Another form of Δc_p can be expressed in terms of the coefficients of Equation (D.1) as follows:

$$\Delta c_p = \alpha + \beta T + \chi T^2 + \delta T^3 \tag{D.8}$$

$$\alpha = \left(\frac{d}{a}a_D + \frac{c}{a}a_C\right) - \left(\frac{b}{a}a_B + a_A\right) \tag{D.9}$$

$$\beta = \left(\frac{d}{a}b_D + \frac{c}{a}b_C\right) - \left(\frac{b}{a}b_B + b_A\right) \tag{D.10}$$

$$\chi = \left(\frac{d}{a}c_D + \frac{c}{a}c_C\right) - \left(\frac{b}{a}c_B + c_A\right) \tag{D.11}$$

$$\delta = \left(\frac{d}{a}d_D + \frac{c}{a}d_C\right) - \left(\frac{b}{a}d_B + d_A\right) \tag{D.12}$$

Using the information given in this section, molar enthalpy of any reaction at any temperature and standard molar Gibbs free energy of any reaction can be calculated once the thermochemical data are available for the species appearing in the related chemical reaction.

D.3. Equilibrium Constants of the Reactions

The values of the reaction equilibrium constants are required both in the evaluation of complex reaction equilibria and in the solution of the reactor models. These situations require the evaluation of equilibrium constants at the temperature of interest. This section describes the method by which equilibrium constant of any reaction at any temperature is evaluated.

The true (dimensionless) equilibrium constant for Reaction (D.3), K, is given as follows (Fogler, 1999):

$$K = \frac{a_C^{c/a} a_D^{d/a}}{a_A a_B^{b/a}} \tag{D.13}$$

This equilibrium constant can be evaluated using the following fundamental relationship:

$$-\Delta G^{o}_{RxN} = RT\ln(K) \tag{D.14}$$

In Equation (D.13), a_j is the activity of species j and can be expressed in terms its activity coefficient, γ_j and partial pressure, P_j as follows:

$$a_j = \gamma_j P_j \tag{D.15}$$

Inserting Equation (D.15) into Equation (D.13) will give the following relationship:

$$K = \frac{\gamma_C^{c/a}\gamma_D^{d/a}}{\gamma_A\gamma_B^{b/a}}\frac{P_C^{c/a}P_D^{d/a}}{P_A P_B^{b/a}} \tag{D.16}$$

In Equation (D.16), the first term including the activity coefficients can be lumped into a single parameter, K_γ. This term is equal to unity if the gases behave ideally, which are assumed to be so in the course of the simulations. Therefore, the latter term including the partial pressures, the pressure equilibrium constant, K_P, becomes equal to the true equilibrium constant, K. This allows the evaluation of K_P at 298 K using Equation (D.14), since the standard molar Gibbs free energy of a reaction can be calculated using Equation (D.5) and the thermochemical data given in Table C.1.

Once K_P is calculated for 298 K (the reference temperature, T_R) as described above, it can be evaluated at any temperature using van't Hoff's equation (Fogler, 1999):

$$\frac{d\ln(K_P)}{dT} = \frac{\Delta H_{RxN,T}}{RT^2} \tag{D.17}$$

The integrated form of Equation (D.17), taking the temperature dependence of the enthalpy of reaction as described in Equation (D.6), is obtained as follows:

$$\frac{\ln[K_P(T)]}{\ln[K_P(T_R)]} = \frac{1}{R}\left[\Delta H^{o}_{RxN}\left(\frac{1}{T}-\frac{1}{T_R}\right)+TERM_1+TERM_2\right] \qquad (D.18)$$

$$TERM_1 = \alpha \ln\left(\frac{T}{T_R}\right)+\frac{\beta}{2}(T-T_R)+\frac{\chi}{6}\left(T^2-T_R^2\right)+\frac{\delta}{12}\left(T^3-T_R^3\right) \qquad (D.19)$$

$$TERM_2 = \left(\frac{1}{T}-\frac{1}{T_R}\right)\left(\alpha T_R+\frac{\beta}{2}T_R^2+\frac{\chi}{3}T_R^3+\frac{\delta}{4}T_R^4\right) \qquad (D.20)$$

Rearranging Equation (D.18) gives K_P for any reaction at any temperature, T:

$$K_P(T) = K_P(T_R)\exp[\text{RHS of Equation (D.18)}] \qquad (D.21)$$

In order to verify the method explained above, the calculated equilibrium constants for methane steam reforming and water-gas shift reactions at certain temperatures are compared with their counterparts given in the literature (Rostrup-Nielsen, 1984). The results are given in Table D.1.

Table D.1. Equilibrium constants for steam reforming of related hydrocarbons and for water-gas shift reaction

Temperature (K)	$CH_4 + H_2O = CO + 3H_2$		$CO + H_2O = CO_2 + H_2$		$CH_3OH + H_2O = CO_2 + 3H_2$	$C_3H_8 + 3H_2O = 3CO + 7H_2$	$i\text{-}C_8H_{18} + 8H_2O = 8CO + 17H_2$
	$K_{P,CALC.}$ (atm^2)	$K_{P,LIT.}$ (atm^2)	$K_{P,CALC.}$ (-)	$K_{P,LIT.}$ (-)	$K_{P,CALC.}$ (atm^2)	$K_{P,CALC.}$ (atm^6)	$K_{P,CALC.}$ (atm^{16})
573	6.138×10^{-8}	6.643×10^{-8}	3.874×10^{1}	3.973×10^{1}	1.347×10^{5}	3.824×10^{-10}	3.252×10^{-17}
623	2.400×10^{-6}	2.600×10^{-6}	2.010×10^{1}	2.066×10^{1}	3.794×10^{5}	2.574×10^{-6}	1.823×10^{-7}
673	5.555×10^{-5}	6.019×10^{-5}	1.158×10^{1}	1.192×10^{1}	9.369×10^{5}	4.865×10^{-3}	3.964×10^{1}
723	8.460×10^{-4}	9.166×10^{-4}	7.246×10^{0}	7.470×10^{0}	2.078×10^{6}	3.336×10^{0}	6.448×10^{8}
773	9.174×10^{-3}	9.945×10^{-3}	4.845×10^{0}	4.999×10^{0}	4.215×10^{6}	1.005×10^{3}	1.282×10^{15}
823	7.519×10^{-2}	8.153×10^{-2}	3.419×10^{0}	3.530×10^{0}	7.932×10^{6}	1.537×10^{5}	4.520×10^{20}
873	4.880×10^{-1}	5.288×10^{-1}	2.522×10^{0}	2.606×10^{0}	1.401×10^{7}	1.338×10^{7}	3.778×10^{25}
923	2.602×10^{0}	2.891×10^{0}	1.930×10^{0}	1.995×10^{0}	2.342×10^{7}	7.244×10^{8}	9.404×10^{29}
973	1.173×10^{1}	1.271×10^{1}	1.523×10^{0}	1.541×10^{0}	3.735×10^{7}	2.618×10^{10}	8.362×10^{33}
1023	4.584×10^{1}	4.966×10^{1}	1.234×10^{0}	1.278×10^{0}	5.718×10^{7}	6.693×10^{11}	3.077×10^{37}
1073	1.582×10^{2}	1.713×10^{2}	1.023×10^{0}	1.059×10^{0}	8.445×10^{7}	1.269×10^{13}	5.289×10^{40}
1123	4.897×10^{2}	5.303×10^{2}	8.643×10^{-1}	8.953×10^{-1}	1.209×10^{8}	1.854×10^{14}	4.689×10^{43}
1173	1.379×10^{3}	1.493×10^{3}	7.426×10^{-1}	7.694×10^{-1}	1.683×10^{8}	2.158×10^{15}	2.330×10^{46}
1223	3.573×10^{3}	3.866×10^{3}	6.475×10^{-1}	6.708×10^{-1}	2.287×10^{8}	2.056×10^{16}	6.960×10^{48}
1273	8.600×10^{3}	9.302×10^{3}	5.720×10^{-1}	5.923×10^{-1}	3.043×10^{8}	1.641×10^{17}	1.326×10^{51}

APPENDIX E: KINETIC PARAMETERS OF SELECTED REACTIONS

Kinetic parameters of the rate expressions describing steam reforming of methane, propane and i-octane expressed in Table 4.3 are given in Table E.1. Parameters are given such that resulting reaction rates are expressed in the units of kmol $kgcat^{-1}$ h^{-1}. Partial pressures are in the units of atm. Parameters of other rate expressions used in this study are available in the corresponding references available in the open literature.

Table E.1. Kinetic parameters of selected steam reforming reactions

Reaction	Rate expression (kmol $kgcat^{-1}$ h^{-1})	Parameters	Catalyst
CH_4+H_2O $=CO+3H_2$	$-r=\frac{kP_{C_1}^{0.96}P_W^{-0.17}}{1+\theta P_H^{0.25}}$	$k=1.05x10^4\exp\left(-\frac{7196}{T}\right)$ $\theta=3.17$	Pt-Ni/δ-Al_2O_3
$C_3H_8+5O_2$ $=3CO_2+4H_2O$	$-r=\frac{kP_{C_3}^{0.93}P_W^{-0.53}}{1+\theta P_H^{0.86}}$	$k=2.43x10^{15}\exp\left(-\frac{22800}{T}\right)$ $\theta=53.1$	Pt-Ni/δ-Al_2O_3
$C_8H_{18}+8H_2O$ $=8CO+17H_2$	$-r=\frac{kP_{C_7}}{\left(1+K''_A P_{C_7}\frac{P_H}{P_W}+K''_B\frac{P_W}{P_H}\right)^2}$	$k=4.3x10^5\exp\left(-\frac{8150}{T}\right)$ $K''_A=2.52x10^1$ $K''_B=8.0x10^{-2}$	Ni/MgO

APPENDIX F: LIST OF PUBLICATIONS OF AHMET KERİM AVCI

- Avcı, A. K., D. L. Trimm, A. E. Aksoylu and Z. İ. Önsan, 2003, "Hydrogen Production by Steam Reforming of n-Butane over Supported Ni and Pt-Ni Catalysts", *Applied Catalysis A: General*, submitted.
- Avcı, A. K., D. L. Trimm, A. E. Aksoylu and Z. İ. Önsan, 2003, "Ignition Characteristics of Pt, Ni and Pt-Ni Catalysts Used for Autothermal Fuel Processing", *Catalysis Letters*, Vol. 88, pp. 17-22.
- Avcı, A. K., D. L. Trimm and Z. İ. Önsan, 2003, "On-board Hydrogen Generation for Fuel Cell Powered Vehicles: The Use of Methanol and Propane", *Topics in Catalysis*, Vol. 22, pp. 359-367.
- Avcı, A. K., D. L. Trimm and Z. İ. Önsan, 2002, "Quantitative Investigation of Catalytic Natural Gas Conversion for Hydrogen Fuel Cell Applications", *Chemical Engineering Journal*, Vol. 90, pp. 77-87.
- Avcı, A. K., Z. İ. Önsan and D. L. Trimm, 2001, "On-board Fuel Conversion for Hydrogen Fuel Cells: Comparison of Different Fuels by Computer Simulations", *Applied Catalysis A: General*, Vol. 216, pp. 243-256.
- Avcı, A. K., D. L. Trimm and Z. İ. Önsan, 2001, "Heterogeneous Reactor Modeling for Simulation of Catalytic Oxidation and Steam Reforming of Methane", *Chemical Engineering Science*, Vol. 56, pp. 641-649.
- Avcı, A. K., M. C. Çamurdan and K. Ö. Ülgen, 2000, "Quantitative Description of Protein Adsorption by Frontal Analysis", *Process Biochemistry*, Vol. 36, pp. 141-148.
- Avcı, A. K., D. L. Trimm and Z. İ. Önsan, 2000, "Simulation of Alternative Catalyst Bed Configurations in Autothermal Hydrogen Production", *Studies in Surface Science and Catalysis*, Vol. 130, pp. 2753-2758.

REFERENCES

Aasberg-Petersen, K., J. H. Bak Hansen, T. S. Christensen, I. Dybkjaer, P. Seier Christensen, C. Stub Nielsen, S. E. L. Winter Madsen and J. R. Rostrup-Nielsen, 2001, "Technologies for Large-Scale Gas Conversion", *Applied Catalysis A: General*, Vol. 221, pp. 379-387.

Ahmed, S. and M. Krumpelt, 2001, "Hydrogen from Hydrocarbon Fuels for Fuel Cells", *International Journal of Hydrogen Energy*, Vol. 26, pp. 291-301.

Akın, A. N., 1996, *Development of Coprecipitated Cobalt-Alumina Catalysts for the Production of C_1-C_4 Hydrocarbons by Carbon Monoxide Hydrogenation*, Ph.D. Dissertation, Boğaziçi University.

Akın, A. N., G. Kılaz, A. İ. İşli and Z. İ. Önsan, 2001, "Development and Characterization of Pt-SnO_2/γ-Al_2O_3 Catalysts", *Chemical Engineering Science*, Vol. 56, pp. 881-888.

Aksoylu, A. E., 1997, *Hydrogenation of Carbon Oxides Using Nickel-Based Monometallic and Bimetallic Catalysts*, Ph.D. Dissertation, Boğaziçi University.

Amadeo, N. E. and M. A. Laborde, 1995, "Hydrogen Production from the Low-Temperature Water-Gas Shift Reaction: Kinetics and Simulation of the Industrial Reactor", *International Journal of Hydrogen Energy*, Vol. 20, pp. 949-956.

Arai, H. and M. Machida, 1996, "Thermal Stabilization of Catalyst Supports and Their Application to High-Temperature Catalytic Combustion", *Applied Catalysis A: General*, Vol. 138, pp. 161-176.

Armor, J. N., 1999, "The Multiple Roles for Catalysis in the Production of H_2", *Applied Catalysis A: General*, Vol. 176, pp. 159-176.

Armor, J. N., 2000, "Energy Efficiency and the Environment. Opportunities for Catalysis", *Applied Catalysis A: General*, Vol. 194-195, pp. 3-11.

Artizzu, P., E. Garbowski, M. Primet, Y. Brulle and J. Saint-Just, 1999, "Catalytic Combustion of Methane on Aluminate-Supported Copper Oxide", *Catalysis Today*, Vol. 47, pp. 83-93.

Aryafar, M. and F. Zaera, 1997, "Kinetic Study of the Catalytic Oxidation of Alkanes over Nickel, Palladium, and Platinum Foils", *Catalysis Letters*, Vol. 48, pp. 173-183.

Ashcroft, A. T., A. K. Cheetham, J. S. Foord, M. L. H. Green, C. P. Gray, A. J. Murrell and P. D. F. Vernon, 1990, "Selective Oxidation of Methane to Synthesis Gas Using Transition Metal Catalysts", *Nature*, Vol. 344, pp. 319-321.

Avcı, A. K., D. L. Trimm and Z. İ. Önsan, 2000, "Simulation of Alternative Catalyst Bed Configurations in Autothermal Hydrogen Production", *Studies in Surface Science and Catalysis*, Vol. 130, pp. 2753-2758.

Avcı, A. K., Z. İ. Önsan and D. L. Trimm, 2001a, "On-board Fuel Conversion for Hydrogen Fuel Cells: Comparison of Different Fuels by Computer Simulations", *Applied Catalysis A: General*, Vol. 216, pp. 243-256.

Avcı, A. K., D. L. Trimm and Z. İ. Önsan, 2001b, "Heterogeneous Reactor Modeling for Simulation of Catalytic Oxidation and Steam Reforming of Methane", *Chemical Engineering Science*, Vol. 56, pp. 641-649.

Avcı, A. K., D. L. Trimm and Z. İ. Önsan, 2002, "Quantitative Investigation of Catalytic Natural Gas Conversion for Hydrogen Fuel Cell Applications", *Chemical Engineering Journal*, Vol. 90, pp. 77-87.

Avcı, A. K., D. L. Trimm and Z. İ. Önsan, 2003, "On-board Hydrogen Generation for Fuel Cell Powered Vehicles: The Use of Methanol and Propane", *Topics in Catalysis*, Vol. 22, pp. 359-367.

Barbier Jr., J. and D. Duprez, 1992, "Hydrogen Formation in Propane Oxidation on Pt-Rh/CeO_2/Al_2O_3 Catalysts", *Applied Catalysis A: General*, Vol. 85, pp. 89-100.

Bartholomew, C. H., 2001, "Mechanisms of Catalyst Deactivation", *Applied Catalysis A: General*, Vol. 212, pp. 17-60.

Basile, F., G. Fornasari, F. Trifiro and A. Vaccari, 2001, "Partial Oxidation of Methane: Effect of Reaction Parameters and Catalyst Composition on the Thermal Profile and Heat Distribution", *Catalysis Today*, Vol. 64, pp. 21-30.

Bharadwaj, S. S. and L. D. Schmidt, 1995, "Catalytic Partial Oxidation of Natural Gas to Syngas", *Fuel Processing Technology*, Vol. 42, pp. 109-127.

Blok, K., R. H. Williams, R. E. Katofsky and C. A. Hendriks, 1997, "Hydrogen Production from Natural Gas, Sequestration of Recovered CO_2 in Depleted Gas Wells and Enhanced Natural Gas Recovery", *Energy*, Vol. 22, pp. 161-168.

Bodke, A. S., S. S. Bharadwaj and L. D. Schmidt, 1998, "The Effect of Ceramic Supports on Partial Oxidation of Hydrocarbons over Noble Metal Coated Monoliths", *Journal of Catalysis*, Vol. 179, pp. 138-149.

Borowiecki, T., A. Golebiowski and B. Stasinska, 1997, "Effects of Small MoO_3 Additions on the Properties of Nickel Catalysts for the Steam Reforming of Hydrocarbons", *Applied Catalysis A: General*, Vol. 153, pp. 141-156.

Boucouvalas Y., Z. L. Zhang and X. E. Verykios, 1996, "Partial Oxidation of Methane to Synthesis Gas via the Direct Reaction Scheme over Ru/TiO_2 Catalyst", *Catalysis Letters*, Vol. 40, pp.189-195.

Bradford, M. C. J. and M. A. Vannice, 1996, "Catalytic Reforming of Methane with Carbon Dioxide over Nickel Catalysts II. Reaction Kinetics", *Applied Catalysis A: General*, Vol. 142, pp. 97-122.

Brown, L., 2001, "A Comparative Study of Fuels for On-board Hydrogen Production for Fuel Cell Powered Automobiles", *International Journal of Hydrogen Energy*, Vol. 26, pp. 381-397.

Browning, D., P. Jones and K. Packer, 1997, "An Investigation of Hydrogen Storage Methods for Fuel Cell Operation with Man-Portable Equipment", *Journal of Power Sources*, Vol. 65, pp. 187-195.

Burch, R., D. J. Crittle and M. J. Hayes, 1999, "C-H Bond Activation in Hydrocarbon Oxidation on Heterogeneous Catalysts", *Catalysis Today*, Vol. 47, pp. 229-234.

Cameron, D. S., 1999, "The Sixth Grove Fuel Cell Symposium", *Platinum Metals Review*, Vol. 43, pp. 149-154.

Chan, S. H. and H. M. Wang, 2000, "Effect of Natural Gas Composition on Autothermal Fuel Reforming Products", *Fuel Processing Technology*, Vol. 64, pp. 221-239.

Choudhary, V. R., A. M. Rajput and A. S. Mamman, 1998, "NiO-Alkaline Earth Oxide Catalysts for Oxidative Methane-to-Syngas Conversion: Influence of Alkaline Earth Oxide on the Surface Properties and Temperature-Programmed Reduction/Reaction by H_2 and Methane", *Journal of Catalysis*, Vol. 178, pp. 576-585.

Ciuparu, D. and L. Pfefferle, 2001, "Methane Combustion Activity of Supported Palladium Catalysts After Partial Reduction", *Applied Catalysis A: General*, Vol. 218, pp. 197-209.

Claridge, J. B., M. L. H. Green, S. C. Tsang, A. P. E. York, A. T. Ashcroft and P. D. Battle, 1993, "A Study of Carbon Deposition on Catalysts During the Partial Oxidation of Methane to Synthesis Gas", *Catalysis Letters*, Vol. 22, pp. 299-305.

Cooper, B. J., 1994, "Catalysis for the Next Decade", *Platinum Metals Review*, Vol. 38, pp. 2-10.

Cubeiro, M. L. and J. L. G. Fierro, 1998, "Selective Production of Hydrogen by Partial Oxidation of Methanol over ZnO-Supported Palladium Catalysts", *Journal of Catalysis*, Vol. 179, pp. 150-162.

De Groote, A. M. and G. F. Froment, 1996, "Simulation of Catalytic Partial Oxidation of Methane to Synthesis Gas", *Applied Catalysis: A General*, Vol. 138, pp. 245-264.

Dicks, A. L., 1996, "Hydrogen Generation from Natural Gas for the Fuel Cell Systems of Tomorrow", *Journal of Power Sources*, Vol. 61, pp. 113-124.

Dietz III, A. G., A. F. Carlsson and L. D. Schmidt, 1996, "Partial Oxidation of C_5 and C_6 Alkanes over Monolith Catalysts at Short Contact Times", *Journal of Catalysis*, Vol. 176, pp. 459-473.

Diskin, A. M., R. H. Cunningham and R. M. Ormerod, 1998, "The Oxidative Chemistry of Methane over Supported Nickel Catalysts", *Catalysis Today*, Vol. 46, pp. 147-154.

Dissanayake, D., M. P. Rosynek, K. C. C. Kharas and J. H. Lunsford, 1991, "Partial Oxidation of Methane to Carbon Monoxide and Hydrogen over a Ni/Al2O3 Catalyst", *Journal of Catalysis*, Vol. 132, pp. 117-127.

Doesburg, E. B. M., K. P. de Jong and J. H. C. van Hooff, 1999, "Preparation of Catalyst Supports, Zeolites and Mesoporous Materials", in R. A. van Santen, P. W. N. M. van Leeuwen, J. A. Moulijn and B. A. Averill (Eds.), *Catalysis: An Integrated Approach*, pp. 433-456, Elsevier, Amsterdam.

Elmasides, C., T. Ioannides and X. E. Verykios, 2000, "Kinetic Model of the Partial Oxidation of Methane to Synthesis Gas Over Ru/TiO_2 Catalyst", *AIChE Journal*, Vol. 46, pp. 1260-1270.

Elnashaie, S. S. E. H., A. M. Adris, A. S. Al-Ubaid and M. A. Soliman, 1990, "On the Non-Monotonic Behaviour of Methane Steam Reforming Kinetics", *Chemical Engineering Science*, Vol. 45, pp. 491-501.

Emonts, B., J. B. Hansen, S. L. Jorgensen, B. Höhlein and R. Peters, 1998, "Compact Methanol Reformer Test for Fuel-Cell Powered Light-Duty Vehicles", *Journal of Power Sources*, Vol. 71, pp. 288-293.

Emonts, B., J. B. Hansen, H. Schmidt, T. Grube, B. Höhlein and R. Peters, 2000, "Fuel Cell Drive System with Hydrogen Generation in Test", *Journal of Power Sources*, Vol. 86, pp. 228-236.

Ferreira-Aparicio, P., I. Rodriguez-Ramos and A. Guerrero-Ruiz, 1997, "Methane Interaction with Silica and Alumina Supported Metal Catalysts", *Applied Catalysis A: General*, Vol. 148, pp. 343-356.

Fogler, H. S., 1999, *Elements of Chemical Reaction Engineering*, 3rd ed., Prentice Hall, New Jersey.

Froment, G. F. and K. B. Bischoff (editors), 1990, *Chemical Reactor Analysis and Design*, 2nd ed., John Wiley & Sons, New York.

Furimsky, E., 1998, "Selection of Catalysts and Reactors for Hydroprocessing", *Applied Catalysis A: General*, Vol. 171, pp. 177-206.

Geankoplis, C. J., 1993, *Transport Processes and Unit Operations*, 3rd ed., Prentice Hall, New Jersey.

Geissler, K., E. Newson, F. Vogel, T. B. Truong, P. Hottinger and A. Wokaun, 2001, "Autothermal Methanol Reforming for Hydrogen Production in Fuel Cell Applications", *Physical Chemistry Chemical Physics*, Vol. 3, pp. 289-293.

Gines, M. J. L., A. J. Marchi and C. R. Apesteguia, 1997, "Kinetic Study of the Reverse Water-Gas Shift Reaction over $CuO/ZnO/Al_2O_3$ Catalysts", *Applied Catalysis A: General*, Vol. 154, pp. 155-171.

Golunski, S., 1998, "HotSpot™ Fuel Processor", *Platinum Metals Review*, Vol. 42, pp. 2-7.

Gray, P. G. and M. I. Petch, 2000, "Advances with HotSpot™ Fuel Processing", *Platinum Metals Review*, Vol. 44, pp. 108-111.

Hanselman, D. and B. Littlefield (editors), 1998, *Mastering MATLAB 5: A Comprehensive Tutorial and Reference*, Prentice-Hall, New Jersey.

Hart, D., 1998, "A Solid Start to the Millennium?", *Chemistry & Industry*, Vol. 9, pp. 344-347.

Heck, R. M. and R. J. Farrauto, 1995, *Catalytic Air Pollution Technology: Commercial Technology*, Van Nostrand Reinhold, New York.

Hickman, D. A. and L. D. Schmidt, 1992, "Synthesis Gas Formation by Direct Oxidation of Methane over Pt Monoliths", *Journal of Catalysis*, Vol. 138, pp. 267-282.

Hickman, D. A. and L. D. Schmidt, 1993, "Production of Syngas by Direct Catalytic Oxidation of Methane", *Science*, Vol. 259, pp. 343-346.

Hilaire, S., X. Wang, T. Luo, R. J. Gorte and J. Wagner, 2001, "A Comparative Study of Water-Gas-Shift Reaction over Ceria Supported Metallic Catalysts", *Applied Catalysis A: General*, Vol. 215, pp. 271-278.

Hohn, K. L. and L. D. Schmidt, 2001, "Partial Oxidation of Methane to Syngas at High Space Velocities over Rh-coated Spheres", *Applied Catalysis A: General*, Vol. 211, pp. 53-68.

Hoogers, G. and D. Thompsett, 1999, "Releasing the Potential of Clean Power", *Chemistry & Industry*, Vol. 20, pp. 796-799.

Horiuchi, T., K. Sakuma, T. Fukui, Y. Kubo, T. Osaki and T. Mori, 1996, "Suppression of Carbon Deposition in the CO_2-reforming of CH_4 by Adding Basic Metal Oxides to a Ni/Al_2O_3 Catalyst", *Applied Catalysis A: General*, Vol. 144, pp. 111-120.

Huff, M. and L. D. Schmidt, 1994, "Production of Olefins by Oxidative Dehydrogenation of Propane and Butane over Monoliths at Short Contact Times", *Journal of Catalysis*, Vol. 149, pp. 127-141.

Ioannides, T., 2001, "Thermodynamic Analysis of Ethanol Processors for Fuel Cell Applications", *Journal of Power Sources*, Vol. 92, pp. 17-25.

Isherwood, K. D., J. R. Linna and P. J. Loftus, 1998, "Using On-board Fuel Reforming by Partial Oxidation to Improve SI Engine Cold-Start Performance and Emissions", *SAE Paper* 980939.

Jamal, Y. and M. L. Wyszynski, 1994, "On-board Hydrogen Generation of Hydrogen-Rich Gaseous Fuels – A Review", *International Journal of Hydrogen Energy*, Vol. 19, pp. 557-572.

Jenkins, J. W. and E. Shutt, 1989, "The Hot Spot™ Reactor", *Platinum Metals Review*, Vol. 33, pp. 118-127.

Jiang, C., 1992, *Studies of the Production of Hydrogen From Methanol Steam Reforming at Low Temperatures* , Ph.D. Dissertation, University of New South Wales.

Jiang, C., D. L. Trimm and M. S. Wainwright, 1995, "New Technology for Hydrogen Production by the Catalytic Oxidation and Steam Reforming of Methanol at Low Temperatures", *Chemical Engineering Technology*, Vol. 18, pp. 1-6.

Jost, K., 1997, "Gasoline-Reforming Fuel Cell", *Automotive Engineering*, pp. 151-152.

Kapteijn., F., G. B. Marin and J. A. Moulijn, 1999, "Cataytic Reaction Engineering", in R. A. van Santen, P. W. N. M. van Leeuwen, J. A. Moulijn and B. A. Averill (Eds.), *Catalysis: An Integrated Approach*, pp. 375-430, Elsevier, Amsterdam.

Keshavaraja, A. and A. V. Ramaswamy, 1996, "Mn-stabilized Zirconia Catalysts for Complete Oxidation of n-Butane", *Applied Catalysis B: Environmental*, Vol. 8, pp. L1-L7.

Kirwan, J. E., A. A. Quader and M. J. Grieve, 1999, "Advanced Engine Management Using On-Board Gasoline Partial Oxidation Reforming for Meeting Super-ULEV (SULEV) Emission Standards", *SAE Paper* 1999-01-2927.

Klaiber, T., 1996, "Fuel Cells for Transport: Can the Promise be Fulfilled? Technical Requirements and Demands from Customers", *Journal of Power Sources*, Vol. 61, pp. 61-69.

Korotkikh, O. and R. Farrauto, 2000, "Selective Catalytic Oxidation of CO in H_2: Fuel Cell Applications", *Catalysis Today*, Vol. 62, pp. 249-254.

Kuvshinov, G. G., Y. I. Mogilnykh and D. G. Kuvshinov, 1998, "Kinetics of Carbon Formation from CH_4-H_2 Mixtures over a Nickel Containing Catalyst", *Catalysis Today*, Vol. 42, pp. 357-360.

Ledjeff-Hey, K., V. Formanski, Th. Kalk and J. Roes, 1998, "Compact Hydrogen Production Systems for Solid Polymer Fuel Cells", *Journal of Power Sources*, Vol. 71, pp. 199-207.

Ledjeff-Hey, K., Th. Kalk, F. Mahlendorf, O. Niemzig, A. Trautmann and J. Roes, 2000, "Portable PEFC Generator with Propane as Fuel", *Journal of Power Sources*, Vol. 86, pp. 166-172.

Lee, J. H., D. L. Trimm and N. W. Cant, 1999, "The Catalytic Combustion of Methane and Hydrogen Sulphide", *Catalysis Today*, Vol. 47, pp. 353-357.

Liu, S., L. Xu, S. Xie, Q. Wang and G. Xiong, 2001, "Partial Oxidation of Propane to Syngas over Nickel Supported Catalysts Modified by Alkali Metal Oxides and Rare-Earth Metal Oxides", *Applied Catalysis A: General*, Vol. 211, pp. 145-152.

Lu, Y., Y. Liu and S. Shen, 1998, "Design of Stable Ni Catalysts for Partial Oxidation of Methane to Synthesis Gas", *Journal of Catalysis*, Vol. 177, pp. 386-388.

Ma, L., 1995, *Hydrogen Production from Steam Reforming of Light Hydrocarbons in an Autothermic System*, Ph.D. Dissertation, University of New South Wales.

Ma, L. and D. L. Trimm, 1996, "Alternative Catalyst Bed Configurations for the Autothermic Conversion of Methane to Hydrogen", *Applied Catalysis A: General*, Vol. 138, pp. 265-273.

Ma, L., D. L. Trimm and C. Jiang, 1996, "The Design and Testing of an Autothermal Reactor for the Conversion of the Light Hydrocarbons to Hydrogen I. The Kinetics of the Catalytic Oxidation of Light Hydrocarbons", *Applied Catalysis A: General*, Vol. 138, pp. 275-283.

Maillet, T., C. Solleau, J. Barbier Jr. and D. Duprez, 1997, "Oxidation of Carbon Monoxide, Propene, Propane and Methane over a Pd/Al_2O_3 Catalyst. Effect of the Chemical State of Pd", *Applied Catalysis B: Environmental*, Vol. 14, pp. 85-95.

Marecot, P., A. Fakche, B. Kellali, G. Mabilon, M. Prigent and J. Barbier Jr., 1994, "Propane and Propene Oxidation over Platinum and Palladium on Alumina: Effects of Chloride and Water", *Applied Catalysis B: Environmental*, Vol. 3, pp. 283-294.

Miao, Q, G. Xiong, S. Sheng, W. Cui, L. Xu and X. Guo, 1997, "Partial Oxidation of Methane to Syngas over Nickel-Based Catalysts Modified by Alkali Metal Oxide and Rare Earth Metal Oxide", *Applied Catalysis A: General*, Vol. 154, pp. 17-27.

Moon, D. J., K. Sreekumar, S. D. Lee, B. G. Lee and H. S. Kim, 2001, "Studies on Gasoline Fuel Processor System for Fuel-Cell Powered Vehicles Application", *Applied Catalysis A: General*, Vol. 215, pp. 1-9.

Morioka, H., Y. Shimizu, M. Sukenobu, K. Ito, E. Tanabe, T. Shishido and K. Takehira, 2001, "Partial Oxidation of Methane to Synthesis Gas over Supported Ni Catalyst Prepared from Ni-Ca/Al-Layered Double Hydroxide", *Applied Catalysis A: General*, Vol. 215, pp. 11-19.

Nakagawa, K., N. Ikenaga, T. Suzuki, T. Kobayashi and M. Haruta, 1998a, "Partial Oxidation of Methane to Synthesis Gas over Supported Iridium Catalysts", *Applied Catalysis A: General*, Vol. 169, pp. 281-290.

Nakagawa, J., K. Anzai, N. Matsui, N. Ikenaga, T. Suzuki, Y. Teng, T. Kobayashi and M. Haruta, 1998b, "Effect of Support on the Conversion of Methane to Synthesis Gas over Supported Iridium Catalysts", *Catalysis Letters*, Vol. 51, pp. 163-167.

Nakagawa, K., N. Ikenaga, Y. Teng, T. Kobayashi and T. Suzuki, 1999a, "Partial Oxidation of Methane to Synthesis Gas over Iridium-Nickel Bimetallic Catalysts", *Applied Catalysis A: General*, Vol. 180, pp. 183-193.

Nakagawa, K., N. Ikenaga, Y. Teng, T. Kobayashi and T. Suzuki, 1999b, "Transient Response of Catalyst Bed Temperature in Pulsed Reaction of Partial Oxidation of Methane to Synthesis Gas over Supported Rhodium and Iridium Catalysts", *Journal of Catalysis*, Vol. 186, pp. 405-413.

Nakamura, J., K. Aikawa, K. Sato and T. Uchijima, 1994, "Role of Support in Reforming of CH4 with CO2 over Rh Catalysts", *Catalysis Letters*, Vol. 25, pp. 265-270.

Northeast Advanced Vehicle Consortium (NAVC), 2000, *Future Wheels*, http://www.navc.org

Neyestanaki, A. K., N. Kumar and L. E. Lindfors, 1995, "Catalytic Combustion of Propane over Pt and Cu modified ZSM-5 Zeolite Catalysts", *Fuel*, Vol. 74, pp. 690-696.

Newsome, D. S., 1980, "The Water-Gas Shift Reaction", *Catalysis Reviews: Science and Engineering*, Vol. 21, pp. 275-318.

O'Connor, R. P., E. J. Klein and L. D. Schmidt, 2000, "High Yields of Synthesis Gas by Millisecond Partial Oxidation of Higher Hydrocarbons", *Catalysis Letters*, Vol. 70, pp. 99-107.

Oklany, J. S., K. Hou and R. Hughes, 1998, "A Simulative Comparison of Dense and Microporous Membrane Reactors for the Steam Reforming of Methane", *Applied Catalysis A: General*, Vol. 170, pp. 13-22.

Opoku-Gyamfi, K. and A. A. Adesina, 1999, "Kinetic Studies of CH_4 Oxidation over Pt-NiO/δ-Al_2O_3 in a Fluidised Bed Reactor", *Applied Catalysis A: General*, Vol. 180, pp. 113-122.

Pena, M. A., J. P. Gomez and J. L. G. Fierro, 1996, "New Catalytic Routes for Syngas and Hydrogen Production", *Applied Catalysis A: General*, Vol. 144, pp. 7-57.

Peppley, B. A., J. C. Amphlett, L. M. Kearns and R. F. Mann, 1999, "Methanol-Steam Reforming on Cu/ZnO/Al_2O_3. Part 1: A Comprehensive Kinetic Model", *Applied Catalysis A: General*, Vol. 179, pp. 31-49.

Perry, R. H., D. W. Green and J. O. Maloney, 1984, *Perry's Chemical Engineers' Handbook*, 6th ed., McGraw-Hill, Singapore.

Prabhu, A. K., R. Radhakrishnan and S. T. Oyama, 1999, "Supported Nickel Catalysts for Carbon Dioxide Reforming of Methane in Plug Flow and Membrane Reactors", *Applied Catalysis A: General*, Vol. 183, pp. 241-252.

Provendier, H., C. Petit, C. Estournes, S. Libs and A. Kiennemann, 1999, "Stabilisation of Active Nickel Catalysts in Partial Oxidation of Methane to Synthesis Gas by Iron Addition", *Applied Catalysis A: General*, Vol. 180, pp. 163-173.

Ralph, T. R., 1999, "Clean Fuel Cell Energy for Today", *Platinum Metals Review*, Vol. 43, pp. 14-17.

Ralph, T. R. and G. A. Hards, 1998, "Powering the Cars and Homes of Tomorrow", *Chemistry & Industry*, Vol. 9, pp. 337-342.

Raman, V., 1997, "Emerging Applications of Hydrogen in Clean Transportation", *Chemistry & Industry*, pp. 771-774.

Rampe, T., A. Heinzel and B. Vogel, 2000, "Hydrogen Generation from Biogenic and Fossil Fuels by Autothermal Reforming", *Journal of Power Sources*, Vol. 86, pp. 536-541.

Rase, H. F., 1990, *Fixed-Bed Reactor Design and Diagnostics*, Butterworths, Massachusetts.

Rastler, D., 2000, "Opportunities and Challenges for Fuel Cells in the Evolving Energy Enterprise", *Fuel Cell Bulletin*, Vol. 19, pp. 7-11.

Reid, R. C., J. M. Prausnitz and B. E. Poling (editors), 1987, *The Properties of Gases and Liquids*, McGraw-Hill, New York.

Rosen, M. A., 1991, "Thermodynamic Investigation of Hydrogen Production by Steam-Methane Reforming", *International Journal of Hydrogen Energy*, Vol. 16, pp. 207-217.

Rostrup-Nielsen, J. R., 1984, "Catalytic Steam Reforming", in J. R. Anderson and M. Boudart (Eds.), *Catalysis, Science & Technology*, Vol. 5, pp. 1-117, Springer-Verlag, Berlin.

Rostrup-Nielsen, J. R., 1997, "Industrial Relevance of Coking", *Catalysis Today*, Vol. 37, pp. 225-232.

Rostrup-Nielsen, J. R., 2000, "New Aspects of Syngas Production and Use", *Catalysis Today*, Vol. 63, pp. 159-164.

Rostrup-Nielsen, J. R. and I. Alstrup, 1999, "Innovation and Science in the Process Industry. Steam Reforming and Hydrogenolysis", *Catalysis Today*, Vol. 53, pp. 311-316.

Rostrup-Nielsen, J. R. and J-H. Bak Hansen, 1993, "CO_2-Reforming of Methane over Transition Metals", *Journal of Catalysis*, Vol. 144, pp. 38-49.

Rostrup-Nielsen, J. R. and L. J. Christiansen, 1995, "Internal Steam Reforming in Fuel Cells and Alkali Poisoning", *Applied Catalysis A: General*, Vol. 126, pp. 381-390.

Ruckenstein, E. and H. Y. Wang, 1999, "Effect of Support on Partial Oxidation of Methane to Synthesis Gas over Supported Rhodium Catalysts", *Journal of Catalysis*, Vol. 187, pp. 151-159.

Ruth, K., M. Hayes, R. Burch, S. Tsubota and M. Haruta, 2000, "The Effects of SO_2 on the Oxidation of CO and Propane on Supported Pt and Au Catalysts", *Applied Catalysis B: Environmental*, Vol. 24, pp. L133-L138.

Slagtern, A., H. M. Swaan, U. Olsbye, I. M. Dahl and C. Mirodatos, 1998, "Catalytic Partial Oxidation of Methane over Ni-, Co- and Fe-based Catalysts", *Catalysis Today*, Vol. 46, pp. 107-115.

Sutton, D., J-F Moisan and J. R. H. Ross, 2001, "Kinetic Study of CO_2 Reforming of Propane over Propane over Ru/Al_2O_3", *Catalysis Letters*, Vol. 75, pp. 175-181.

Takano, A., T. Tagawa and S. Goto, 1994, "Carbon Dioxide Reforming of Methane on Supported Nickel Catalysts", *Journal of Chemical Engineering of Japan*, Vol. 27, pp. 727-731.

Thevenin, P. O., A. G. Ersson, H. M. J. Kusar, P. G. Menon and S. G. Jaras, 2001, "Deactivation of High Temperature Combustion Catalysts", *Applied Catalysis A: General*, Vol. 212, pp. 189-197.

Thomas, C. E., B. D. James, F. D. Lomax Jr and I. F. Kuhn Jr, 2000, "Fuel Options for the Fuel Cell Vehicle: Hydrogen, Methanol or Gasoline?", *International Journal of Hydrogen Energy*, Vol. 25, pp. 551-567.

Tindall, B. M. and D. L. King, 1994, "Designing Steam Reformers for Hydrogen Production", *Hydrocarbon Processing*, Vol. 73, pp. 69-75.

Tomishige, K., S. Kanazawa, K. Suzuki, M. Asadullah, M. Sato, K. Ikushima and K. Kunimori, 2002, "Effective Heat Supply from Combustion to Reforming in Methane Reforming with CO_2 and O_2: Comparison Between Ni and Pt Catalysts", *Applied Catalysis A: General*, Vol. 233, pp. 35-44.

Torniainen, P. M., X. Chu and L. D. Schmidt, 1994, "Comparison of Monolith-Supported Metals for the Direct Oxidation of Methane to Syngas", *Journal of Catalysis*, Vol. 176, pp. 1-10.

Trimm, D. L., 1980, *Design of Industrial Catalysts*, Elsevier, Amsterdam.

Trimm, D. L., 1983, "Catalytic Combustion", *Applied Catalysis*, Vol. 7, pp. 249-282.

Trimm, D. L., 1999, "Catalysts for the Control of Coking During Steam Reforming", *Catalysis Today*, Vol. 49, pp. 3-10.

Trimm, D. L., 2001, "The Regeneration or Disposal of Deactivated Heterogeneous Catalysts", *Applied Catalysis A: General*, Vol. 212, pp. 153-160.

Trimm, D. L. and C. W. Lam, 1980, "The Combustion of Methane on Platinum-Alumina Fibre Catalysts", *Chemical Engineering Science*, Vol. 35, pp. 1405-1413.

Trimm, D. L. and Z. İ. Önsan, 2001, "Onboard Fuel Conversion for Hydrogen-Fuel-Cell-Driven Vehicles", *Catalysis Reviews: Science and Engineering*, Vol. 43, pp. 31-84.

Tsipouriari, V. A., Z. Zhang and X. E. Verykios, 1998, "Catalytic Partial Oxidation of Methane to Synthesis Gas over Ni-based Catalysts", *Journal of Catalysis*, Vol. 179, pp. 283-291.

Tsotsis, T. T., A. M. Champagnie, S. P. Vasileiadis, Z. D. Ziaka and R. G. Minet, 1992, "Packed Bed Catalytic Membrane Reactors", *Chemical Engineering Science*, Vol. 47, pp. 2903-2908.

Twigg, M. V. and M. S. Spencer, 2001, "Deactivation of Supported Copper Metal Catalysts for Hydrogenation Reactions", *Applied Catalysis A: General*, Vol. 212, pp. 161-174.

Urban, P. M., A. Funke, J. T. Müller, M. Himmen and A. Docter, 2001, "Catalytic Processes in Solid Polymer Electrolyte Fuel Cell Systems", *Applied Catalysis A: General*, Vol. 221, pp. 459-470.

Utaka, T., K. Sekizawa and K. Eguchi, 2000, "CO Removal by Oxygen-Assisted Water Gas Shift Reaction over Supported Cu Catalysts", *Applied Catalysis A: General*, Vol. 194-195, pp. 21-26.

van de Beld, L., M. C. van der Ven and K. R. Westerterp, 1995, "A Kinetic Study of the Complete Oxidation of Ethene, Propane and Their Mixtures on a Pd/Al_2O_3 Catalyst", *Chemical Engineering and Processing*, Vol. 34, pp. 469-478.

van Looij, F. and J. W. Geus, 1997, "Nature of the Active Phase of a Nickel Catalyst during the Partial Oxidation of Methane to Synthesis Gas", *Journal of Catalysis*, Vol. 168, pp. 154-163.

Vemeiren, W. J. M., E. Blomsma and P. A. Jacobs, 1992, "Catalytic and Thermodynamic Approach of Oxyreforming Reaction of Methane", *Catalysis Today*, Vol. 13, pp. 427-436.

Velu, S., K. Suzuki and T. Osaki, 1999, "Selective Production of Hydrogen by Partial Oxidation of Methanol over Catalysts Derived from CuZnAl-layered Double Hydroxides", *Catalysis Letters*, Vol. 62, pp. 159-167.

Velu, S., K. Suzuki, M. P. Kapoor, F. Ohashi and T. Osaki, 2001, "Selective Production of Hydrogen for Fuel Cells via Oxidative Steam Reforming of Methanol over CuZnAl(Zr)-oxide Catalysts", *Applied Catalysis A: General*, Vol. 213, pp. 47-63.

Veser, G. and L. D. Schmidt, 1996, "Ignition and Extinction in the Catalytic Oxidation of Hydrocarbons over Platinum", *AIChE Journal*, Vol. 42, pp. 1077-1087.

Veser, G., M. Ziauddin and L. D. Schmidt, 1999, "Ignition in Alkane Oxidation on Noble-Metal Catalysts", *Catalysis Today*, Vol. 47, pp. 219-228.

Vielstich, W. and T. Iwasita, 1997, in G. Ertl, H. Knozinger, J. Weitkamp (Eds.), *Handbook of Heterogeneous Catalysis*, pp. 2090, Wiley-VCH, New York.

Wainwright, M. S. and D. L. Trimm, 1995, "Methanol Synthesis and Water-Gas Shift Reactions on Ranney Copper-Catalysts", *Catalysis Today*, Vol. 23, pp. 29-42.

Wakao, N. and S. Kaguei (editors), 1982, *Heat and Mass Transfer in Packed Beds*, Gordon and Breach Science Publishers, New York.

Wang, X. and R. J. Gorte, 2001, "Steam Reforming of n-Butane on Pd/Ceria", *Catalysis Letters*, Vol. 73, pp. 15-19.

Widjaja, H., K. Sekizawa, K. Eguchi and H. Arai, 1999, "Oxidation of Methane over Pd/mixed Oxides for Catalytic Combustion", *Catalysis Today*, Vol. 47, pp. 95-101.

Witt, P. M. and L. D. Schmidt, 1996, "Effect of Flow Rate on the Partial Oxidation of Methane and Ethane", *Journal of Catalysis*, Vol. 163, pp. 465-475.

Wu, H., L. Liu and S. Yang, 2001, "Effects of Additives on Supported Noble Metal Catalysts for Oxidation of Hydrocarbons and Carbon Monoxide", *Applied Catalysis A: General*, Vol. 211, pp. 159-165.

Xu, J. and G. F. Froment, 1989a, "Methane Steam Reforming, Methanation and Water-Gas Shift: I. Intrinsic Kinetics", *AIChE Journal*, Vol. 35, pp. 88-96.

Xu, J. and G. F. Froment, 1989b, "Methane Steam Reforming: II. Diffusional Limitations and Reactor Simulation", *AIChE Journal*, Vol. 35, pp. 97-103.

Yamazaki, O., K. Tomishige and K. Fujimoto, 1996, "Development of Highly Stable Nickel Catalyst for Methane-Steam Reaction under Low Steam to Carbon Ratio", *Applied Catalysis A: General*, Vol. 136, pp. 49-56.

Yazawa, Y., N. Kagi, S. Komai, A. Satsuma, Y. Murakami and T. Hattori, 2001, "Kinetic Study of Support Effect in the Propane Combustion over Platinum Catalyst", *Catalysis Letters*, Vol. 72, pp. 157-160.

Zhang, T. and M. D. Amiridis, 1998, "Hydrogen Production via the Direct Cracking of Methane over Silica-Supported Nickel Catalysts", *Applied Catalysis A: General*, Vol. 167, pp. 161-172.

Zum Mallen, M. P. and L. D. Schmidt, 1996, "Oxidation of Methanol over Polycrystalline Rh and Pt: Rates, OH Desorption, and Model", *Journal of Catalysis*, Vol. 161, pp. 230-246.